



## **CARBON-BASED MEMBRANE BIOREACTORS FOR THE ANAEROBIC DECOLORIZATION OF DYES**

**Mohammad Shaiful Alam Amin**

**ADVERTIMENT.** L'accés als continguts d'aquesta tesi doctoral i la seva utilització ha de respectar els drets de la persona autora. Pot ser utilitzada per a consulta o estudi personal, així com en activitats o materials d'investigació i docència en els termes establerts a l'art. 32 del Text Refós de la Llei de Propietat Intel·lectual (RDL 1/1996). Per altres utilitzacions es requereix l'autorització prèvia i expressa de la persona autora. En qualsevol cas, en la utilització dels seus continguts caldrà indicar de forma clara el nom i cognoms de la persona autora i el títol de la tesi doctoral. No s'autoritza la seva reproducció o altres formes d'explotació efectuades amb finalitats de lucre ni la seva comunicació pública des d'un lloc aliè al servei TDX. Tampoc s'autoritza la presentació del seu contingut en una finestra o marc aliè a TDX (framing). Aquesta reserva de drets afecta tant als continguts de la tesi com als seus resums i índexs.

**ADVERTENCIA.** El acceso a los contenidos de esta tesis doctoral y su utilización debe respetar los derechos de la persona autora. Puede ser utilizada para consulta o estudio personal, así como en actividades o materiales de investigación y docencia en los términos establecidos en el art. 32 del Texto Refundido de la Ley de Propiedad Intelectual (RDL 1/1996). Para otros usos se requiere la autorización previa y expresa de la persona autora. En cualquier caso, en la utilización de sus contenidos se deberá indicar de forma clara el nombre y apellidos de la persona autora y el título de la tesis doctoral. No se autoriza su reproducción u otras formas de explotación efectuadas con fines lucrativos ni su comunicación pública desde un sitio ajeno al servicio TDR. Tampoco se autoriza la presentación de su contenido en una ventana o marco ajeno a TDR (framing). Esta reserva de derechos afecta tanto al contenido de la tesis como a sus resúmenes e índices.

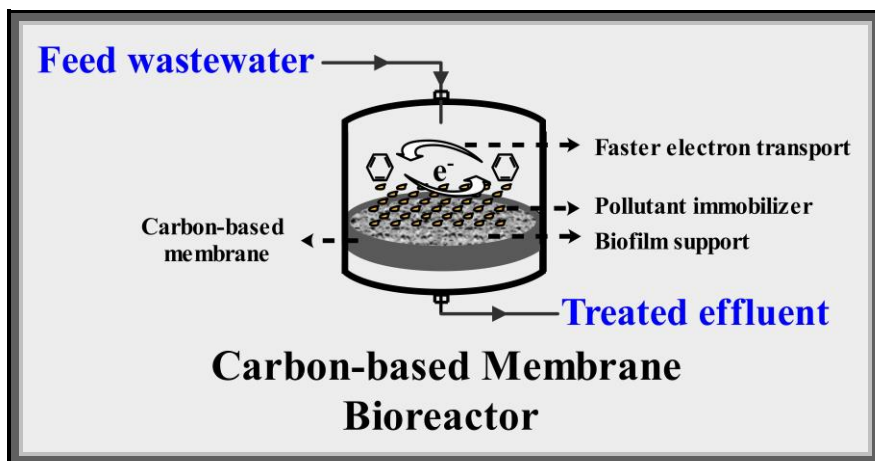
**WARNING.** Access to the contents of this doctoral thesis and its use must respect the rights of the author. It can be used for reference or private study, as well as research and learning activities or materials in the terms established by the 32nd article of the Spanish Consolidated Copyright Act (RDL 1/1996). Express and previous authorization of the author is required for any other uses. In any case, when using its content, full name of the author and title of the thesis must be clearly indicated. Reproduction or other forms of for profit use or public communication from outside TDX service is not allowed. Presentation of its content in a window or frame external to TDX (framing) is not authorized either. These rights affect both the content of the thesis and its abstracts and indexes.



# CARBON-BASED MEMBRANE BIOREACTORS FOR THE ANAEROBIC DECOLORIZATION OF DYES

---

MOHAMMAD SHAIFUL ALAM AMIN



DOCTORAL THESIS

2022

UNIVERSITAT ROVIRA I VIRGILI

CARBON-BASED MEMBRANE BIOREACTORS FOR THE ANAEROBIC DECOLORIZATION OF DYES

Mohammad Shaiful Alam Amin

# **Carbon-based Membrane Bioreactors for the Anaerobic Decolorization of Dyes**

DOCTORAL THESIS

**Mohammad Shaiful Alam Amin**

Supervised by:

**Dr. Josep Font Capafons**

Department of Chemical Engineering



UNIVERSITAT  
ROVIRA i VIRGILI

A Thesis submitted in partial fulfillment of the requirements of the  
degree of doctor from the Universitat Rovira i Virgili in  
Nanoscience, Materials and Chemical Engineering Program

**Tarragona 2022**

UNIVERSITAT ROVIRA I VIRGILI

CARBON-BASED MEMBRANE BIOREACTORS FOR THE ANAEROBIC DECOLORIZATION OF DYES

Mohammad Shaiful Alam Amin



UNIVERSITAT  
ROVIRA I VIRGILI

ESCOLA TÈCNICA SUPERIOR D'ENGINYERIA QUÍMICA  
DEPARTAMENT D'ENGINYERIA QUÍMICA

Avinguda dels Països Catalans, 26  
Campus Sescelades  
43007 Tarragona (Spain)  
Tels.: +34 977 55 9646  
Fax: +34 977 55 9621  
e-mail: [jose.font@urv.cat](mailto:jose.font@urv.cat)

I STATE that the present study, entitled “Carbon-based Membrane Bioreactors for the Anaerobic Decolorization of Dyes”, presented by Mohammad Shaiful Alam Amin for the award of the degree of Doctor, has been carried out under my supervision at the Department of Chemical Engineering of this university.

Tarragona, February 1, 2022

### Doctoral Thesis Supervisor

José Font  
Capafons - DNI  
39856271P  
(AUT)

Firmado  
digitalmente por  
José Font Capafons -  
DNI 39856271P  
(AUT)  
Fecha: 2022.02.01  
21:05:44 +01'00'

Dr. Josep Font Capafons

UNIVERSITAT ROVIRA I VIRGILI

CARBON-BASED MEMBRANE BIOREACTORS FOR THE ANAEROBIC DECOLORIZATION OF DYES

Mohammad Shaiful Alam Amin

*“To my loving parents and wife,  
without whom this thesis would not be possible”*



UNIVERSITAT ROVIRA I VIRGILI

CARBON-BASED MEMBRANE BIOREACTORS FOR THE ANAEROBIC DECOLORIZATION OF DYES

Mohammad Shaiful Alam Amin

# Acknowledgments

“Al-Ḥamdu lillāhi Rabbil-'Ālamīn” All praise and thanks are for Allah, the lord of all creations. I am indebted to Allah for his kindness and blessings that enabled me to complete my thesis.

First and foremost, I am thankful to my supervisor Dr. Josep Font, for his helpful instruction, constructive criticism, and encouragement. His inspiration and supervision helped me to work independently towards completing the research in due time. His guidance and support helped me to accomplish this degree.

I would also like to express my gratitude to all of the present and former members of the PISET research group, with whom I have had the pleasure of meeting and working. The last three years have gone by surprisingly quickly with this pleasant environment of this research group. Thank you so much to everyone!

I would like to express my gratitude to Dr. Magdalena Constantí from the Interfibio group at the Universitat of Rovira i Virgili for her help with biofilm characterization. I also thank her for devoting so much attention to me and introducing me to the world of bacterial DNA extraction and analysis.

My deepest gratitude is extended to Dr. Esther Torrens Serrahima for her unwavering assistance and support throughout the years. I want to thank Núria Juanpere Mitjana for all her help with all the administrative issues. My earnest thanks to all my friends: Oleg, Kasia, Jacky, Mary, Margarita for all the memories, experiences, and funs.

I am also grateful for the support granted by the European Union's Horizon 2020 research and innovation programme under the Marie Skłodowska-Curie grant agreement No. 713679 and from the Universitat Rovira i Virgili (URV).

Finally, my deep and sincere gratitude to my family for their continuous and unparalleled love, help, advice, and support. Love to my children, Ayaat and Abdullah, whose presence always motivates me to finish my degree with expediency. Though I could not give them much more time, I believe we will have many years of great times together. I am thankful to my brother, Md. Shariful Alam, for always being there for me as a friend. I am always indebted to my parents for providing me with the opportunities and experiences that shaped me for this position.

Last but not least, I'd like to express my gratitude to my wife, Trisha, who, despite all of my quirk and moods, continues to love, countless sacrifices, and support me throughout this entire process.

# Table of Contents

<b>SUMMARY .....</b>	<b>1</b>
<b>CHAPTER 1. INTRODUCTION .....</b>	<b>5</b>
<b>1. WATER POLLUTION .....</b>	<b>7</b>
<b>2. AZO DYE REMOVAL PROCESSES .....</b>	<b>9</b>
2.1 Conventional and Advance Treatment Procedures .....	9
2.2 Ceramic-supported Carbon-based Membrane Bioreactor .....	11
<b>3. HYPOTHESIS AND OBJECTIVES OF THE THESIS .....</b>	<b>13</b>
<b>4. THESIS OUTLINE .....</b>	<b>15</b>
<b>CHAPTER 2. COMPARATIVE ANAEROBIC DECOLORIZATION OF AZO DYES BY CARBON-BASED MEMBRANE BIOREACTOR.....</b>	<b>23</b>
<b>1. INTRODUCTION .....</b>	<b>25</b>
<b>2. MATERIALS AND METHODS .....</b>	<b>28</b>
2.1 Materials.....	28
2.2 Preparation of Ceramic-supported Carbon Membrane .....	30
2.3 Membrane Characterization .....	31
2.4 Microbial Analysis .....	31
2.5 Experimental Set-up for Anaerobic Biodegradation .....	32
2.6 Analytical Methods .....	34
<b>3. RESULTS AND DISCUSSIONS .....</b>	<b>35</b>
3.1 Morphological Structure Analysis .....	35
3.2 Impact of the Carbon Layer on Flux and Resistance .....	38
3.3 Role of the Carbon Layer on Anaerobic Biodegradation of Azo Dye ..	40
3.4 Effect of Precursor Concentration on Azo Dye Decolorization.....	43
3.5 Effect of Flux and Feed Concentration on Azo Dye Decolorization ....	45
3.6 Comparative Decolorization of Azo Dyes .....	47
3.7 Microbial Community Analysis .....	50
<b>4. CONCLUSIONS .....</b>	<b>53</b>

<b>CHAPTER 3. CERAMIC-SUPPORTED GRAPHENE OXIDE MEMBRANE BIOREACTOR FOR THE ANAEROBIC DECOLORIZATION OF AZO DYES .....</b>	<b>67</b>
<b>1. INTRODUCTION .....</b>	<b>69</b>
<b>2. EXPERIMENTAL.....</b>	<b>72</b>
2.1 Fabrication of Ceramic-supported GO Membrane (CSGOM).....	72
2.2 Experimental Set-up for Anaerobic Biodegradation .....	74
2.3 CSGOM Membrane Characterization .....	76
2.4 Microbial Analysis.....	77
<b>3. RESULT AND DISCUSSION .....</b>	<b>78</b>
3.1 Morphological Structure of CSGOM.....	78
3.2 Impact of the GO Layer on Flux and Resistance .....	84
3.3 Role of the Graphene Oxide Layer on Anaerobic Biodecolorization of Azo Dyes.....	87
3.4 Effect of Flux and Feed Concentration on Azo Dye Decolorization ....	91
3.5 Comparative Decolorization of Azo Dyes .....	94
3.6 Microbial Community Analysis.....	97
<b>4. CONCLUSIONS .....</b>	<b>100</b>
<b>CHAPTER 4. COMPACT CARBON-BASED MEMBRANE REACTORS FOR THE INTENSIFIED ANAEROBIC DECOLORIZATION OF DYE EFFLUENTS .....</b>	<b>113</b>
<b>1. INTRODUCTION .....</b>	<b>115</b>
<b>2. MATERIALS AND METHODS .....</b>	<b>118</b>
2.1 Fabrication of Ceramic-supported Carbon Membrane.....	118
2.2 Experimental Set-up for Anaerobic Biodegradation .....	119
2.3 Membrane Characterization .....	120

<b>3. RESULT AND DISCUSSION .....</b>	<b>122</b>
3.1 Structural and Chemical Characterization of Ceramic-supported Carbon Membranes .....	122
3.2 Impact of the Carbonaceous Layer on Flux and Resistance.....	128
3.3 Role of the Membrane Precursors on Anaerobic Decolorization of Dye Molecules .....	131
3.4 Biodecolorization Performance of CSCM and CSGOM .....	133
<b>4. CONCLUSIONS .....</b>	<b>139</b>
<b>CHAPTER 5. COMPACT TUBULAR CARBON-BASED MEMBRANE BIOREACTORS FOR ANAEROBIC DECOLORIZATION OF AZO DYES</b>	<b>151</b>
<b>1. INTRODUCTION .....</b>	<b>153</b>
<b>2. EXPERIMENTAL.....</b>	<b>155</b>
2.1 Preparation of Tubular Ceramic-supported Carbon Membrane.....	155
2.2 Experimental Set-up for Anaerobic Biodegradation .....	156
2.3 Membrane Characterization .....	158
2.4 Analytical Methods .....	158
<b>3. RESULT AND DISCUSSION .....</b>	<b>159</b>
3.1 Structural and Chemical Characterization of Tubular Ceramic-supported Carbon Membranes .....	159
3.2 Permeate Flux and Hydraulic Resistance of the Tubular Carbon-based Membranes.....	161
3.3 Role of the Membrane Type on Anaerobic Decolorization of Dyes...	163
3.4 TCSCM and TCSGOM Performance for Decolorization of Azo Dyes ....	165
.....	165
<b>4. CONCLUSIONS .....</b>	<b>170</b>

<b>CHAPTER 6. BIOFILM MODEL DEVELOPMENT AND PROCESS ANALYSIS OF ANAEROBIC BIO-DIGESTION OF AZO DYES .....</b>	<b>177</b>
<b>1. INTRODUCTION .....</b>	<b>179</b>
<b>2. MATERIALS AND METHODS .....</b>	<b>183</b>
2.1 Preparation of Bioreactors.....	183
2.2 Process Configuration .....	184
2.3 Analytical Procedure .....	185
2.4 Model Development.....	185
2.5 Reactor Configuration, Simulation Parameters and Initial Conditions ....	189
2.6 Model Calibration and Validation.....	190
<b>3. RESULTS AND DISCUSSIONS .....</b>	<b>191</b>
3.1 Model Calibration .....	191
3.2 Model Validation .....	193
3.3 Model Evaluation with Various Types of Dye.....	194
3.4 Model Evaluation with Differing Supporting Materials .....	197
3.5 Effect of External Carbon Source on Anaerobic Bio-digestion of Dyes...	199
3.6 Interaction Between HRT and Acetate to Dye Ratio on Anaerobic Bio-digestion of Dyes.....	201
<b>4. CONCLUSIONS .....</b>	<b>203</b>
<b>CHAPTER 7. CONCLUSIONS AND FUTURE WORK .....</b>	<b>213</b>
<b>1. GENERAL CONCLUSIONS.....</b>	<b>215</b>
<b>2. FUTURE WORK.....</b>	<b>217</b>

## Summary

The textile dyeing sector is the world's second most polluting industry, responsible for 20% of global water pollution. This polluted water not only ruins the environment but also harms people because it enters the food chain in a variety of ways, including drinking water. Many industrially developed or developing countries face many problems in treating textile industrial effluent waste materials that mainly contain azo dye waste, which is typically xenobiotic and recalcitrant in nature. Dye-containing wastewater mixed with freshwater reduces the amount of dissolved oxygen in the water and causes catastrophic damage to aquatic animals and the environment. The presence of these compounds in the effluents must reduce to use or reuse water. For this reason, environmentally friendly wastewater treatment is now a top concern of nations around the world.

The presence of a modest quantity of such recalcitrants in massive volumes of wastewater failed to treat and remove them efficiently by conventional treatment processes, including physical, chemical, physicochemical, and biological methods. Researchers worldwide have been working on different techniques such as incineration, chemical precipitation, ionic exchange, catalytic and non-catalytic oxidation, peroxidation, anaerobic treatment, membrane filtrations, anaerobic biological activated carbon for the treatment of textile wastewater.

The significant factors for dye removal from textile wastewater are operating cost, installation cost, retention time, secondary sludge, or toxic byproduct. Toxic byproducts or sludges are highly environmental pollutants that need further treatment. Considering all of these, membrane separation processes and biological treatment are the most cost-effective eco-friendly



methods. Our previous research demonstrated the beneficial effect of the biological activated carbon on anaerobic dye degradation. Thus, an anaerobic compact bioreactor greatly enhanced the mineralization of this compound. However, this new system had some imperfections, such as decolorization efficiency with higher flux and dye concentration and weak electron shuttle mechanism between carbonaceous surface and microbes.

Therefore, this thesis exploits a novel system that integrates the electron carrier and separation element into a single unit. The idea is to combine the membrane separation and bio-reduction processes by inoculating or growing anaerobic biofilms on top of ceramic-supported carbon membranes. UF ceramic composite support with the pore sizes equivalent to 50 kg·mol<sup>-1</sup> molecular weight cut-off (MWCO), comprised of ZrO<sub>2</sub> and TiO<sub>2</sub>, was chosen because of the superb physical, chemical, and thermal stability that provides longevity and reusability of the membrane. The carbon-based membranes were prepared from several carbonaceous materials, for example, Matrimid 5218 polyimide and exfoliated graphene oxide solution. The flat and tubular ceramic-supported carbon-based membranes were fabricated using both membrane precursors. Spin coating and up-flow method were employed to deposit the polyimide layer over and inside the ceramic support, respectively, to synthesize flat and tubular membranes. The coated membranes were then carbonized at high temperatures in an inert atmosphere to achieve their final shape. On the contrary, both the ceramic-supported flat and tubular graphene oxide membrane utilized the vacuum-assisted filtration of exfoliated graphene oxide solution to achieve the carbon-based graphene oxide membrane.

Due to the feasibility of using carbonaceous material with anaerobic microorganisms, an optimization study was conducted on decolorizing dye molecules with structurally different dye molecules. The influence of amounts and membrane precursors (Matrimid 5218 and Graphene Oxide) over the carbon-based membrane was investigated based on two independent factors: feed concentration and permeate flux. As a result of this study, both ceramic-supported nano-sized carbon-based membranes were able to decolorize mono azo Acid Orange 7 (AO7), diazo Reactive Black 5 (RB5), and triazo Direct Blue 71 (BD71). The ceramic-supported graphene oxide membrane (CSGOM) facilitates a better electron transport mechanism than the ceramic-supported matrimid membrane (CSCM) that enhances the color removal rate in this integrated anaerobic membrane bioreactors. That's why at a higher feed concentration ( $100 \text{ mg}\cdot\text{mL}^{-1}$ ) and permeate flux ( $0.10 \text{ L}\cdot\text{m}^{-2}\cdot\text{h}^{-1}$ ), CSGOM shows three times higher decolorization rate than CSCM.

Since the single compact carbon-based membrane bioreactor was demonstrated to be an effective technology for enhanced decolorization of azo dyes, similar reactors worked well with other dyes instead of the individual azo dyes. In such an experiment, the color removal properties of an azo dye mixture (ADM) (equimolar ratio of AO7, RB5, and DB71), phenothiazine Methylene Blue (MB), and sticky fluorescent Rhodamine B (RhB) dye solution were studied. CSGOM performs optimally in each scenario, regardless of the operating conditions or parameters. This concept is later applied to the tubular membrane as this module has high crossflow and pressure drop as well as a low tendency to fouling and ease of cleaning. As in prior trials, the tubular ceramic-supported graphene oxide membrane (TCSGOM) decolorized azo dye more efficiently than the ceramic-supported carbon-based membrane (TCSCM).

Finally, the thesis studies the kinetic model of the biodecolorization process of the CSGOM bioreactor in order to determine the ideal operating parameters for maximum dye removal. More precisely, the model was used to study the effect of critical operating factors on the dye removal mechanism, including dye structures, initial dye concentration, and permeate flux. This study also scrutinized the hydrolysis behavior of complex dye molecules and the effect of biofilm support materials. The results suggest that the external carbon sources and hydraulic retention time be optimized for the maximum biodecolorization rate.

# Chapter 1. Introduction

The first chapter of this thesis presents an overview of water pollution as well as the severe environmental effect caused by the dyestuff molecules, mainly the azo dye. This section summarizes traditional water treatment and several advanced alternative methods for removing azo dyes from wastewater. It describes the hypothesis and objective of this novel compact ceramic-supported carbon membrane bioreactor that combines anaerobic biological processes with membrane filtration to remove azo and other dyes. Afterward, highlighted the topics of each chapter that focused on improving dye decolorization by conducting several experiments, for example, the influence of membrane precursors, inflow feed concentrations and outflow permeate flow, membrane modules (flat and tubular), and dye structure. Finally, it introduces a biofilm model kinetics to optimize the decolorization process.



## 1. Water Pollution

The crisis of pure water is increasing day by day due to population growth, wastage of water resources, and increasing use of water in industry. Globally, as the industry develops, the severity of water pollution is increasing at an alarming rate. Rivers and canals are being polluted by untreated liquid wastes and toxic chemicals from industries, as seen in Figure 1. Most of these pollutants are recalcitrant or resistive, which has adverse effects on wastewater quality [1]. Due to this contamination, pure water changes into a dark black opaque color. This blockage the underwater sunlight transmission, as a result, disrupt the photosynthetic process [2]. Furthermore, it lowers the oxygen level in the water and causes the death of the plants and animals that reside beneath of water surface [3]. That deficiency of oxygen and the presence of toxic substances resulted in the death of numerous fish, later which eventually became a source of water pollution. Moreover, it becomes impossible to use the polluted water for drinking and household purposes because of its bad odors. Sometimes the wastewater has seeped into the ponds and arable lands during the monsoons or floods. As a result, the crop is being destroyed and the environment as well. A recent study has found the existence of dyes and toxic substances in vegetables and fruits grown by using this pollutant water [4].

Very common and harmful pollutants in the wastewater effluent are the azo dyes that discharged from the textile and garment industries. The azo dyes are mainly comprised of azo bond ( $-\text{N}=\text{N}-$ ) in addition to the several chromophores ( $-\text{C}=\text{C}-$ ,  $-\text{C}\equiv\text{N}-$ ), auxochromes ( $-\text{OH}$ ,  $-\text{NH}_2$ ) and other functional groups ( $-\text{COOH}$ ,  $-\text{CH}_3$ ,  $\text{O}-\text{CH}_3$ ,  $-\text{SO}_3\text{H}$ ) in different structural positions [5]. In a dye structure, the occurrences of the azo bond can happen many times. Thus, monoazo dye includes one azo linkage, while diazo and

## 1. Introduction

triazo dye contains two and three, respectively. It is the largest group of synthetic dyes, and compared to the use of other dyes, it represents approximately 70% [6]. As a result, worldwide, millions of tons of these azo dye containing waste are annually discharged from a variety of industries such as textile, paint, food, pharmaceuticals and cosmetics [7, 8].



<https://www.textiletoday.com.bd/invisible-price-pay-producing-garment-concerning-environment/>



<https://www.weforum.org/agenda/2020/01/fashion-industry-carbon-unsustainable-environment-pollution/>



<https://www.nytimes.com/2013/07/15/world/asia/bangladesh-pollution-told-in-colors-and-smells.html>



<https://www.reuters.com/article/us-bangladesh-rivers-idUSTRE54I04G20090519>

**Figure 1.** Water pollution in Bangladesh.

Generally, the azo dyes are developed to be chemically and photolytically stable, which makes them recalcitrant that are slowly biodegradable or non-biodegradable in the aquatic environment. That means after the mixing of dyestuffs molecules in water, it poses a massive obstacle to potential treatment, which causes them to remain in the environment for a long time. In addition, because most azo dyes are water-soluble and readily absorbed

through skin contact and inhalation, they raise the risk of cancer and allergic disease. Even the azo dyes breakdown products (aromatic amines and arylamine) are highly cytotoxic and carcinogenic [9]. Thus, the presence of azo dyes either on the surface or groundwater is highly hazardous to the living organism. Therefore, the necessity of finding solutions to this problem caused by dye-containing wastewater does not require any more discussion. It is decidedly essential to ensure that wastewater treatment processes are operating efficiently to avoid problems with contamination of azo dyes substances.

## **2. Azo Dye Removal Processes**

### **2.1 Conventional and Advance Treatment Procedures**

For ensuring a safe and healthy aquatic environment, the pollutants present in effluent wastewater need to be kept within a permissible limit [10, 11]. Dye-containing industrial wastewater could be treated independently or in combination by chemical, physical, physicochemical, and biological methods [12-15].

For the degradation of dye, as seen in Figure 2, most commonly applied chemical methods are ozonation, advanced oxidation processes and photocatalytic degradation [16, 17]. The ozonation process has been demonstrated to effectively decolorization, COD removal, and improved biodegradability [18-20]. As ozone is applied in its gaseous state, therefore, overall volume and sludge do not increase significantly. However, a large amount of ozone is used, which makes the process expensive [21]. Advanced Oxidation Processes such as electrochemical oxidation, Fenton and Fenton-like processes are efficiently capable to reduce COD, color, and toxicity [22, 23]. One major disadvantage of this method is the production of sludge,



which requires further treatment. The same difficulty has also been experienced for the physicochemical methods such as coagulation-flocculation or adsorption [24]. Some traditional physical methods, such as adsorption or filtration techniques, have also been successfully applied in textile industry [25, 26]; however, their main drawbacks are high investment cost and fouling [27]. Nanofiltration and reverse osmosis can be applied for the treatment of textile-processing wastewaters. These separation processes are very fast and the requirements are less [28]. The weaknesses of these processes are flux decline and membrane fouling, which leads to higher operating cost. Biological treatment or activated sludge process is very attractive, as it requires an insignificant amount of chemicals or even any at all. For biological treatment, however, the space required for installing treatment facilities is quite large [29].

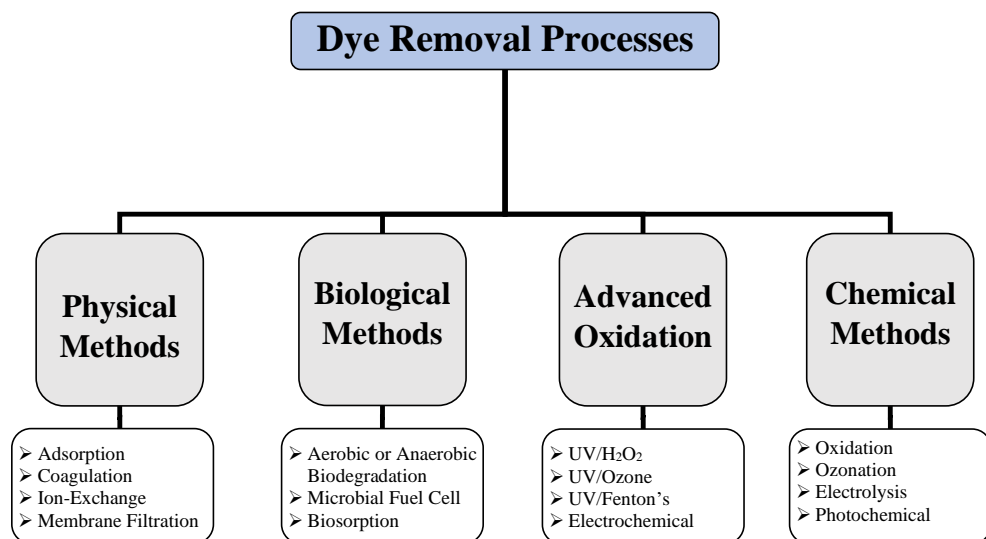


**Figure 2.** Decolorization processes applied to treat the dye-containing wastewater.

The biological treatment approach based on the anaerobic reduction of the azo dyes has gained more popularity because of their cost-effectiveness, environmental friendliness, and the fact that they create less hazardous and/or non-toxic substances. Because the aerobic conditions limit NADH usage, which hinders the electron transport from NADH to azo bonds [30]. On the contrary, anaerobic bacteria facilitated the electron transport from the bacterial cell to azo bonds, which act as an electron acceptor for this dye reduction system. Finally, the cleavage of bonds leads to the decolorization of azo dyes by forming colorless products. Furthermore, the intermediate products undergo the aerobic or anaerobic biodegradation treatment process to remove the dye from the wastewater. A recent study demonstrates that the use of mixed microbial consortiums in the anaerobic decolorization process is more efficient than the pure culture [31-33]. Over the last decades, several bioreactor configurations such as packed-bed [34], continuous flow stirred-tank [35], up-flow anaerobic sludge blanket [36] or membrane bioreactors [37] were tested. Almost in all experiments, the reduction of dye and color was quite significant, but the process was relatively slow.

## **2.2 Ceramic-supported Carbon-based Membrane Bioreactor**

Some of the conventional and advanced treatment procedures have already proved to be capable of removing these pollutants but still are not low-cost and efficient technologies. In such a case, specifically dedicated processes must be applied to their elimination. However, the bacterial azo reduction is enhanced by redox mediators, an interaction between the bacteria to the azo dyes [38]. Therefore, the coupling of anaerobic bioreactor and external carbon source has attracted increasing interest both academically and commercially because of the inherent advantages that the process offers over conventional biological wastewater treatment systems [39-41]. Activated

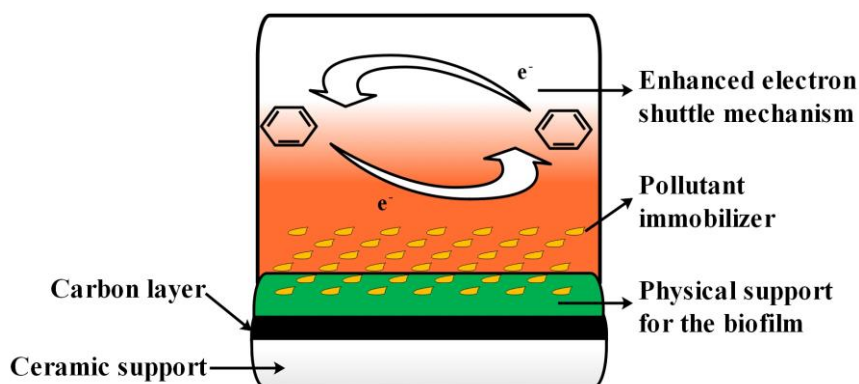
carbon and/or biologically activated carbon has been extensively tested for azo dye reduction and it seems very promising technology [9, 42, 43]. In order to avoid the over biomass production and clogging, carbon particles can be deposited onto ceramic or polymeric supports [44-47]. Moreover, these carbon particles sometimes help to reduce fouling problems.

It is possible to optimize and enhance the anaerobic azo dye reduction system by designing and fabricating novel ceramic-supported carbon membranes (CSCM) anaerobic bioreactors, which integrated the anaerobic biodegradation process with membrane filtration. In this process, a carbon layer is deposited over the ceramic supports (an ultrafiltration membrane). The carbon coating is usually composed of different selective carbon precursors such as polyacrylonitrile, polydopamine, carbon fiber, and polyimides. During the biodecolorization, a biofilm on top of CSCM is formed using the mixed anaerobic bacteria. Thus, the carbon layer acts as physical support for biofilm formation. In addition, the CSCM serves as a redox mediator to enhance the color removal rate [9, 47]. It is also worked as a pollutant immobilizer by adsorption mechanism (functioned as a selective barrier).

Moreover, this compact single unit can overcome some operational problems related to fouling and biomass retention. Therefore, it is expected that the ceramic-supported carbon membranes bioreactor will be capable of producing highly treated effluents without the need for subsequent purification steps. This new compact reactor concept will reduce operating costs and improve disposal performance, thus obtaining an effluent potentially free of contaminants and microorganisms.

### 3. Hypothesis and Objectives of the Thesis

One hypothesis of this thesis is the formation of a carbon layer over the ceramic supports (an ultrafiltration membrane) that facilitates the anaerobic decolorization of dye effluents. Figure 3 graphically depicts the triple benefit of a carbon layer during the dye removal process.



**Ceramic-supported carbon membrane**

**Figure 3.** Role of ceramic-supported carbon membrane in biodecolorization of azo dyes.

Following the previous assumption, the carbon layer's conductivity can increase by preparing it from different polymeric precursors. However, it should be noted that the carbon layer must maintain two criteria: the conduciveness of the carbon layer and the desired permeate flux through the membrane. A similar hypothesis is considered for both ceramic-supported flat and tubular membranes.

The effluent color is one of the most visible signs of water pollution. The main objective of this thesis (as shown in Figure 4) is to design, conduct and study the operation conditions of the carbon-based membrane bioreactor to decolorize the model dye solutions containing wastewater. Anaerobic

biodecolorization studies were carried out to determine the bioreactor's robustness and overall performance of several dyes to compare and identify the possible impact of their atomic mass, charge, shape, structure, and functional groups.

The following objectives have been accomplished in order to achieve the goal:

- Fabrication of flat ceramic-supported carbon membrane (CSCM) by the carbonization of Matrimid 5218 polyimide solution and implement the CSCM bioreactor for the decolorization of monoazo Acid Orange 7 (AO7), diazo Reactive Black 5 (RB5), and triazo Direct Blue 71 (DB71) dyes (Chapter 2).
- Evaluation of the novel ceramic-supported graphene oxide membrane (CSGOM) for use in anaerobic bioreduction of AO7, RB5, and DB71 (Chapter 3).
- Application of the CSCM and CSGOM bioreactors for the anaerobic decolorization of the other selected dyes such as Azo Dye Mixture (ADM), Methylene Blue (MB), Rhodamine Blue (RhB) (Chapter 4).
- Preparation of Tubular CSCM and CSGOM membranes and study the dye bioreduction of AO7, RB5, and DB71 (Chapter 5).
- Development of biofilm kinetic model of the biodecolorization process of the CSGOM bioreactor (Chapter 6).

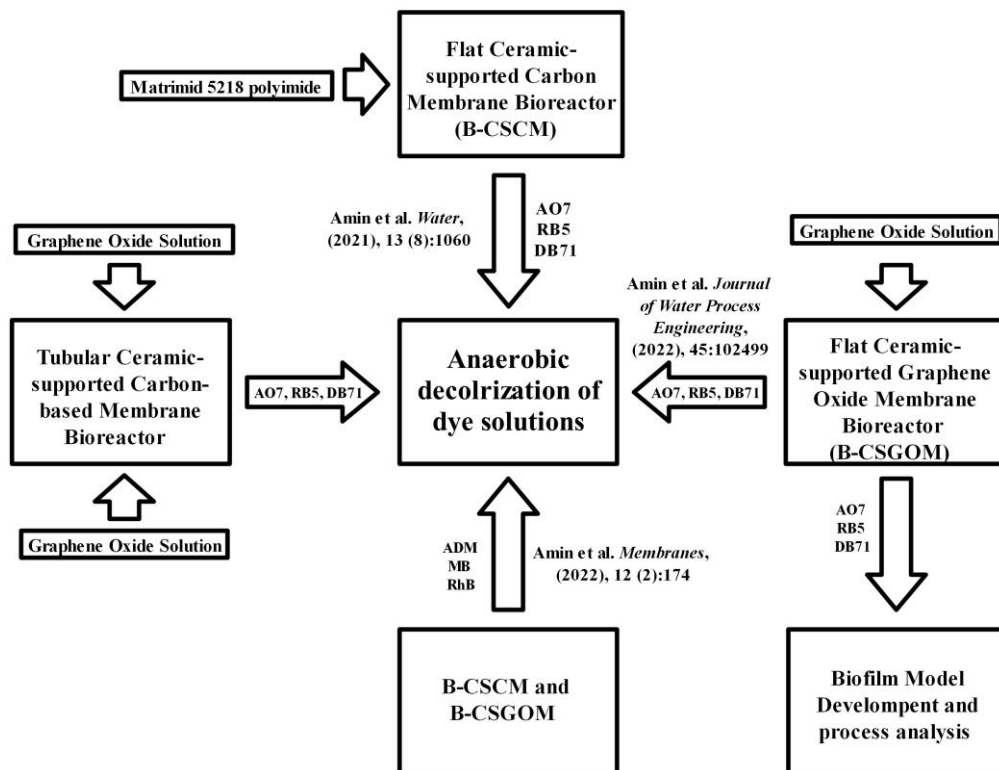


**Figure 4.** Summary of the experimental research work.

## 4. Thesis Outline

The research work is divided into seven chapters, which are summarized below:

- **Chapter 1** provides an overview of the work and its objectives.
- **Chapter 2** demonstrated the synthesis and use of B-CSCM in reducing the color of three structurally different azo dyes using CSCM bioreactors. This work has been published in the journal *Water*.
- **Chapter 3** discusses the synthesis of partly oxidized graphene and its subsequent use in fabricating graphene-based membranes to improve

its performance throughout various biological activities. In detail, the ceramic-supported graphene oxide membranes (BCSGOM) are prepared using exfoliated graphene oxide solution. This work has been published in the *Journal of Water Process Engineering*.

- **Chapter 4** reports the comparative color removal between the CSCM and CSGOM bioreactors. The model dye solutions are i) an equimolar mixture of AO7, RB5, and DB71 solutions, ii) Methylene Blue, and iii) Rhodamine Blue. This work has been published in the journal *Membranes*.
- **Chapter 5** presents the synthesis of tubular ceramic-supported carbon-based membrane using Matrimid 5218 and graphene oxide (GO) solution. The comparative decolorization analysis of several structurally different azo dye solution (AO7, RB5 and DB71) were studied using the TCSCM and TCSGOM bioreactors. The publication is in preparation.
- **Chapter 6** describes the modified biofilm kinetics model of the CSGOM bioreactors to optimize the process parameters and enhancing the biodecolorization of model azo dye solutions. The manuscript is under internal revision.
- **Chapter 7** summarizes the thesis's significant findings and makes recommendations for further research on the topic.

## References:

1. Nawaz, M. S., Gadelha, G., Khan, S. J., and Hankins, N., Microbial toxicity effects of reverse transported draw solute in the forward osmosis membrane bioreactor (FO-MBR). *Journal of Membrane Science*, 2013. 429, 323-329.
2. dos Santos, A. B., Cervantes, F. J., and van Lier, J. B., Review paper on current technologies for decolourisation of textile wastewaters: Perspectives for anaerobic biotechnology. *Bioresource Technology*, 2007. 98(12), 2369-2385.
3. Corso, C. R. and Maganha de Almeida, A. C., Bioremediation of dyes in textile effluents by *Aspergillus oryzae*. *Microb Ecol*, 2009. 57(2), 384-90.
4. Sakamoto, M., Ahmed, T., Begum, S., and Huq, H., Water Pollution and the Textile Industry in Bangladesh: Flawed Corporate Practices or Restrictive Opportunities? *Sustainability*, 2019. 11(7), 1951.
5. Benkhaya, S., M'Rabet, S., and El Harfi, A., Classifications, properties, recent synthesis and applications of azo dyes. *Heliyon*, 2020. 6(1), 03271.
6. Saratale, R. G., Saratale, G. D., Chang, J. S., and Govindwar, S. P., Bacterial decolorization and degradation of azo dyes: A review. *Journal of the Taiwan Institute of Chemical Engineers*, 2011. 42(1), 138-157.
7. Zheng, Z., Levin, R. E., Pinkham, J. L., and Shetty, K., Decolorization of polymeric dyes by a novel *Penicillium* isolate. *Process Biochemistry*, 1999. 34(1), 31-37.
8. Brás, R., Isabel A. Ferra, M., Pinheiro, H. M., and Gonçalves, I. C., Batch tests for assessing decolourisation of azo dyes by methanogenic and mixed cultures. *Journal of Biotechnology*, 2001. 89(2), 155-162.



9. Mezohegyi, G., Kolodkin, A., Castro, U. I., Bengoa, C., Stuber, F., Font, J., Fabregat, A., and Fortuny, A., Effective Anaerobic Decolorization of Azo Dye Acid Orange 7 in Continuous Upflow Packed-Bed Reactor Using Biological Activated Carbon System. *Industrial & Engineering Chemistry Research*, 2007. 46(21), 6788-92.
10. Poots, V. J. P., McKay, G., and Healy, J. J., Removal of Basic Dye from Effluent Using Wood as an Adsorbent. *Journal (Water Pollution Control Federation)*, 1978. 50(5), 926-935.
11. Rani, D. and Dahiya, R. P., COD and BOD removal from domestic wastewater generated in decentralised sectors. *Bioresource Technology*, 2008. 99(2), 344-349.
12. Beydilli, M. I., Pavlostathis, S. G., and Tincher, W. C., Biological Decolorization of the Azo Dye Reactive Red 2 under Various Oxidation-Reduction Conditions. *Water Environment Research*, 2000. 72(6), 698-705.
13. Manu, B., Physico-chemical treatment of indigo dye wastewater. *Coloration Technology*, 2007. 123(3), 197-202.
14. Karcher, S., Kornmüller, A., and Jekel, M., Anion exchange resins for removal of reactive dyes from textile wastewaters. *Water Research*, 2002. 36(19), 4717-4724.
15. Papić, S., Koprivanac, N., and Božić, A. L., Removal of reactive dyes from wastewater using Fe (III) coagulant. *Coloration Technology*, 2000. 116(11), 352-358.
16. Uddin, M. J., Islam, M. A., Haque, S. A., Hasan, S., Amin, M. S. A., and Rahman, M. M., Preparation of nanostructured TiO<sub>2</sub>-based photocatalyst by controlling the calcining temperature and pH. *International Nano Letters*, 2012. 2(1), 19.

17. Papić, S., Koprivanac, N., Božić, A. L., Vujević, D., Dragičević, S. K., Kušić, H., and Peternel, I., Advanced Oxidation Processes in Azo Dye Wastewater Treatment. *Water Environ. Res.*, 2006. 78(6), 572-579.
18. Koyuncu, İ. and Afşar, H., Decomposition of dyes in the textile wastewater with ozone. *Journal of Environmental Science and Health. Part A: Environmental Science and Engineering and Toxicology*, 1996. 31(5), 1035-1041.
19. Liakou, S., Kornaros, M., and Lyberatos, G., Pretreatment of azo dyes using ozone. *Water Science and Technology*, 1997. 36(2), 155-163.
20. Tzitzzi, M., Vayenas, D. V., and Lyberatos, G., Pretreatment of Textile Industry Wastewaters with Ozone. *Water Science and Technology*, 1994. 29(9), 151-160.
21. Xu, Y., Lebrun, R. E., Gallo, P.-J., and Blond, P., Treatment of Textile Dye Plant Effluent by Nanofiltration Membrane. *Separation Science and Technology*, 1999. 34(13), 2501-2519.
22. Slokar, Y. M. and Majcen Le Marechal, A., Methods of decoloration of textile wastewaters. *Dyes and Pigments*, 1998. 37(4), 335-356.
23. Hansson, H., Kaczala, F., Marques, M., and Hogland, W., Photo-Fenton and Fenton Oxidation of Recalcitrant Industrial Wastewater Using Nanoscale Zero-Valent Iron. *International Journal of Photoenergy*, 2012. 2012, 11.
24. Lau, Y.-Y., Wong, Y.-S., Teng, T.-T., Morad, N., Rafatullah, M., and Ong, S.-A., Coagulation-flocculation of azo dye Acid Orange 7 with green refined laterite soil. *Chemical Engineering Journal*, 2014. 246, 383-390.
25. Robinson, T., McMullan, G., Marchant, R., and Nigam, P., Remediation of dyes in textile effluent: a critical review on current treatment

- technologies with a proposed alternative. *Bioresource Technology*, 2001. 77(3), 247-255.
26. Galán, J., Rodríguez, A., Gómez, J. M., Allen, S. J., and Walker, G. M., Reactive dye adsorption onto a novel mesoporous carbon. *Chemical Engineering Journal*, 2013. 219, 62-68.
  27. Zhang, J., Wang, L., Zhang, G., Wang, Z., Xu, L., and Fan, Z., Influence of azo dye-TiO<sub>2</sub> interactions on the filtration performance in a hybrid photocatalysis/ultrafiltration process. *Journal of Colloid and Interface Science*, 2013. 389(1), 273-283.
  28. Buckley, C. A., *Membrane Technology for the Treatment of Dyehouse Effluents*. *Water Science and Technology*, 1992. 25(10), 203-209.
  29. Islam, M. A., Amin, M. S. A., and Hoinkis, J., Optimal design of an activated sludge plant: theoretical analysis. *Applied Water Science*, 2013. 3(2), 375-386.
  30. Chang, J.-S., Chou, C., and Chen, S.-Y., Decolorization of azo dyes with immobilized *Pseudomonas luteola*. *Process Biochemistry*, 2001. 36(8), 757-763.
  31. Kodam, K. M., Soojhawon, I., Lokhande, P. D., and Gawai, K. R., Microbial decolorization of reactive azo dyes under aerobic conditions. *World Journal of Microbiology and Biotechnology*, 2005. 21(3), 367-370.
  32. Khehra, M. S., Saini, H. S., Sharma, D. K., Chadha, B. S., and Chimni, S. S., Decolorization of various azo dyes by bacterial consortium. *Dyes and Pigments*, 2005. 67(1), 55-61.
  33. Yu, L., Zhang, X.-Y., Wang, S., Tang, Q.-W., Xie, T., Lei, N.-Y., Chen, Y.-L., Qiao, W.-C., Li, W.-W., and Lam, M. H.-W., Microbial community structure associated with treatment of azo dye in a start-up

- anaerobic sequenced batch reactor. *Journal of the Taiwan Institute of Chemical Engineers*, 2015. 54, 118-124.
34. Mielgo, I., Moreira, M. T., Feijoo, G., and Lema, J. M., A packed-bed fungal bioreactor for the continuous decolourisation of azo-dyes (Orange II). *Journal of Biotechnology*, 2001. 89(2), 99-106.
  35. Ong, S.-A., Toorisaka, E., Hirata, M., and Hano, T., Treatment of azo dye Orange II in aerobic and anaerobic-SBR systems. *Process Biochemistry*, 2005. 40(8), 2907-2914.
  36. Brás, R., Gomes, A., Ferra, M. I. A., Pinheiro, H. M., and Gonçalves, I. C., Monoazo and diazo dye decolourisation studies in a methanogenic UASB reactor. *Journal of Biotechnology*, 2005. 115(1), 57-66.
  37. Spagni, A., Casu, S., and Grilli, S., Decolourisation of textile wastewater in a submerged anaerobic membrane bioreactor. *Bioresource Technology*, 2012. 117, 180-185.
  38. Keck, A., Klein, J., Kudlich, M., Stolz, A., Knackmuss, H. J., and Mattes, R., Reduction of azo dyes by redox mediators originating in the naphthalenesulfonic acid degradation pathway of *Sphingomonas* sp. strain BN6. *Applied and environmental microbiology*, 1997. 63(9), 3684-3690.
  39. Rodríguez-reinoso, F., The role of carbon materials in heterogeneous catalysis. *Carbon*, 1998. 36(3), 159-175.
  40. Demirbas, A., Agricultural based activated carbons for the removal of dyes from aqueous solutions: A review. *Journal of Hazardous Materials*, 2009. 167(1), 1-9.
  41. Thines, R. K., Mubarak, N. M., Nizamuddin, S., Sahu, J. N., Abdullah, E. C., and Ganesan, P., Application potential of carbon nanomaterials in

- water and wastewater treatment: A review. *Journal of the Taiwan Institute of Chemical Engineers*, 2017. 72, 116-133.
42. Mezohegyi, G., Bengoa, C., Stuber, F., Font, J., Fabregat, A., and Fortuny, A., Novel bioreactor design for decolourisation of azo dye effluents. *Chemical Engineering Journal*, 2008. 143(1), 293-298.
43. Mezohegyi, G., Fabregat, A., Font, J., Bengoa, C., Stuber, F., and Fortuny, A., Advanced Bioreduction of Commercially Important Azo Dyes: Modeling and Correlation with Electrochemical Characteristics. *Industrial & Engineering Chemistry Research*, 2009. 48(15), 7054-7059.
44. Tian, J.-y., Chen, Z.-l., Nan, J., Liang, H., and Li, G.-b., Integrative membrane coagulation adsorption bioreactor (MCABR) for enhanced organic matter removal in drinking water treatment. *Journal of Membrane Science*, 2010. 352(1), 205-212.
45. Shkavro, Z. N., Kochkodan, V. M., Ognyanova, R., Budinova, T., and Goncharuk, V. V., Combined ultrafiltration-adsorption water purification of the cationic violet dye. *Journal of Water Chemistry and Technology*, 2010. 32(2), 101-106.
46. Yang, Y., Chen, R., and Xing, W., Integration of ceramic membrane microfiltration with powdered activated carbon for advanced treatment of oil-in-water emulsion. *Separation and Purification Technology*, 2011. 76(3), 373-377.
47. Chang, S., Waite, T. D., Ong, P. E. A., and Schaefer, A., Assessment of Trace Estrogenic Contaminants Removal by Coagulant Addition, Powdered Activated Carbon Adsorption and Powdered Activated Carbon/Microfiltration Processes. *Journal of Environmental Engineering*, 2004. 130(7), 736-742.

## Chapter 2. Comparative Anaerobic Decolorization of Azo Dyes by Carbon-based Membrane Bioreactor

### ABSTRACT

This study used a novel integrated technology of ceramic-supported carbon membrane (CSCM) to degrade azo dyes through an anaerobic mixed culture. The CSCM worked simultaneously as biofilm support, redox mediator, and nano-filter to enhance the dye decolorization efficiency. The decolorization of Acid Orange 7 (AO7) was initially investigated with and without microorganisms in both ceramic support (CS) and CSCM reactors. The CSCM bioreactor (B-CSCM), operated with microorganisms, gave a maximum decolorization of 98% using a CSCM evolved from 10% weight (wt.) of Matrimid 5218 solution. To know the influence of permeate flow, feed concentration, and dye structure on the decolorization process, different B-CSCMs for dye removal experiments were studied over monoazo AO7, diazo Reactive Black 5 (RB5), and triazo Direct Blue 71 (DB71). The highest color removal, operated with 50 mg·L<sup>-1</sup> feed solution and 0.05 L·m<sup>-2</sup>·h<sup>-1</sup> of permeate flux, was 98%, 82%, and 72%, respectively, for AO7, RB5, and DB71. By increasing these parameters to 100 mg·L<sup>-1</sup> and 0.10 L·m<sup>-2</sup>·h<sup>-1</sup>, the decolorization rate of dye solution still achieved 37% for AO7, 30% for RB5, and 26% for DB71. In addition, the system was run for weeks without apparent loss of activity. These findings make evident that the combined phenomena taking place in CSCM bioreactor result in an efficient, cost-effective, and eco-friendly azo dye decolorization method.



## 1. Introduction

Azo dyes represent the largest class of dyestuffs used in textile, paint, food, pharmaceuticals, and cosmetics industries in different stages. Every year, approximately a half-million tons of dyes are used worldwide, of which about 15% are later found in the effluent streams. This fact poses an enormous threat to the environment, especially due to water pollution [1]. The degraded product or byproduct of the dyes generated from this undesirable discharge poses an adverse effect on the water quality by increasing the color, toxicity, biochemical oxygen demand (BOD), and chemical oxygen demand (COD) [2]. This contaminated water obstructs sunlight transmission, which causes a severe problem for photosynthetic organisms [3]. Besides, wastewater also does significant genotoxic and carcinogenic damage to human health [4] in addition to aquatic life [5]. With the limited supply and rising demand for water for the agricultural and industrial sectors, the situation is getting out of hand [6]. Therefore, wastewater treatments need to be implemented for a safe and healthy aquatic environment by keeping contaminants within permissible limits [7, 8].

Generally, azo dyes in the aquatic environment behave as xenobiotic and recalcitrant compounds creating a massive barrier to potential treatment [9]. Several removals or decolorization methods based on physical, chemical, physicochemical, and biological processes were previously examined independently or in combination to resolve this problem and decolorize the azo dyes [10-13]. Photocatalytic degradation [14], Ozonation [15], Advanced Oxidation Processes [16], and a combined photocatalytic and electrochemical oxidation process [17] are among the most widely applied chemical methods used in recent years. For instance, Montanaro et al. [18] reported the efficient



coumarin degradation using UV-assisted electrochemical oxidation on boron doped diamond anodes. Yet the acceptable cost and the ineptness of a large-scale operation still make it incompatible for practical application. The ozonation process was shown to be an improved process to amend the biodegradability by reducing the color and COD [19, 20]. Although this process reduced the overall volume and sludge, it is quite expensive due to the high operating cost associated with the generation of ozone [21]. Electrochemical oxidation [22] and Fenton peroxidation [23] are the most used advanced oxidation processes, all of them efficiently able to decrease COD, color, and toxicity [24]. However, excess sludge formation later requires its disposal or secondary treatment. The same difficulty was also experienced with the coagulation-flocculation system [25, 26]. Conventional methods like activated carbon adsorption and filtration techniques were also extensively applied in the textile industry [27, 28]. The nature and solubility of the azo dyes in this treatment process increase the filtration resistance and cake filter that raise the operating cost [29, 30]. In comparison, a quite quick and convenient approach is membrane separation [31, 32]. This process is still limited due to membrane fouling and a high operating cost, in addition to its inherent non-destructive nature. Microorganism-assisted biological methods in aerobic or anaerobic environments are often appealing and effective systems to decolorize the azo dyes in wastewater [33].

Recently, more attention has been paid to the anaerobic decolorization of azo dyes for treating industrial wastewater [34]. Compared to the pure culture, the use of mixed microbial consortium in the anaerobic reactor shows efficient decolorization, as it is more capable of handling the heterogeneity of micropollutants in industrial effluents [24, 35]. Though the bioreduction of dye and subsequent color removal was quite significant, the

process is relatively slow. Using redox mediators, which improves the transfer of the electron from electron sources to dye molecules, considerable dye removal is achieved at a shorter residence time [36]. For example, flavin enzyme cofactors and quinone compounds as redox mediators have widely demonstrated a positive impact on the anaerobic dye decolorization system [37, 38]. Apart from these, carbonaceous materials act as a redox mediator and essential physical support for the microorganism to form a biofilm. Granular or powdered activated carbon was effectively examined in a variety of anaerobic decolorization methods such as MBR [39], packed-bed [40], up-flow anaerobic packed bed [41], continuous flow stirred-tank [42], up-flow anaerobic sludge blanket [43], and membrane bioreactors [44]. Some significant problems were noted due to over biomass production, pore blocking, and drag of microorganisms through the effluent stream. Further secondary treatment is needed to get rid of this, which again raises the treatment expenses.

The current work is aimed to establish a novel anaerobic azo dye decolorization method, taking into consideration all the above drawbacks and the benefit of activated carbon. The proposed methodology integrates membrane separation and bio-reduction processes by the inoculation or formation of anaerobic biofilm on top of ceramic-supported carbon membranes. This compact single unit reactor concept is able to generate highly treated effluents without needing additional purification steps. As a result, it presents a relatively low-cost treatment process with enhanced disposal performance. To accomplish this, the azo dye removal method was performed by coupling CSCM and an anaerobic bioreactor. The carbon-based membrane in the anaerobic bioreactor helps to form biofilm by retaining microorganisms on its surface. At the same time, the carbon layer

acts as a redox mediator to increase the decolorization rate [9, 45]. Moreover, it works as an additional filter medium for retaining dyes and degradation products by a molecular sieve mechanism. Overall, it is an applied example of process intensification principles by enhancing the dye removal through the promotion of a stable biofilm; the increase of the biodegradation rate and the retention of products allows deep biodegradation. This study examines these triple roles of carbon membrane on the anaerobic biodegradation of monoazo Acid Orange 7 (AO7), diazo Reactive Black 5 (RB5), and triazo Direct Blue 71 (DB71) dyes from synthetic wastewater under mixed microbial culture at constant flux. Additionally, the influence of some critical parameters, such as precursor concentration for carbon membrane synthesis, dye structure, feed flow rate, and inlet concentration in the B-CSCM, were assessed to enhance and optimize the decolorization process.

## 2. Materials and Methods

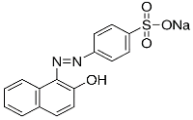
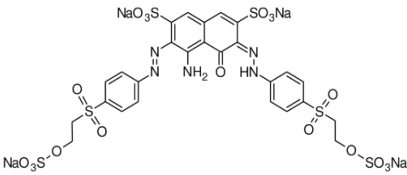
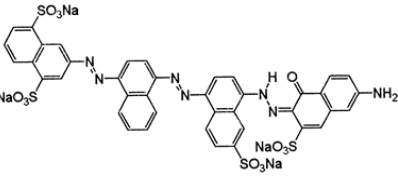
### 2.1 Materials

Matrimid 5218 (3,3',4,4'-benzophenonetetracarboxylic dianhydride and diamino-phenylindane, Huntsman Advanced Materials, Texas, USA), a commercial thermoplastic polyimide, was used as a carbon precursor, and NMP (1-methyl-2-pyrrolidone, Sigma Aldrich, ref. 328634, Spain) as precursor solvent for the synthesis of the carbon-based membrane.

AO7 (dye content  $\geq 85\%$ , ACROS Organics, ref. 416561000, Spain), RB5 (dye content  $\geq 50\%$ , Sigma Aldrich, ref. 306452, Spain), and DB71 (dye content  $\geq 50\%$ , Sigma Aldrich, ref. 212407, Spain) colorants were used for preparing synthetic wastewater. The type and complexity of the dye structures and their main properties are collected in Table 1. Sodium Acetate

(Sigma Aldrich, ref. 110191, Spain), a readily biodegradable co-substrate, was employed as a secondary carbon source for the microorganisms.

**Table 1.** Structure, composition, and properties of selected azo dyes.

Azo Dyes	Structure	Type	Solubility in Water
Acid Orange 7 $(C_{16}H_{11}N_2NaO_4S)$ MW: $350.3 \text{ g}\cdot\text{mol}^{-1}$ $\lambda_{\text{max}}$ : 484 nm		Monoazo CI: 15510	$116 \text{ g}\cdot\text{L}^{-1}$ (35 °C)
Reactive Black 5 $(C_{26}H_{21}N_5Na_4O_{19}S_6)$ MW: $991.8 \text{ g}\cdot\text{mol}^{-1}$ $\lambda_{\text{max}}$ : 587 nm		Diazo CI: 20505	$100 \text{ g}\cdot\text{L}^{-1}$ (30 °C)
Direct Blue 71 $(C_{40}H_{23}N_7Na_4O_{13}S_4)$ MW: $1029.9 \text{ g}\cdot\text{mol}^{-1}$ $\lambda_{\text{max}}$ : 585 nm		Triazo CI: 34140	$10 \text{ g}\cdot\text{L}^{-1}$ (60 °C)

The basal media [46] for growth of microorganisms was composed of the following compounds ( $\text{mg}\cdot\text{L}^{-1}$ ):  $\text{MnSO}_4\cdot\text{H}_2\text{O}$  (0.155),  $\text{CuSO}_4\cdot 5\text{H}_2\text{O}$  (0.285),  $\text{ZnSO}_4\cdot 7\text{H}_2\text{O}$  (0.46),  $\text{CoCl}_2\cdot 6\text{H}_2\text{O}$  (0.26),  $(\text{NH}_4)_6\text{Mo}_7\text{O}_{24}$  (0.285),  $\text{K}_2\text{HPO}_4$  (21.75),  $\text{Na}_2\text{HPO}_4\cdot 2\text{H}_2\text{O}$  (33.40),  $\text{KH}_2\text{PO}_4$  (8.50),  $\text{FeCl}_3\cdot 6\text{H}_2\text{O}$  (29.06),  $\text{CaCl}_2$  (13.48)  $\text{MgSO}_4\cdot 7\text{H}_2\text{O}$  (15.2),  $\text{NH}_4\text{Cl}$  (190.90). Each of the chemicals for preparing the nutrient solution was purchased from Sigma Aldrich (Spain) and used as received. Ultrapure water (Millipore Milli-Q system, Molsheim, France) was employed in the entire research work. Nitrogen gas (Linde, Spain) served to pressurize the feed tank and give the constant flux to operate

the biodegradation process and purge any oxygen to maintain anaerobic conditions.

Soil DNA Isolation Plus Kit (Norgen Biotek Corporation, ref. 64000, Ontario, Canada),  $\lambda$  DNA/HindIII Markers (New England Biolab Inc. ref. N3012S, Massachusetts, USA), Agarose (Sigma Aldrich, ref. 1.16801, Spain), TBE buffer (Sigma Aldrich, ref. 574796, Spain), and DNA Ladder (New England Biolab Inc. ref. N0552S, Massachusetts, USA) were used to detect microorganisms from biofilm samples.

## 2.2 Preparation of Ceramic-supported Carbon Membrane

The polymeric precursor solution was prepared by dispersing the desired amount of dry Matrimid (2, 5, and 10% wt.) in NMP under mild mechanical stirring for 12 h. The mixture was placed in ultrasonic baths to remove the tiny air bubbles from the polymeric solution. Finally, the carbon membrane was obtained by forming a homogeneous layer of Matrimid precursor on the surface of the ceramic support (diameter: 47 mm, thickness: 2.5 mm of thickness and molecular weight cut-off: 50 kg·mol<sup>-1</sup>; TAMI Industries, France). This thin polymer film was attained by a two-step spin coating method adopted from previous works [47, 48]. The initial ramp was run for 10 s at 500 rpm, followed by a final spin at 3000 rpm for 30 s. Ceramic support was then dried at 110 °C for 24 h to settle the coated film, and was subsequently washed with methanol and cured at 80-100 °C for 3 h to remove the traces of solvent impurities that may produce defected membranes. Afterward, the membrane was set into a horizontal tube furnace (Thermolyne F79440, Barnstead Thermolyne Corporation, Iowa, USA) for the pyrolysis process. The membrane was then subjected to stabilization and final carbonization steps at 300 °C and 800 °C, respectively. The

carbonization environment was preserved strictly within an inert atmosphere, at a nitrogen flow rate of  $500 \text{ mL}\cdot\text{min}^{-1}$ , to avoid the undesired burning off and chemical disruption on the membrane surface [49]. During this process, the heating ramp rate was set at  $1 \text{ }^\circ\text{C}\cdot\text{min}^{-1}$  above  $200 \text{ }^\circ\text{C}$  to prevent cracking. In the end, the carbon membranes were allowed to cool under room temperature.

### 2.3 Membrane Characterization

The morphology of CSCM and its chemical composition were recorded by Environmental Scanning Electron Microscopy (ESEM, FEI Quanta 600, Virginia, USA), coupled with energy dispersive X-ray Spectrometry (EDX, Oxford Instrument, UK). Topography and conductivity of the membrane surface were observed using Atomic Force Microscopy (AFM, Molecular Imaging Pico SPM II (Pico Plus), Bid Service, New Jersey, USA). The images were recorded at room temperature in tapping mode with a resonance frequency of 1 Hz in air and then processed by WSxM 5.0 software [50]. Pure water permeability of both ceramic support and ceramic-supported carbon membranes was examined by using a lab-scale filtration cell (TAMI disc holder with  $0.00131 \text{ m}^2$  of filtration area, TAMI Industries, France).

### 2.4 Microbial Analysis

Anaerobic biofilm created in CSCM bioreduction operation was examined separately by Transmission Electron Microscopy (TEM JEOL, JEM-1011, Massachusetts, USA) and by DNA isolation kits. Before testing, the carbon membrane was taken out from the reactor, washed with ultrapure water, and scratched a little bit hard to extract the microorganism from the membrane surface. In order to perform the DNA extraction, 1.5 mL of the

wet sludge sample was transferred to a 1.7 mL microcentrifuge tube. Then, samples went under a process to extract its DNA [51]. After extraction, the sample was run through Denaturing gradient gel electrophoresis (DGGE) gel electron and then to a Gel Documentation System (Bio-Rad Laboratories SA, Spain) to detect the presence of DNA. The final bacterial diversity studies were performed under variable regions (V3 and V4) of the prokaryotic 16S ribosomal RNA gene (16S rRNA). To obtain the results, the 16S rRNA gene was amplified using the primary pairs 341F-532R and 515F-806R. The Agilent 2100 Bioanalyzer (Agilent Technologies, California, USA) and its associated DNA 7500 Reagent kit (Agilent Technologies, California, USA) were used to assess the library quality, length, and concentration.

## 2.5 Experimental Set-up for Anaerobic Biodegradation

A scheme of the lab-scale CSCM bioreactor system is shown in Figure 1. The compact bioreactor consisted of a filtration cell holding the 47 mm diameter CSCM with a retentate chamber of 5 mL. The 200 mL feed solution was comprised of a 1:3 ratio of azo dye and sodium acetate and basal media with microelements described previously. The feed bottle was kept in a refrigerator (Selecta Group SA, Spain) at  $1 \pm 1$  °C to prevent the uncontrolled growth of microorganisms and thus to avoid the consumption of sodium acetate outside the bioreactor. Nitrogen gas was flowing into the feed tank to pressurize the system and control the flux through the membrane by manually setting the transmembrane pressure (TMP). Besides, sparging of nitrogen gas in the liquid phase at the feed tank served to maintain the negative redox potential as a measure of the anaerobic condition throughout the process needed to conduct the dye biodecolorization [52].

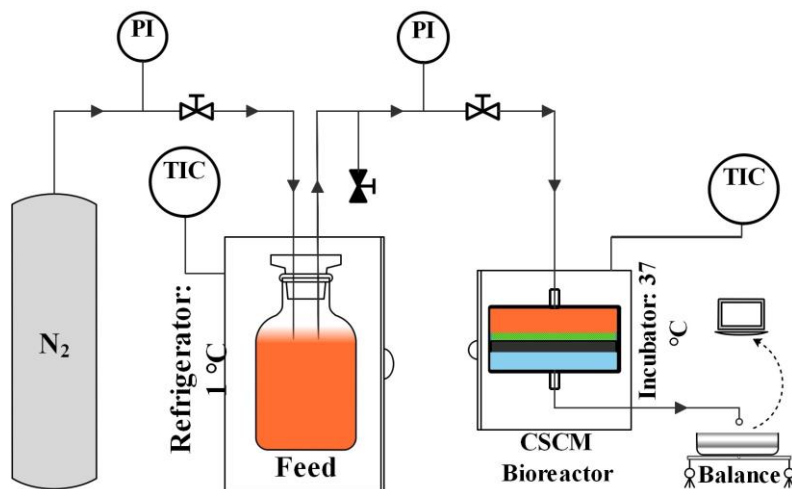


**Figure 1.** Ceramic-supported carbon membrane bioreactor experimental set-up.

The CSCM bioreactor was started by placing anaerobic sludge on the top of the membrane surface as a microbial seed. The anaerobic sludge source was the untreated aerobic secondary sludge from recirculation obtained from a municipal wastewater treatment plant (Reus, Spain). Initially, it was allowed for partial digestion under anaerobic conditions for a week. After that, the sludge was filtered through glass wool and then flowed into filter paper to get the single-cell or single-spore. The compact CSCM bioreactor was operated in anaerobic dead-end filtration mode at a temperature of  $37 \pm 1$  °C to enhance the efficiency of microbial strains capable of decolorizing azo dyes [24, 53]. At the beginning of each experiment, CSCM bioreactor flux was kept constant at  $0.05 \text{ L}\cdot\text{m}^{-2}\cdot\text{h}^{-1}$  and later changed to 0.075 and  $0.10 \text{ L}\cdot\text{m}^{-2}\cdot\text{h}^{-1}$  for further investigations.



## 2.6 Analytical Methods

The permeate flux was computed from the quotient of the permeate flow rate and active surface area of the membrane: Equation (1)

$$J = \frac{V}{t} \cdot \frac{1}{A} \quad (1)$$

where  $J$  is the permeate flux ( $\text{L m}^{-2} \text{h}^{-1}$ ),  $V$  the volume of permeate (L),  $t$  the filtration time (h), and  $A$  the membrane area ( $\text{m}^2$ ).

The resistance of CS and CSCM can be calculated by using Equation (2):

$$R = \frac{\Delta P}{\mu J} \quad (2)$$

where  $R$  is the resistance ( $\text{m}^{-1}$ ),  $\Delta P$  is the transmembrane pressure applied (Pa), and  $\mu$  is the viscosity of the permeate corrected to experimental temperature (Pa·s).

The decolorization achieved was measured spectrophotometrically, using UV/VIS4000n Spectrophotometers (DINKO Instruments, Spain), whereas the maximum absorption wavelength was fixed at 484 nm for AO7, 597 nm for RB5, and 585 nm for DB71. The decolorization percentage ( $D$ ) was calculated using Equation 3:

$$D (\%) = \frac{A_o - A}{A_o} \times 100 \quad (3)$$

$A_o$  and  $A$  are the absorbance of feed and treated samples during the biodegradation process, respectively.

### **3. Results and Discussions**

#### **3.1 Morphological Structure Analysis**

The ESEM images represent the morphology of the CS, and CSCM resulted from carbonization of 10% wt. polymeric precursor. The surface view and cross section of the CS and CSCM are shown in Figure 2 a-d. The CS was found to have three layers, with the smallest active porous layer at the top, an intermediate layer in the middle, and a porous supporting layer at the bottom. In CSCM, an extra 1.09  $\mu\text{m}$  porous carbon layer was observed besides these three layers (as shown in Figure 2d). Each carbon and supported layer, however, was not uniform and represented uneven thickness and level.

The surface view of CSCM shows that the coating was homogeneous and defect-free, as the comparison of Figures 2a,b evidences. It is obtained by maintaining the optimum coating processes and carbonization conditions [47, 54, 55]. The statistical distribution of pore size revealed that the pore size of CSCM was in several textures and grains. A rough analysis of the average pore sizes, based on SEM and AFM imaging, showed more than 80% of the total pores were found in the range 10-25 nm. Desired information from the SEM and AFM images were extracted by ImageJ and SPIP software. These results revealed that the formation of the carbon membrane modified the support pore size from 40 nm to less than 20 nm, which may nearly be classified into the nanoporous membrane family.

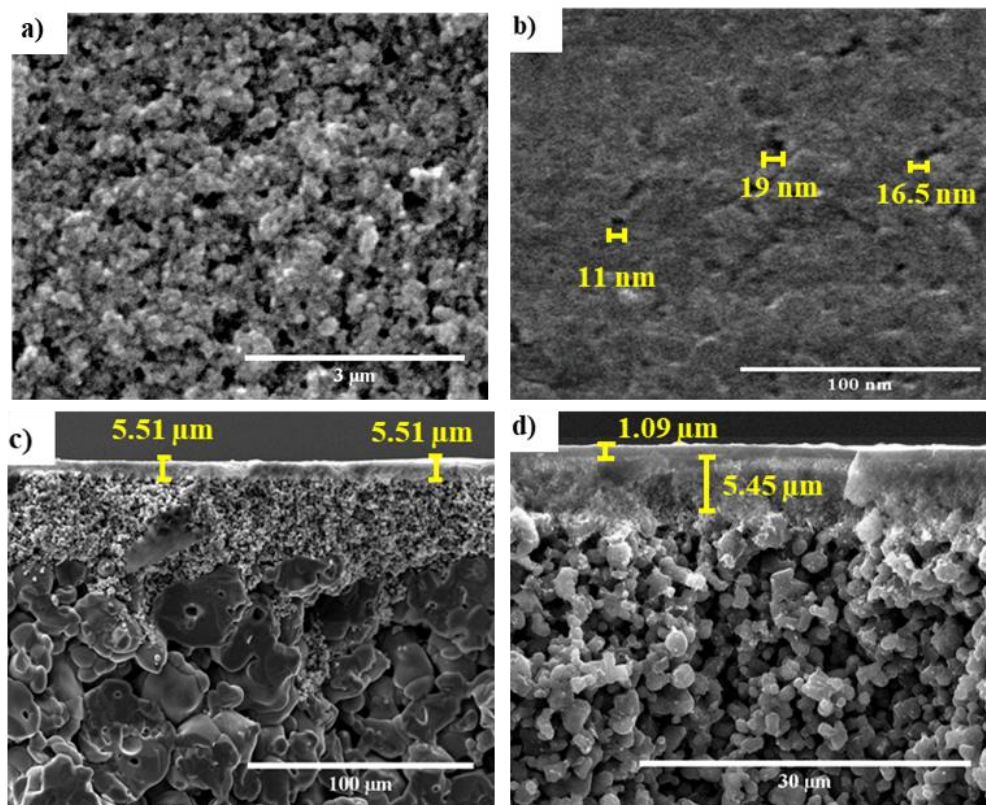


**Figure 2.** Scanning electron micrographs on the surface of (a, b) Ceramic support (CS) and 10% wt. CSCM, and (c, d) the cross section of CS and 10% wt. CSCM.

The elemental chemical composition of CS and CSCM was studied with ESEM-EDX inspection (Table 2). It confirmed that the CS was composed of  $\text{TiO}_2$  and  $\text{ZrO}_2$  layers. Whereas for CSCM, the analysis suggests a typical composite membrane that contains a carbon-rich layer on the top (9.8 to 65.6 wt.% of carbon, depending on precursor concentration), as carbon percentage increased with increasing precursor concentration.

**Table 2.** Environmental scanning electron microscopy-energy dispersive x-ray spectrometry analysis; composition (wt.%) of the CS and CSCM.

	C	O	Ti	Zr
CS	n.d.	44.0	52.2	3.8
CSCM (2% wt. of Matrimid)	9.8	25.9	2.6	61.7
CSCM (5% wt. of Matrimid)	34.5	19.1	1.2	45.2
CSCM (10% wt. of Matrimid)	65.6	3.1	0.6	30.7

Topographic and current sensing images of the carbon membranes were obtained with AFM (at a random area of  $1 \times 1 \mu\text{m}^2$ ) and current sensing atomic force microscopy (CSAFM), as shown in Figure 3a-c. Tapping mode AFM, which avoids the drag of tips across the sample surface [56], was employed in this experiment to achieve the high-resolution topographic images of the CSCM surface. AFM section images of Figure 3a showed that the CSCM surface was slightly rough and comparatively thin.

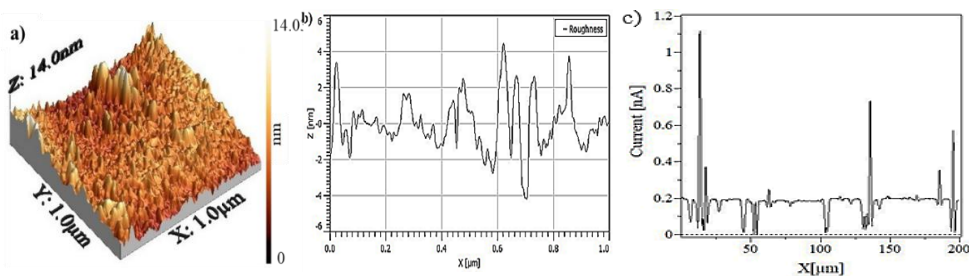


**Figure 3.** Atomic force microscopy images of CSCM (a) 3D topography, (b) roughness profile, and (c) current distribution.

The surface roughness deviation of the carbon membrane was measured, resulting in 1.10 nm and 1.48 nm in which the deviation was smaller. Despite that, the rough surfaces could have a beneficial impact on the bioreduction

application due to the more vigorous attachment of the biofilm to the surface [57]. CSAFM images (Figure 3c) provide a distribution that reflects the local conductance on the carbon-based membrane surfaces. It appeared that the CSCM surface was conductive, which could improve the biodegradation rate by the electron shuttle mechanism [36]. Though there is no clear correlation between the structures observed in the current image and topographical characteristics, it may be anticipated, as the topography corresponds to the morphological structures that rely on the membrane synthesis process.

### 3.2 Impact of the Carbon Layer on Flux and Resistance

The permeate flux and hydraulic resistance mostly govern the membrane filtration process. A comparative experiment was performed between the CS and CSCMs to assess these characteristics. Variation of the flux and resistance of CS and CSCMs (prepared by 2, 5, 10, 15 and 20% wt. of Matrimid solution) are presented in Figure 4a,b. Not surprisingly, CS exhibits higher flux,  $62.3 \text{ L}\cdot\text{m}^{-2}\cdot\text{h}^{-1}$ . In the case of CSCM, it gradually decreases with increasing precursor concentration, and the lowest flux ( $7.5 \text{ L}\cdot\text{m}^{-2}\cdot\text{h}^{-1}$ ) was obtained for the CSCM made of 15% wt. of Matrimid polyimide solution. In comparison to the ceramic support, it is observed that the pure water flux for 2% wt., 5% wt., 10% wt., and 15% wt. CSCM dropped 27%, 44%, 66%, and 88%, respectively. The pure water permeance (PWP) obtained from the slope of Figure 4a) also showed a similar pattern where the highest permeance ( $77.8 \text{ L}\cdot\text{m}^{-2}\cdot\text{h}^{-1}\cdot\text{bar}^{-1}$ ) was obtained for CS, and thereafter, the PWP of the 15% wt. CSCM decreased up to  $9.5 \text{ L}\cdot\text{m}^{-2}\cdot\text{h}^{-1}\cdot\text{bar}^{-1}$ .

As the permeate flux and hydraulic resistance depend on each other, an analogous hydraulic resistance feature was seen between the CS and CSCMs. The overall resistance of the support and carbon membranes are seen in the bar chart of Figure 4b, whereas the resistance of CS was assumed to be constant in CSCMs. In addition, the line graph represents the resistance due to the coated carbon layer on different CSCMs. It is observed that the ceramic support shows  $5.16 \pm 0.04 \times 10^{12} \text{ m}^{-1}$  of hydraulic resistance at different TMPs. In CSCM, the deposited carbon layer on the top of the ceramic support added more resistance than CS, which mainly depends on the polymer concentration used to prepare the carbon membrane.

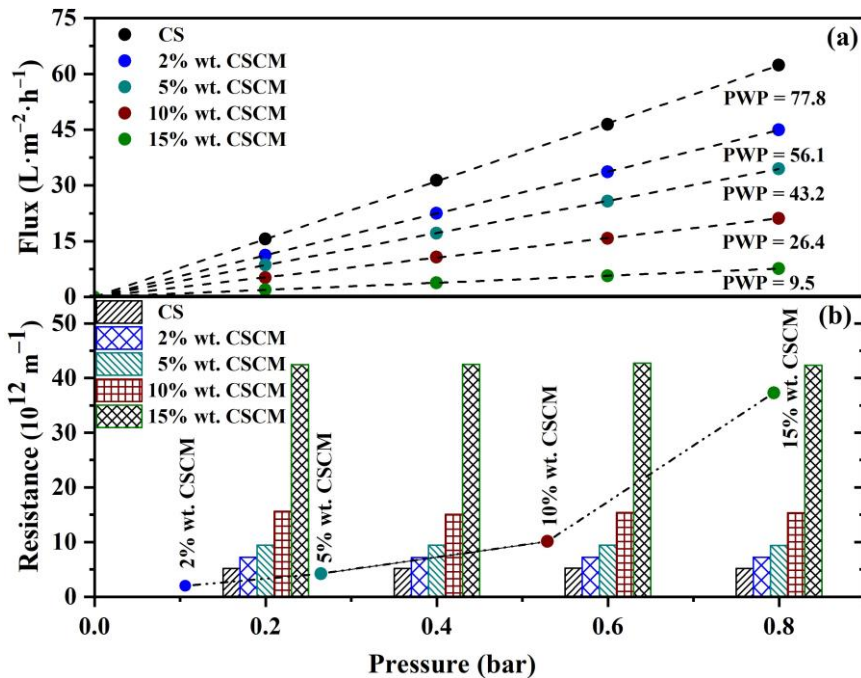


**Figure 4.** Variation of (a) pure water flux and (b) resistance of CS and CSCM at 25 °C. Overall resistance is displayed as a bar chart, and the line graph illustrates the resistance of the coated carbon layer. PWP in  $\text{L} \cdot \text{m}^{-2} \cdot \text{h}^{-1} \cdot \text{bar}^{-1}$ .

Nermen et al. [58] identified that the increase in precursor concentration increased the thickness of the membrane and decreased porosity, resulting in a decline in the permeability rate. Therefore, a higher initial concentration of polymer will facilitate lower hydraulic permeability and maximize the resistance of the resulting carbon membrane. Accordingly, the highest resistance was observed in flowed order: 15% wt. > 10% wt. > 5% wt. > 2% wt. CSCM. Moreover, the CSCM made of 20% wt. Matrimid solution was essentially non-porous, as no flux was obtained even at the highest TMP tested.

### **3.3 Role of the Carbon Layer on Anaerobic Biodegradation of Azo Dye**

The continuous experimental treatment was carried out under anaerobic conditions to promote the reduction of the model azo dye, AO7. The comparative decolorization of azo dye was studied between the ceramic support and ceramic-supported carbon membrane. In these experiments (as shown in Figure 5), reactors that use a mixed microbial consortium are referred to as B-CS and B-CSCM, while reactors that do not use it are referred to as R-CS and R-CSCM. The carbon-based membrane reactors were composed of 2% wt. Matrimid polyimide solution. Four compact reactors were operated at once over 50 mg·L<sup>-1</sup> AO7 feed solutions. During the ten consecutive days of operation, it is evident that the presence of a carbon layer was found to have a significant influence on the decolorization of AO7, as shown in Figure 5. Overall, it was observed that CSCM bioreactors (B-CSCM) performed a maximum decolorization rate.

For all reactors, above 85% decolorization was achieved within the first 12 h. The dye removal was initially driven by the preferential adsorption of dye molecules over the surface of materials showing this apparent high

removal. Over time, dye saturates all the solid materials, resulting in a sudden drop in dye removal performance. Following three days on stream, for R-CS, permeate and feed solution showed the same concentration, meaning that the membrane became saturated, so adsorption no longer occurred, and there was not bioreduction of the dye at all. Meanwhile, decolorization of R-CSCM reactors dropped from 80% to 10% in six days, and then the reduction was stable at 7%. This behavior is attributed to the nano-sized membrane pores developed in the carbon layer, in which this residual decolorization was controlled mainly by a sieving mechanism [59].

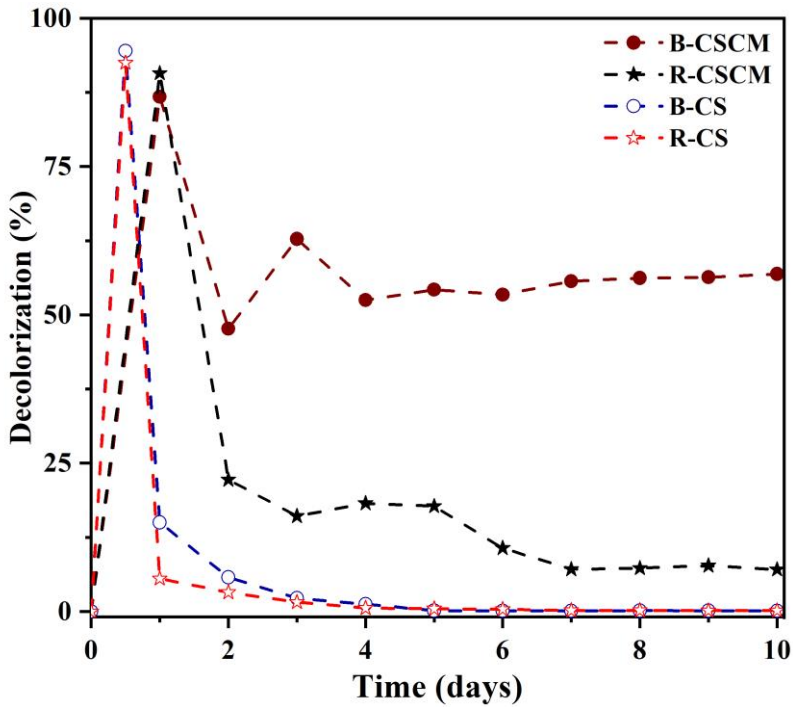


**Figure 5.** AO7 disappearance in CS and CSCM reactors; CS and CSCM bioreactor; Flux =  $0.05 \text{ L}\cdot\text{m}^{-2}\cdot\text{h}^{-1}$ ,  $[\text{AO7}] = 50 \text{ mg}\cdot\text{L}^{-1}$  and  $T = 37 \text{ }^\circ\text{C}$ . CSCM: 2% wt. polymeric precursor.



The most efficient and improved conversion, nearly 51%, was attained by the B-CSCM reactor. In B-CSCM, filtration and biodegradation simultaneously occur. The compact reactor took a minimum of two days to stabilize the system, which was faster than other studies in different systems [42, 60]. This fact clearly demonstrated that the deposited carbon layer plays a critical role as biofilm support, redox mediator [61], and filtration unit. The size of CSCM pores was much smaller than that of the microorganism so that they could not get into the pores to block them. As a result, biofilm and the degradation products were retained on the membrane surface, and microorganisms metabolized the substrate better [46]. In the absence of the carbon layer, it appears that B-CS was unsuccessful to perform efficiently. In this case, the microorganisms were probably unable to create a stable dense biofilm on the membrane surface, because the bacteria were washed out by the permeate flow due to their smaller size compared to the support pores. Thus, the novel one-step compact unit (B-CSCM) was able to combine dye and microorganism retention properly and promote both biofilm growth and electron transferability to furnish an effective dye removal process through anaerobic bioreduction.

At the end of the B-CSCM experiment, backflushing cleaning was used to check the recoverability of the membrane. Thus, the initial permeate flux was obtained without any apparent structural modification or loss due to bioreduction activity. Therefore, the system can be reused for weeks without mechanical or chemical damage.

### 3.4 Effect of Precursor Concentration on Azo Dye Decolorization

The anaerobic bioreduction of the model azo dye compound was investigated in three different B-CSCMs, which contained the carbon membrane made from 2% wt., 5% wt., and 10% wt. of Matrimid solution, respectively. For these B-CSCMs (as shown in Figure 6), the highest decolorization (98%) was observed for the CSCM prepared with a concentration of 10% wt. CSCM, whereas the lowest (51%) color removal was observed for 2% wt. CSCM.

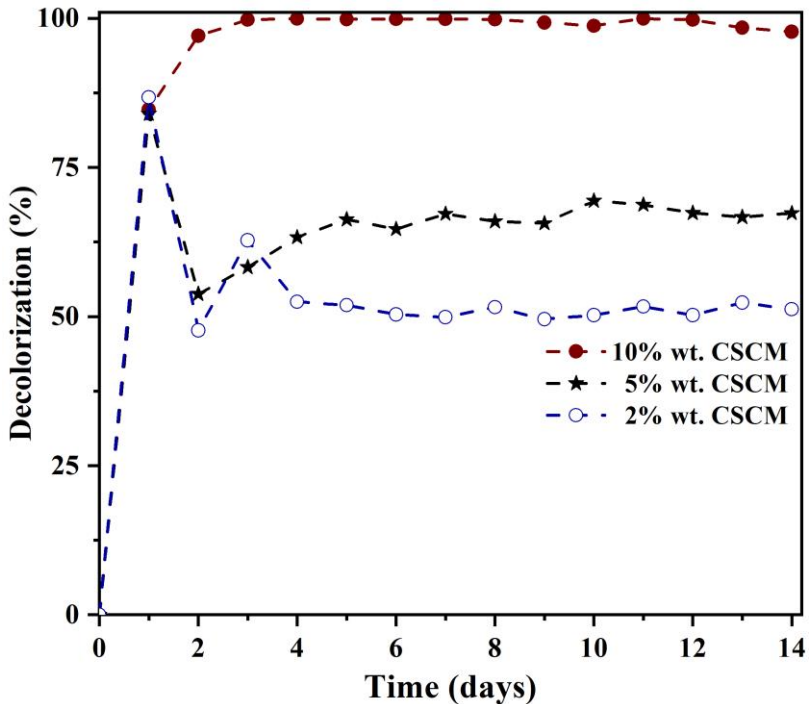


**Figure 6.** Influence of precursor concentration on anaerobic bioreduction of AO7; Flux =  $0.05 \text{ L} \cdot \text{m}^{-2} \cdot \text{h}^{-1}$ ,  $[\text{AO7}] = 50 \text{ mg} \cdot \text{L}^{-1}$  and  $T = 37 \text{ }^\circ\text{C}$

The results revealed that this 98% of decolorization was attained at a removal rate of  $49 \text{ g} \cdot \text{m}^{-3} \cdot \text{d}^{-1}$ . The various conventional, batch, continuous, and discontinuous biosystems, such as packed bed reactors (PBRs) or

sequential anaerobic-aerobic processes, operated with different initial dye concentrations and showed that high AO7 conversion (>90%) required a longer contact time (10-15 days) than B-CSCM [9, 46, 60, 62]. Using the mixed culture under batch condition, Brás et al. [63] reported AO7 decolorization of up to 90% after four days of operation. Similarly, Evangelista-Barreto et al. [64] (achieved 96-98% of color removal) and Bragger et al. (decolorized up to 95%) [65] also published identical decolorization results for pure culture.

Antonio et al. [66] investigated catalyst loading and discovered that increasing the catalyst load improves azo dye decolorization efficiency. Similarly, the above results proved that the decolorization efficiency was boosted by the amount of carbonaceous material deposited on the ceramic-supported membrane. The ESEM-EDX analysis (Table 2) confirms that the increasing precursor concentration raises the carbon content in the CSCM superficial layer. The high concentration of polymeric precursor mostly creates a membrane with a smaller pore size due to the slow evaporation of solvent [67]. This smaller pore-sized carbon-rich layer makes the CSCM easier to serve as an effective organic adsorbent and immobilization support. Besides, an increase in carbon content in the CSCMs enhanced their redox mediator capacity and, thus, their biodegradation activity.

The same evidence is illustrated in Figure 6, which raised the decolorization of AO7 as the precursor concentration of CSCM increased. For example, polymer content changes from 2% to 10% wt. had doubled decolorization effectiveness. Conversely, the extreme rise in precursor concentration decreased the pore size and permeability of the CSCM, which was not favorable for lack of flux in this compact treatment unit at reasonable

TMP pressure. Considering this fact, the CSCM that consisted of 15% and 20% wt. of Matrimid solution was not used in the process of bioreduction. Thereafter, 10% wt. of Matrimid precursor was chosen for all subsequent tests.

### **3.5 Effect of Flux and Feed Concentration on Azo Dye Decolorization**

A series of B-CSCMs were simultaneously operated to assess the impact of initial AO7 dye concentration and permeate flux on decolorization efficiency. Consequently, three B-CSCMs were run at feed concentrations of 50, 75, and 100 mg·L<sup>-1</sup>, respectively. Each reactor was started from the lowest flux (0.05 L·m<sup>-2</sup>·h<sup>-1</sup>), and when the steady operation was achieved, step by step, flux was first increased to 0.075 L·m<sup>-2</sup>·h<sup>-1</sup> and finally to 0.10 L·m<sup>-2</sup>·h<sup>-1</sup>. The permeate flux was set by varying the operating pressure. A small fluctuation was observed in the operating flux, and it was controlled by modifying the TMP; nonetheless, the decolorization rate was very stable. The decolorization efficiency depicted in Figure 7 illustrates that the maximum color removal was obtained at a low flux (0.05 L·m<sup>-2</sup>·h<sup>-1</sup>) and initial concentration (50 mg·L<sup>-1</sup>); as expected, it declined with higher permeate flux and feed concentration. In that low flux-region, the color removal was essentially complete, and no differences can be observed for the different feed concentrations. After that, for B-CSCMs operating with 100 mg·L<sup>-1</sup> of dye solutions, it was observed that the gradual reduction of decolorization was due to the rise of feed concentration and permeate flow. Results showed that efficiency of decolorization decreased to 60% at a flux of 0.075 L·m<sup>-2</sup>·h<sup>-1</sup>, and 36% for 0.10 L·m<sup>-2</sup>·h<sup>-1</sup>.

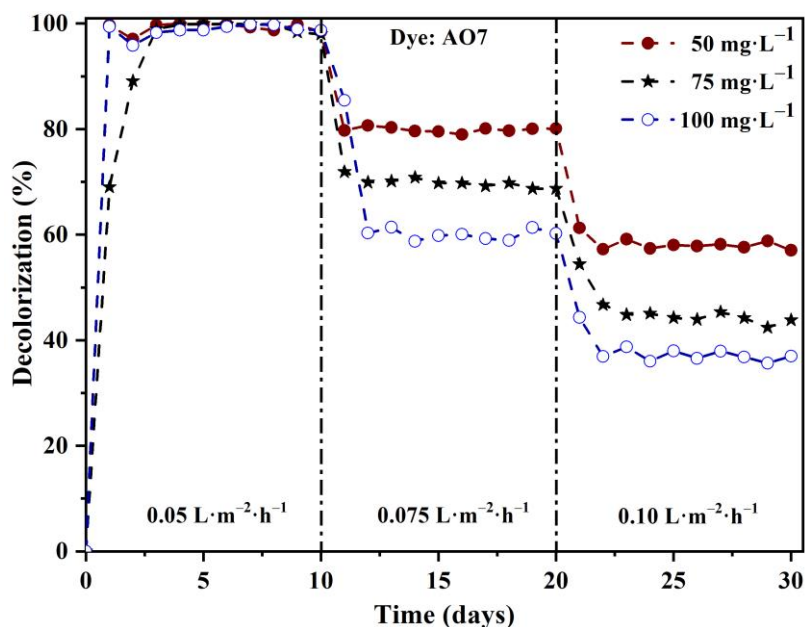


**Figure 7.** Decolorization of AO7 at different permeate flux and feed concentrations. CSCM: 10% wt. polymeric precursor.

As stated in Figure 7, at a flux of  $0.05 \text{ L}\cdot\text{m}^{-2}\cdot\text{h}^{-1}$ , dye biodegradation efficiency was almost identical for all concentrations of AO7 feed solutions within the first ten days of the experiments. In this interval, there was an average of 98% decolorization for all concentrated AO7 dye solutions (Figure 7). This result indicates that the amount of biomass was high enough to guarantee the total biodegradation of the dye. Even though the concentration was doubled from its initial point ( $50$  to  $100 \text{ mg}\cdot\text{L}^{-1}$ ), due to the large contact time at low flux [68], the increased dye concentration had no adverse impact on individual bacterial microbial population. At a flux of  $0.075 \text{ L}\cdot\text{m}^{-2}\cdot\text{h}^{-1}$ , the decolorization efficiency of B-CSCMs of  $50$ ,  $75$ , and  $100 \text{ mg}\cdot\text{L}^{-1}$  dye solution was decreased at  $80\%$ ,  $69\%$ , and  $60\%$ , respectively, as shown in Figure 7. Subsequently, their performance reduced to  $58\%$ ,  $45\%$ , and  $36\%$ , respectively, when the permeate flux was increased up to  $0.10$

$\text{L}\cdot\text{m}^{-2}\cdot\text{h}^{-1}$ . The obtained results were in line with previous findings reported by Meitiniarti et al. [69] and Ding et al. [70], where it was observed that the color removal rate declined from 98% to 58%, while the AO7 dye concentration increased to  $140\text{ mg}\cdot\text{L}^{-1}$ .

It should be noted that higher permeate flux or higher feed concentration at the reactor means higher dye load rate, which reduces the microorganism's tolerance [71]. Therefore, the decolorization ability was probably reduced because of the shortage of biomass in the biodegradation process [72]. Such a significant adverse pattern was observed in other systems for the decolorization of AO7 [73, 74]. One reason could be the presence of sulfonic acid ( $-\text{SO}_3\text{H}$ ) group in the azo dye structure, which significantly suppressed the microbial growth at higher dye concentrations [75]. Nonhydrolyzed organic matter and heavy metals may also inhibit bacterial growth and might be another cause for toxicity at higher concentrations.

### 3.6 Comparative Decolorization of Azo Dyes

A set of B-CSCMs was prepared to check the anaerobic bioreduction of structurally different azo dyes; in this case, azo dyes containing one azo bond, monoazo AO7; two azo bonds, diazo RB5 or three azo bonds, triazo DB71. Again, the effect of feed concentration and flux was explored. As shown in Figure 8a-c, the results of these experiments indicate that the decolorization rate of all azo dye solutions decreased with increasing dye concentration and permeate flux. The mono azo dye solution at a low flux ( $0.05\text{ L}\cdot\text{m}^{-2}\cdot\text{h}^{-1}$ ) showed the maximum color removal, 98%, in all operations.

Overall, the azo dye solutions exhibited different decolorization levels, mainly depending on the number of azo bonds. The structural differences,

such as the functional groups, number of azo bonds, morphology, and position of the benzene ring, have been reported to cause variations in decolorization rate [76, 77]. The decolorization is typically higher for simple low molecular weight azo dyes; on the contrary, the color removal becomes smaller for the complex large weight dye molecules. Therefore, irrespective of the initial dye concentration and permeate flux, monoazo dye decolorization was significantly higher than for diazo and triazo dyes. For instance, under different dye concentrations and fluxes, decolorization of AO7 ranged between 98% and 32%; additionally, RB5 and DB71 varied from 82% to 30% and from 70% to 26%, respectively. Thus, it was proved that the present method also successfully deals with complex azo dyes, and the decolorization trends were consistent with other previous research [78-80].

As for previous results, the color removal of such dyes for various concentrations tested decreased with increasing permeate flux and feed dye concentration. It was observed that with the gradual raise in permeate flux (0.05, 0.075, and 0.10 L·m<sup>-2</sup>·h<sup>-1</sup>) and feed dye concentrations (50, 75, and 100 mg·L<sup>-1</sup>), the rate of decolorization of RB5 and DB71 was consistently less than for AO7. At higher flux (0.10 L·m<sup>-2</sup>·h<sup>-1</sup>), the percentage of decolorization was lowered to 59%, 41%, and 32% for a 50 mg·L<sup>-1</sup> solution of AO7, RB5, and DB71, respectively. When the feed dye concentration increased up to 100 mg·L<sup>-1</sup>, the decolorization of dye solution was additionally reduced to 37% for AO7, 30% for RB5, and 26% for DB71. The reason for the reduction in removal rate was probably that the high concentration of dyes hindered biofilm growth, and later this adverse environment was responsible for some microbial death.

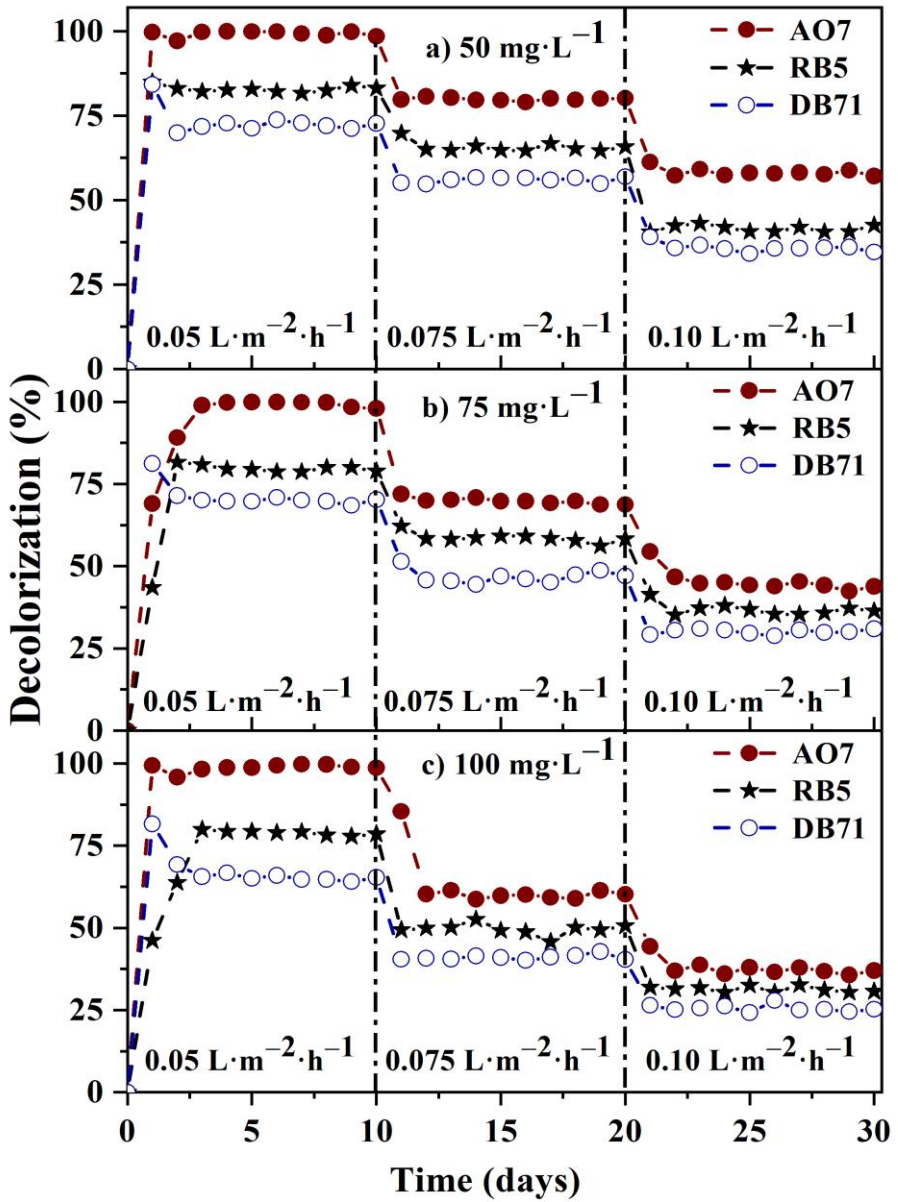


**Figure 8.** Decolorization of AO7, RB5, and DB71 dyes at different concentrations and fluxes; (a) 50 mg·L<sup>-1</sup>, (b) 75 mg·L<sup>-1</sup>, and (c) 100 mg·L<sup>-1</sup> dye solution at 37 °C. CSCM: 10% wt. polymeric precursor.



In any case, all B-CSCMs showed stable performance. The short contact time, i.e., high flux inhibits prolonged toxicity and dye deposition on biomass, makes the environment more favorable for microorganisms to outlive. This finding reflects those of Franciscon et al. [79], where the dyes with mono azo bonds were more likely to decolorize quicker than those with diazo or triazo groups. However, at a lower flux ( $0.05 \text{ L}\cdot\text{m}^{-2}\cdot\text{h}^{-1}$ ), the decolorization effect by the initial dye concentration was not observed very much. For instance, Figure 8a-c showed that, at this stage, around 98%, 80%, and 68% of decolorization was achieved for the various concentrations of AO7, RB5, and DB71, respectively. It is assumed that the dye decolorization response with higher contact time favors the well-built microbial growth and efficient biodegradation operation. Hence, there was a significant correlation between feed dye concentration and permeate flux, and an optimum value should be required to operate the decolorization process efficiently.

### 3.7 Microbial Community Analysis

After biodegradation of the AO7 dye, the bacterial cell morphology of biofilm that formed over the B-CSCM was evaluated by TEM analysis. At different magnifications, Figure 9 shows the presence of microorganisms on the biofilm sample. The microscopy images showed that most of the microorganisms could belong to the community of bacillus and vibrio bacteria. Some fungi may also be present as the inoculum was prepared from a mixed anaerobic microbial consortium obtained from a conventional wastewater treatment plant, where typically numerous groups of microorganisms exist.

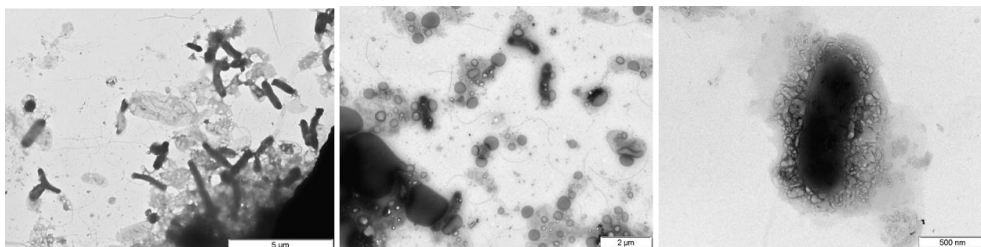


**Figure 9.** Transmission electron microscopy images of biofilm sample after biodegradation.

Afterward, the DNA of the biofilm sample was collected to confirm the existence of microorganisms. DGGE fingerprint patterns (Figure 10) indicate that active microbial colonies existed in the biofilm sample. This analysis, however, was insufficient to give more detailed information on microbial diversity.

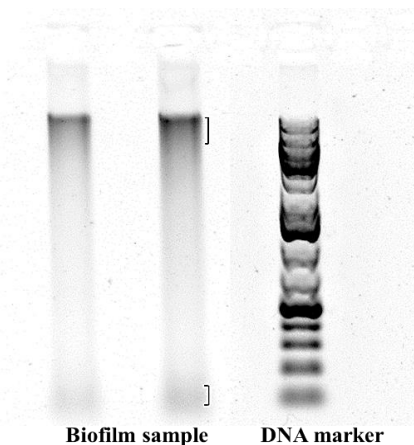


**Figure 10.** Denaturing gradient gel electrophoresis fingerprints of microbial communities of biofilm.

The taxonomical studies were performed by PCR amplifying to determine the microbial species and genus distribution of biofilm samples. In total, 357 bacterial operational taxonomic units (OTUs) and 43 fungal OTUs

were detected in the samples studied. The mixed anaerobic microbial culture used in this biodecolorization experiment was responsible for the existence of numerous bacterial and fungal species. Alpha diversity analysis assessed by the QIIME (V1.9.1) showed that the microbial richness (Chao1 Index: 1989.93 for bacterial and 41.19 for fungal species) and the diversity (Shannon Indices: 6.69 for bacterial and 1.91 for fungal species and Simpson indices: 0.925 for bacterial and 0.471 for fungal species) of bacteria were more dominant than the fungi.

As illustrated in Figure 11 a-b, bacterial analysis showed that the *Comamonadaceae* (39%) was the most prevalent bacterial community, followed by *AUTHM297* (13%), *Desulfovibrio* (4%), *Victivallaceae* (3%), *Ruminococcaceae* (3%), *Porphyromonadaceae* (2%), *Bacteroidales* (1.8%), *Clostridiales* (1.8%), *Mollicutes* (1.7%), *Treponema* (1.6%), and *Xanthomonadaceae* (1.4%). The largest phylum consisted of Proteobacteria (54%), followed by *Thermotogae* (13%), *Firmicutes* (9.2%), and *Bacteroidetes* (6.9%). Fungi phyla distribution revealed that 90% of OTUs were not matched with any fungal taxonomic category. The rest of the OTUs was prevalent by *Ascomycota* (9.3%), composed by the genus *Candida* (0.5%) and the genus *Pseudallescheria* (8.5%).

The role of *Proteobacteria* and *Firmicutes* during the degradation of dye solution by microbial communities was proven in several studies [81, 82]. Cui et al. [83] revealed that the bacterial community (rich in *Proteobacteria* and *Firmicutes*) present in anaerobic sludge efficiently decolorized the azo, anthraquinone, and triphenylmethane dyes. Under anaerobic or microaerobic conditions, *Firmicutes* bacteria promoted the ability of *Proteobacteria* to decolorate azo dyes [84]. What is more, other bacterial species such as

*Bacteroidetes* [85], *Desulfovibrio* [86], and *Clostridia* [87] were capable of decolorization of dye solutions. Separately, some of the fungal species were also known to be capable of decolorizing the textile azo dyes [88].

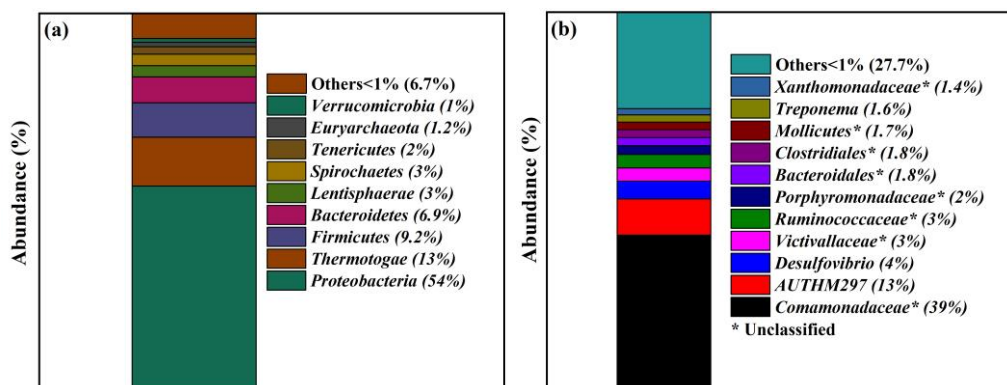


**Figure 11.** Microbial community in the mixed bacterial culture: (a) bacterial phyla and (b) bacterial genus distribution.

## 4. Conclusions

The concept of a compact one-step B-CSCM was implemented for the anaerobic decolorization of structurally different dyes, AO7, RB5, and DB71, without the need for subsequent purification steps.

Stable carbon-layers were synthesized with designed thickness, using Matrimid polymer precursor, over a commercial ceramic flat element. Long-term operation demonstrated a robust operation without apparent loss of chemical and mechanical properties.

The triple role of CSCM, such as attachment of microorganisms to grow biofilms, redox mediator for better electron transfer, and nano-filter to retain the dyes, demonstrated better efficiency and removal rate in B-CSCMs.

Stable performance of anaerobic biodegradation was achieved for all types of azo dyes and operation conditions. Comparatively, for any feed concentration and permeate flux, AO7 azo dye shows a higher decolorization rate. Diazo and triazo dyes seem to be more reluctant to biodecolorization.

For the maximum decolorization extent (98% for AO7, 80% for RB5 and 69% for DB71), it seems that an increase in dye concentration at low permeate flux ( $0.05 \text{ L}\cdot\text{m}^{-2}\cdot\text{h}^{-1}$ ) causes no limitation to the biodegradation process. In contrast, high permeate flux, that is, lower contact time, reduced the removal rate of any concentrated dye solution.

The metagenomics results and microbial activity tests indicate that the *proteobacteria* and *firmicutes* were mainly responsible for dye decolorization.

### **Acknowledgements:**

This project has been supported by the European Union's Horizon 2020 research and innovation programme under the Marie Skłodowska-Curie grant agreement No. 713679 and by the Universitat Rovira i Virgili (URV), contract 2017MFP-COFUND-18. Funding for this research was provided by Ministerio de Ciencia, Innovación y Universidades, the Agencia Estatal de Investigación (AEI) and the European Regional Development Fund (ERDF), project RTI2018-096467-B-I00. The authors research group is recognized by the Comissionat per a Universitats i Recerca, DIUE de la Generalitat de Catalunya (2017 SGR 396), and supported by the Universitat Rovira i Virgili (2019PFR-URV-33). We would like thank Dr. Constantí for her contribution to the bacterial community characterization.

**References:**

1. Shanker, U., Rani, M., and Jassal, V., Degradation of hazardous organic dyes in water by nanomaterials. *Environmental Chemistry Letters*, 2017. 15(4), 623-642.
2. Puvaneswari, N., Jayarama, M., and Gunasekaran, P., Toxicity assessment and microbial degradation of azo dyes. *Indian journal of experimental biology*, 2006. 44, 618-26.
3. dos Santos, A. B., Cervantes, F. J., and van Lier, J. B., Review paper on current technologies for decolourisation of textile wastewaters: Perspectives for anaerobic biotechnology. *Bioresource Technology*, 2007. 98(12), 2369-2385.
4. Alves de Lima, R. O., Bazo, A. P., Salvadori, D. M. F., Rech, C. M., de Palma Oliveira, D., and de Aragão Umbuzeiro, G., Mutagenic and carcinogenic potential of a textile azo dye processing plant effluent that impacts a drinking water source. *Mutation Research/Genetic Toxicology and Environmental Mutagenesis*, 2007. 626(1), 53-60.
5. Lellis, B., Fávoro-Polonio, C. Z., Pamphile, J. A., and Polonio, J. C., Effects of textile dyes on health and the environment and bioremediation potential of living organisms. *Biotechnology Research and Innovation*, 2019. 3(2), 275-290.
6. Nawaz, M. S., Gadelha, G., Khan, S. J., and Hankins, N., Microbial toxicity effects of reverse transported draw solute in the forward osmosis membrane bioreactor (FO-MBR). *Journal of Membrane Science*, 2013. 429, 323-329.
7. Poots, V. J. P., McKay, G., and Healy, J. J., Removal of Basic Dye from Effluent Using Wood as an Adsorbent. *Journal (Water Pollution Control Federation)*, 1978. 50(5), 926-935.

8. Rani, D. and Dahiya, R. P., COD and BOD removal from domestic wastewater generated in decentralised sectors. *Bioresource Technology*, 2008. 99(2), 344-349.
9. Mezohegyi, G., Kolodkin, A., Castro, U. I., Bengoa, C., Stuber, F., Font, J., Fabregat, A., and Fortuny, A., Effective Anaerobic Decolorization of Azo Dye Acid Orange 7 in Continuous Upflow Packed-Bed Reactor Using Biological Activated Carbon System. *Industrial & Engineering Chemistry Research*, 2007. 46(21), 6788-92.
10. Beydilli, M. I., Pavlostathis, S. G., and Tincher, W. C., Biological Decolorization of the Azo Dye Reactive Red 2 under Various Oxidation-Reduction Conditions. *Water Environment Research*, 2000. 72(6), 698-705.
11. Manu, B., Physico-chemical treatment of indigo dye wastewater. *Coloration Technology*, 2007. 123(3), 197-202.
12. Karcher, S., Kornmüller, A., and Jekel, M., Anion exchange resins for removal of reactive dyes from textile wastewaters. *Water Research*, 2002. 36(19), 4717-4724.
13. Papić, S., Koprivanac, N., and Božić, A. L., Removal of reactive dyes from wastewater using Fe (III) coagulant. *Coloration Technology*, 2000. 116(11), 352-358.
14. Uddin, M. J., Islam, M. A., Haque, S. A., Hasan, S., Amin, M. S. A., and Rahman, M. M., Preparation of nanostructured TiO<sub>2</sub>-based photocatalyst by controlling the calcining temperature and pH. *International Nano Letters*, 2012. 2(1), 1-10.
15. Koyuncu, İ. and Afşar, H., Decomposition of dyes in the textile wastewater with ozone. *Journal of Environmental Science and Health*.

- Part A: Environmental Science and Engineering and Toxicology, 1996. 31(5), 1035-1041.
16. Papić, S., Koprivanac, N., Božić, A. L., Vujević, D., Dragičević, S. K., Kušić, H., and Peternel, I., Advanced Oxidation Processes in Azo Dye Wastewater Treatment. *Water Environment Research*, 2006. 78(6), 572-579.
  17. Ennouri, R., Lavecchia, R., Zuurro, A., Elaoud, S. C., and Petrucci, E., Degradation of chloramphenicol in water by oxidation on a boron-doped diamond electrode under UV irradiation. *Journal of Water Process Engineering*, 2021. 41, 101995.
  18. Montanaro, D., Lavecchia, R., Petrucci, E., and Zuurro, A., UV-assisted electrochemical degradation of coumarin on boron-doped diamond electrodes. *Chemical Engineering Journal*, 2017. 323, 512-519.
  19. Liakou, S., Kornaros, M., and Lyberatos, G., Pretreatment of azo dyes using ozone. *Water Science and Technology*, 1997. 36(2), 155-163.
  20. Tzitzis, M., Vayenas, D. V., and Lyberatos, G., Pretreatment of Textile Industry Wastewaters with Ozone. *Water Science and Technology*, 1994. 29(9), 151-160.
  21. Xu, Y., Lebrun, R. E., Gallo, P.-J., and Blond, P., Treatment of Textile Dye Plant Effluent by Nanofiltration Membrane. *Separation Science and Technology*, 1999. 34(13), 2501-2519.
  22. Ghanbarlou, H., Pedersen, N. L., Simonsen, M. E., and Muff, J., Nitrogen-Doped Graphene Iron-Based Particle Electrode Outperforms Activated Carbon in Three-Dimensional Electrochemical Water Treatment Systems. *Water*, 2020. 12(11), 3121.
  23. Hansson, H., Kaczala, F., Marques, M., and Hogland, W., Photo-Fenton and Fenton Oxidation of Recalcitrant Industrial Wastewater Using



- Nanoscale Zero-Valent Iron. *International Journal of Photoenergy*, 2012. 2012, 11.
24. Khehra, M. S., Saini, H. S., Sharma, D. K., Chadha, B. S., and Chimni, S. S., Decolorization of various azo dyes by bacterial consortium. *Dyes and Pigments*, 2005. 67(1), 55-61.
  25. Lau, Y.-Y., Wong, Y.-S., Teng, T.-T., Morad, N., Rafatullah, M., and Ong, S.-A., Coagulation-flocculation of azo dye Acid Orange 7 with green refined laterite soil. *Chemical Engineering Journal*, 2014. 246, 383-390.
  26. Islam, M. A., Amin, M. S. A., and Hoinkis, J., Optimal design of an activated sludge plant: theoretical analysis. *Applied Water Science*, 2013. 3(2), 375-386.
  27. Robinson, T., McMullan, G., Marchant, R., and Nigam, P., Remediation of dyes in textile effluent: a critical review on current treatment technologies with a proposed alternative. *Bioresource Technology*, 2001. 77(3), 247-255.
  28. Galán, J., Rodríguez, A., Gómez, J. M., Allen, S. J., and Walker, G. M., Reactive dye adsorption onto a novel mesoporous carbon. *Chemical Engineering Journal*, 2013. 219, 62-68.
  29. Zhang, J., Wang, L., Zhang, G., Wang, Z., Xu, L., and Fan, Z., Influence of azo dye-TiO<sub>2</sub> interactions on the filtration performance in a hybrid photocatalysis/ultrafiltration process. *Journal of Colloid and Interface Science*, 2013. 389(1), 273-283.
  30. Wanyonyi, W. C., Onyari, J. M., Shiundu, P. M., and Mulaa, F. J., Effective biotransformation of Reactive Black 5 Dye Using Crude Protease from *Bacillus Cereus* Strain KM201428. *Energy Procedia*, 2019. 157, 815-824.

31. Buckley, C. A., Membrane Technology for the Treatment of Dyehouse Effluents. *Water Science and Technology*, 1992. 25(10), 203-209.
32. Żyła, R., Ledakowicz, S., Boruta, T., Olak-Kucharczyk, M., Foszpańczyk, M., Mrozińska, Z., and Balcerzak, J., Removal of Tetracycline Oxidation Products in the Nanofiltration Process. *Water*, 2021. 13(4), 555.
33. Gupta, V. K., Khamparia, S., Tyagi, I., Jaspal, D., and Malviya, A., Decolorization of Mixture of Dyes: A Critical Review. *Global Journal of Environmental Science and Management*, 2015. 1(1), 71-94.
34. Mubashar, M., Naveed, M., Mustafa, A., Ashraf, S., Shehzad Baig, K., Alamri, S., Siddiqui, M. H., Zabochnicka-Świątek, M., Szota, M., and Kalaji, H. M., Experimental Investigation of *Chlorella vulgaris* and *Enterobacter* sp. MN17 for Decolorization and Removal of Heavy Metals from Textile Wastewater. *Water*, 2020. 12(11), 3034.
35. Yu, L., Zhang, X.-Y., Wang, S., Tang, Q.-W., Xie, T., Lei, N.-Y., Chen, Y.-L., Qiao, W.-C., Li, W.-W., and Lam, M. H.-W., Microbial community structure associated with treatment of azo dye in a start-up anaerobic sequenced batch reactor. *Journal of the Taiwan Institute of Chemical Engineers*, 2015. 54, 118-124.
36. Keck, A., Klein, J., Kudlich, M., Stolz, A., Knackmuss, H. J., and Mattes, R., Reduction of azo dyes by redox mediators originating in the naphthalenesulfonic acid degradation pathway of *Sphingomonas* sp. strain BN6. *Applied and environmental microbiology*, 1997. 63(9), 3684-3690.
37. Saratale, R. G., Saratale, G. D., Chang, J. S., and Govindwar, S. P., Bacterial decolorization and degradation of azo dyes: A review. *Journal of the Taiwan Institute of Chemical Engineers*, 2011. 42(1), 138-157.

38. Cervantes, F., van der Zee, F., Lettinga, G., and Field, J., Enhanced decolorisation of Acid Orange 7 in a continuous UASB reactor with quinones as redox mediators. *Water science and technology: a journal of the International Association on Water Pollution Research*, 2001. 44, 123-128.
39. Asif, M. B., Ren, B., Li, C., Maqbool, T., Zhang, X., and Zhang, Z., Powdered activated carbon – Membrane bioreactor (PAC-MBR): Impacts of high PAC concentration on micropollutant removal and microbial communities. *Science of The Total Environment*, 2020. 745, 141090.
40. Mielgo, I., Moreira, M. T., Feijoo, G., and Lema, J. M., A packed-bed fungal bioreactor for the continuous decolourisation of azo-dyes (Orange II). *Journal of Biotechnology*, 2001. 89(2), 99-106.
41. Mezohegyi, G., Bengoa, C., Stuber, F., Font, J., Fabregat, A., and Fortuny, A., Novel bioreactor design for decolourisation of azo dye effluents. *Chemical Engineering Journal*, 2008. 143(1), 293-298.
42. Ong, S.-A., Toorisaka, E., Hirata, M., and Hano, T., Treatment of azo dye Orange II in aerobic and anaerobic-SBR systems. *Process Biochemistry*, 2005. 40(8), 2907-2914.
43. Brás, R., Gomes, A., Ferra, M. I. A., Pinheiro, H. M., and Gonçalves, I. C., Monoazo and diazo dye decolourisation studies in a methanogenic UASB reactor. *Journal of Biotechnology*, 2005. 115(1), 57-66.
44. Spagni, A., Casu, S., and Grilli, S., Decolourisation of textile wastewater in a submerged anaerobic membrane bioreactor. *Bioresource Technology*, 2012. 117, 180-185.
45. Chang, S., Waite, T. D., Ong, P. E. A., and Schaefer, A., Assessment of Trace Estrogenic Contaminants Removal by Coagulant Addition,

- Powdered Activated Carbon Adsorption and Powdered Activated Carbon/Microfiltration Processes. *Journal of Environmental Engineering*, 2004. 130(7), 736-742.
46. García-Martínez, Y., Bengoa, C., Stüber, F., Fortuny, A., Font, J., and Fabregat, A., Biodegradation of acid orange 7 in an anaerobic–aerobic sequential treatment system. *Chemical Engineering and Processing - Process Intensification*, 2015. 94, 99-104.
  47. Sazali, N., Salleh, W. N. W., Nordin, N. A. H. M., and Ismail, A. F., Matrimid-based carbon tubular membrane: Effect of carbonization environment. *Journal of Industrial and Engineering Chemistry*, 2015. 32, 167-171.
  48. Fuertes, A. B., Nevskaia, D. M., and Centeno, T. A., Carbon composite membranes from Matrimid® and Kapton® polyimides for gas separation. *Microporous and Mesoporous Materials*, 1999. 33(1), 115-125.
  49. Kiyono, M., Williams, P. J., and Koros, W. J., Effect of pyrolysis atmosphere on separation performance of carbon molecular sieve membranes. *Journal of Membrane Science*, 2010. 359(1), 2-10.
  50. Horcas, I., Fernández, R., Gómez-Rodríguez, J. M., Colchero, J., Gómez-Herrero, J., and Baro, A. M., WSXM: A software for scanning probe microscopy and a tool for nanotechnology. *Review of Scientific Instruments*, 2007. 78(1), 013705.
  51. NorgenBiotek. Soil DNA Isolation Kit. 2016. [cited 2020; Available from: <https://norgenbiotek.com/sites/default/files/resources/Soil-DNA-Isolation-Plus-Kit-Insert-PI64000-1.pdf>]
  52. Lourenço, N. D., Novais, J. M., and Pinheiro, H. M., Effect of some operational parameters on textile dye biodegradation in a sequential batch reactor. *Journal of Biotechnology*, 2001. 89(2), 163-174.

53. El Bouraie, M. and El Din, W. S., Biodegradation of Reactive Black 5 by *Aeromonas hydrophila* strain isolated from dye-contaminated textile wastewater. *Sustainable Environment Research*, 2016. 26(5), 209-216.
54. Ismail, N. H., Salleh, W. N. W., Sazali, N., and Ismail, A. F., Effect of intermediate layer on gas separation performance of disk supported carbon membrane. *Separation Science and Technology*, 2017. 52(13), 2137-2149.
55. Barsema, J. N., Klijnstra, S. D., Balster, J. H., van der Vegt, N. F. A., Koops, G. H., and Wessling, M., Intermediate polymer to carbon gas separation membranes based on Matrimid PI. *Journal of Membrane Science*, 2004. 238(1), 93-102.
56. Boussu, K., Van der Bruggen, B., Volodin, A., Snauwaert, J., Van Haesendonck, C., and Vandecasteele, C., Roughness and hydrophobicity studies of nanofiltration membranes using different modes of AFM. *Journal of Colloid and Interface Science*, 2005. 286(2), 632-638.
57. Shimp, R. J. and Pfaender, F. K., Effects of surface area and flow rate on marine bacterial growth in activated carbon columns. *Applied and environmental microbiology*, 1982. 44(2), 471-477.
58. Maximous, N., Nakhla, G., Wan, W., and Wong, K., Preparation, characterization and performance of Al<sub>2</sub>O<sub>3</sub>/PES membrane for wastewater filtration. *Journal of Membrane Science*, 2009. 341(1), 67-75.
59. Abid, M. F., Zablouk, M. A., and Abid-Alameer, A. M., Experimental study of dye removal from industrial wastewater by membrane technologies of reverse osmosis and nanofiltration. *Iranian Journal of Environmental Health Science & Engineering*, 2012. 9(1), 1-9.

60. Méndez-Paz, D., Omil, F., and Lema, J. M., Anaerobic treatment of azo dye Acid Orange 7 under batch conditions. *Enzyme and Microbial Technology*, 2005. 36(2), 264-272.
61. Mezohegyi, G., van der Zee, F. P., Font, J., Fortuny, A., and Fabregat, A., Towards advanced aqueous dye removal processes: A short review on the versatile role of activated carbon. *Journal of Environmental Management*, 2012. 102, 148-164.
62. Manu, B. and Chaudhari, S., Anaerobic decolorisation of simulated textile wastewater containing azo dyes. *Bioresource Technology*, 2002. 82(3), 225-231.
63. Brás, R., Isabel A. Ferra, M., Pinheiro, H. M., and Gonçalves, I. C., Batch tests for assessing decolourisation of azo dyes by methanogenic and mixed cultures. *Journal of Biotechnology*, 2001. 89(2), 155-162.
64. Evangelista-Barreto, N. S., Albuquerque, C. D., Vieira, R. H. S. F., and Campos-Takaki, G. M., Cometabolic Decolorization of the Reactive Azo Dye Orange II by *Geobacillus stearothermophilus* UCP 986. *Textile Research Journal*, 2009. 79(14), 1266-1273.
65. Bragger, J. L., Lloyd, A. W., Soozandehfar, S. H., Bloomfield, S. F., Marriott, C., and Martin, G. P., Investigations into the azo reducing activity of a common colonic microorganism. *International Journal of Pharmaceutics*, 1997. 157(1), 61-71.
66. Zuorro, A., Lavecchia, R., Monaco, M. M., Iervolino, G., and Vaiano, V., Photocatalytic Degradation of Azo Dye Reactive Violet 5 on Fe-Doped Titania Catalysts under Visible Light Irradiation. *Catalysts*, 2019. 9(8), 645.
67. Tan, X. and Rodrigue, D., A Review on Porous Polymeric Membrane Preparation. Part II: Production Techniques with Polyethylene,

- Polydimethylsiloxane, Polypropylene, Polyimide, and Polytetrafluoroethylene. *Polymers*, 2019. 11(8), 1310.
68. Rahimi, M., Aghel, B., Sadeghi, M., and Ahmadi, M., Using Y-shaped microreactor for continuous decolorization of an Azo dye. *Desalination and Water Treatment*, 2014. 52(28-30), 5513-5519.
69. Meitiniarti, I., Soetarto, E. S., Sugiharto, E., and Timotius, K., Optimum concentration of glucose and Orange II for growth and decolorization of Orange II by *Enterococcus faecalis* ID6017 under static culture. *Microb Indones*, 2008. 2, 73-78.
70. Ding, J., Zhang, Y., Quan, X., and Chen, S., Anaerobic biodecolorization of AO7 by a newly isolated Fe (III)-reducing bacterium *Sphingomonas* strain DJ. *Journal of Chemical Technology & Biotechnology*, 2015. 90(1), 158-165.
71. Chen, B.-Y., Chen, S.-Y., and Chang, J.-S., Immobilized cell fixed-bed bioreactor for wastewater decolorization. *Process Biochemistry*, 2005. 40(11), 3434-3440.
72. Popli, S. and Patel, U. D., Destruction of azo dyes by anaerobic-aerobic sequential biological treatment: a review. *International Journal of Environmental Science and Technology*, 2015. 12(1), 405-420.
73. Mutambanengwe, C. C. Z., Togo, C. A., and Whiteley, C. G., Decolorization and Degradation of Textile Dyes with Biosulfidogenic Hydrogenases. *Biotechnology Progress*, 2007. 23(5), 1095-1100.
74. Kiriakidou, F., Kondarides, D. I., and Verykios, X. E., The effect of operational parameters and TiO<sub>2</sub>-doping on the photocatalytic degradation of azo-dyes. *Catalysis Today*, 1999. 54(1), 119-130.

75. Chen, B.-Y., Understanding decolorization characteristics of reactive azo dyes by *Pseudomonas luteola*: toxicity and kinetics. *Process Biochemistry*, 2002. 38(3), 437-446.
76. Khan, R., Bhawana, P., and Fulekar, M. H., Microbial decolorization and degradation of synthetic dyes: a review. *Reviews in Environmental Science and Bio/Technology*, 2013. 12(1), 75-97.
77. Solís, M., Solís, A., Pérez, H. I., Manjarrez, N., and Flores, M., Microbial decolouration of azo dyes: A review. *Process Biochemistry*, 2012. 47(12), 1723-1748.
78. Chen, K.-C., Wu, J.-Y., Liou, D.-J., and Hwang, S.-C. J., Decolorization of the textile dyes by newly isolated bacterial strains. *Journal of Biotechnology*, 2003. 101(1), 57-68.
79. Franciscon, E., Zille, A., Fantinatti-Garboggini, F., Silva, I. S., Cavaco-Paulo, A., and Durrant, L. R., Microaerophilic–aerobic sequential decolourization/biodegradation of textile azo dyes by a facultative *Klebsiella* sp. strain VN-31. *Process Biochemistry*, 2009. 44(4), 446-452.
80. Garcia-Segura, S., Centellas, F., Arias, C., Garrido, J. A., Rodríguez, R. M., Cabot, P. L., and Brillas, E., Comparative decolorization of monoazo, diazo and triazo dyes by electro-Fenton process. *Electrochimica Acta*, 2011. 58, 303-311.
81. Chen, Y., Zhang, L., Feng, L., Chen, G., Wang, Y., Zhai, Z., and Zhang, Q., Exploration of the key functional strains from an azo dye degradation microbial community by DGGE and high-throughput sequencing technology. *Environmental Science and Pollution Research*, 2019. 26(24), 24658-24671.



82. Köchling, T., Ferraz, A. D. N., Florencio, L., Kato, M. T., and Gavazza, S., 454-Pyrosequencing analysis of highly adapted azo dye-degrading microbial communities in a two-stage anaerobic-aerobic bioreactor treating textile effluent. *Environmental Technology*, 2017. 38(6), 687-693.
83. Cui, D., Zhang, H., He, R., and Zhao, M., The Comparative Study on the Rapid Decolorization of Azo, Anthraquinone and Triphenylmethane Dyes by Anaerobic Sludge. *International journal of environmental research and public health*, 2016. 13(11), 1053.
84. Balapure, K. H., Jain, K., Chattaraj, S., Bhatt, N. S., and Madamwar, D., Co-metabolic degradation of diazo dye-Reactive blue 160 by enriched mixed cultures BDN. *Journal of Hazardous Materials*, 2014. 279, 85-95.
85. Zhang, L., Sun, Y., Guo, D., Wu, Z., and Jiang, D., Molecular diversity of bacterial community of dye wastewater in an anaerobic sequencing batch reactor. *African journal of microbiology research*, 2012. 6, 6444-6453.
86. Yoo, E., Libra, J., and Adrian, L., Mechanism of Dye Reduction of Azo Dyes in Anaerobic Mixed Culture. *Journal of Environmental Engineering-ASCE*, 2001. 127, 844-849.
87. Fernando, E., Keshavarz, T., and Kyazze, G., Simultaneous co-metabolic decolourisation of azo dye mixtures and bio-electricity generation under thermophillic (50°C) and saline conditions by an adapted anaerobic mixed culture in microbial fuel cells. *Bioresource Technology*, 2013. 127, 1-8.
88. Prigione, V., Grosso, I., Tigini, V., Anastasi, A., and Varese, G. C., Fungal Waste-Biomasses as Potential Low-Cost Biosorbents for Decolorization of Textile Wastewaters. *Water*, 2012. 4(4), 770-784.

## Chapter 3. Ceramic-supported Graphene Oxide Membrane Bioreactor for the Anaerobic Decolorization of Azo Dyes

### ABSTRACT

A continuous compact membrane bioreactor consisted of ceramic-supported graphene oxide membrane (CSGOM) was implemented for the first time for anaerobic biodecolorization of monoazo Acid Orange 7 (AO7), diazo Reactive Black 5 (RB5), and triazo Direct Blue 71 (DB71) solutions, showing excellent decolorization potential. The membrane was prepared by vacuum filtration of various graphene oxide solutions using a UF ceramic flat element. The decolorization efficiency of the CSGOM bioreactor, made from 1 mg·mL<sup>-1</sup> of GO solution (B-CSGOM-1), was investigated for several structurally distinct azo dyes, initial feed concentrations, and permeate fluxes. Maximum color removal was achieved under low feed concentration (50 mg·L<sup>-1</sup>) and permeate flux (0.05 L·m<sup>-2</sup>·h<sup>-1</sup>), reaching 99% for AO7, 96% RB5, and 92% for DB71. At this low permeate flux, the biodecolorization was stable for all azo dye solutions irrespective of the feed concentration. In a subsequent experiment under higher feed concentration and permeate flux (100 mg·L<sup>-1</sup> and 0.10 L·m<sup>-2</sup>·h<sup>-1</sup>), the decolorization slightly fell to 93%, 85%, and 81% for monoazo, diazo, and triazo solutions, respectively. The existence of anaerobic bacteria (*Geobacter* and *Pseudomonas Guangdongensis*) in the B-CSGOM-1 biofilm confirms that they could perform efficient biodegradation of azo dye molecules in association with the graphene oxide membrane.

---

Amin, M. S. A., Stüber, F., Giralt, J., Fortuny, A., Fabregat, A., and Font, J., Ceramic-supported graphene oxide membrane bioreactor for the anaerobic decolorization of azo dyes. *Journal of Water Process Engineering*, 2022. 45, 102499. DOI: 10.1016/j.jwpe.2021.102499 (JIF = 5.485, 9/98 in Water Resources)



## 1. Introduction

Global water pollution occurred in all sources, including canals, lakes, rivers, oceans, and underground reservoirs. It usually happened when unwanted substances, from either humankind or environment, mix with water. Industrial effluents are the primary source of contaminant substances for water pollution. For instance, every year, 0.28 million tons of textile dyes are discharged in the aquatic environment as industrial waste [1]. About half of the textile dyes belong to the azo dye group, which is also extensively used in leather, medical, food, and personal care products [2, 3]. The disposal of this untreated dyestuff poses a severe threat to the aquatic ecosystem as well as biodiversity [4]. It changes the natural appearance of the water becoming a dark, opaque, and colored liquid hindering the photosynthesis process due to the deficient transmission of sunlight in such water [5]. The dye effluents and their decomposed products are mostly detrimental, even at a very low concentration. This contaminated water, if used for drinking, household, or agricultural purposes, may cause toxicity, mutagenicity, and carcinogenicity on the human body [6]. Therefore, efficient wastewater treatment is highly required to maintain and control water pollution in this situation.

Several methods for treating dye-containing wastewater have been investigated, including physicochemical (adsorption, coagulation-flocculation, filtration, ion-exchange), biological, photocatalysis by UV irradiation, advanced oxidation processes, and combined process [7, 8]. Still, these treatment processes have faced some disadvantages, including addition of enormous amounts of chemicals, installation and operating costs, space requirements, secondary treatments, and poor process efficiency [9, 10]. On the other hand, membrane-based separation processes have attracted tremendous attention in the wastewater treatment over the few decades due to

its easy operation, low operating cost and energy consumption, small carbon footprint, and environmental suitability [11-13]. Besides, other eco-friendly, efficient dye removal processes are those based on biological mechanisms. Among the various biological methods, anaerobic treatments are very simple, less expensive azo dye removal processes [14]. This also produces less potentially dangerous substances, which eliminates the need to treat subsequently the biodegradable byproducts [7, 15]. However, no single process for removing azo dyes from textile effluent is efficiently and economically viable yet [16]. Therefore, the advantages of both anaerobic pathway and membrane separation process can be coupled in a single compact reactor as a successful technique for the intensified biodecolorization of azo dye. The key for implementing effectively this alternative is the selection of membrane precursors that can successfully be coupled with the anaerobic process.

In this sense, nowadays, graphene oxide (GO) is considered a prospective precursor for the synthesis of membranes because of its unique two-dimensional structure that consisted of the functional polar oxidized zone and pristine graphite zone [17]. The water molecules accumulate inside the interlayers of the oxidized region, and the other zone increases the liquid permeation [18]. Besides, the nanoporous GO membrane imparts surface functionality, electrical conductivity, and mechanical stability, making it possible to produce a low-cost membrane for a large-scale operation such as wastewater treatment and molecular separation [19]. Pure GO (single or multilayer graphene) and GO composite (GO surface-modified, stacked graphene, graphene mixed-matrix) membrane are reported to be fabricated by filtration-assisted, casting, spin coating, and layer by layer assembly method [20]. Vacuum-assisted filtration is most commonly used to obtain either free-

standing or supported GO membranes of all preparation techniques. In recent years, GO and GO-composite membranes have demonstrated the ability to retain azo dyes [17, 21]. Still, it is under consideration to further improve the GO membrane durability, longevity, and water permeability without losing decolorization performance. So, it is important to obtain a compact treatment process with stable, robust, and high azo dye removal potential.

A nano-sized ceramic-supported carbon membrane (CSCM) was synthesized in our earlier work [22]. This form of the membrane was capable of decolorizing structurally different azo dyes. However, the effectiveness of the decolorization was limited at higher permeate flux and feed concentration, while it is an essential matter to attain the maximum decolorization performance for practical application. Taking this into account, this work is aimed at finding a robust and durable compact anaerobic membrane bioreactor for a better biodecolorization rate. The novelty of this study lies on the application of conductive graphene oxide membrane in combination with the anaerobic biofilm process for the successful removal of azo dye from dye-containing wastewater. It is worth that anaerobic bacteria such as *Geobacter* and *Pseudomonas* can perform extracellular electron transfer in an aqueous solution. As a result of the use of microorganisms and GO membrane, both the bacteria and the GO layer provide faster and more efficient electron transfer for azo dye bond (-N=N-) breaking, thus enhancing the decolorization performance under anaerobic conditions. Additionally, the nano-sized ceramic-supported graphene oxide membrane (CSGOM) acts as biofilm support and pollutant immobilizer to improve the azo dye removal rate. The optimum concentration of the GO solution for the preparation of CSGOM and its decolorization performance by anaerobic biodegradation were examined. Ceramic-supported graphene oxide membrane bioreactor (B-

CSGOM) was first implemented for the monoazo Acid Orange 7 (AO7) decolorization process. Afterward, variations of critical parameters for B-CSGOM performance, for example, azo dye with different structures, molecular weight and functional groups, initial feed concentration, and permeate flux, were explored to enhance and optimize the bioreduction of azo dyes. Finally, the biofilm was examined to identify microbial species involved in this anaerobic process in order to understand and, subsequently, improve the biodecolorization by means of CSGOM.

## 2. Experimental

### 2.1 Fabrication of Ceramic-supported GO Membrane (CSGOM)

Vacuum-assisted deposition of the synthesized graphene oxide layer over the ceramic support ( $ZrO_2$ - $TiO_2$  ultrafiltration flat membrane; diameter: 47 mm; thickness: 2.5 mm; molecular weight cut-off: 50  $kg \cdot mol^{-1}$ ; TAMI Industries, France) was used to prepare the CSGOM membrane. Firstly, a modified Hummer method [23] was employed to obtain the graphene oxide powder. A homogeneous mixture of 2.5 g of graphite powder ( $<20 \mu m$ , Sigma Aldrich, ref. 282863) and 2 g of  $NaNO_3$  (Honeywell Fluka™, ref. 15603430) was made in 70 mL of  $H_2SO_4$  (Honeywell Fluka™ 95-98%, ref. 32051) solution. The mixture was then placed in an ice bath and mixed with 10 g of  $KMnO_4$  (PanReac AppliChem, ref. 141527), and followed by stirring overnight at 50 °C. Thereafter, 10 g of  $KMnO_4$  and 70 mL of Milli-Q water (Millipore Milli-Q system, Molsheim, France) were added and stirred for 24 h. The mixture was transferred into a beaker containing 400 mL of ice water, and 3 mL of  $H_2O_2$  (Acros Organics, ref. 411880025) were added and kept stirred at room temperature. The graphite oxide solution was purified by a 500 mL solution of 0.5 wt.%  $H_2O_2$  and 3 wt.%  $H_2SO_4$ . The graphite oxide

pellet was centrifuged at 3000 rpm and the supernatant discarded. After repeating it five times, the solid was exfoliated in water in a sonication bath for 2 h to obtain graphene oxide. The GO pellets were dried for 48 h at 60 °C and then grounded using mortar and pestle to obtain the GO powder.

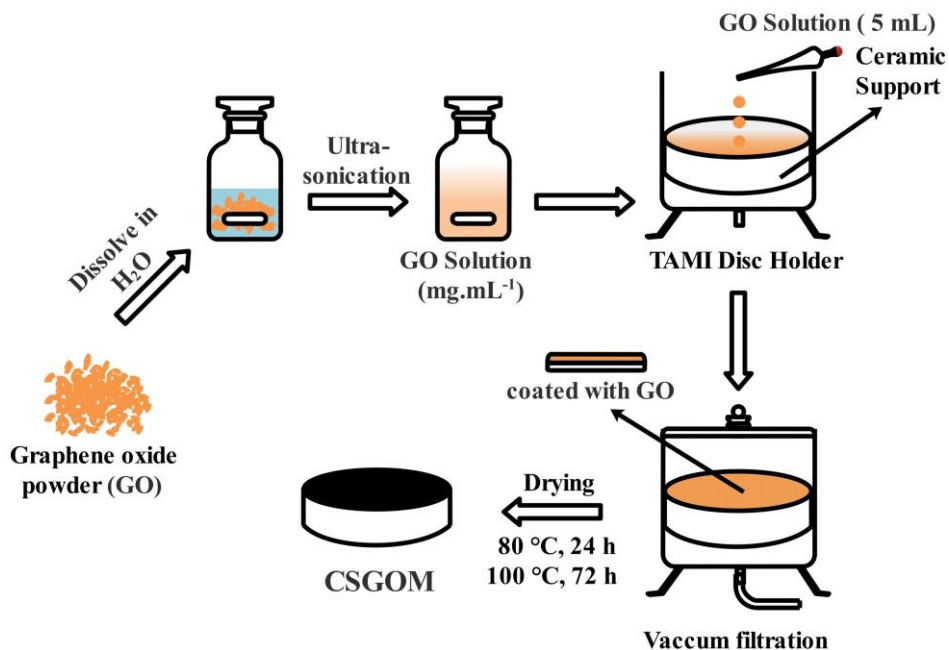


**Figure 1:** Fabrication process of the ceramic-supported GO Membrane (CSGOM).

The schematic diagram of the synthesis of CSGOM is illustrated in Figure 1. The process begins with preparing different concentrations of homogeneous GO solution ( $\text{mg}\cdot\text{mL}^{-1}$ ) by dissolving the desired amount of previously synthesized GO powder in deionized water, which was sonicated by 45 minutes in an ultrasonic bath. Then, 5 mL of GO solution was poured over the ceramic support placed inside the filtration cell (INSIDE DisRAM holder, TAMI Industries, France). After 15 minutes of vacuum filtration, a controllable graphene oxide layer was formed on the ceramic support surface.



The coating was settled by first drying at 80 °C for 24 h and then at 100 °C for 72 h. Following the above procedure, a total of four GO membranes were prepared using a variety of precursor concentrations; these were denoted as CSGOM-0.5, CSGOM-1, CSGOM-2, and CSGOM-4, respectively, for the membrane synthesized with 0.5, 1, 2, and 4 mg·mL<sup>-1</sup> of exfoliated GO solutions.

## 2.2 Experimental Set-up for Anaerobic Biodegradation

**Figure 2** shows a scheme of the lab-scale B-CSGOM system used in this study. The compact bioreactor was made of a filtration cell that held the CSGOM membrane with 5 mL of retentate chamber. AO7 (ACROS Organics, ref. 416561000), diazo Reactive Black 5 (RB5) (Sigma Aldrich, ref. 306452), and triazo Direct Blue 71 (DB71) (Sigma Aldrich, ref. 212407) were selected as model compounds to generate the artificial wastewater. As co-substrate, Sodium Acetate (SA) (Sigma Aldrich, ref. 110191) was used as a carbon source and electron donor for microorganisms and azo reduction. The dye and SA were dissolved in Milli-Q water at a 1:3 mass ratio to make the synthetic feed solution. After that, 1 mL of each basic medium (BM), used as a source of microorganism nutrients, was added to the feed solution. There were six basal media; BM 1 contained 0.155 mg·L<sup>-1</sup> MnSO<sub>4</sub>·H<sub>2</sub>O, 0.285 mg·L<sup>-1</sup> CuSO<sub>4</sub>·5H<sub>2</sub>O, 0.46 mg·L<sup>-1</sup> ZnSO<sub>4</sub>·7 H<sub>2</sub>O, 0.26 mg·L<sup>-1</sup> CoCl<sub>2</sub>·6H<sub>2</sub>O and 0.285 mg·L<sup>-1</sup> (NH<sub>4</sub>)<sub>6</sub>Mo<sub>7</sub>O<sub>24</sub>; BM 2 contained 21.75 mg·L<sup>-1</sup> K<sub>2</sub>HPO<sub>4</sub>, 33.40 mg·L<sup>-1</sup> Na<sub>2</sub>HPO<sub>4</sub>·2H<sub>2</sub>O, 8.50 mg·L<sup>-1</sup> KH<sub>2</sub>PO<sub>4</sub>; BM 3 was 29.06 mg·L<sup>-1</sup> FeCl<sub>3</sub>·6H<sub>2</sub>O solution; BM 4 was 13.48 mg·L<sup>-1</sup> CaCl<sub>2</sub> solution; BM 5 was 15.2 mg·L<sup>-1</sup> MgSO<sub>4</sub>·7H<sub>2</sub>O solution; and BM 6 was 190.90 mg·L<sup>-1</sup> NH<sub>4</sub>Cl solution. All the chemicals used in this BM were analytical grade chemicals (Sigma Aldrich), and the solutions of these chemicals were made by dissolution in Milli-Q water.

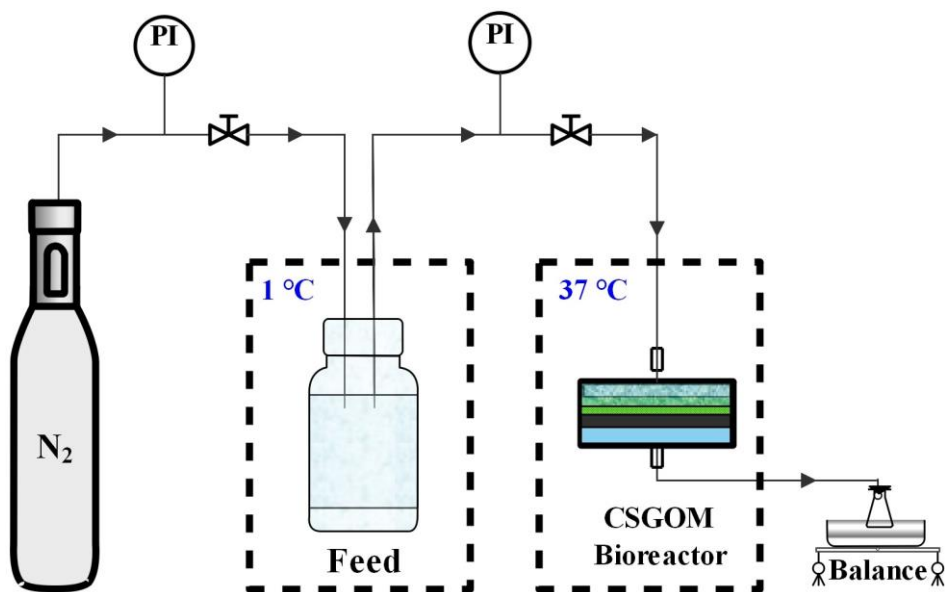


**Figure 2.** CSGOM bioreactor experimental set-up.

The feed solution was kept at 1 °C to prevent microbial growth in the feed stream that ensured a stable sodium acetate concentration. The reactor was sealed tightly after 5 mL of secondary anaerobic sludge (municipal WWTP Reus, Spain) was placed over the CSGOM membrane. Continuous sparging of nitrogen through the feed solution (Purity >99.99 %, Linde) helped to maintain the negative redox potential, needed to favor dye decolorization rate [24]; this resulted in the obtained anaerobic conditions throughout the system. Moreover, nitrogen pressure fixed the operation of TMP, thus controlling the permeate flux. The compact bioreactor was run under dead-end filtration mode at a temperature of  $37 \pm 1$  °C to boost the efficiency of microbial strains that were capable of decoloring azo dyes [25, 26].

### 2.3 CSGOM Membrane Characterization

The morphology, thickness, and elemental composition of graphene oxide membranes were characterized by the Field Emission Scanning Electron Microscope with Focused Ion Beam (FESEM-FIB, Scios 2 Dual Beam, Thermo Scientific, USA). Atomic Force Microscopy (AFM, Molecular Imaging Pico Plus 2500, Bid Service, USA) was used to examine the membrane surface and conductivity.

Raman scattering measurements to characterize the carbon product were carried out at room temperature with a Renishaw inVia Raman Confocal Microscope System w/Leica DM 2500M at 633 nm. Furthermore, to confirm the phase purity and crystallinity of the CSGOM membrane, a Siemens D5000 diffractometer, Bragg-Brentano parafocusing geometry, and vertical  $\theta$ - $\theta$  goniometer under the  $\text{CuK}_\alpha$  wavelength of 1.54056 Å at 40 kV and 30 mA, was used for X-ray Diffraction (XRD). The data was obtained using a sample rotation (0.05° angular step at 3s per step) and analyzed with the aid of diffract-plus software.

The filtration performance of CSGOM was inspected using equations 1 and 2 as straightforward method to determine membrane flux and hydraulic resistance.

$$J = \frac{V}{t} \cdot \frac{1}{A} \quad (1)$$

$$H_R = \frac{\Delta P}{\mu} \cdot \frac{1}{J} \quad (2)$$

where  $J$  is the permeate flux ( $\text{L} \cdot \text{m}^{-2} \cdot \text{h}^{-1}$ ),  $V$  the volume of permeate (L) collected in a given time,  $t$  the filtration time (h),  $A$  the membrane area ( $\text{m}^2$ ),

$H_R$  is the resistance ( $m^{-1}$ ),  $\Delta P$  is the transmembrane pressure (bar), and  $\mu$  is the viscosity ( $Pa \cdot s$ ) of the permeate corrected to experimental temperature.

Dye removal was evaluated by measuring the dye concentration using a UV/VIS4000n Spectrophotometer (DINKO Instruments, Spain) at the corresponding maximum absorbance wavelength at 484 nm for AO7, 597 nm for RB5, and 585 nm for DB71. The decolorization percentage (D) was calculated using equation 3.

$$D (\%) = \frac{A_o - A}{A_o} \times 100 \quad (3)$$

where  $A_o$  and  $A$  are the absorbance of feed and treated samples for each biodegradation test, respectively.

## 2.4 Microbial Analysis

The microbial diversity of the biofilm evolved during the anaerobic bioreduction of dye was examined using DNA isolation kits (Norgen Biotek Corporation, ref. 64000). In this extraction technique, the bio-samples were collected from the membrane surface and its DNA extracted [27]; 500 ng of extracted DNA were used for library preparation to apply DNA Illumina sequencing employing Illumina DNA Prep kit (Illumina, Inc.). All libraries were evaluated with the TapeStation High Sensitivity DNA kit (Agilent Technologies) and quantified with Qubit (Invitrogen Corporation). The filtered reads were matched to unique clade-specific marker genes using MetaPhlAn 3 to determine the taxonomic profile. Relative abundances and alpha diversity measures (Shannon and chao1 indexes) were calculated using MetaPhlAn's relative proportions.



Raman spectra shown in **Figure 4** can provide additional evidence for the presence of GO in the CSGOM-1. High intensity peaks in the Raman spectra of CSGOM-1 indicate the expected conjugated and carbon-carbon double bonds of graphene. In general, the D peak is caused by  $sp^3$  carbon atoms with a disordered or defective carbon structure, while the G peak is originated from the vibration of the aromatic structure of  $sp^2$  hybrid carbon atoms. It also reflects the same characteristics as XRD, whereas the tetragonal  $ZrO_2$  is observed at  $262\text{ cm}^{-1}$  ( $E_g$ ) [33] and for rutile  $TiO_2$  peaks at  $448\text{ cm}^{-1}$  ( $E_g$ ) and  $611\text{ cm}^{-1}$  ( $A_{1g}$ ) [34]. The typical D and G bands for the CSGOM-1 are found at  $1351\text{ cm}^{-1}$  and  $1605\text{ cm}^{-1}$ , respectively. The quotient  $I_D/I_G$ , the D and G band's intensity ratio, is a common way to express the defect degree of materials. It is found to be 1.02 for CSGOM-1, which is consistent with reported values in the literature [35]. This ratio suggests that the GO membrane is relatively stable and resistant to environment conditions. Furthermore, the absence of a 2D band at  $2700\text{ cm}^{-1}$  indicates that all the graphite layers were essentially oxidized during the oxide formation step [36]. The morphology of both CS and CSGOM-1 were examined by FESEM.

**Figure 5(a-b)** demonstrates that both ceramic support and ceramic-supported graphene oxide membranes are typical porous surfaces [22, 37]. Part of the of the graphene oxide deposited on the ceramic support appears as an aggregate or was broken down into smaller particles that penetrated into the ceramic support to form a GO- $ZrO_2$  composite [23]. It seems that, once the pores were shrinking or blocked, the homogeneous GO layer was formed, over a first zone of the composite GO- $ZrO_2$  and then over the original  $ZrO_2$  section. Probably, interaction on the membrane surface is mainly due to the attraction between  $ZrO_2$  oxygens and either or both hydroxyl and carboxylic groups of graphene oxide [38, 39]. As expected, the GO layer deposited

reduced the pore size of the virgin CS surface. In addition to the visual inspection of the FESEM images, ImageJ software was used to analyze the surface pores of CS and CSGOM-1. Compared to the CS, it is found that the pore size of the CSGOM-1 is significantly lowered, where more than 80% of the pores being around 25 nm, in the range of transition from ultra to nanofiltration.

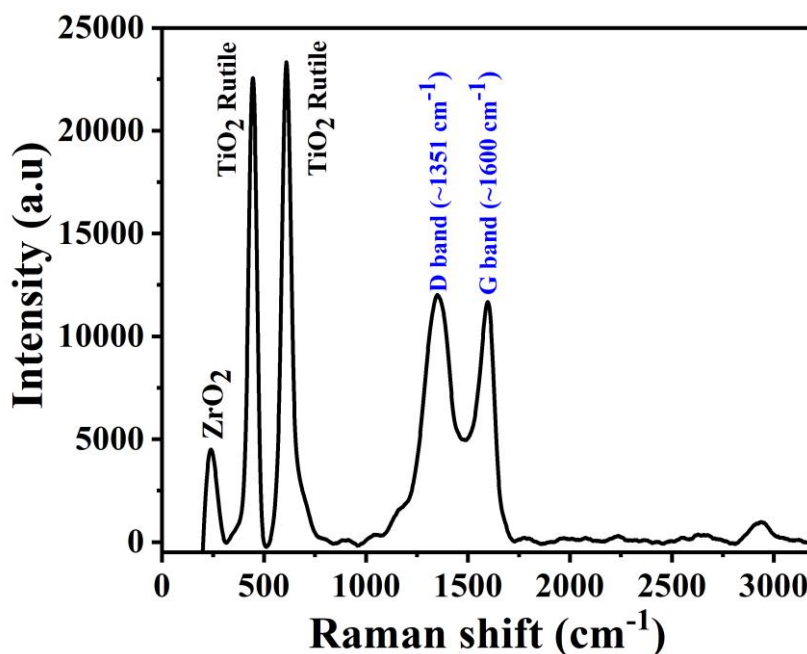


**Figure 4.** Raman spectra of ceramic-supported graphene oxide membrane

The cross-sectional images of both CS and CSGOM-1 (**Figure 5(c-d)**) revealed a clear disparity between the support and the membrane. The bottom part in both cases is the titanium oxide layer. There are then two more layers of zirconium oxide above the titanium oxide layer: the smaller active porous layer and the intermediate porous layer.

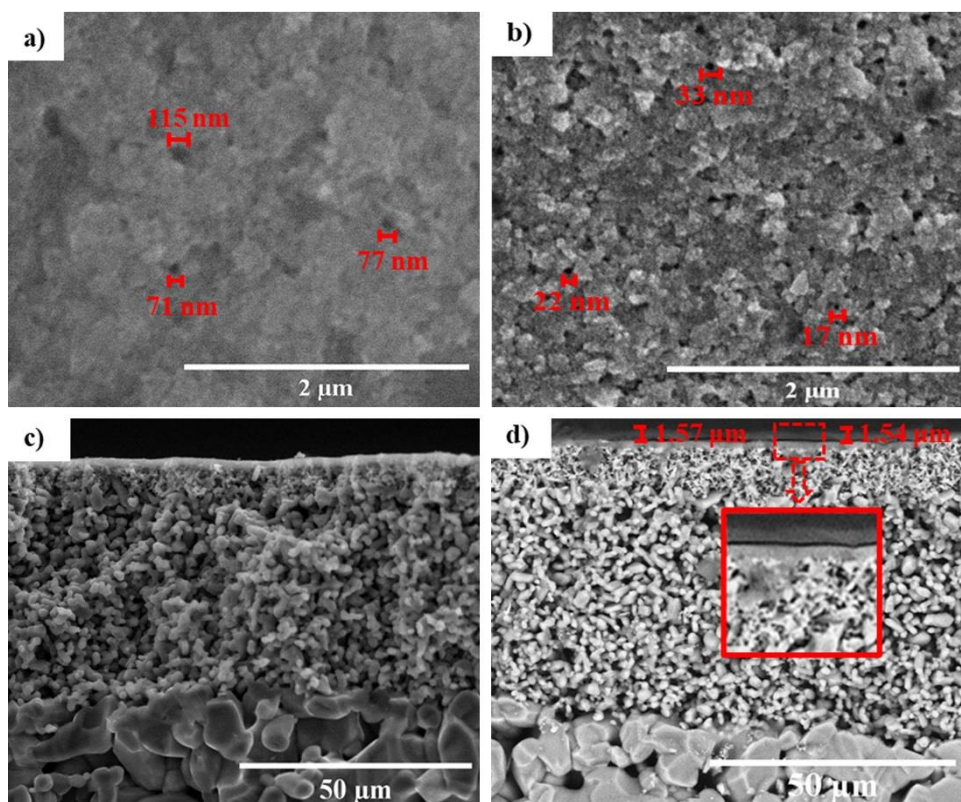


**Figure 5.** FESEM micrographs on the surface of a) CS and b) CSGOM-1, and the cross section of c) CS and d) CSGOM-1 (deposited GO amounts: 2.6 mg).

However, another layer is clearly visible in the CSGOM-1, which corresponds to the synthesized graphene oxide membrane. This configuration is in line with that found by Octávia et al. [40], who demonstrated the fabrication of a uniform GO-Zirconia composite membrane. The 1.55 μm thick GO layer is firmly adhered to the ceramic support, indicating the success of CSGOM-1 preparation using the vacuum-assisted method.



**Table 1** lists the GO content and elementary composition of CSGOM synthesized with various concentrations of GO solution. As expected, the GO content (0.8 to 3.9 mg) of the top layer of CSGOM increases in proportion to the initial solution concentration of membrane precursors. The FESEM-EDX analysis of the GO membrane provided more detailed information about this layer composition.

**Table 1.** Surface analysis of the CS and CSGOM-1

	GO content (mg)	C	O	Ti	Zr
		(wt.%)			
CS	n.d.	n.d.	44.0	22.2	33.8
CSGOM-0.5 (0.5 mg·mL <sup>-1</sup> )	0.8	13.7	42.2	17.0	27.1
CSGOM-1 (1 mg·mL <sup>-1</sup> )	2.6	49.4	37.0	3.1	10.5
CSGOM-2 (2 mg·mL <sup>-1</sup> )	3.3	61.3	35.9	n.d.	2.8
CSGOM-4 (4 mg·mL <sup>-1</sup> )	3.9	66.8	33.1	n.d.	0.1

As expected, the results show that CS is made of ZrO<sub>2</sub> and TiO<sub>2</sub>, although the content of zirconia is higher than titania as the analysis rather falls upon the upper layer of the virgin layer, described as a selective zirconia band. In turn, the CSGOM have a carbon-rich layer on top (13.7 to 66.8 wt.% of carbon) together with ZrO<sub>2</sub> and TiO<sub>2</sub>. The amount of carbon content is greater when increasing the concentration of exfoliated GO solution during coating and, subsequently, the relative content of ZrO<sub>2</sub> and TiO<sub>2</sub> is decreased. Obviously, the data is in accordance with the fact that the incident beam energy (5 keV) for all measurements penetrated a given depth through the CSGOM surface. Thus, the thicker GO layer on the membrane surface allows passing a shorter distance, and therefore the analysis was able to quantify fewer elements deeper inside the membrane composite. Furthermore, as the concentration of the precursor solution rises, more GO particles begin to

penetrate the GO-ZrO<sub>2</sub> composite layer, which means deposited deep inside the ceramic support. As a result, the precursor concentration increases from 2 to 4 mg·mL<sup>-1</sup> had almost no significant changes in the carbon content measured on the membrane surface.

The multilayer 3D topography, height, and current profile of CSGOM-1 were investigated by using AFM (at a random area of 500x500 nm<sup>2</sup>) and CSAFM (current sensing atomic force microscopy); the data is shown in **Figure 6 (a-b)**. The mean roughness and root mean square (RMS) roughness analysis of the membrane surface yielded 7.5 and 9.4 nm, respectively. According to a rough estimate based on AFM imaging with SPIP<sup>TM</sup> software, most of the pores in CSGOM-1 were in the 17-33 nm range, which compares well with estimates made by FESEM.

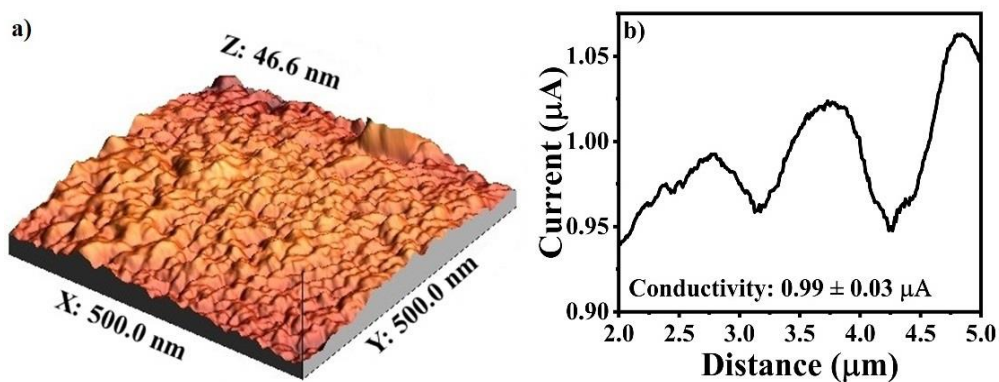


**Figure 6.** AFM images of CSGOM-1 a) 3D Topography b) Current distribution

The CSAFM images also provide the current distribution profile of the CSGOM-1 membrane (**Figure 6b**). The results demonstrate the local conductance on graphene oxide surfaces, which should enhance the rate of biodegradation through the electron shuttle mechanism [41].

### 3.2 Impact of the GO Layer on Flux and Resistance

A set of tests were conducted to investigate the effect of depositing different amounts of membrane precursor (produced by varying the concentration of GO solution) on filtration characteristics represented by membrane flux, and the derived parameters pure water permeance (PWP) and hydraulic resistance ( $H_R$ ). As expected, the membrane without GO, CS, showed the highest flux,  $62.3 \text{ L}\cdot\text{m}^{-2}\cdot\text{h}^{-1}$ . The pure water flux of the ceramic support ( $\text{ZrO}_2\text{-TiO}_2$  based ultrafiltration flat membrane) is mainly influenced by the membrane properties such as thickness, homogeneity, and porosity. Additional single or multilayer GO was formed over the ceramic support in CSGOM, resulting in an increment of hydraulic resistance. Moreover, the GO particles reduce the pore size of the ceramic support. Thus, a membrane without the GO always possessed the highest water flux. Similar results are shown in **Figure 7**, where the flux decreased linearly with increasing GO thickness, which correlates with the increasing precursor concentration for CSGOM preparation (0.5, 1 and  $2 \text{ mg}\cdot\text{mL}^{-1}$  GO). The lowest pure water flux ( $4.1 \text{ L}\cdot\text{m}^{-2}\cdot\text{h}^{-1}$ ) was observed for the membrane made of  $2 \text{ mg}\cdot\text{mL}^{-1}$  of GO solution (CSGOM-2). In comparison to CS, the pure water flux for CSGOM-0.5, CSGOM-1, CSGOM-2 dropped 63%, 83%, and 93%, respectively. Giménez et al. [23] also found strong flux drops, 47% and 77%, for GO membranes prepared from 0.05 and  $0.5 \text{ mg}\cdot\text{mL}^{-1}$  of GO over a  $0.04 \mu\text{m}$  pore size ceramic support. The derived PWP follows these trends, so CS exhibits maximum permeance ( $77.8 \text{ L}\cdot\text{m}^{-2}\cdot\text{h}^{-1}\cdot\text{bar}^{-1}$ ) and it then decreases up to  $5.1 \text{ L}\cdot\text{m}^{-2}\cdot\text{h}^{-1}\cdot\text{bar}^{-1}$  for CSGOM-2 (**Figure 7**).

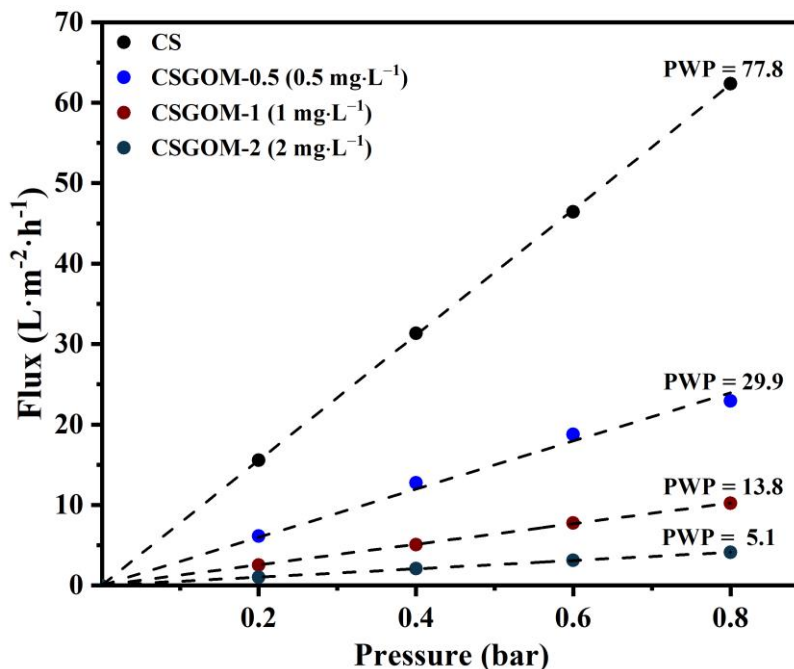


**Figure 7.** Variation of pure water flux and pure water permeability of CS and CSGOM at 25 °C. (PWP in  $\text{L}\cdot\text{m}^{-2}\cdot\text{h}^{-1}\cdot\text{bar}^{-1}$ )

From the permeances given in **Figure 7**, the total resistance of the CS and CSGOM were estimated, and the specific contribution of the GO layer was calculated considering the ceramic support resistance to be constant in the membranes containing GO. The hydraulic resistance of the ceramic support was estimated to be as  $5.2\pm 0.1\cdot 10^{12} \text{ m}^{-1}$ . It has been noted that GO load during preparation of graphene oxide membranes has a significant impact on permeate flux, thus in the hydraulic resistance. Since permeate flux and hydraulic resistance are interconnected functions, higher graphene oxide content membrane must result in more resistance. During fabrication, the ceramic support pores (GO-ZrO<sub>2</sub> region) were first entirely filled and then formed on top the GO multilayer. It was also observed that the thickness of the deposited GO layer grew as the GO concentration was increased, which in turn decreased the membrane flux [42, 43] and increased the hydraulic

resistance. Hence, the CSGOM resistances increased from  $1.51 \pm 0.04 \cdot 10^{13} \text{ m}^{-1}$  to  $8.64 \pm 0.13 \cdot 10^{13} \text{ m}^{-1}$  as the concentration of GO solution during coating increased from 0.5 to 2  $\text{mg} \cdot \text{mL}^{-1}$ . Therefore, the CS gives less than one third of the total resistance in CSGOM. Further increase of GO concentration up to 4  $\text{mg} \cdot \text{mL}^{-1}$  in CSGOM-4 preparation made the membrane essentially impermeable due to the formation of a very thick, dense, and nonporous GO layer on the membrane surface that prevents water molecules from passing across [44, 45].

On the other hand, a low concentration of GO solution ( $< 0.5 \text{ mg} \cdot \text{mL}^{-1}$ ) failed to form a uniform, stable GO-Ceramic membrane because of lack of carbon content and non-homogeneous layer formation on the membrane surface. Lou et al. [46] found that a membrane prepared from 0.05, 0.10, and 0.5  $\text{mg} \cdot \text{mL}^{-1}$  GO solution was not good enough for practical application. Moreover, in a membrane prepared with a high GO concentration ( $\geq 4 \text{ mg} \cdot \text{mL}^{-1}$ ), the GO layer can peel up easily after swelling and detached from the surface. Therefore, it is inferred that the CSGOM preparation technique must meet two critical requirements. GO load must be suitable to create a homogeneous and tightly bound GO layer and permeate flux should be at the desired level. In this study, it was found that the CSGOM-1, with an estimated 1.55  $\mu\text{m}$  GO layer thickness showed a permeance of  $13.8 \text{ L} \cdot \text{m}^{-2} \cdot \text{h}^{-1} \cdot \text{bar}^{-1}$ . This was comparable to other attempts available in the literature such as a polyacrylonitrile nanofibrous mat supported ( $8.2 \text{ L} \cdot \text{m}^{-2} \cdot \text{h}^{-1} \cdot \text{bar}^{-1}$ ) and an electrospray nanofiltration ( $11.3 \text{ L} \cdot \text{m}^{-2} \cdot \text{h}^{-1} \cdot \text{bar}^{-1}$ ) GO membrane [47]. Even though the carbon wall or channel is hydrophobic in nature, the slip flow theory indicates that it can assist in transporting the liquid between the GO layers [42]. As per this principle, the water molecules first proceed to the hydrophilic edges and defects of the GO layer, which act as a gate for water

flow. The liquids are usually deposited in those gates and then slip through the hydrophobic nanochannel. As a result, graphene oxide membrane displays acceptable permeate flux despite having a thicker layer. Based on these facts, 0.5 and 1 mg·mL<sup>-1</sup> of GO solution appears to be the optimum concentration for forming the membranes properly, combining enough flux and robustness needed for the wastewater treatment process.

### 3.3 Role of the Graphene Oxide Layer on Anaerobic Biodecolorization of Azo Dyes

The capability of the graphene oxide membrane for anaerobic azo dye decolorization was checked out, with and without the formation of biofilm. Four different reactor combinations were used: mixed microbial consortium on CS (B-CS), mixed microbial consortium on CSGOM (B-CSGOM), no microbial consortium on CS (R-CS), and no microbial consortium on CSGOM (R-CSGOM). In all cases, initially, 50 mg·L<sup>-1</sup> feed solution of AO7 was used as it falls within the typical range (10 to 50 mg·L<sup>-1</sup>) of dye concentrations in real textile effluents [48]. In all the cases, a constant flux of 0.05 L·m<sup>-2</sup>·h<sup>-1</sup> was maintained in a dead-end filtration mode. Furthermore, two graphene oxide membranes produced from 0.5 and 1 mg·mL<sup>-1</sup> of GO solution (CSGOM-0.5 and CSGOM-1) were used to investigate the impact of graphene oxide content on the decolorization process. As above commented, the thickness of the GO layer on the membrane surface is easily adjusted by changing the precursor concentration. Since the membrane flux is dependent on the thickness of the deposited graphene oxide layer (resistance) of the CSGOM, transmembrane pressure from 0.5 to 2.0 bar was adjusted in the experiments to maintain a constant flow irrespective of the different membrane thicknesses. **Figure 8** includes the removal evolution for all the cases during a period of 10 days, since the start until a steady operation was

reached. Overall, the results confirmed that the presence of the GO layer had a significant effect on the decolorization of AO7. The color removal attained was larger at the highest GO load (B-CSGOM-1 consisting of the membrane made of  $1 \text{ mg}\cdot\text{mL}^{-1}$  of GO solution), giving a decolorization of 99%.

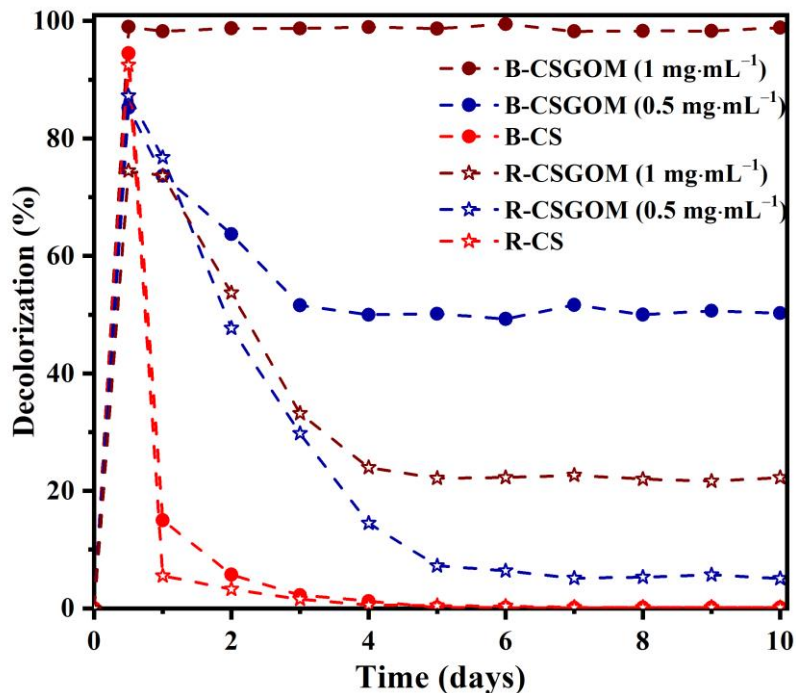


**Figure 8.** Decolorization of AO7 in CS and CSGOM reactors; CS and CSGOM bioreactors; Flux =  $0.05 \text{ L}\cdot\text{m}^{-2}\cdot\text{h}^{-1}$ , AO7 concentration in feed solution =  $50 \text{ mg}\cdot\text{L}^{-1}$  and  $T = 37 \text{ }^\circ\text{C}$ .

All the reactors apparently showed a good efficiency during the first 12 hours as they decolorized more than 75% of the azo dye solution. Actually, this initial decolorization was basically due to the adsorption of the dye on the membrane surfaces, so it is not a true removal. Once the membrane became saturated, the color removal efficiency dropped suddenly, except for B-CSGOM-1, stabilizing rapidly around a mostly steady value. The B-CS and

R-CS completely lost any decolorization ability after two days. In the case of R-CS, once saturated the membrane material, the only possible mechanism to remove dyes could be the membrane retention, which fails since the pore size of the support element (UF range) is too high in comparison to the dye dimensions (NF range). Although B-CS was operated with the mixed microbial consortium, the desired biodecolorization did not occur because of the probable absence of an active biofilm or even microorganisms on the ceramic support, which can probably be ascribed to the fact that the permeate flow washed out the bacteria before forming a biofilm because of their size relatively smaller than the support pores. After four days of operation, the decolorization rate stabilized at approximately 22% for CSGOM-1 and 10% after six days with CSGOM-0.5. In this case, the membranes are partially able to retain the dye due to the nano-sized pores of the CSGOM surface created after GO layer formation. Therefore, this limited capacity of dye removal can essentially be attributed to molecular sieving mechanism.

Only for B-CSGOMs (blue and brown circles in **Figure 8**), there was a true biodegradation of the dye. The highest decolorization (99%) was observed for the B-CSGOM-1 prepared with a concentration of  $1 \text{ mg}\cdot\text{mL}^{-1}$  of GO, whereas only 51% of color removal was observed using B-CSGOM-0.5 made from  $0.5 \text{ mg}\cdot\text{mL}^{-1}$  GO. Only dye decomposition caused by the anaerobic action of the microorganisms can account for the high level of decolorization observed in this study. However, a great difference is observed between the performance of the B-CSGOM-1 and B-CSGOM-0.5, where the load of GO seems to favor the biodecomposition. To form an efficient biofilm or anaerobic membrane scaffold, microorganisms must be selectively attached to the graphene oxide surface. The essence of the microbial activity and the consistency of the GO layer have a direct impact on adhesion



performance. Thus, the improved performance in B-CSGOMs was due to the concurrent occurrence of physical sieving and anaerobic biodegradation. As in previous studies using ceramic-supported carbon-based membrane bioreactors [22], the GO layer of B-CSGOM also played a triple role in the anaerobic decolorization of azo dyes since it performs as a pollutant immobilizer, support for the biofilm, and electron transporter. Graphene-oxide membranes are more conductive than Matrimid-based carbon membranes [22], thus contributing to a faster electron shuttle mediator mechanism. Moreover, the surface of the nanoporous graphene oxide membrane improves the microbial metabolism and retains the degradation products, which globally enhances the decolorization performance [49].

Compared with previous studies (the up-flow packed-bed reactor filled with biological activated carbon) with a similar objective [50], the B-CSGOM-1 was also stabilized in a shorter retention time to achieve the almost complete (99%) decolorization of AO7. On the other hand, our configuration shows better performance if compared to other attempts based on GO. Shital et al. [51] assessed AO7 removal by adsorption with reduced graphene oxide (RGO), combined RGO-Photolysis, RGO-Oxidation with  $H_2O_2$ , and RGO-Oxidation with photo radiation process, and found 10% removal by RGO alone and a maximum of 80% by combined RGO-Oxidation with UV-radiation.

Since GO plays a critical role in this process, it was expected that its load in the GO layer impact somehow on the dye removal. For instance, in an oxidation process, Lee et al. [52] investigated GO load and discovered that the increase of the load improved the dye removal efficiency. As previously noted, FESEM-EDX measurements (**Table 1**) confirmed the increase of the

GO concentration in the precursor solution from 0.5 to 1 mg·mL<sup>-1</sup> improves the GO content of CSGOM from 0.8 to 2.6 mg. This latter higher load creates a membrane with smaller pore size responsible of dye adsorption and biofilm immobilization, therefore, both enhanced [53]. Moreover, the carbon-rich CSGOM enhances the redox mediator role due to the greater availability of sites with redox properties, which also contributes to improve the biodegradation performance. **Figure 8** corroborates this trend, as raise of carbon content from 13.7% to 49.4% on CSGOM-1 almost doubled the decolorization (from 51 to 98%). Further application of a CSGOM-2 and CSGOM-4, as commented above, gave a less or non-permeable membrane, so the CSGOM-1 was taken as the most favorable balance between flux and decolorization.

### 3.4 Effect of Flux and Feed Concentration on Azo Dye Decolorization

The effect of feed concentration and permeate flux on the decolorization process of B-CSGOM-1 was evaluated by varying AO7 concentrations (50, 75, and 100 mg·L<sup>-1</sup>) and permeate fluxes (0.05, 0.075, and 0.10 L·m<sup>-2</sup>·h<sup>-1</sup>). All experiments were conducted for 30 days continuous operation, with a flow of 0.05 L·m<sup>-2</sup>·h<sup>-1</sup> within the first 10 days, 0.075 L·m<sup>-2</sup>·h<sup>-1</sup> for the second 10 days, and finally at 0.10 L·m<sup>-2</sup>·h<sup>-1</sup> until the end. The transmembrane pressure (TMP) was adjusted when needed to keep a constant permeate flux. Though slight, accumulated membrane fouling during the process would lower the permeate flux if not corrected. **Figure 9** depicts the change in AO7 decolorization for the three feed concentrations tested during the three periods of different permeate flux. As can be seen, irrespective of the conditions, the decolorization reached over 90% although the expected trends for feed concentration and permeate flux were observed. B-CSGOM-1 with a feed concentration of 50 mg·L<sup>-1</sup> and a permeate flux of 0.05 L·m<sup>-2</sup>·h<sup>-1</sup> achieved the

maximum AO7 removal, 99%. At a higher permeate flux ( $0.10 \text{ L}\cdot\text{m}^{-2}\cdot\text{h}^{-1}$ ), the decolorization slightly decreased to 97%, 95%, and 93%, at the AO7 feed solution concentrations of 50, 75, and  $100 \text{ mg}\cdot\text{L}^{-1}$  respectively. Along with **Figure 9**, **Table 2** illustrates the amount of dye removed and the percentage of decolorization during the B-CSGOM-1 process. It is worth noting that when the feed concentration and permeate flux increase, decolorization usually reduces but the amount of decolorized dye is progressively growing. In this experiment, a maximum equivalent consumption of  $9.3 \text{ mg}\cdot\text{m}^{-2}\cdot\text{h}^{-1}$  was obtained for  $100 \text{ mg}\cdot\text{L}^{-1}$  AO7 at a  $0.10 \text{ L}\cdot\text{m}^{-2}\cdot\text{h}^{-1}$  flux.

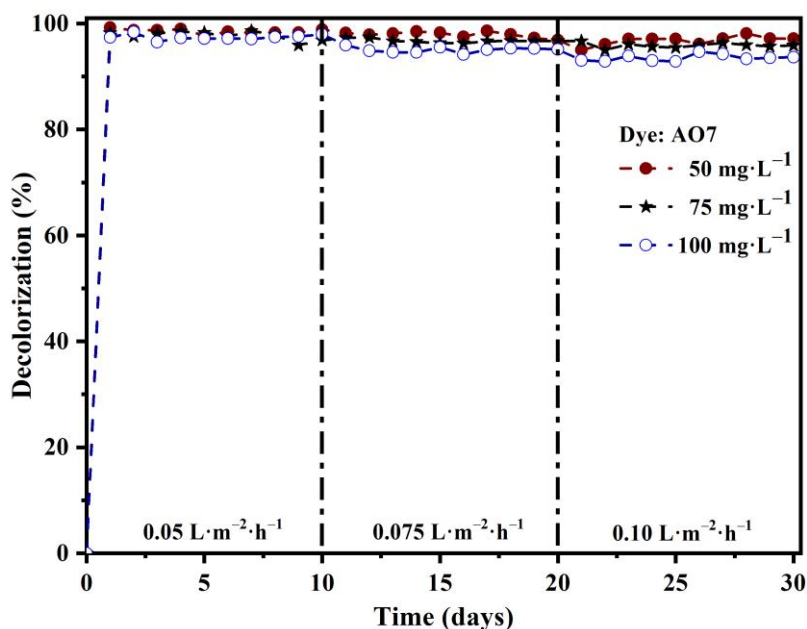


**Figure 9.** Influence of feed concentration and permeate flux on anaerobic decolorization of AO7 using B-CSGOM-1.

Color removal was thoroughly stable at the low flux-region, with no significant differences observed for the three different feed concentrations. The low permeate flow allowed the dye molecules to interact with bacteria

enough time to reach large biodegradation [54]. After 30 days of operation, even increasing permeate flux, the B-CSGOM-1 gave around 97% of azo dye decolorization for the 50 mg·L<sup>-1</sup> feed solution. Increasing the flux, even the falling decolorization percentage, the absolute amount of AO7 removal by the B-CSGOM-1 increased from 2.5 to 4.7 mg·m<sup>-2</sup>·h<sup>-1</sup>. These decolorization and dye removal findings concluded that the amount of biomass was sufficient to assure almost complete biodegradation of the dye. Anyway, even when the AO7 feed concentration and permeate flux doubled, the microorganisms were able to attain high levels of decolorization. Thus, the decolorization for 75 and 100 mg·L<sup>-1</sup> feed solution at 0.075 and 0.10 L·m<sup>-2</sup>·h<sup>-1</sup> flux was only reduced to 98-95% and 97-93%, respectively. Simultaneously, the Total Organic Carbon (TOC) and Chemical Oxygen Demand (COD) of each dye solution were reduced by more than 85% and 95%, respectively, in all conditions. The effluent properties achieved by B-CSGOM-1 were highly suitable for environmental emissions (details are given in Table A). Besides, these conditions furnish more absolute dye removal, which reach 7.1 and 9.3 mg·m<sup>-2</sup>·h<sup>-1</sup> for 75 and 100 mg·L<sup>-1</sup> feed solutions, respectively. The results were much better than those obtained using conventional discontinuous biological systems at several AO7 concentrations [50, 55, 56]. In a similar reactor configuration and operations conditions using carbon-based membranes instead of GO [22], the decolorization attained was 58%, 45%, and 36% for 50, 75, and 100 mg·L<sup>-1</sup> of AO7 solutions, respectively, while over 93% removal was achieved using the present B-CSGOM-1 in the ranges tested. This suggests that the GO plays a dominant role during the dye biodegradation, being much more efficient than carbon-based membrane made using Matrimid 5218 as a precursor [22]. Probably the potential of GO

as a redox mediator enhanced the transfer of electrons to the azo bond of the dye molecule, leading to easier cleavage of the azo bond [57].

**Table 2.** Summary of the decolorization and dye removal in B-CSGOM-1 tests.

Flux ( $L \cdot m^{-2} \cdot h^{-1}$ )	Decolorization (%)			Dye Removal Rate ( $mg \cdot m^{-2} \cdot h^{-1}$ )		
	0.05	0.075	0.10	0.05	0.075	0.10
Concentration ( $mg \cdot L^{-1}$ )						
50	99	98	97	2.5	3.7	4.7
75	98	97	95	3.7	5.4	7.2
100	97	95	93	4.9	7.1	9.3

However, regardless of the color removal, this compact bioreactor unit is more compatible with higher feed concentration and permeate flux to remove the amount of azo dye as the microorganisms of the B-CSGOM-1 is highly capable of coping with the growing dye loads. Consequently, it might be more productive to operate the B-CSGOM-1 at a greater permeate flux.

### 3.5 Comparative Decolorization of Azo Dyes

A comparative biodecolorization of three structurally different azo dyes (mono azo AO7, diazo RB5, and triazo DB71) were investigated in the anaerobic B-CSGOM-1s under various permeate fluxes and feed concentrations. The extent of decolorization of azo dye solutions varied depending on the number of azo bonds present in the dye structure. **Figure 10(a-c)** illustrates this fact. In general, for the three azo dyes, the decolorization declined as feed concentration and permeate fluxes increased. As expected, for all experimental conditions, mono azo AO7 dye reported the highest color removal (99-93%), which was significantly higher than for

diazo (96-85 %) and triazo (92-81%) dyes. Franciscon et al. [58] previously demonstrated that the monoazo dye removal was faster and more efficient than diazo and triazo using a sequential microaerophilic-aerobic treatment with *Klebsiella* sp. strain VN-3. Anyway, the absolute quantity of dye removal for all azo dyes as well progresses with increasing feed concentration or permeate flux, although it reduces when raising the number of azo bonds and AO7 hence exhibits the highest dye removal of  $9.3 \text{ mg}\cdot\text{m}^{-2}\cdot\text{h}^{-1}$  while DB71 the lowest  $8.1 \text{ mg}\cdot\text{m}^{-2}\cdot\text{h}^{-1}$ .

It must be considered that the contact time (directly related to the permeate flux) can affect the removal capacity, which is also varied depending on dye properties and microorganism behavior against each specific dye [59]. In B-CSGOM-1, as when increasing feed concentration, a higher permeate flux adds additional dye load with more chromophores and auxochromes content in the decolorization process. Additionally, the high flux minimizes biomass retention time within the bioreactor, thereby declining microbial biodecolorization [60, 61]. As a result, under high feed concentration ( $100 \text{ mg}\cdot\text{L}^{-1}$ ), changing permeate flux from  $0.05$  to  $0.075 \text{ L}\cdot\text{m}^{-2}\cdot\text{h}^{-1}$  and finally to  $0.10 \text{ L}\cdot\text{m}^{-2}\cdot\text{h}^{-1}$ , the decolorization reduced to 93% for AO7, 85% for RB5, and 81% for DB71. The corresponding dye removal for AO7, RB5, and DB71 was calculated to be 9.3, 8.5, and  $8.07 \text{ mg}\cdot\text{m}^{-2}\cdot\text{h}^{-1}$ , respectively.

Under identical operating conditions, the structural properties and nature of the azo dyes, for example, meta, ortho, and para position of the electron-withdrawing groups ( $-\text{NO}_2$ ,  $-\text{C}\equiv\text{N}$ ,  $-\text{SO}_3\text{H}$ ,  $-\text{SO}_2\text{NH}_2$ ) to azo bond, presence of electron-releasing groups ( $-\text{OH}$ ,  $-\text{R}$ ,  $-\text{NH}_2$ ) and other functional groups ( $-\text{CH}_3$ ,  $\text{O}-\text{CH}_3$ ), the number of azo bonds and high molecular weight of the dye

molecules have been reported to cause variations in decolorization rate [62-64].

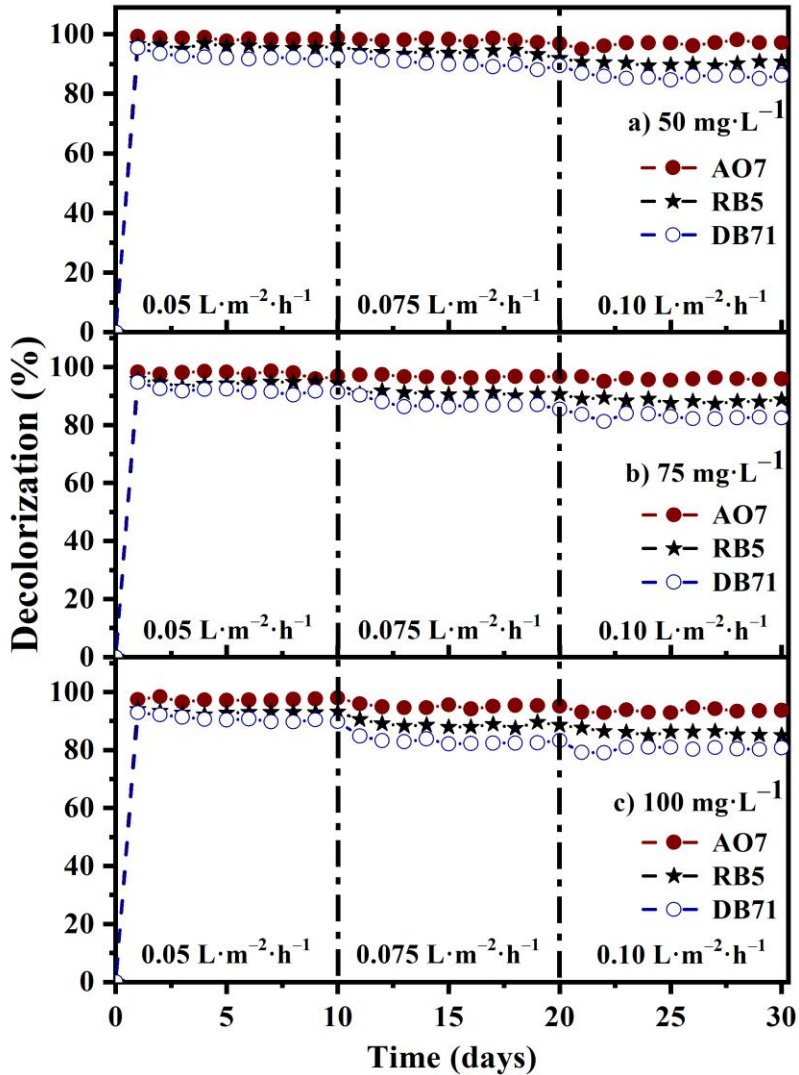


**Figure 10.** Anaerobic decolorization of AO7, RB5, and DB71 dyes at various concentrations and fluxes; a) 50 mg·L<sup>-1</sup>, b) 75 mg·L<sup>-1</sup> and c) 100 mg·L<sup>-1</sup> dye solution at 37 °C.

Increase of both permeate flux and feed dye concentration, brought more reactive groups into the anaerobic bioreactor. It has been reported that an excess amount of  $-SO_3H$  groups in the azo dye structure readily reduced microbial growth [65]. In addition, a rise of toxicity in the degradation process led to inadequate biomass to dye ratio and spoiled the active sites of the biofilm. Consequently, microbial biomass yield at higher feed concentration probably remains lower due to excess dye toxicity to microorganisms. Compatible trends can be seen in **Figure 10(a-c)**, in which the percentage of decolorization of dyes declines as the initial feed concentration or permeate flux increases. Anyway, it has been proved that the bioreactor configuration here introduced successfully decolorized the various azo dyes tested, in line with results reported elsewhere [22, 66].

### 3.6 Microbial Community Analysis

Since the active biofilm evolved from conventional secondary sludge taken from a municipal WWTP after an acclimation period, it is interesting to elucidate which type of microorganism remained prevalent for the dye biodegradation. Therefore, FESEM analysis was applied to measure the presence of microorganisms in the B-CSGOM biofilm after the DB71 biodegradation. **Figure 11(a-b)** displays the surface and cross-sectional view of the biofilm formed over the GO layer. On the biofilm surface, significant quantities of microorganisms with an average size of  $1.51 \mu m$  were detected. Cross-section analysis revealed a biofilm thickness of about  $1.83 \mu m$  over the GO membrane (**Figure 11c**).



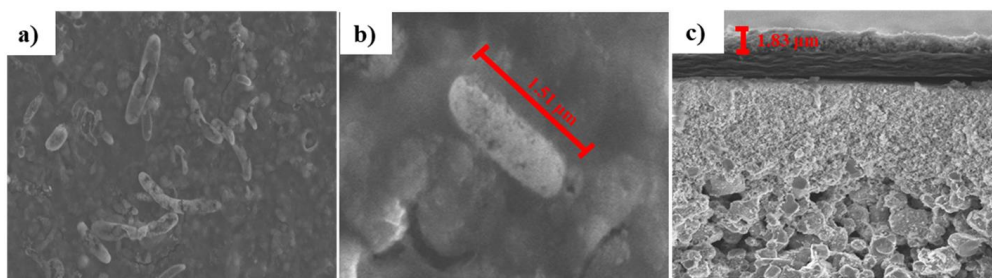


**Figure 11.** Micrograph of FESEM images of biofilm sample after biodecolorization of azo dyes. a) Biofilm surface b) Size of the microorganism c) Biofilm thickness

The biofilm specimen of distinct B-CSGOM-1 bioreactors was used to extract the DNA of bacteria. Three DNA samples were collected from the CSGOM-1 bioreactors operated with 50, 75, and 100 mg·L<sup>-1</sup> of DB71 solutions and were then compared with the original anaerobic sludge (inoculum). DNA Illumina sequencing was used to examine the microbial populations of bacteria, archaea, viruses, and single-celled eukaryotes in these four samples. The sequencing run produced 32.8 million reads that reduce to 30.6 million reads after quality filtering. Although raw anaerobic sludge contained both bacteria and archaea, no archaea were found after bioreactor operation. **Figure 12** depicts the schematic bar diagram and comparison of bacterial phyla for the four samples.

According to species richness, chao1 indexes show that anaerobic sludge (15.24) was the most diverse, and B-CSGOM-1 with 50 mg·L<sup>-1</sup> DB71 (7.54) was less. Overall, among the 53 bacterial taxonomic units (OTUs), the species *Pseudomonas guangdongensis* was the most prevalent in all samples, while *Geobacter sulfurreducens* was abundant in all biofilms but not in the initial anaerobic sludge.

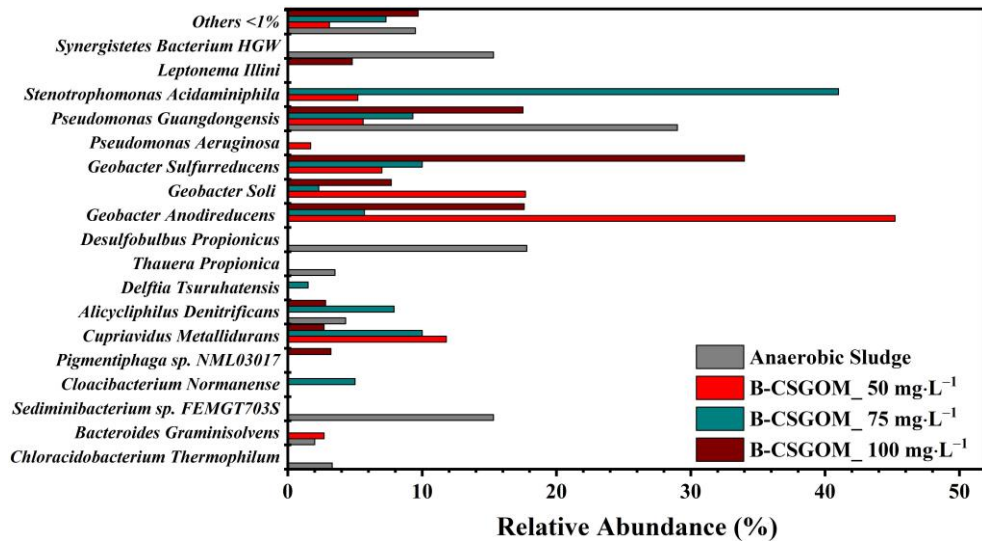


**Figure 12.** Schematic bar diagram of bacterial phyla in the B-CSGOM; (■) Anaerobic sludge, B-CSGOM of (■)50 mg·L<sup>-1</sup>, (■) 75 mg·L<sup>-1</sup> and (■) 100 mg·L<sup>-1</sup>

In all cases, bacterial growth solely depended on the concentration of feed solution. For example, the presence of a significant number of *Geobacter sulfurreducens* (35%) was observed in the biofilm that treated 100 mg·L<sup>-1</sup> DB71 solution, and the lowest (7%) was found for 50 mg·L<sup>-1</sup> of DB71 solution. Similarly, presence of *Pseudomonas guangdongensis* in biofilm was enhanced increasing inflow dye concentration, but the highest was still in the original anaerobic sludge. The results revealed that activities of both *Geobacter sulfurreducens* and *Pseudomonas guangdongensis* were increased with increasing dye concentration.

Several studies have proven the role of *Geobacter sulfurreducens* in the anaerobic biodegradation of azo dye solution [67, 68]. Moreover, the extracellular electron transfer capability of *Geobacter sulfurreducens* and *Geobacter soli* might enable them to play an important role during the

biodecolorization process [69]. In addition, *Geobacter anodireducens*, which were present in B-CSGOM, can exchange more electrons and more rapidly than *Geobacter sulfurreducens* and *Geobacter soli* [70]. Higher content of these bacteria in B-CSGOM operated with 50 mg·L<sup>-1</sup> of DB71 could contribute to get a more stable and better decolorization performance (as shown in **Figure 10a**). Nevertheless, other bacterial species such as *Stenotrophomonas acidaminiphila* [71], *Pseudomonas guangdongensis* [72], *Cupriavidus Metallidurans* [73] were known as a potential decolorizing organism. All they were significantly present in B-CSGOM biofilm and probably took part in the decolorization.

## 4. Conclusions

To the best of our knowledge, this is the first time that a dead-end membrane filtration element with a ceramic-supported graphene oxide layer has been used for anaerobic azo dye decolorization. Different concentrations of GO solution were examined to investigate their formation of CSGOM and subsequent performance over the anaerobic biodecolorization process. Due to the suitable membrane permeability, resistance, and maximum decolorization during the azo dye removal process, CSGOM-1 made from 1 mg·mL<sup>-1</sup> GO solution was identified as the optimal for this integrated compact bioreactor that provides a novel, robust, and effective color removal process.

The conductive surface of the GO membrane enhances faster electron transfer in B-CSGOM if compared to other carbon-based processes reported. In all operating conditions, the dye removal performance for monoazo AO7 was stable and higher than for RB5 and DB71. High decolorization rates of structurally distinct azo dyes (99% for AO7, 96% for RB5, and 92% for

DB71) were achieved at the lowest permeate flux ( $0.05 \text{ L}\cdot\text{m}^{-2}\cdot\text{h}^{-1}$ ) and feed concentration ( $50 \text{ mg}\cdot\text{L}^{-1}$ ).

The microbial community found in the B-CSGOM-1 mainly contained anaerobic *Geobacter* (*Soli*, *Anodireducens*, *Sulfurreducens*) and *Pseudomonas Guangdongensis*; all are recognized to be able to decolorize azo dyes in anaerobic conditions.

### **Acknowledgements:**

This project has been supported by the European Union's Horizon 2020 research and innovation programme under the Marie Skłodowska-Curie grant agreement No. 713679 and by the Universitat Rovira i Virgili (URV), contract 2017MFP-COFUND-18. This article was possible thanks to the grant RTI2018-096467-B-I00 funded by MCIN/AEI/ 10.13039/501100011033 and “ERDF A way of making Europe”. The authors research group is recognized by the Comissionat per a Universitats i Recerca, DIUE de la Generalitat de Catalunya (2017 SGR 396), and supported by the Universitat Rovira i Virgili (2019PFR-URV-33). We would like to thank Dr. Constantí for her contribution to the bacterial community characterization.

### **References:**

1. Jin, X.-C., Liu, G.-Q., Xu, Z.-H., and Tao, W.-Y., Decolorization of a dye industry effluent by *Aspergillus fumigatus* XC6. *Applied Microbiology and Biotechnology*, 2007. 74(1), 239-243.
2. Garcia-Segura, S. and Brillas, E., Combustion of textile monoazo, diazo and triazo dyes by solar photoelectro-Fenton: Decolorization, kinetics and degradation routes. *Applied Catalysis B: Environmental*, 2016. 181, 681-691.

3. Chen, Y., Feng, L., Li, H., Wang, Y., Chen, G., and Zhang, Q., Biodegradation and detoxification of Direct Black G textile dye by a newly isolated thermophilic microflora. *Bioresource Technology*, 2018. 250, 650-657.
4. dos Santos, A. B., Cervantes, F. J., and van Lier, J. B., Review paper on current technologies for decolourisation of textile wastewaters: Perspectives for anaerobic biotechnology. *Bioresource Technology*, 2007. 98(12), 2369-2385.
5. Elshahawy, M. F., Mahmoud, G. A., Raafat, A. I., Ali, A. E.-H., and Soliman, E. s. A., Fabrication of TiO<sub>2</sub> Reduced Graphene Oxide Based Nanocomposites for Effective of Photocatalytic Decolorization of Dye Effluent. *Journal of Inorganic and Organometallic Polymers and Materials*, 2020. 30(7), 2720-2735.
6. Lellis, B., Fávares-Polonio, C. Z., Pamphile, J. A., and Polonio, J. C., Effects of textile dyes on health and the environment and bioremediation potential of living organisms. *Biotechnology Research and Innovation*, 2019. 3(2), 275-290.
7. Prigione, V., Grosso, I., Tigrini, V., Anastasi, A., and Varese, G. C., Fungal Waste-Biomasses as Potential Low-Cost Biosorbents for Decolorization of Textile Wastewaters. *Water*, 2012. 4(4), 770-784.
8. Uddin, M. J., Islam, M. A., Haque, S. A., Hasan, S., Amin, M. S. A., and Rahman, M. M., Preparation of nanostructured TiO<sub>2</sub>-based photocatalyst by controlling the calcining temperature and pH. *International Nano Letters*, 2012. 2(1), 1-10.
9. Hai, F. I., Yamamoto, K., and Fukushi, K., Hybrid Treatment Systems for Dye Wastewater. *Critical Reviews in Environmental Science and Technology*, 2007. 37(4), 315-377.

10. Islam, M. A., Amin, M. S. A., and Hoinkis, J., Optimal design of an activated sludge plant: theoretical analysis. *Applied Water Science*, 2013. 3(2), 375-386.
11. Shannon, M. A., Bohn, P. W., Elimelech, M., Georgiadis, J. G., Mariñas, B. J., and Mayes, A. M., Science and technology for water purification in the coming decades. *Nature*, 2008. 452(7185), 301-310.
12. Goh, K., Jiang, W., Karahan, H. E., Zhai, S., Wei, L., Yu, D., Fane, A. G., Wang, R., and Chen, Y., All-Carbon Nanoarchitectures as High-Performance Separation Membranes with Superior Stability. *Advanced Functional Materials*, 2015. 25(47), 7348-7359.
13. Gin, D. L. and Noble, R. D., Designing the Next Generation of Chemical Separation Membranes. *Science*, 2011. 332(6030), 674.
14. García-Martínez, Y., Chirinos, J., Bengoa, C., Stüber, F., Font, J., Fortuny, A., and Fabregat, A., Fast Aqueous Biodegradation of Highly-Volatile Organic Compounds in a Novel Anaerobic Reaction Setup. *Environments*, 2018. 5, 115.
15. Savant, D. V., Abdul-Rahman, R., and Ranade, D. R., Anaerobic degradation of adsorbable organic halides (AOX) from pulp and paper industry wastewater. *Bioresource Technology*, 2006. 97(9), 1092-1104.
16. van der Zee, F. P. and Villaverde, S., Combined anaerobic-aerobic treatment of azo dyes—A short review of bioreactor studies. *Water Research*, 2005. 39(8), 1425-1440.
17. Thebo, K. H., Qian, X., Zhang, Q., Chen, L., Cheng, H.-M., and Ren, W., Highly stable graphene-oxide-based membranes with superior permeability. *Nature Communications*, 2018. 9(1), 1486.

18. Dreyer, D. R., Park, S., Bielawski, C. W., and Ruoff, R. S., The chemistry of graphene oxide. *Chemical Society Reviews*, 2010. 39(1), 228-240.
19. Ma, J., Ping, D., and Dong, X., Recent Developments of Graphene Oxide-Based Membranes: A Review. *Membranes*, 2017. 7(3), 52.
20. Song, N., Gao, X., Ma, Z., Wang, X., Wei, Y., and Gao, C., A review of graphene-based separation membrane: Materials, characteristics, preparation and applications. *Desalination*, 2018. 437, 59-72.
21. Zhang, P., Gong, J.-L., Zeng, G.-M., Deng, C.-H., Yang, H.-C., Liu, H.-Y., and Huan, S.-Y., Cross-linking to prepare composite graphene oxide-framework membranes with high-flux for dyes and heavy metal ions removal. *Chemical Engineering Journal*, 2017. 322, 657-666.
22. Amin, M. S. A., Stüber, F., Giralt, J., Fortuny, A., Fabregat, A., and Font, J., Comparative Anaerobic Decolorization of Azo Dyes by Carbon-based Membrane Bioreactor. *Water*, 2021. 13(8), 1060.
23. Giménez-Pérez, A., Bikkarolla, S. K., Benson, J., Bengoa, C., Stüber, F., Fortuny, A., Fabregat, A., Font, J., and Papakonstantinou, P., Synthesis of N-doped and non-doped partially oxidised graphene membranes supported over ceramic materials. *Journal of Materials Science*, 2016. 51(18), 8346-8360.
24. Lourenço, N. D., Novais, J. M., and Pinheiro, H. M., Effect of some operational parameters on textile dye biodegradation in a sequential batch reactor. *Journal of Biotechnology*, 2001. 89(2), 163-174.
25. Khehra, M. S., Saini, H. S., Sharma, D. K., Chadha, B. S., and Chimni, S. S., Decolorization of various azo dyes by bacterial consortium. *Dyes and Pigments*, 2005. 67(1), 55-61.

26. El Bouraie, M. and El Din, W. S., Biodegradation of Reactive Black 5 by *Aeromonas hydrophila* strain isolated from dye-contaminated textile wastewater. *Sustainable Environment Research*, 2016. 26(5), 209-216.
27. NorgenBiotek. Soil DNA Isolation Kit. 2016. [cited 2020; Available from: <https://norgenbiotek.com/sites/default/files/resources/Soil-DNA-Isolation-Plus-Kit-Insert-PI64000-1.pdf>]
28. Johra, F. T., Lee, J.-W., and Jung, W.-G., Facile and safe graphene preparation on solution based platform. *Journal of Industrial and Engineering Chemistry*, 2014. 20(5), 2883-2887.
29. Thema, F. T., Moloto, M. J., Dikio, E. D., Nyangiwe, N. N., Kotsedi, L., Maaza, M., and Khenfouch, M., Synthesis and Characterization of Graphene Thin Films by Chemical Reduction of Exfoliated and Intercalated Graphite Oxide. *Journal of Chemistry*, 2013. 2013, 150536.
30. Bikkarolla, S. K., Cumpson, P., Joseph, P., and Papakonstantinou, P., Oxygen reduction reaction by electrochemically reduced graphene oxide. *Faraday Discussions*, 2014. 173(0), 415-428.
31. Ruppert, A. M., Agulhon, P., Grams, J., Wąchała, M., Wojciechowska, J., Świerczyński, D., Cacciaguerra, T., Tanchoux, N., and Quignard, F., Synthesis of TiO<sub>2</sub>-ZrO<sub>2</sub> Mixed Oxides via the Alginate Route: Application in the Ru Catalytic Hydrogenation of Levulinic Acid to Gamma-Valerolactone. *Energies*, 2019. 12(24), 4706.
32. Luo, Q., Cai, Q.-z., Li, X.-w., Pan, Z.-h., Li, Y.-j., Chen, X.-d., and Yan, Q.-s., Preparation and characterization of ZrO<sub>2</sub>/TiO<sub>2</sub> composite photocatalytic film by micro-arc oxidation. *Transactions of Nonferrous Metals Society of China*, 2013. 23(10), 2945-2950.



33. Siu, G. G., Stokes, M. J., and Liu, Y., Variation of fundamental and higher-order Raman spectra of  $ZrO_2$  nanograins with annealing temperature. *Physical Review B*, 1999. 59(4), 3173-3179.
34. Ocaña, M., Garcia-Ramos, J. V., and Serna, C. J., Low-Temperature Nucleation of Rutile Observed by Raman Spectroscopy during Crystallization of  $TiO_2$ . *Journal of the American Ceramic Society*, 1992. 75(7), 2010-2012.
35. Bikkarolla, S. K., Yu, F., Zhou, W., Joseph, P., Cumpson, P., and Papakonstantinou, P., A three-dimensional  $Mn_3O_4$  network supported on a nitrogenated graphene electrocatalyst for efficient oxygen reduction reaction in alkaline media. *Journal of Materials Chemistry A*, 2014. 2(35), 14493-14501.
36. Zou, W., Gu, B., Sun, S., Wang, S., Li, X., Zhao, H., and Yang, P., Preparation of a graphene oxide membrane for air purification. *Materials Research Express*, 2019. 6(10), 105624.
37. Hu, Y., Wei, J., Liang, Y., Zhang, H., Zhang, X., Shen, W., and Wang, H., Zeolitic Imidazolate Framework/Graphene Oxide Hybrid Nanosheets as Seeds for the Growth of Ultrathin Molecular Sieving Membranes. *Angew. Chem. Int. Ed.*, 2016. 55(6), 2048-2052.
38. Wang, L., Zhao, J., Bai, S., Zhao, H., and Zhu, Z., Significant catalytic effects induced by the electronic interactions between carboxyl and hydroxyl group modified carbon nanotube supports and vanadium species for NO reduction with  $NH_3$  at low temperature. *Chemical Engineering Journal*, 2014. 254, 399-409.
39. Oh, Y. J., Yoo, J. J., Kim, Y. I., Yoon, J. K., Yoon, H. N., Kim, J.-H., and Park, S. B., Oxygen functional groups and electrochemical capacitive behavior of incompletely reduced graphene oxides as a thin-

- film electrode of supercapacitor. *Electrochimica Acta*, 2014. 116, 118-128.
40. Vieira, O., Ribeiro, R. S., Pedrosa, M., Lado Ribeiro, A. R., and Silva, A. M. T., Nitrogen-doped reduced graphene oxide – PVDF nanocomposite membrane for persulfate activation and degradation of water organic micropollutants. *Chemical Engineering Journal*, 2020. 402, 126117.
  41. Keck, A., Klein, J., Kudlich, M., Stolz, A., Knackmuss, H. J., and Mattes, R., Reduction of azo dyes by redox mediators originating in the naphthalenesulfonic acid degradation pathway of *Sphingomonas* sp. strain BN6. *Applied and environmental microbiology*, 1997. 63(9), 3684-3690.
  42. Wang, J., Zhang, P., Liang, B., Liu, Y., Xu, T., Wang, L., Cao, B., and Pan, K., Graphene Oxide as an Effective Barrier on a Porous Nanofibrous Membrane for Water Treatment. *ACS Applied Materials & Interfaces*, 2016. 8(9), 6211-6218.
  43. Yi, R., Xia, X., Yang, R., Yu, R., Dai, F., Chen, J., Liu, W., Wu, M., Xu, J., and Chen, L., Selective reduction of epoxy groups in graphene oxide membrane for ultrahigh water permeation. *Carbon*, 2021. 172, 228-235.
  44. Xu, K., Feng, B., Zhou, C., and Huang, A., Synthesis of highly stable graphene oxide membranes on polydopamine functionalized supports for seawater desalination. *Chemical Engineering Science*, 2016. 146, 159-165.
  45. Han, Y., Xu, Z., and Gao, C., Ultrathin Graphene Nanofiltration Membrane for Water Purification. *Advanced Functional Materials*, 2013. 23(29), 3693-3700.

46. Lou, Y., Liu, G., Liu, S., Shen, J., and Jin, W., A facile way to prepare ceramic-supported graphene oxide composite membrane via silane-graft modification. *Applied Surface Science*, 2014. 307, 631-637.
47. Chen, L., Moon, J.-H., Ma, X., Zhang, L., Chen, Q., Chen, L., Peng, R., Si, P., Feng, J., Li, Y., Lou, J., and Ci, L., High performance graphene oxide nanofiltration membrane prepared by electrospaying for wastewater purification. *Carbon*, 2018. 130, 487-494.
48. Ong, S.-A., Toorisaka, E., Hirata, M., and Hano, T., Decolorization of azo dye (Orange II) in a sequential UASB–SBR system. *Separation and Purification Technology*, 2005. 42(3), 297-302.
49. García-Martínez, Y., Bengoa, C., Stüber, F., Fortuny, A., Font, J., and Fabregat, A., Biodegradation of acid orange 7 in an anaerobic–aerobic sequential treatment system. *Chemical Engineering and Processing - Process Intensification*, 2015. 94, 99-104.
50. Mezohegyi, G., Kolodkin, A., Castro, U. I., Bengoa, C., Stuber, F., Font, J., Fabregat, A., and Fortuny, A., Effective Anaerobic Decolorization of Azo Dye Acid Orange 7 in Continuous Upflow Packed-Bed Reactor Using Biological Activated Carbon System. *Industrial & Engineering Chemistry Research*, 2007. 46(21), 6788-92.
51. Ovhall, S. D., Rodrigues, C. S. D., and Madeira, L. M., Photocatalytic wet peroxide assisted degradation of Orange II dye by reduced graphene oxide and zeolites. *Journal of Chemical Technology & Biotechnology*, 2021. 96(2), 349-359.
52. Lee, S., Amaranatha Reddy, D., and Kim, T. K., Well-wrapped reduced graphene oxide nanosheets on Nb<sub>3</sub>O<sub>7</sub>(OH) nanostructures as good electron collectors and transporters for efficient photocatalytic

- degradation of rhodamine B and phenol. *RSC Advances*, 2016. 6(43), 37180-37188.
53. Tan, X. and Rodrigue, D., A Review on Porous Polymeric Membrane Preparation. Part II: Production Techniques with Polyethylene, Polydimethylsiloxane, Polypropylene, Polyimide, and Polytetrafluoroethylene. *Polymers*, 2019. 11(8),
54. Rahimi, M., Aghel, B., Sadeghi, M., and Ahmadi, M., Using Y-shaped microreactor for continuous decolorization of an Azo dye. *Desalination and Water Treatment*, 2014. 52(28-30), 5513-5519.
55. Meitiniarti, I., Soetarto, E. S., Sugiharto, E., and Timotius, K., Optimum concentration of glucose and Orange II for growth and decolorization of Orange II by *Enterococcus faecalis* ID6017 under static culture. *Microb Indones*, 2008. 2, 73-78.
56. Ding, J., Zhang, Y., Quan, X., and Chen, S., Anaerobic biodecolorization of AO7 by a newly isolated Fe (III)-reducing bacterium *Sphingomonas* strain DJ. *Journal of Chemical Technology & Biotechnology*, 2015. 90(1), 158-165.
57. Xiao, X., Li, T.-T., Lu, X.-R., Feng, X.-L., Han, X., Li, W.-W., Li, Q., and Yu, H.-Q., A simple method for assaying anaerobic biodegradation of dyes. *Bioresource Technology*, 2018. 251, 204-209.
58. Franciscon, E., Zille, A., Fantinatti-Garboggini, F., Silva, I. S., Cavaco-Paulo, A., and Durrant, L. R., Microaerophilic-aerobic sequential decolourization/biodegradation of textile azo dyes by a facultative *Klebsiella* sp. strain VN-31. *Process Biochemistry*, 2009. 44(4), 446-452.
59. Ewida, A. Y. I., El-Sesy, M. E., and Abou Zeid, A., Complete degradation of azo dye acid red 337 by *Bacillus megaterium*

- KY848339.1 isolated from textile wastewater. *Water Science*, 2019. 33(1), 154-161.
60. Chen, B.-Y., Chen, S.-Y., and Chang, J.-S., Immobilized cell fixed-bed bioreactor for wastewater decolorization. *Process Biochemistry*, 2005. 40(11), 3434-3440.
61. Popli, S. and Patel, U. D., Destruction of azo dyes by anaerobic-aerobic sequential biological treatment: a review. *International Journal of Environmental Science and Technology*, 2015. 12(1), 405-420.
62. Khan, R., Bhawana, P., and Fulekar, M. H., Microbial decolorization and degradation of synthetic dyes: a review. *Reviews in Environmental Science and Bio/Technology*, 2013. 12(1), 75-97.
63. Hsueh, C.-C. and Chen, B.-Y., Comparative study on reaction selectivity of azo dye decolorization by *Pseudomonas luteola*. *Journal of Hazardous Materials*, 2007. 141(3), 842-849.
64. Solís, M., Solís, A., Pérez, H. I., Manjarrez, N., and Flores, M., Microbial decolouration of azo dyes: A review. *Process Biochemistry*, 2012. 47(12), 1723-1748.
65. Chen, B.-Y., Understanding decolorization characteristics of reactive azo dyes by *Pseudomonas luteola*: toxicity and kinetics. *Process Biochemistry*, 2002. 38(3), 437-446.
66. Garcia-Segura, S., Centellas, F., Arias, C., Garrido, J. A., Rodríguez, R. M., Cabot, P. L., and Brillas, E., Comparative decolorization of monoazo, diazo and triazo dyes by electro-Fenton process. *Electrochimica Acta*, 2011. 58, 303-311.
67. Liu, Y.-N., Zhang, F., Li, J., Li, D.-B., Liu, D.-F., Li, W.-W., and Yu, H.-Q., Exclusive Extracellular Bioreduction of Methyl Orange by Azo

- Reductase-Free *Geobacter sulfurreducens*. *Environmental Science & Technology*, 2017. 51(15), 8616-8623.
68. Fang, Z., Song, H.-L., Cang, N., and Li, X.-N., Performance of microbial fuel cell coupled constructed wetland system for decolorization of azo dye and bioelectricity generation. *Bioresource Technology*, 2013. 144, 165-171.
69. Cai, X., Huang, L., Yang, G., Yu, Z., Wen, J., and Zhou, S., Transcriptomic, Proteomic, and Bioelectrochemical Characterization of an Exoelectrogen *Geobacter soli* Grown with Different Electron Acceptors. *Front Microbiol*, 2018. 9, 1075.
70. Sun, D., Wan, X., Liu, W., Xia, X., Huang, F., Wang, A., Smith, J. A., Dang, Y., and Holmes, D. E., Characterization of the genome from *Geobacter anodireducens*, a strain with enhanced current production in bioelectrochemical systems. *RSC Advances*, 2019. 9(44), 25890-25899.
71. Khehra, M. S., Saini, H. S., Sharma, D. K., Chadha, B. S., and Chimni, S. S., Comparative studies on potential of consortium and constituent pure bacterial isolates to decolorize azo dyes. *Water Research*, 2005. 39(20), 5135-5141.
72. Yang, G., Han, L., Wen, J., and Zhou, S., *Pseudomonas guangdongensis* sp. nov., isolated from an electroactive biofilm, and emended description of the genus *Pseudomonas* Migula 1894. *Int. J. Syst. Evol. Microbiol*, 2013. 63(Pt\_12), 4599-4605.
73. Jaramillo, A. C., Cobas, M., Hormaza, A., and Sanromán, M. Á., Degradation of Adsorbed Azo Dye by Solid-State Fermentation: Improvement of Culture Conditions, a Kinetic Study, and Rotating Drum Bioreactor Performance. *Water, Air, & Soil Pollution*, 2017. 228(6), 205.

## Appendix:

### The properties of feed and permeate quality

The typical properties of the dye-containing feed solution and treated effluent quality are listed in Table A.

**Table A.** Water quality of the feed and treated effluent

Dye	Concentration	TOC		COD	
		Feed	Effluent	Feed	Effluent
AO7	50	86.8	6.4	310	10
	75	96.9	7.9	340	8
	100	102.4	7.8	410	9
RB5	50	56.3	12.2	220	7
	75	70.2	10.3	259	8
	100	88.6	14.3	319	7
DB71	50	53.4	8.6	208	12
	75	83.3	13.4	296	13
	100	110.5	5.7	382	13

\* Unit of the concentration, TOC and COD are in (mg·mL<sup>-1</sup>).

\*\* The TOC and COD measurements were analyzed by Lovibond testing kit vials Vario 420761 and Vario 2420710 respectively.

## Chapter 4. Compact Carbon-based Membrane Reactors for the Intensified Anaerobic Decolorization of Dye Effluents

### Abstract:

Carbon-based membranes integrated with anaerobic biodegradation are presented as a unique wastewater treatment approach to deal with dye effluents. This study explores the scope of Ceramic-supported carbon membrane bioreactors (B-CSCM) and Ceramic-supported graphene oxide membrane bioreactors (B-CSGOM) to decolorize azo dye mixtures (ADM) and other dyes. The ADM mixture was prepared using an equimolar composition of monoazo Acid Orange 7, diazo Reactive Black 5, and triazo Direct Blue 71 dye aqueous solutions. Later, like the ADM experiment, both compact units were investigated for their ability to biodecolorization of Methylene Blue (MB) and Rhodamine B (RhB) dye solutions, which do not belong to the azo family. The obtained outcomes revealed that the conductive surface of the ceramic-supported graphene oxide membrane (CSGOM) resulted in a more efficient and higher color removal of all dye solutions than B-CSCM under a wide feed concentration and permeate flux ranges. The maximum color removal at low feed concentration ( $50 \text{ mg}\cdot\text{L}^{-1}$ ) and permeate flux ( $0.05 \text{ L}\cdot\text{m}^{-2}\cdot\text{h}^{-1}$ ) was 96% for ADM, 98% for MB, and 94% for RhB, whereas it was 89%, 94% and 66%, respectively, for B-CSCM. This suggests that the robust, cost-effective, efficient nanostructures of B-CSGOM can successfully remove diverse azo dye solutions from wastewater better than the B-CSCM does.

---

Amin, M. S. A., Stüber, F., Giral, J., Fortuny, A., Fabregat, A., and Font, J., Compact Carbon-based Membrane Reactors for the Intensified Anaerobic Decolorization of Dye Effluents. *Membranes*, 2022. 12 (2), 174. DOI: 10.3390/membranes12020174 (JIF = 4.106, 21/91 in Polymer Sciences)





## 1. Introduction

Dye molecules are widely applied for coloring in various sectors such as the textile, pulp and paper, leather, drug, food, and cosmetics industries. Their use has increased rapidly in recent decades, resulting in massive discharges of toxic, mutagenic, carcinogenic, and mostly recalcitrant dye effluents into the environment [1]. The presence of this dyestuff waste in industrial effluent has a detrimental effect on the ecosystem, the human body, and animals [2]. The dyed waste turns the color of the water into an unpleasant hue that negatively impacts the photosynthesis process and the amount of dissolved oxygen in aquatic life [3,4]. Moreover, dye-containing wastewater makes water sources unsuitable for drinking and for household and industrial purposes [5]. As a result, developing a simple, economical, and sustainable wastewater treatment for removing dye-containing effluent from the environment is considered a critical issue.

At present, several physical, chemical, and biological wastewater treatment methods such as adsorption, photocatalysis, coagulation, electrocoagulation, advanced oxidation, ozonation, filtration processes and membrane bioreactors have been examined extensively [6-8]. Since most dyestuff molecules are chemically stable and notably soluble in water, it is difficult to remove them using the traditional treatment process [9,10]. In addition, most of these treatment procedures become less appealing due to the higher installation and operating cost, moderate efficiency, duration of the treatment and evolving secondary pollution [11,12]. What is more, this secondary solid waste might be toxic in nature and poses additional environmental problems associated with sludge treatment and disposal. The dye removal process using a membrane is one of the most convenient and cost-effective applications. Membrane units are capable of overcoming some

of the previously described limits, such as reduced equipment size, lower energy usage and capital costs [13,14]. Additionally, they may eliminate the need for chemicals, making them an environmentally friendly and accessible choice. Among the membrane separation processes, ultrafiltration and nanofiltration are the most used for dye removal; however, fouling limits the membrane flux as well as its performance [11]. In recent years, reverse osmosis (RO) filtration followed by ultrafiltration or nanofiltration has proven effective in removing dye molecules; nevertheless, installation cost remains a significant challenge for its wide application. Electrodialysis and ion-exchange membranes, on the other hand, are also tested for the treatment of water and wastewater.

Due to the effective performance when addressing suspended solids, color and high Biochemical Oxygen Demand (BOD) loads, biological treatment processes are widely used in Wastewater Treatment Plants (WWTPs). These processes can occur in the presence or absence of oxygen (aerobic and anaerobic conditions, respectively). Compared to aerobic treatment, anaerobic biodegradation is a simple and less expensive azo dye decolorization approach [15]. However, in this process, the electron transport between the microorganisms and the dye molecules become the limiting steps that reduce the biodegradability and increase the residence time. Therefore, when searching for an environmentally friendly treatment process for decolorizing dyes from wastewater, it seems that the combination of anaerobic biodegradation and membrane separation processes would be perfectly complementary.

Most of the materials employed for membrane separation used in wastewater treatment are essentially non-conductive in nature [16]. However, a faster electron transfer mechanism in the anaerobic dye reduction is the crux

for an effective treatment method [17]. Daniela et al. [18,19] reported that conductive graphene-based composite ion-change membranes could be used for wastewater treatment purposes. Nonetheless, they may not be feasible in terms of cost, which could cause incompetence for large-scale operations with practical applications. Therefore, besides the good mechanical and chemical stability, carbon-based membranes exhibit a conductive layer on the top of their surface that can be integrated with the anaerobic process for dye decolorization [20,21]. Carbon membranes are usually derived from the carbonization of organic polymer materials such as polyimide, cellulose, melamine, polyethersulfone, polyacrylonitrile and the like, in an inert atmosphere [22,23]. A nanostructured carbon membrane for wastewater treatment shows thermally and electrically conductive properties synthesized by graphitic oxide and carbon nanotubes [24,25]. In our previous work, we synthesized two types of ceramic-supported carbon membranes [21,26]. One of the membranes was fabricated by the carbonization of Matrimid 5218 and another one by the vacuum filtration of exfoliated graphene oxide solution. Notably, both the Ceramic-supported Matrimid Membrane (CSCM) and the Ceramic-supported Graphene Oxide Membrane (CSGOM) displayed good electron conductivity that integrated the membrane separation with the anaerobic biodegradation to achieve a successful azo dye decolorization process.

To the best of our knowledge, it is the first time that the removal of azo dye mixture (ADM), phenothiazine Methylene Blue (MB) and sticky fluorescence Rhodamine B (RhB) solutions were conducted in an integrated membrane filtration with an anaerobic biodegradation process. For this, two compact membrane bioreactors using carbonized Matrimid, and graphene oxide membranes were studied to decolorize the dye molecules. These two

carbon-based membranes were compared to select a more suitable configuration for the anaerobic biodecolorization of azo dye wastewater. Throughout the experiments, the decolorization rate of dye solution was examined under several feed concentrations and permeate fluxes.

## 2. Materials and Methods

### 2.1 Fabrication of Ceramic-supported Carbon Membrane

The carbon-based membranes were synthesized from several membrane precursors to compare their suitability for the biodecolorization of dyestuff molecules. For this purpose, two membranes were prepared over porous ceramic support ( $ZrO_2$ - $TiO_2$  microfiltration flat element, diameter: 47 mm; thickness: 2.5 mm; molecular weight cut-off:  $50 \text{ kg}\cdot\text{mol}^{-1}$ ; TAMI Industries, Nyons, France) using either a 10% wt. of Matrimid 5218 (Huntsman Advanced Materials, The Woodlands, TX, USA) in NMP (1-methyl-2-pyrrolidone, Sigma Aldrich, ref. 328634, Madrid, Spain), or a  $1 \text{ mg}\cdot\text{mL}^{-1}$  graphene oxide solution, respectively. In CSCM, the polymeric solution was deposited on the support by a two-step spin coating method. After 24 h of drying, the carbon membrane was finally formed by carbonizing it at  $800 \text{ }^\circ\text{C}$  under an inert atmosphere [21]. For the other carbon-based membrane (CSGOM), the exfoliated graphene oxide solution was prepared by the modified Hummer method using  $20 \text{ }\mu\text{m}$  of pristine graphite powder (Sigma Aldrich, ref. 282863, Madrid, Spain) [27]. The porous graphene oxide layer was deposited over the ceramic support by vacuum-assisted filtration of 3-5 mL of  $1 \text{ mg}\cdot\text{mL}^{-1}$  graphene oxide solution using the filtration cell [26]. The desired thickness of the uniform GO layer was formed within 15 min of vacuum filtration. The membrane was subsequently dried at  $80 \text{ }^\circ\text{C}$  for 24 h and subsequently  $100 \text{ }^\circ\text{C}$  for 72 h to get a stable and robust CSGOM.

## 2.2 Experimental Set-up for Anaerobic Biodegradation

Anaerobic biodecolorization of the dyestuff molecule by carbon-based membrane bioreactor (B-CSCM and B-CSGOM) process is depicted in Figure 1. Nitrogen gas (Purity > 99.99 %, Linde, Valencia, Spain) flowed in the feed tank to pump the feed solution to the two membrane bioreactors and modulated the permeate flux by changing the transmembrane pressure (TMP). In addition, it was used to maintain the anaerobic conditions throughout the decolorization process. Thus, the entire system achieves a negative redox potential that forces the suitable conditions for the action of anaerobic microorganisms [28]. The feed solution was composed of dye, Sodium Acetate (Sigma Aldrich, ref. 110191, Madrid, Spain), and basal media (1 mL from each set). The concentration of Sodium acetate was three times (1:3 molar ratio) higher than the dye in each feed solution. Depending on the test, three different types of feed solutions were used as synthetic feed. The first feed was an equimolar solution of monoazo AO7 (ACROS Organics, ref. 416561000, Geel, Belgium), diazo RB5 (Sigma Aldrich, ref. 306452, Madrid, Spain), and triazo DB71 (Sigma Aldrich, ref. 212407, Madrid, Spain). The second and third were the solution of Methylene Blue (Fluka, ref. 66720, Madrid, Spain) and Rhodamine B (Fluka, ref. R6626, Madrid, Spain), respectively. On the other hand, were basal media with microelements ( $\text{mg}\cdot\text{L}^{-1}$ ) composed by  $\text{MnSO}_4\cdot\text{H}_2\text{O}$  (0.155),  $\text{CuSO}_4\cdot 5\text{H}_2\text{O}$  (0.285),  $\text{ZnSO}_4\cdot 7\text{H}_2\text{O}$  (0.46),  $\text{CoCl}_2\cdot 6\text{H}_2\text{O}$  (0.26),  $(\text{NH}_4)_6\text{Mo}_7\text{O}_{24}$  (0.285),  $\text{K}_2\text{HPO}_4$  (21.75),  $\text{Na}_2\text{HPO}_4\cdot 2\text{H}_2\text{O}$  (33.40),  $\text{KH}_2\text{PO}_4$  (8.50),  $\text{FeCl}_3\cdot 6\text{H}_2\text{O}$  (29.06),  $\text{CaCl}_2$  (13.48)  $\text{MgSO}_4\cdot 7\text{H}_2\text{O}$  (15.2),  $\text{NH}_4\text{Cl}$  (190.90). All the analytical grade chemicals were purchased from Sigma Aldrich (Madrid, Spain) and dissolved in Milli-Q water (Millipore Milli-Q system, Molsheim, France).

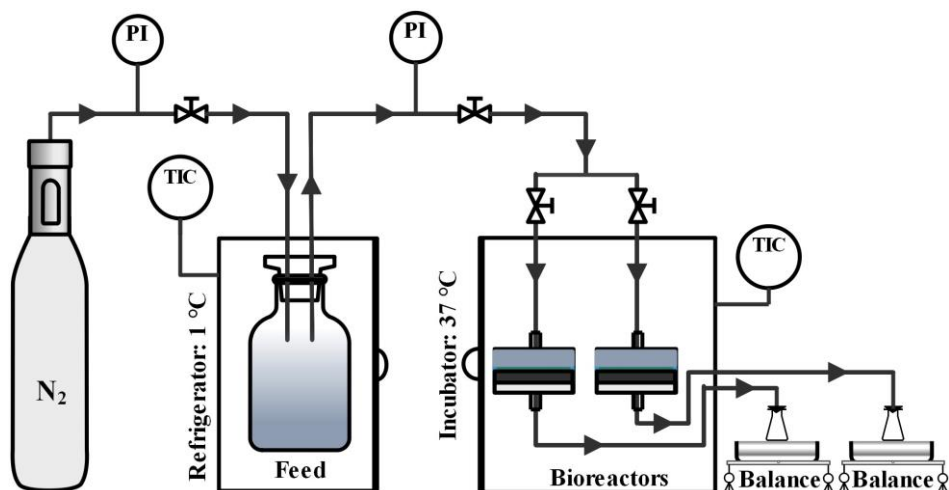


**Figure 1.** Experimental set-up for anaerobic decolorization of dye molecules by CSCM and CSGOM.

The temperature has a significant impact on decolorization performance and microbial population in this compact membrane bioreactor. Thus, the feed solution was kept at 1 °C to prevent microbial growth on the feed tank and maintain its actual dye and co-substrate (Sodium Acetate) composition. After placing 5 mL of secondary anaerobic sludge (collected from municipal WWTP Reus, Spain) over the carbon-based membrane, the membrane bioreactor, which was a direct-filtration cell (TAMI Industries, Nyons, France), was sealed tightly and then, operated at  $37 \pm 1$  °C under constant flux dead-end filtration mode. At this temperature, the microbial strains are able to give the best biodecolorization rate [29].

### 2.3 Membrane Characterization

The Combined Focused Ion Beam-Scanning Electron Microscope (FIB-SEM, Scios 2 Dual Beam, Thermo Scientific, MA, USA) examined and compared the surface, cross-section, and elemental composition of both CSCM and CSGOM. Atomic Force Microscope (AFM) using Molecular Imaging Pico Plus 2500 (Bid Service, NJ, USA) examined the membrane

surface and conductivity. Further, chemical structures and microstructures of the carbon-based membranes were analyzed, respectively, through Fourier Transform Infrared (FT-IR) spectrophotometer (FT/IR-6700, JASCO, Tokyo, Japan) and X-ray Diffraction (XRD) diffractometer (Siemens D5000, Germany under the  $\text{CuK}\alpha$  wavelength of  $1.54056 \text{ \AA}$  at 40 kV and 30 mA), respectively.

The filtration performance was assessed by means of membrane flux, pure water permeance (PWP), hydraulic resistance, and calculated using equations 1-3,

$$J = \frac{\Delta V}{\Delta t} \cdot \frac{1}{A} \quad (1)$$

$$\text{PWP} = \frac{J}{\Delta P} \quad (2)$$

$$H_R = \frac{\Delta P}{\mu} \cdot \frac{1}{J} \quad (3)$$

where  $J$  is the permeate flux ( $\text{L} \cdot \text{m}^{-2} \cdot \text{h}^{-1}$ ),  $V$  is the volume of permeate (L),  $t$  the filtration time (h),  $A$  the membrane area ( $\text{m}^2$ ),  $H_R$  is the hydraulic resistance ( $\text{m}^{-1}$ ),  $\Delta P$  is the transmembrane pressure (bar), and  $\mu$  is the viscosity of the permeate corrected to the experimental temperature ( $\text{Pa} \cdot \text{s}$ ).

The decolorization ( $D$ ) during the anaerobic bioreduction of the azo dye was measured using UV/VIS4000n Spectrophotometers (DINKO Instruments, Barcelona, Spain) and computed by equation 4,

$$D (\%) = \frac{A_0 - A}{A_0} \times 100 \quad (4)$$

$A_0$  and  $A$  are the absorbance of feed and treated samples during the biodegradation process, respectively.



### 3. Result and Discussion

#### 3.1 Structural and Chemical Characterization of Ceramic-supported Carbon Membranes

The FTIR spectrum of carbon-based membranes shown in Figure 2 helps to reveal the presence of diverse functional groups, including carboxylic, hydroxyl, epoxy, and imide, that also exhibited the appropriate molecular orientation. For the polymeric membrane and CSCM, before and after the carbonization of the membrane, the structural changes were observed through the transformation of the polymeric chains to the carbon membrane. The representative bands of the polymeric membrane (Matrimid 5218) were obtained at 1714 and 1360  $\text{cm}^{-1}$ , indicating the stretching of C=O and C-N groups [30]. The aromatic C=C bending vibration, C-N-C transverse stretching, and presence of C-H aromatic monosubstituted benzene were found at 1501, 1089, and 718  $\text{cm}^{-1}$ , respectively [31]. In the case of CSCM, compared to the initial polymeric membrane, no apparent bands were observed after its carbonization under a nitrogen atmosphere. This fact was similar to that observed by Sazali et al. [32], where they synthesized the Matrimid-based carbon membrane at different pyrolysis temperatures and polymeric compositions.

The peaks for numerous oxygen-containing functional groups, such as O-H, C=O, and C-O, were visible in the CSGOM spectra, which agrees well with earlier research and illustrates that the graphite exists mostly oxidized into GO [33,34]. In summary, the broad peak at 3370  $\text{cm}^{-1}$  confirms the presence of hydroxyl groups on the GO layer of CSGOM while the peak at 1725  $\text{cm}^{-1}$  indicates the C=O stretching vibration of carboxylic acid positioned at the edge of the GO structure. The absorption peaks at 1620,

1223, and 1055  $\text{cm}^{-1}$ , respectively, were obtained due to the aromatic C=C stretching, epoxy, and alkoxy C-O stretching vibration.

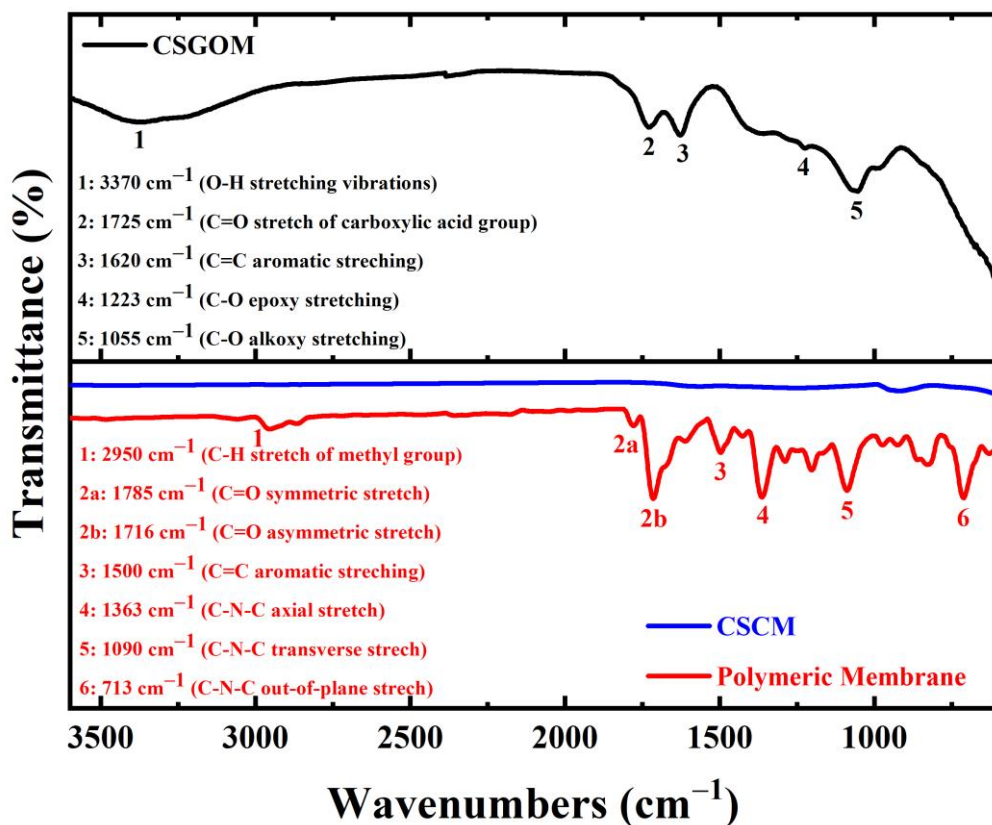


**Figure 2.** FTIR spectra of the polymeric membrane, CSCM and CSGOM (CSCM: 10% wt. Matrimid and CSGOM: 1  $\text{mg}\cdot\text{L}^{-1}$  GO solution).

The microstructure and interlayer distance of the ceramic support and ceramic-supported carbon-based membranes were determined using XRD diffraction, as shown in Figure 3. In CS, CSCM and CSGOM diffractograms, identical peaks were obtained at  $2\theta = 28, 36, 39, 41, 43, 55$  and  $57^\circ$  due to the presence of rutile,  $\text{TiO}_2$  [35], and  $2\theta = 30, 35, 50, 60,$  and  $63^\circ$  own to the presence of tetragonal  $\text{ZrO}_2$  [36], which is consistent with the information

provided by the supplier of the ceramic support, consisting of layers of  $ZrO_2$  and  $TiO_2$ .

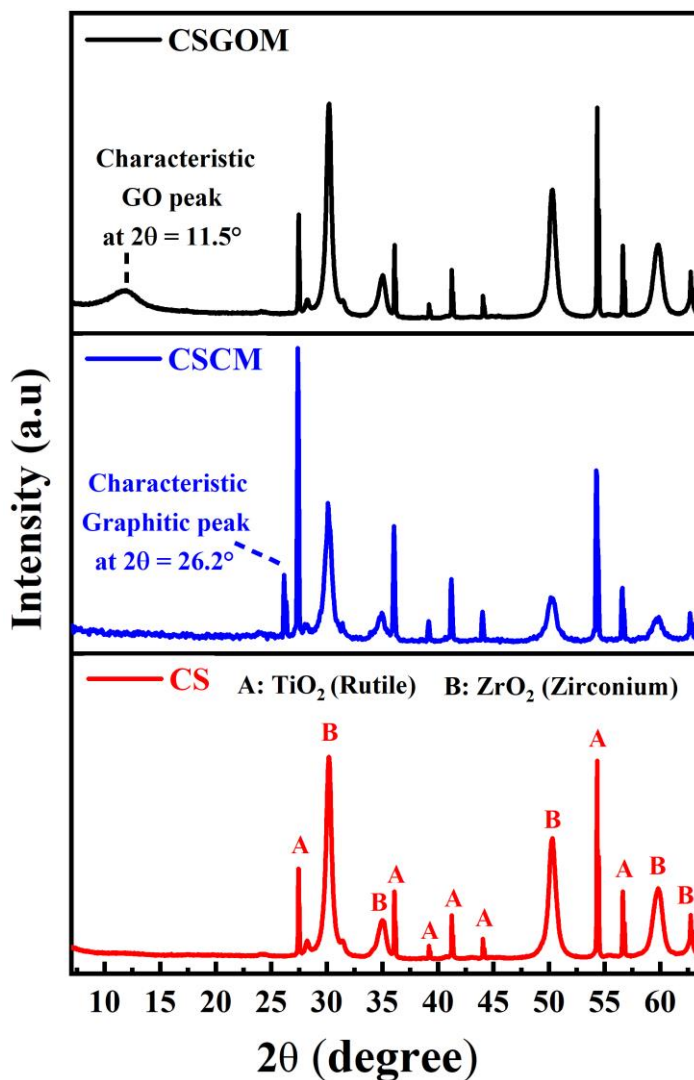


**Figure 3.** X-ray diffractogram of the ceramic support (CS) and the ceramic-supported carbon-based membrane (CSCM: 10% wt. Matrimid and CSGOM:  $1 \text{ mg}\cdot\text{L}^{-1}$  GO solution).

Furthermore, the diffraction peak located at  $2\theta = 26.2^\circ$  is an indication that the CSCM consisted of highly graphitized carbon with an interlayer distance of  $3.6 \text{ \AA}$ , which corresponds to the (002) plane of crystalline graphite [37]. Besides, the GO crystal plane (001) was clearly visible at  $2\theta = 11.5^\circ$  (as shown in CSGOM diffractogram in Figure 3) with the interlayer spacing of  $7.3 \text{ \AA}$  that was larger than graphite atomic spacing [38]. The absence of a peak at  $26.2^\circ$  means that all graphite molecules were completely oxidized to generate graphene oxide, and no graphitic contaminations were obtained [39]. This was expected as the oxygen-containing groups were attached to each layer edge to raise the spacing between the sheets, which aided GO exfoliation in the aqueous medium and increased the hydrophilicity [40].

The surface and cross-sectional views of the carbon-based membranes were studied using FESEM, which shows crucial morphological features for their application in the anaerobic decolorization process. As illustrated in Figures 4(a-b), the top view of these carbon membranes clearly exhibits a defect-free smooth and porous carbon layer that was quite similar to previous studies [21,26]. The pore size of the resulting carbon membrane differed between the two alternatives. The difference between both membranes was the pore size and thickness of the respective synthesized carbon layers. The average pore size was found to be  $35 \text{ \mu m}$  for CSCM and  $20 \text{ \mu m}$  for CSGOM. On the other hand, the thickness was, respectively,  $0.88$  and  $1.78 \text{ \mu m}$  for CSCM and CSGOM, as depicted in Figure 4 (c-d). The thinner layer in CSCM was due to the optimal spin coating method and high carbonization temperature maintained during the preparation of this membrane [41]. For the same reason, FESEM-EDX analysis observed higher carbon content in CSCM (64%) than that of the CSGOM (49%).

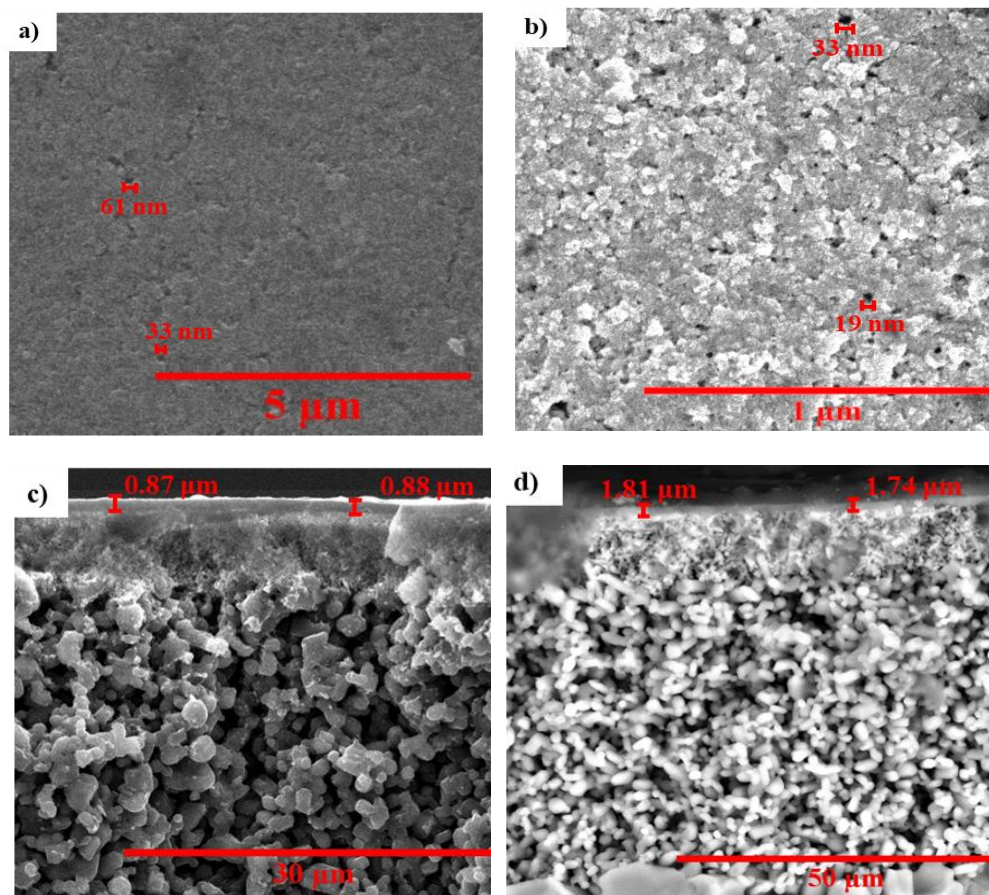


**Figure 4.** FESEM micrographs on the surface of a-b) CSCM and CSGOM, and c-d) the cross section of CSCM and CSGOM (CSCM: 10% wt. Matrimid and CSGOM: 1 mg·L<sup>-1</sup> GO solution).

The membrane surface roughness and conductivity were further investigated using AFM (at a random area of 5x5 μm<sup>2</sup>) and CSAFM (current sensing atomic microscopy) images. The 3D topography and current profile of these experiments are shown in Figure 5(a-d). The root-mean-square (RMS) roughness of the carbon layer attained for the CSGOM surface was at 80.12 nm, while the CSCM exhibited the lowest surface roughness at 32.94 nm. This fact was attributed to the less porous structure of the carbonized

Matrimid membrane, as shown by SEM images. This means a less porous structure but represents a smoother surface. In Figure 5(c-d), the current distribution of the surface of the membrane was compared, and the local conductance on the graphene oxide membrane surfaces was found better than that of the CSCM. However, the rough conductive GO surfaces could improve the biodecolorization because of the more vigorous attachment of the biofilm to the surface and the intensified electron shuttle mechanism [42,43].

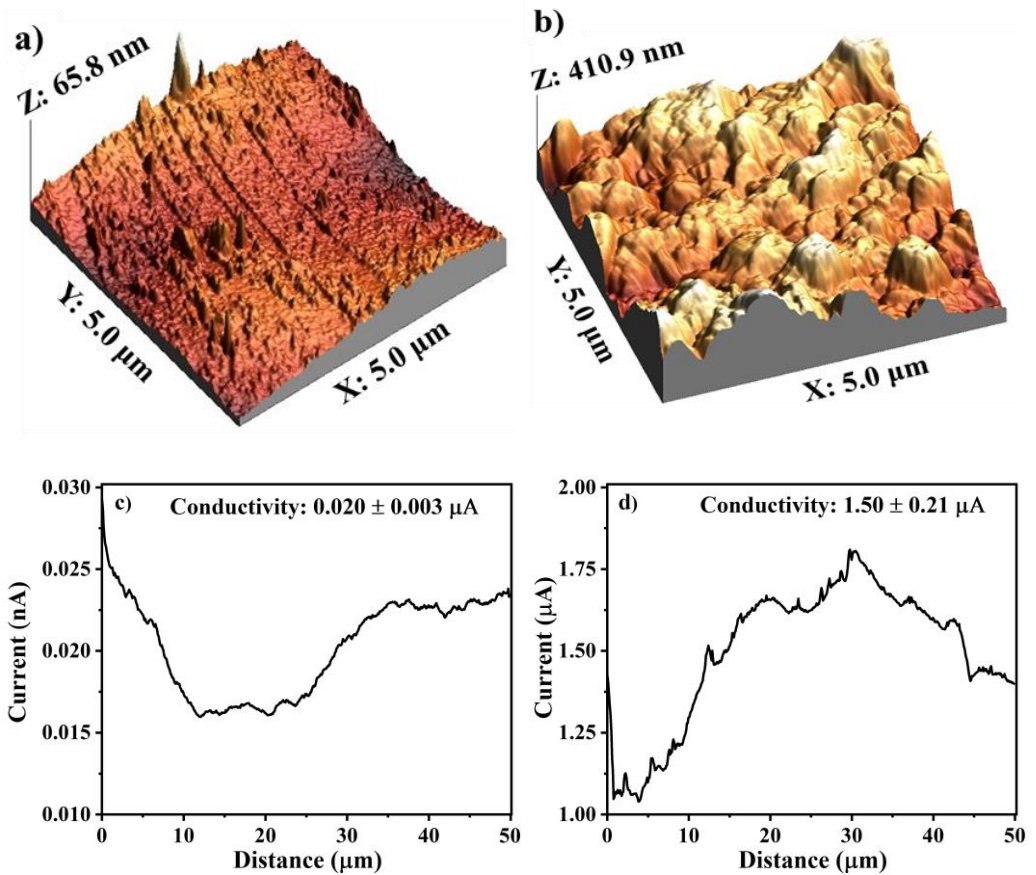


**Figure 5.** AFM images of CSCM and CSGOM a-b) 3D Topography and c-d) current distribution.

Therefore, it is possible to conclude from the above results that the compact membrane bioreactor made with a graphene oxide layer may be a more suitable solution for the dye bioreduction method.

### 3.2 Impact of the Carbonaceous Layer on Flux and Resistance

The effect of membrane precursors (Matrimid 5218 or exfoliated GO solution) on filtration parameters such as permeate flux, pure water permeance (PWP), and hydraulic resistance ( $H_R$ ) was examined by as of experiments. Figure 6 displays the results of this comparative study, where the units were either the ceramic support (CS), CSCM (produced with 10% wt. of Matrimid solution), and CSGOM (made with  $1 \text{ mg}\cdot\text{mL}^{-1}$  of exfoliated GO solution). A simple comparison shows that the ceramic support gives the maximum permeate flux,  $62.3 \text{ L}\cdot\text{m}^{-2}\cdot\text{h}^{-1}$ , and  $77.8 \text{ L}\cdot\text{m}^{-2}\cdot\text{h}^{-1}\cdot\text{bar}^{-1}$  of PWP. At the same range of operating conditions, the lowest water flux ( $10.2 \text{ L}\cdot\text{m}^{-2}\cdot\text{h}^{-1}$ ) and PWP ( $12.9 \text{ L}\cdot\text{m}^{-2}\cdot\text{h}^{-1}\cdot\text{bar}^{-1}$ ) were observed for CSGOM, which is less than 84% and 50%, respectively, than for CS and CSCM. In addition, a bar chart depicting the hydraulic resistance of the CS, CSCM, and CSGOM is shown at the bottom of Figure 6. Since both variables are directly related, CS displayed the lowest hydraulic resistance ( $5.25 \pm 0.1 \times 10^{12} \text{ m}^{-1}$ ), while CSGOM has the highest.

Membrane thickness and pore size greatly influence the membrane performance by altering the permeate flux and hydraulic resistance [44]. In this study, in addition to the  $\text{TiO}_2\text{-ZrO}_2$  layers of the ceramic support, we deposited an additional carbon layer on top of the support in each case. As a result, the membrane flux drops as well as the hydraulic resistance rises. Comparing the FESEM images of the two membranes synthesized over the ceramic support, the thickness of the defect-free carbon layer in CSCM was



found to be smaller than that of CSGOM; on the contrary, the average pore size was relatively greater.

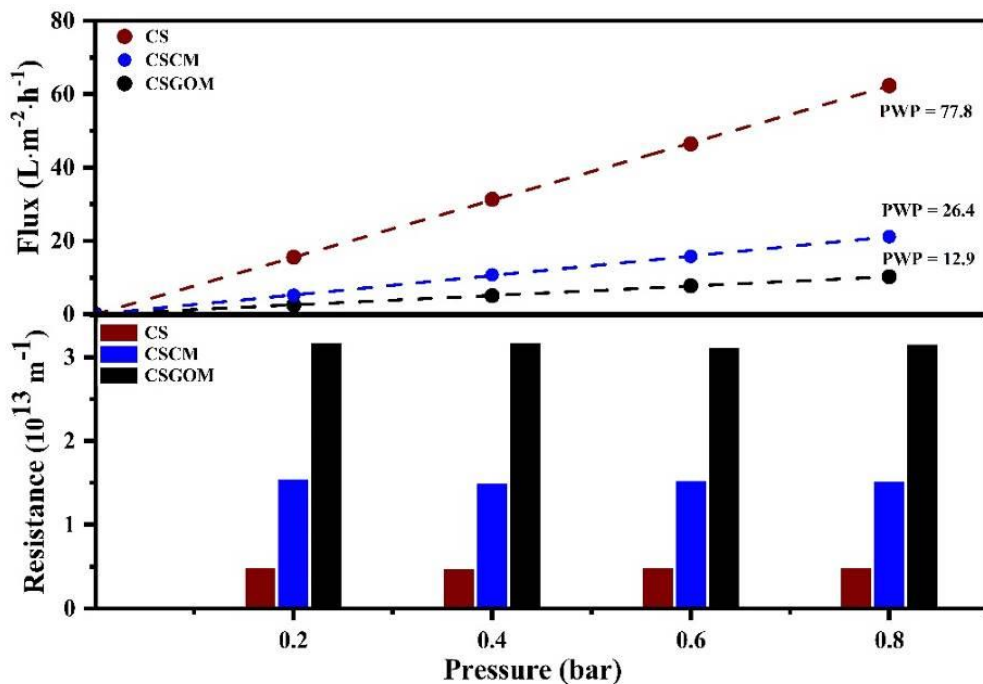


**Figure 6.** Variation of pure water flux, permeance, and resistance of CS, CSCM and CSGOM at 25 °C. CSCM: 10% wt. of Matrimid and CSGOM: 1 mg·mL<sup>-1</sup> of GO.

Thus, the initial PWP (77.8 L·m<sup>-2</sup>·h<sup>-1</sup>·bar<sup>-1</sup>) and resistance (5.25±0.1×10<sup>12</sup> m<sup>-1</sup>) of the porous ceramic support changed after deposition of the carbonaceous layer. Due to the relatively larger thickness and smaller pore size of CSGOM than CSCM, PWP was recorded at 12.9 L·m<sup>-2</sup>·h<sup>-1</sup>·bar<sup>-1</sup>; on the other hand, in CSCM, it was 26.4 L·m<sup>-2</sup>·h<sup>-1</sup>·bar<sup>-1</sup>. Similarly, the hydraulic resistance rises to 1.50 ± 0.2×10<sup>13</sup> m<sup>-1</sup> in CSCM and 3.15 ± 0.3×10<sup>13</sup> m<sup>-1</sup> in CSGOM.



These results align with the trends observed by Sazali et al. [45], which indicated that the high carbonization temperature and precursors concentration were the keys for fabricating a thin carbon-based membrane. In the case of CSGOM, the membrane was prepared by vacuum-assisted filtration of an exfoliated GO solution with a concentration of  $1 \text{ mg}\cdot\text{mL}^{-1}$ . The viscosity of the GO solution is much lower than that of Matrimid 5218, so it easily filled the internal ceramic support pore (GO-ZrO<sub>2</sub> region) and then formed the mono or multilayer of GO on the top of CS. Due to the internal blockage or filling of the support pore, the hydraulic resistance and permeability through the membrane were usually disrupted [46].

Our recent work demonstrated the selection of the most appropriate precursor is critical to achieving a porous, permeable carbon-based membrane [21, 26]. In CSGOM, this is essential because the carbon layer thickness on the membrane surface increases as the GO concentration increases, resulting in a decrease in membrane flux [47]. Again, when the membrane is derived from a high precursor concentration ( $>3 \text{ mg}\cdot\text{mL}^{-1}$ ), the GO layer can easily peel away from the surface or causes swelling of the layer [48]. On the other hand, GO membrane synthesized with low GO solution ( $0.05\text{-}0.5 \text{ mg}\cdot\text{mL}^{-1}$ ) provide low carbon content that was not suitable for anaerobic biodecolorization application. A thicker and less porous GO layer was required to establish a defect-free GO layer with high carbon content and flux on CSGOM. Thus, compared to the CSGOM, pure water flux and permeance values were higher in CSCM. Since permeate flux and hydraulic resistance are interdependent, higher hydraulic resistance was observed in the CSGOM due to its less porosity and formation of GO-ZrO<sub>2</sub> layers inside the ceramic support.

### 3.3 Role of the Membrane Precursors on Anaerobic Decolorization of Dye Molecules

The combined effect of the filtration and anaerobic bioreduction of dye solutions in compact bioreactors was evaluated using carbon-based membranes (both CSCM and CSGOM) and ceramic support (CS). This study used  $50 \text{ mg}\cdot\text{L}^{-1}$  azo dye mixture (ADM) of feed solution that contained an equimolar mixture of the monoazo AO7, diazo RB5, and triazo DB71. All reactors were operated in dead-end filtration mode and maintained with a constant permeate flux of  $0.05 \text{ L}\cdot\text{m}^{-2}\cdot\text{h}^{-1}$ . These concentrations in the feed solution were selected because they fall within the range owing to dye residues in industrial or textile wastewater, which is generally found between 10 and  $50 \text{ mg}\cdot\text{L}^{-1}$  [49]. In this test, the reactors operated with microorganisms are referred to as B-CS, B-CSCM, and B-CSGOM; in turn, reactors without microorganisms are labeled R-CS, R-CSCM, and R-CSGOM, respectively. As illustrated in Figure 7, the simultaneous presence of the carbon layer and microorganisms has a significant effect on the bioreduction of ADM during the decolorization process. Both compact carbon-based membrane bioreactors, B-CSCM and B-CSGOM, gave very high decolorization rates under anaerobic conditions, the B-CSGOM achieving a maximum of 99% of dye removal rate.

At the start of the anaerobic decolorization process, up to 12 hours, all the reactors accomplished more than 75% of the dye removal rate. Unlike the two carbon-based membrane bioreactors, the decolorization rate for all the other reactors progressively declined; it is noteworthy that, after 48 hours of operation, the color removal for B-CS and R-CS dropped to almost zero. This strongly suggests that the dye was initially removed due to adsorption by the porous support and carbon membrane but, once saturated, they were not able anymore to remove color. Even though B-CS was used in conjunction with

microorganisms, the color removal was negligible, too. It seems that the microorganisms were washed out from the reactor by the permeate flow because of the lack of nano-sized structure or support suitable to form a stable biofilm, as it happens in the other carbon-based membranes.

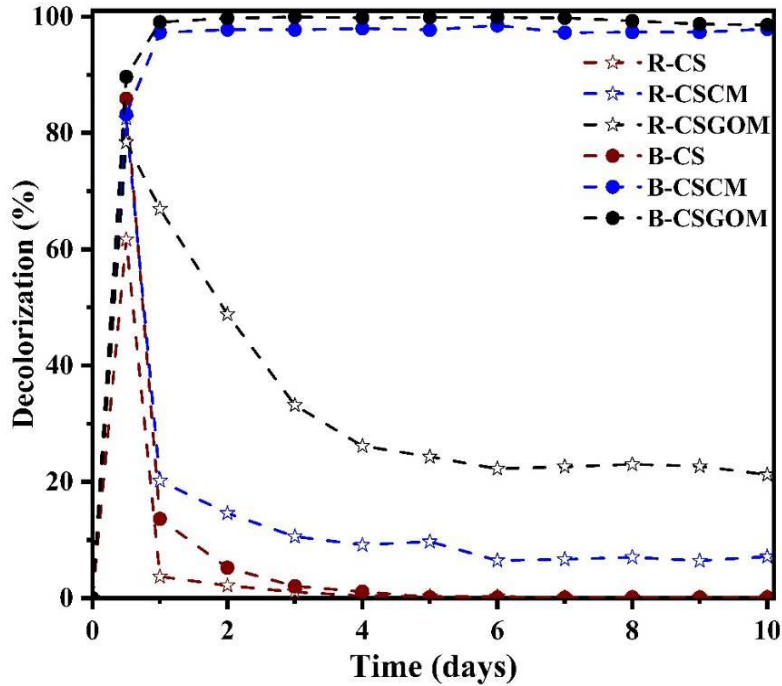


**Figure 7.** Decolorization of azo dye mixture in CS, CSCM and CSGOM reactors, and CS, CSCM and CSGOM bioreactors. Flux =  $0.05 \text{ L}\cdot\text{m}^{-2}\cdot\text{h}^{-1}$ ,  $[\text{ADM}]_0 = 50 \text{ mg}\cdot\text{L}^{-1}$  and  $T = 37 \text{ }^\circ\text{C}$ .

For CSGOM and CSCM, because of having a nanoporous carbon layer on the top, decolorization gradually decreased to reach a stable 20% for R-CSGOM and 6% for R-CSCM. In this case, the pore size of the carbonaceous layers was able to reject partially the dyes, although both the adsorption site and pore size decreased with the time on stream [50]. The highest decolorization, 99%, was observed for the bioreactor operated with CSGOM, while 97% of color removal was observed for B-CSCM. Overall, it means

that the carbon layer derived from the carbonization of the Matrimid, and graphene oxide has no adverse effect on bacterial growth for the successive formation of active biofilm [51-53]. As with the results obtained from the earlier ceramic-supported carbon-based membrane bioreactor experiments [21,26], these membranes perform triple roles in anaerobic dye decolorization. The carbon membrane served as biofilm support, redox mediator, and pollutant immobilizer that also retain the degradation products. In this way, the one-pass compact carbon-based membrane bioreactor has shown enhanced decolorization performance for azo dye mixtures.

Following each successful biodecolorization experiment, the membrane was cleaned using Milli-Q water backflushing. As a result, the initial permeate flux was regained without modifying the membrane properties, so it can be reused for subsequent color removal operation without any additional conditioning.

### **3.4 Biodecolorization Performance of CSCM and CSGOM**

After demonstration of stable and excellent performance by the carbon-based membrane bioreactors, the B-CSCM and B-CSGOM were investigated for long-term operation for the biodecolorization of structurally different dyes. Azo dye mixture, thiazine MB, and fluoresce RhB dye solutions were examined under various permeate fluxes and feed concentrations. Initially, all compact reactors were run with  $50 \text{ mg}\cdot\text{L}^{-1}$  of dye solution at a permeate flux of  $0.05 \text{ L}\cdot\text{m}^{-2}\cdot\text{h}^{-1}$ . After obtaining consistent decolorization, the system was left to operate for 10 days; then, the flow rate was first increased to  $0.075 \text{ L}\cdot\text{m}^{-2}\cdot\text{h}^{-1}$  and, finally, at 20 days, up to  $0.1 \text{ L}\cdot\text{m}^{-2}\cdot\text{h}^{-1}$ . Similar procedures were repeated for compact bioreactors consisting of  $75$  and  $100 \text{ mg}\cdot\text{L}^{-1}$  of feed solution operated for the anaerobic decolorization of azo dyes.

Figure 8 collects all the decolorization performance data. Besides the influence of the feed concentration and permeate flow, it is shown that the biodecolorization effectiveness of different dye solutions widely depends on the number and nature of azo bonds and functional groups present in the dye structure. Apart from this, membrane properties, such as membrane precursors, pore size, and thickness, also played a relevant role in decolorization performance. It must be noted that all the dye decolorization removals decreased when feed concentration and permeate flux increased. In all experiments, the highest decolorization was achieved for the lowest feed concentration and permeate flow. Comparing again the performance of the bioreactors containing carbon-based membranes, B-CSGOM exhibits greater decolorization under all feed concentrations and fluxes. According to Figure 8, the maximum decolorization in the B-CSGOM system was 96%, 98%, and 94% for ADM, MB, and RhB, respectively, obtained for 50 mg·L<sup>-1</sup> of dye solutions at a permeate flux of 0.05 L·m<sup>-2</sup>·h<sup>-1</sup>). On the contrary, the lowest decolorization was in B-CSCM experiments using 100 mg·L<sup>-1</sup> feed solutions and 0.10 L·m<sup>-2</sup>·h<sup>-1</sup> flow, which only achieved 84% for ADM, 84% for MB, and 22% for RhB.

In terms of lifetime, the B-CSGOM was more stable in all operating situations and produced better results. This indicates that the properties of the membrane precursor were responsible for most of the dye removal capacity in the carbon-based membrane bioreactors operated under identical conditions. Thus, in addition to providing the required energy for microbial growth, it works as a redox mediator by enhancing the electron transfer to the azo, hydrogen, and other bonds of the dye molecule, thereby breaking the bonds to achieve the effective biodegradation of dyes [17].

## 4. Compact Carbon-based Membrane Reactors for the Intensified Anaerobic Decolorization of Dye effluents

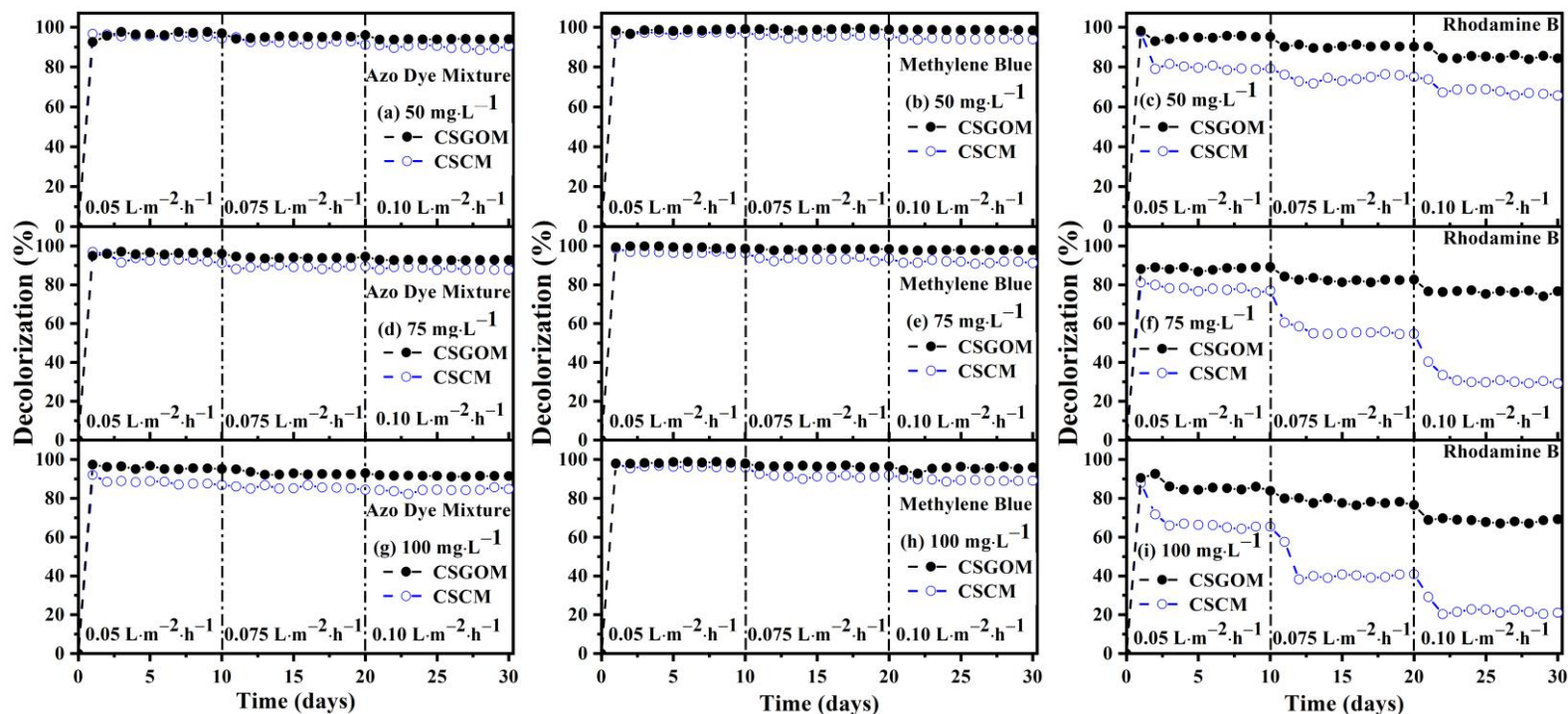


**Figure 8.** Anaerobic decolorization of Azo dye mixture, Methylene Blue, and Rhodamine B dyes at various concentrations and fluxes; a-c)  $50 \text{ mg}\cdot\text{L}^{-1}$ , d-f)  $75 \text{ mg}\cdot\text{L}^{-1}$  and g-i)  $100 \text{ mg}\cdot\text{L}^{-1}$  dye solution at  $37^\circ\text{C}$ . CSCM: 10% wt. of Matrimid and CSGOM:  $1 \text{ mg}\cdot\text{mL}^{-1}$  of GO.

However, regardless of the flux, the difference of the decolorization between B-CSCM and B-CSGOM was rather low for ADM and MB, whereas this was indeed noticeable for RhB. In general, the color removal efficiency for ADM (96-94% in B-CSGOM and 95-88% in B-CSCM), MB (98% in B-CSGOM and 96% in B-CSCM), and RhB (94-84% in B-CSGOM and 79-66% in B-CSCM) was remarkably steady at low permeate flux,  $0.05 \text{ L}\cdot\text{m}^{-2}\cdot\text{h}^{-1}$ , as illustrated by Figure 8, with no significant steady changes found when the feed concentrations were first increased up to  $75 \text{ mg}\cdot\text{L}^{-1}$  and then up to  $100 \text{ mg}\cdot\text{L}^{-1}$ . The results obtained were mostly consistent and, in some cases, showed much better decolorization performance than those using conventional adsorption, photocatalysis, filtration, and bacterial treatment process for decolorizing the dye mixture, Methylene Blue, and Rhodamine Blue dye solutions [2,16,54]. It must be noted that dye removal levels reached here were similar to those obtained using nanofiltration coupled with wet oxidation, PVDF membrane sensitized nano zeolite, MBR with electrocoagulation, Ag/Pd-loaded ZnO nanofiber membrane with UV irradiation; where it was shown over 85% of color removal [55-58]. Some other membrane-based dye removal treatment processes, such as nanofiltration under unstirred batch and continuous crossflow mode [59], activated carbon-PVDF Blend Membrane [60], showed the limitations and were capable of decolorizing just up to 70%.

During the biodecolorization process, the biomass load was sufficient to form active biofilms to ensure complete biodegradation of the dyes, even with the short contact times associated to one-pass direct filtration operation. Even so, low permeate flow allowed the dye molecules to interact sufficiently with the microorganisms, stimulating the effective biodecolorization rate [61,62], although higher permeate flux is of course detrimental for achieving high

biodegradation [63,64]. Therefore, the increase of the permeate flux from 0.05 to 0.075  $\text{L}\cdot\text{m}^{-2}\cdot\text{h}^{-1}$  and, finally, to 0.1  $\text{L}\cdot\text{m}^{-2}\cdot\text{h}^{-1}$  provides declining decolorization of ADM, MB, and RhB dye solutions up to 94%, 98%, and 85%, respectively, in B-CSGOM, which are more evident for B-CSCM, were they decreased to 89% for ADM, 94% for MB, and 66% for the most reluctant RhB.

Increased feed concentration of dye molecules introduced more reactive groups into the anaerobic bioreactor, as did when increasing permeate flux. In such conditions, the excess load of functional groups causes an inadequate biomass to dye ratio [16,63]. Therefore, some dye molecules escape the membrane reactor without undergoing adequate biodegradation. Additionally, the toxicity effect of the dye molecules affects active sites in the biofilm, reducing the decolorization effectiveness of the membrane reactor. These features were reflected in Figure 8(a-c), where the color removal for each of the dye solutions and compact bioreactors declined as the initial feed concentration or permeate flux increased so the load to the anaerobic biodegradation system rises. The feed concentration firstly was increased from 50 to 75  $\text{mg}\cdot\text{L}^{-1}$  and, later, to 100  $\text{mg}\cdot\text{L}^{-1}$ , in B-CSGOM; accordingly, the decolorization rate for the ADM, MB, and RhB solutions was reduced to 91%, 96%, and 67%, respectively. Whereas for B-CSCM, it was decreased to 84% for ADM, 88% for MB, and 22% for RhB. In an earlier investigation, the color removal rate of individually administered AO7, RB5, and BD71 solutions was respectively 34-58% in B-CSCM and 86-97% in B-CSGOM [21,26].

For the azo dye mixture, this study achieved a decolorization up to 90% and 94 % for B-CSCM and B-CSGOM, respectively. In the instance of ADM, the mixed solution exhibited a synergic effect, which increased the



biodecolorization of the ADM compared to the individual dye. Additionally, the mixture of numerous azo dyes and their metabolic products boosts the carbon sources or food available to the microbe that improves the bioreduction of dye molecules. B-CSGOM, on the other hand, performs significantly better than B-CSCM because its GO layer is more conductive than the CSCM carbon layer to escalate the biodegradation performance.

As can be seen, color removal for the MB exhibited less sensitivity to the bioreactor configuration and operating conditions. This treatment behavior can be influenced by the factors that dye removal efficacy varies, such as dye structure with different bonds and functional groups, dye concentration, external carbon and nitrogen sources, electron donor, redox mediator, food to microorganism ratio, and the microorganism growth [65,66]. Increasing feed concentration of ADM in the bioreactor means more azo bonds but also that more other functional groups were entered into the biodegradation system. On the contrary, the rate of biodecolorization of the RhB dye solution was the lowest in all cases. RhB molecules are coalesced by nature and easily stick into the pores or the biofilm. As a result, activity and development of the microbial were prevented, which reduced the biodegradability performance of RhB. The reason for the two-and-a-half-fold higher rate of RhB decolorization in B-CSGOM in comparison to B-CSCM should be assigned to the best capacity of graphene oxide to transfer electrons, which is critical for this more structurally complex dye.

## 4. Conclusions

In this study, the feasibility of two carbon-based membranes integrated with the anaerobic process proved to be efficient for treating several dye solutions. The systems were tested to decolorize azo dye mixtures made of monoazo Acid Orange 7, diazo Reactive Black 5, and triazo Direct Blue 71 dyes. In addition, they were tested over the phenothiazine, Methylene Blue, and the sticky fluorescence Rhodamine B (RhB), too.

It was found that the enhanced electron transfer mechanism of graphene oxide in the CSGOM unit seems to be superior to the carbonaceous layer present in the CSCM configuration. Additionally, this nanoscaled GO layer appears to stimulate the establishment of stable biofilms and to retain better dye molecules and biodegradation derived compounds.

Under the lowest feed concentration ( $50 \text{ mg}\cdot\text{L}^{-1}$ ) and permeate flux ( $0.05 \text{ L}\cdot\text{m}^{-2}\cdot\text{h}^{-1}$ ), maximum decolorization of the dye solutions in CSGOM bioreactor was 96% for ADM, 98% for MB, and 94% for RhB; in turn, for B-CSCM, it was 89%, 94%, and 66%. In response to increasing feed and flux, after 30 days of operation, the decolorization rate of ADM and MB was only 8-12% and 2-5% lower in B-CSCM and B-CSGOM, respectively. RhB demonstrated to be more reluctant, so the decolorization lowered up to 67% B-CSGOM and only 26% in B-CSCM for the more unfavorable conditions, higher feed concentration and flux.

The present investigation shows that compact graphene oxide membrane-based anaerobic biosystems can be successfully applied for the decolorization of a wide variety of isolate or mixed dye molecules.

The definition of the kinetics describing the anaerobic bioreduction of azo dyes is highly needed in order to optimize the decolorization performance so the implementation at large scale could be lowered. In this sense, operation

at higher permeate flux or availability of more conductive membranes would be desirable, too.

### **Acknowledgements:**

This project has been supported by the European Union's Horizon 2020 research and innovation programme under the Marie Skłodowska-Curie grant agreement No. 713679 and by the Universitat Rovira i Virgili (URV), contract 2017MFP-COFUND-18. This article was possible thanks to the grant RTI2018-096467-B-I00 funded by MCIN/AEI/ 10.13039/501100011033 and “ERDF A way of making Europe”. The authors research group is recognized by the Comissionat per a Universitats i Recerca, DIUE de la Generalitat de Catalunya (2017 SGR 396), and supported by the Universitat Rovira i Virgili (2021PFR-URV-87).

### **References:**

1. Adeel, S., Saeed, M., Shahzad, M., Haq, A., Muneer, M., Younas, M., Decolorization of Rhodamine B Dye in Aqueous Medium. *Chiang Mai Journal of Science*. 2015. 42, 730-44.
2. Gupta, V. K., Khamparia, S., Tyagi, I., Jaspal, D., Malviya, A., Decolorization of mixture of dyes: A critical review. *Global Journal of Environmental Science and Management*. 2015. 1(1), 71-94.
3. Holkar, C. R., Jadhav, A. J., Pinjari, D. V., Mahamuni, N. M., Pandit, A. B., A critical review on textile wastewater treatments: Possible approaches. *Journal of Environmental Management*. 2016. 182, 351-66.

4. Elshahawy, M. F., Mahmoud, G. A., Raafat, A. I., Ali, A. E.-H., Soliman, E. s. A., Fabrication of TiO<sub>2</sub> Reduced Graphene Oxide Based Nanocomposites for Effective of Photocatalytic Decolorization of Dye Effluent. *Journal of Inorganic and Organometallic Polymers and Materials*. 2020. 30(7), 2720-35.
5. Pavithra, K. G., P, S. K., V, J., P, S. R., Removal of colorants from wastewater: A review on sources and treatment strategies. *Journal of Industrial and Engineering Chemistry*. 2019. 75, 1-19.
6. Ledakowicz, S., Paździor, K., Recent Achievements in Dyes Removal Focused on Advanced Oxidation Processes Integrated with Biological Methods. *Molecules*. 2021. 26(4), 870.
7. Wang, Y., Pan, J., Li, Y., Zhang, P., Li, M., Zheng, H., Zhang, X., Li, H., and Du, Q., Methylene blue adsorption by activated carbon, nickel alginate/activated carbon aerogel, and nickel alginate/graphene oxide aerogel: a comparison study. *Journal of Materials Research and Technology*. 2020. 9(6), 12443-60.
8. Uddin, M. J., Islam, M. A., Haque, S. A., Hasan, S., Amin, M. S. A., Rahman, M. M., Preparation of nanostructured TiO<sub>2</sub>-based photocatalyst by controlling the calcining temperature and pH. *International Nano Letters*. 2012. 2(1), 1-10.
9. Lellis, B., Fávaro-Polonio, C. Z., Pamphile, J. A., Polonio, J. C., Effects of textile dyes on health and the environment and bioremediation potential of living organisms. *Biotechnology Research and Innovation*. 2019. 3(2), 275-90.

10. Hassan, M. M., Carr, C. M., A critical review on recent advancements of the removal of reactive dyes from dyehouse effluent by ion-exchange adsorbents. *Chemosphere*. 2018. 209, 201-19.
11. Caprarescu, S., Miron, A. R., Purcar, V., Radu, A.-L., Sarbu, A., Ion-Ebrasu, D., Atanase, L.-I., Ghiurea, M., Efficient removal of Indigo Carmine dye by a separation process. *Water Science and Technology*. 2016. 74(10), 2462-73.
12. Modrogan, C., Căprărescu, S., Dăncilă, A. M., Orbuleț, O. D., Grumezescu, A. M., Purcar, V., Radițoiu, V., Fierascu, R. C., Modified Composite Based on Magnetite and Polyvinyl Alcohol: Synthesis, Characterization, and Degradation Studies of the Methyl Orange Dye from Synthetic Wastewater. *Polymers*. 2021. 13(22), 3911.
13. Islam, M. A., Amin, M. S. A., Hoinkis, J., Optimal design of an activated sludge plant: theoretical analysis. *Applied Water Science*. 2013. 3(2), 375-86.
14. Obotey Ezugbe, E., Rathilal, S., Membrane Technologies in Wastewater Treatment: A Review. *Membranes*. 2020. 10(5), 89.
15. García-Martínez, Y., Chirinos, J., Bengoa, C., Stüber, F., Font, J., Fortuny, A., Fabregat, A., Fast Aqueous Biodegradation of Highly-Volatile Organic Compounds in a Novel Anaerobic Reaction Setup. *Environments*. 2018. 5, 115.
16. Tao, P., Xu, Y., Song, C., Yin, Y., Yang, Z., Wen, S., Wang, S., Liu, H., Li, S., Li, C., Wang, T., and Shao, M., A novel strategy for the removal of rhodamine B (RhB) dye from wastewater by coal-based carbon

- membranes coupled with the electric field. *Separation and Purification Technology*. 2017. 179, 175-83.
17. Xiao, X., Li, T.-T., Lu, X.-R., Feng, X.-L., Han, X., Li, W.-W., Li, Q., Yu, H.-Q., A simple method for assaying anaerobic biodegradation of dyes. *Bioresource technology*. 2018. 251, 204-9.
  18. Ion-Ebrasu, D., Pollet, B. G., Spinu-Zaulet, A., Soare, A., Carcadea, E., Varlam, M., Caprarescu, S., Graphene modified fluorinated cation-exchange membranes for proton exchange membrane water electrolysis. *International Journal of Hydrogen Energy*. 2019. 44(21), 10190-6.
  19. Ion-Ebrasu, D., Pollet, B. G., Caprarescu, S., Chitu, A., Trusca, R., Niculescu, V., Gabor, R., Carcadea, E., Varlam, M., and Vasile, B. S., Graphene inclusion effect on anion-exchange membranes properties for alkaline water electrolyzers. *International Journal of Hydrogen Energy*. 2020. 45(35), 17057-66.
  20. Pan, Z., Song, C., Li, L., Wang, H., Pan, Y., Wang, C., Li, J., Wang, T., and Feng, X., Membrane technology coupled with electrochemical advanced oxidation processes for organic wastewater treatment: Recent advances and future prospects. *Chemical Engineering Journal*. 2019. 376, 120909.
  21. Amin, M. S. A., Stüber, F., Giralt, J., Fortuny, A., Fabregat, A., Font, J., Comparative Anaerobic Decolorization of Azo Dyes by Carbon-based Membrane Bioreactor. *Water*. 2021. 13(8), 1060.
  22. Khraisheh, M., Elhenawy, S., AlMomani, F., Al-Ghouti, M., Hassan, M. K., Hameed, B. H., Recent Progress on Nanomaterial-Based Membranes for Water Treatment. *Membranes*. 2021. 11(12), 995.

23. Isaeva, V. I., Vedenyapina, M. D., Kurmysheva, A. Y., Weichgrebe, D., Nair, R. R., Nguyen, N. P., Kustov, L. M., Modern Carbon-Based Materials for Adsorptive Removal of Organic and Inorganic Pollutants from Water and Wastewater. *Molecules*. 2021. 26(21), 6628.
24. Manawi, Y., Kochkodan, V., Hussein, M. A., Khaleel, M. A., Khraisheh, M., Hilal, N., Can carbon-based nanomaterials revolutionize membrane fabrication for water treatment and desalination? *Desalination*. 2016. 391, 69-88.
25. Perreault, F., Fonseca de Faria, A., Elimelech, M., Environmental applications of graphene-based nanomaterials. *Chemical Society Reviews*. 2015. 44(16), 5861-96.
26. Amin, M. S. A., Stüber, F., Giralt, J., Fortuny, A., Fabregat, A., Font, J., Ceramic-supported graphene oxide membrane bioreactor for the anaerobic decolorization of azo dyes. *Journal of Water Process Engineering*. 2022. 45, 102499.
27. Giménez-Pérez, A., Bikkarolla, S. K., Benson, J., Bengoa, C., Stüber, F., Fortuny, A., Fabregat, A., Font, J., and Papakonstantinou, P., Synthesis of N-doped and non-doped partially oxidised graphene membranes supported over ceramic materials. *Journal of Materials Science*, 2016. 51(18), 8346-8360.
28. Chen, A., Yang, B., Zhou, Y., Sun, Y., Ding, C., Effects of azo dye on simultaneous biological removal of azo dye and nutrients in wastewater. *Royal Society Open Science*. 2018. 5(8), 180795.

29. El Bouraie, M., El Din, W. S., Biodegradation of Reactive Black 5 by *Aeromonas hydrophila* strain isolated from dye-contaminated textile wastewater. *Sustainable Environment Research*. 2016. 26(5), 209-16.
30. Sazali, N., Salleh, W. N. W., Md Nordin, N. A. H., Harun, Z., Ismail, A. F., Matrimid-based carbon tubular membranes: The effect of the polymer composition. *Journal of Applied Polymer Science*. 2015. 132(33), 42394.
31. Dohade, M., Incorporation of carbon nanofibers into a Matrimid polymer matrix: Effects on the gas permeability and selectivity properties. *Journal of Applied Polymer Science*. 2018. 135(12), 46019.
32. Sazali, N., Salleh, W. N. W., Nordin, N. A. H. M., Ismail, A. F., Matrimid-based carbon tubular membrane: Effect of carbonization environment. *Journal of Industrial and Engineering Chemistry*. 2015. 32, 167-71.
33. Rattana, Chaiyakun, S., Witit-anun, N., Nuntawong, N., Chindaudom, P., Oaew, S., Kedkeaw, C., Limsuwan, P., Preparation and characterization of graphene oxide nanosheets. *Procedia Engineering*. 2012. 32, 759-64.
34. Wang, J., Zhang, P., Liang, B., Liu, Y., Xu, T., Wang, L., Cao, B., Pan, K., Graphene Oxide as an Effective Barrier on a Porous Nanofibrous Membrane for Water Treatment. *ACS Applied Materials & Interfaces*. 2016. 8(9), 6211-8.
35. Luo, Q., Cai, Q.-z., Li, X.-w., Pan, Z.-h., Li, Y.-j., Chen, X.-d., Yan, Q.-s., Preparation and characterization of ZrO<sub>2</sub>/TiO<sub>2</sub> composite



- photocatalytic film by micro-arc oxidation. *Transactions of Nonferrous Metals Society of China*. 2013. 23(10), 2945-50.
36. Ruppert, A. M., Agulhon, P., Grams, J., Wąchała, M., Wojciechowska, J., Świerczyński, D., Cacciaguerra, T., Tanchoux, N., and Quignard, F., Synthesis of TiO<sub>2</sub>-ZrO<sub>2</sub> Mixed Oxides via the Alginate Route: Application in the Ru Catalytic Hydrogenation of Levulinic Acid to Gamma-Valerolactone. *Energies*, 2019. 12(24), 4706.
37. Ismail, N. H., Salleh, W. N. W., Sazali, N., Ismail, A. F., Development and characterization of disk supported carbon membrane prepared by one-step coating-carbonization cycle. *Journal of Industrial and Engineering Chemistry*. 2018. 57, 313-21.
38. Johra, F. T., Lee, J.-W., Jung, W.-G., Facile and safe graphene preparation on solution based platform. *Journal of Industrial and Engineering Chemistry*. 2014. 20(5), 2883-7.
39. Bikkarolla, S. K., Cumpson, P., Joseph, P., Papakonstantinou, P., Oxygen reduction reaction by electrochemically reduced graphene oxide. *Faraday Discussions*. 2014. 173(0), 415-28.
40. Thema, F. T., Moloto, M. J., Dikio, E. D., Nyangiwe, N. N., Kotsedi, L., Maaza, M., Khenfouch, M., Synthesis and Characterization of Graphene Thin Films by Chemical Reduction of Exfoliated and Intercalated Graphite Oxide. *Journal of Chemistry*. 2013. 2013, 150536.
41. Ismail, N. H., Salleh, W. N. W., Sazali, N., Ismail, A. F., Yusof, N., Aziz, F., Disk supported carbon membrane via spray coating method: Effect of carbonization temperature and atmosphere. *Separation and Purification Technology*. 2018. 195, 295-304.

42. Wu, S., Zhang, B., Liu, Y., Suo, X., Li, H., Influence of surface topography on bacterial adhesion: A Review. *Biointerphases*. 2018. 13(6), 060801.
43. Oder, M., Arlič, M., Bohinc, K., Fink, R., Escherichia coli biofilm formation and dispersion under hydrodynamic conditions on metal surfaces. *International Journal of Environmental Health Research*. 2018. 28(1), 55-63.
44. Niu, F., Huang, M., Cai, T., Meng, L., Effect of Membrane Thickness on Properties of FO Membranes with Nanofibrous Substrate. *IOP Conference Series: Earth and Environmental Science*. 2018. 170, 052005.
45. Ismail, N. H., Salleh, W. N. W., Sazali, N., Ismail, A. F., Effect of intermediate layer on gas separation performance of disk supported carbon membrane. *Separation Science and Technology*. 2017. 52(13), 2137-49.
46. Yang, M., Zhao, C., Zhang, S., Li, P., Hou, D., Preparation of graphene oxide modified poly(m-phenylene isophthalamide) nanofiltration membrane with improved water flux and antifouling property. *Applied Surface Science*. 2016. 394, 149-159.
47. Xu, K., Feng, B., Zhou, C., Huang, A., Synthesis of highly stable graphene oxide membranes on polydopamine functionalized supports for seawater desalination. *Chemical Engineering Science*. 2016. 146, 159-65.

48. Lou, Y., Liu, G., Liu, S., Shen, J., Jin, W., A facile way to prepare ceramic-supported graphene oxide composite membrane via silane-graft modification. *Applied Surface Science*. 2014. 307, 631-7.
49. Yaseen, D. A., Scholz, M., Textile dye wastewater characteristics and constituents of synthetic effluents: a critical review. *International Journal of Environmental Science and Technology*. 2019. 16(2), 1193-226.
50. Xu, N., Guo, D., Xiao, C., Fe/Mn oxide decorated polyacrylonitrile hollow fiber membrane as heterogeneous Fenton reactor for methylene blue decolorization. *Journal of Applied Polymer Science*. 2019. 136(46), 48217.
51. Ming, J., Sun, D., Wei, J., Chen, X., Zheng, N., Adhesion of Bacteria to a Graphene Oxide Film. *ACS Applied Bio Materials*. 2020. 3(1), 704-12.
52. Chen, H. Q., Gao, D., Wang, B., Zhao, R. F., Guan, M., Zheng, L. N., Zhou, X. Y., Chai, Z. F., and Feng, W. Y., Graphene oxide as an anaerobic membrane scaffold for the enhancement of *B. adolescentis* proliferation and antagonistic effects against pathogens *E. coli* and *S. aureus*. *Nanotechnology*. 2014. 25(16), 165101.
53. Mezohegyi, G., Bengoa, C., Stuber, F., Font, J., Fabregat, A., Fortuny, A., Novel bioreactor design for decolourisation of azo dye effluents. *Chemical Engineering Journal*. 2008. 143(1), 293-8.
54. Hashemi Salehi, M., Yousefi, M., Hekmati, M., Balali, E., Application of palladium nanoparticle-decorated *Artemisia abrotanum* extract-modified graphene oxide for highly active catalytic reduction of

- methylene blue, methyl orange and rhodamine B. *Applied Organometallic Chemistry*. 2019. 33(10), e5123.
55. Dhale, A. D., Mahajani, V. V., Studies in treatment of disperse dye waste: membrane-wet oxidation process. *Waste Management*. 2000. 20(1), 85-92.
56. Zhang, X.-b., Hu, Y.-p., Yang, W., Feng, M.-b., Ag-loaded and Pd-loaded ZnO nanofiber membranes: preparation via electrospinning and application in photocatalytic antibacterial and dye degradation. *Applied Nanoscience*. 2021.
57. Ismail, A. M., Menazea, A. A., Ali, H., Selective adsorption of cationic azo dyes onto zeolite nanorod-based membranes prepared via laser ablation. *Journal of Materials Science: Materials in Electronics*. 2021. 32(14), 19352-67.
58. Ravadelli, M., da Costa, R. E., Lobo-Recio, M. A., Akaboci, T. R. V., Bassin, J. P., Lapolli, F. R., Belli, T. J., Anoxic/oxic membrane bioreactor assisted by electrocoagulation for the treatment of azo-dye containing wastewater. *Journal of Environmental Chemical Engineering*. 2021. 9(4), 105286.
59. Chakraborty, S., Purkait, M. K., DasGupta, S., De, S., Basu, J. K., Nanofiltration of textile plant effluent for color removal and reduction in COD. *Separation and Purification Technology*. 2003. 31(2), 141-51.
60. Ye, Q., Li, J., Han, Q., Xu, M., Jiang, L., Yan, B., Preparation of Activated Carbon-PVDF Blend Membrane and Its Effect on the Decolorization of Azo Dyes. *IOP Conference Series: Earth and Environmental Science*. 2021. 793(1), 012012.

61. Rahimi, M., Aghel, B., Sadeghi, M., Ahmadi, M., Using Y-shaped microreactor for continuous decolorization of an Azo dye. *Desalination and Water Treatment*. 2014. 52(28-30), 5513-9.
62. Ewida, A. Y. I., El-Sesy, M. E., Abou Zeid, A., Complete degradation of azo dye acid red 337 by *Bacillus megaterium* KY848339.1 isolated from textile wastewater. *Water Science*. 2019. 33(1), 154-61.
63. Li, Q., Tang, X., Sun, Y., Wang, Y., Long, Y., Jiang, J., Xu, H., Removal of Rhodamine B from wastewater by modified *Volvariella volvacea*: batch and column study. *RSC Advances*. 2015. 5(32), 25337-47.
64. Popli, S., Patel, U. D., Destruction of azo dyes by anaerobic–aerobic sequential biological treatment: a review. *International Journal of Environmental Science and Technology*. 2015. 12(1), 405-20.
65. Khan, R., Bhawana, P., Fulekar, M. H., Microbial decolorization and degradation of synthetic dyes: a review. *Reviews in Environmental Science and Bio/Technology*. 2013. 12(1), 75-97.
66. Solís, M., Solís, A., Pérez, H. I., Manjarrez, N., Flores, M., Microbial decolouration of azo dyes: A review. *Process Biochemistry*. 2012. 47(12), 1723-48.

## Chapter 5. Compact Tubular Carbon-based Membrane Bioreactors for Anaerobic Decolorization of Azo Dyes

### Abstract:

This research investigates a highly efficient compact tubular ceramic-supported carbon-based membrane reactor integrated with the anaerobic biodegradation to decolorize the azo dyes. Two carbon-based membranes, produced using Matrimid 5218 and graphene oxide (GO) solutions, are evaluated for the comparative color removal of three structurally different azo dyes, Acid Orange 7 (AO7), Reactive Black 5 (RB5), and Direct Blue 71 (DB71). The results indicated that the tubular ceramic-supported graphene oxide membrane bioreactor (B-TCSGOM) was more efficient and effective at removing color from all dye solutions than the ceramic-supported carbonized membrane bioreactor (B-TCSCM) over a wide range of feed concentrations. In both the reactors, the highest decolorization was achieved at low feed concentration ( $50 \text{ mg}\cdot\text{L}^{-1}$ ), and in B-TCSGOM, removal was 94% for AO7, 90% for RB5, and 88% for DB71, whereas 88%, 85%, and 69%, respectively, in B-TCSCM. These findings indicate that the robust conductive nanoporous surface of B-TCSGOM makes it more effective at removing different azo dye solutions from wastewater.

---



## 1. Introduction

Textile industries are now one of the pillars of the contemporary economy. The manufacturing of clothes has increased due to the growth of the population, and as a consequence, the environmental impact associated with these processes has also increased [1]. Among the different textile manufacturing processes, the dyeing process is primarily responsible for water pollution as it uses a high amount of water to dissolve the azo dyes that give color to the products. This produces an enormous amount of wastewater, which poses a severe threat to the environment. Some azo dyes may be carcinogenic and cause several allergies [2]. Furthermore, it is also reported that they can affect neural, cardiac, and pulmonary systems and cause reproductive problems [3]. The dyestuff wastewater treatment technologies have evolved over the years, and they can be divided into three broad categories: advanced oxidation processes (AOPs), biological treatments, and physicochemical treatment methods.

The most common physicochemical treatments are precipitation, adsorption, and membrane technology [4]. The difference between coagulation and flocculation is that the second one needs the addition of a reagent to produce the aggregation. In the case of the adsorption processes, the dye molecules are adsorbed on the surface of the solid surface. In these cases, it is essential to point out that they are expensive even if they are easy to operate. Moreover, their application is limited by the use of some hazardous coagulants [5] as well as the generation of toxic sludge and its high cost of adsorption disposal [6].



AOPs are treatment technologies that allow oxidizing the organic compounds present in wastewater by exploiting the reactivity of hydroxyl radicals ( $\cdot\text{OH}$ ) [7]. The literature has widely studied Fenton, Photo-Fenton, and ozonation processes [8-10] and shows the dye removal capabilities from wastewater. However, to optimize and enhance the performance of these processes, special attention to the process variables such as pH, reagent dose, pollutant concentration, temperature, UV source, etc., are required [11]. In addition, it may produce secondary pollutants which are required to undergo furthermore treatment. Thus, the high operating cost (high amount of acid, base, and energy consumption) makes it difficult to be applied on an industrial scale [12].

Biological treatments are processes in which organic contaminants act as nutrients for microorganisms [13]. These methods are typically employed in wastewater treatment plants because of their capability of removing suspended particles and color as well as keeping the biochemical oxygen demand at the desired level. These treatments can be aerobic or anaerobic that operate with or without oxygen. Despite being fully implemented in the industry due to their competitive cost, long residence time, and extensive facilities, it is difficult to remove such contaminants in continuous mode [14].

In the last years, membrane technology has gained the attention of researchers and has become a potential wastewater treatment process. Membrane units allow overcoming some of the mentioned limitations: the more diminutive size of the equipment, less energy consumption, and low capital cost. Moreover, it may not use chemicals, thus being an environmentally-friendly and accessible alternative [14]. However, the lifetime of the membranes is short, and their surface is exposed to fouling.

Combining different methods can obtain a better contaminant azo dye removal process. Among all the possible alternatives, the coupling of membrane technology and anaerobic digestion is an effective solution, giving rise to anaerobic membrane bioreactors systems [15, 16]. In these works, the researcher used the flat ceramic supports to prepare a carbon-based membrane that usually showed the highest chemical and thermal resistance, making them suitable for industrial wastewater treatment. However, among the different geometries, tubular and hollow-fiber membranes present better performance than the flat-sheet module, as they present higher mechanical strength and resistance to high cross-flow velocities. Considering this, the main objective of this work is to synthesize the ceramic-supported tubular carbon-based membrane. As first option, one of the membranes is synthesized by the carbonization of Matrimid 5218 polyimide solution. In contrast, the other tubular membrane is made of graphene oxide by vacuum-assisted filtration of exfoliated graphene oxide solution. One of the innovative aspects of this study is the integration of the tubular carbon-based membranes with the anaerobic biodegradation method to successfully remove azo dye from dye-containing wastewater, which is the first of its kind to the best of our knowledge. The decolorization of Acid Orange 7 (AO7), Reactive Black 5 (RB5), and Direct Blue 71 (DB71) dye solutions were investigated at various feed solution concentrations.

## **2. Experimental**

### **2.1 Preparation of Tubular Ceramic-supported Carbon Membrane**

The ultrafiltration tubular ceramic membrane (inner diameter: 3 mm, length: 250 mm, molecular weight cut-off: 50 kg·mol<sup>-1</sup>, TAMI Industries, France) served as the ceramic support for depositing the carbon layer. The ceramic-supported tubular carbon membrane (TCSCM) used 10% wt.

Matrimid 5218 (Huntsman Advanced Materials, The Woodlands, TX, USA) as membrane precursor that was prepared by dissolving the desired amount of polymeric precursors in NMP (1-methyl-2-pyrrolidone, Sigma Aldrich, ref. 328634, Spain). In TCSCM, the polymeric layer inside the tubular ultrafiltration support was formed by flowing (up-flow) of precursor solution, in-out, through the membrane, continuously for 60 minutes. The membrane was subsequently dried for one hour before the repetition of the coating protocol. In the following step, the coated membrane was allowed to dry for 24 hours before the carbon membrane was created by carbonization at 800 °C under an inert atmosphere [15].

For the another carbon-based membrane, ceramic-supported tubular graphene oxide membrane (TCSGOM), the membrane precursor was exfoliated graphene oxide (GO) solution, which was generated using a modified Hummer method [17] from 20 µm of pristine graphite powder (Sigma Aldrich, ref. 282863, Spain). The porous graphene oxide layer on the TCSGOM was formed by vacuum-assisted filtration, in-out, of 3-5 mL of 1 mg·mL<sup>-1</sup> homogenous GO solution over the ceramic substrate in a filtration cell (INSIDE DisRAM holder, TAMI Industries, France). Following filtering for thirty minutes, the membrane was first dried at 80 °C for 24 hours and then at 100 °C for 72 hours to obtain a stable and robust TCSGOM.

## 2.2 Experimental Set-up for Anaerobic Biodegradation

Figure 1 illustrates the comparative anaerobic biodecolorization of azo dyes using both carbon-based membrane bioreactors (B-TCSCM and B-TCSGOM). The monoazo AO7 (ACROS Organics, ref. 416561000, Spain) was used as first feed solution to test. Afterwards, the second and third were diazo RB5 (Sigma Aldrich, ref. 306452, Spain) and triazo DB71 (Sigma Aldrich, ref. 212407, Spain) solutions. The dye, Sodium Acetate (Sigma

Aldrich, ref. 110191, Spain), and basal medium were combined to form the artificial feed solution in each experiment [16]. The basal media, formed by six sets of microelements ( $\text{mg}\cdot\text{L}^{-1}$ ), contains i)  $\text{MnSO}_4\cdot\text{H}_2\text{O}$  (0.155),  $\text{CuSO}_4\cdot 5\text{H}_2\text{O}$  (0.285),  $\text{ZnSO}_4\cdot 7\text{H}_2\text{O}$  (0.46),  $\text{CoCl}_2\cdot 6\text{H}_2\text{O}$  (0.26),  $(\text{NH}_4)_6\text{Mo}_7\text{O}_{24}$  (0.285), ii)  $\text{K}_2\text{HPO}_4$  (21.75),  $\text{Na}_2\text{HPO}_4\cdot 2\text{H}_2\text{O}$  (33.40),  $\text{KH}_2\text{PO}_4$  (8.50), iii)  $\text{FeCl}_3\cdot 6\text{H}_2\text{O}$  (29.06), iv)  $\text{CaCl}_2$  (13.48) v)  $\text{MgSO}_4\cdot 7\text{H}_2\text{O}$  (15.2), and vi)  $\text{NH}_4\text{Cl}$  (190.90). All chemicals were obtained from Sigma Aldrich (Spain) and dissolved in Milli-Q water (Millipore Milli-Q system, Molsheim, France).

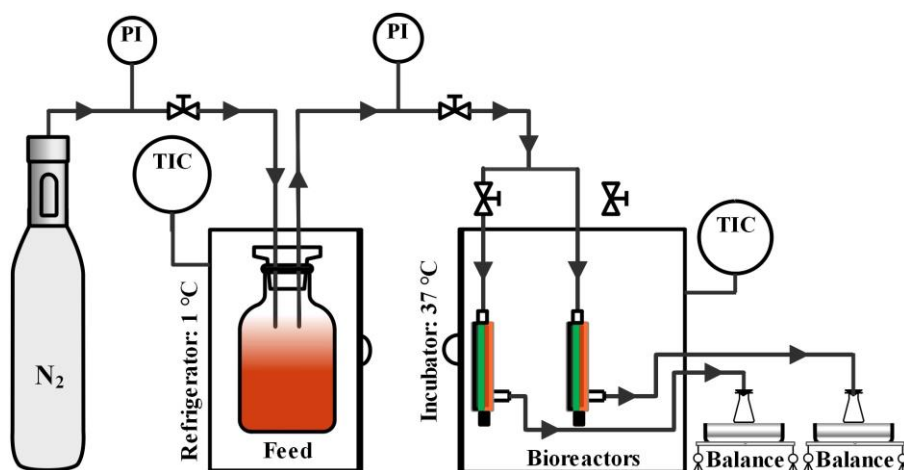


**Figure 1.** Experimental set-up for anaerobic decolorization of dye molecules by TCSCM and TCSGOM.

Firstly, the TCSCM and TCSGOM membranes were inserted in the appropriate filtration cells, which perform as reactors. Following, 5 mL of secondary anaerobic sludge (collected from the municipal WWTP in Reus, Spain) was injected inside the tubular carbon-based membranes. The continuous flow of the nitrogen gas (purity >99.99%, Linde, Spain) into the feed tank allows the feed solution to be driven to the bioreactor. The gas flow was adjusted throughout the operation to maintain a transmembrane pressure

(TMP) and a negative redox potential, to assure suitable conditions for the decolorization [18]. In addition, the feed tank and the temperature of the bioreactor were operated at  $1\pm 1$  °C and  $37\pm 1$  °C, respectively, to attain the maximum color removal [19, 20].

### 2.3 Membrane Characterization

The chemical structures of the tubular carbon membranes were analyzed using the Fourier Transform Infrared (FT-IR) spectrophotometer (FT/IR-6700, JASCO, Tokyo, Japan). Further, the deposited carbon layer pore size, thickness, and microelements were examined by combined Focused Ion Beam-Scanning Electron Microscope (FIB-SEM, Scios 2 Dual Beam, Thermo Scientific, MA USA).

### 2.4 Analytical Methods

Membrane flux, pure water permeance (PWP), and hydraulic resistance were used to determine the filtration performance, which was computed using equations 1-3,

$$J = \frac{\Delta V}{\Delta t} \cdot \frac{1}{A} \quad (1)$$

$$\text{PWP} = \frac{J}{\Delta P} \quad (2)$$

$$H_R = \frac{\Delta P}{\mu} \cdot \frac{1}{J} \quad (3)$$

where  $J$  denotes the permeate flux through the tubular membrane ( $\text{L}\cdot\text{m}^{-2}\cdot\text{h}^{-1}$ ),  $V$  is the permeate volume that passes through the membrane (L),  $t$  the filtration time (h),  $A$  the membrane filtration area ( $\text{m}^2$ ),  $H_R$  is the hydraulic resistance ( $\text{m}^{-1}$ ),  $\Delta P$  is the transmembrane pressure (bar), and  $\mu$  is the viscosity of water ( $\text{Pa}\cdot\text{s}$ ).

A UV/VIS4000n Spectrophotometer (DINKO Instruments, Spain) was used to quantify the decolorization (D) that occurred during the anaerobic bioreduction of the azo dye which was then calculated using equation 4.

$$D (\%) = \frac{A_o - A}{A_o} \times 100 \quad (4)$$

$A_o$  and  $A$  are the absorbance of feed and permeate liquid, i.e., before and after the biodegradation process.

### 3. Result and Discussion

#### 3.1 Structural and Chemical Characterization of Tubular Ceramic-supported Carbon Membranes

The functional groups of the TCSCM and TCSGOM were characterized by FTIR and are depicted in Figure 2(a-b). The peaks at  $1717.23 \text{ cm}^{-1}$  in TCSGOM (Figure 2a) are attributable to the C=O group, whereas the peak at  $1601.23 \text{ cm}^{-1}$  owns to the presence of the  $\text{sp}^2$  bond for the aromatic C=C skeletal vibrations. A moderate peak shows the stretching vibrations of the C-OH bond at  $1417.23 \text{ cm}^{-1}$ . Another distinctive signal at  $1039.78 \text{ cm}^{-1}$  corresponds to the C-O-C groups, demonstrating that pristine graphite has been completely oxidized [21]. In Figure 2b, the typical FTIR spectra of the polymeric membrane, before the carbonization, shows at  $2955.12$ ,  $1713.23$ ,  $1497.31$ ,  $1368.98$ ,  $1090.01$ , and  $712.16 \text{ cm}^{-1}$ , the stretch of the methyl group (C-H), C=O, C=C, C-N-C axial, C-N-C transverse, and C-H (monosubstituted of benzene) groups, respectively [22, 23]. After carbonization, the spectrum, represented by the blue line in Figure 2b, does not show apparent peaks from  $3600$  to  $600 \text{ cm}^{-1}$ . This proves that the polymeric precursor completely decomposes and break its chemical structure during carbonization [22, 24].

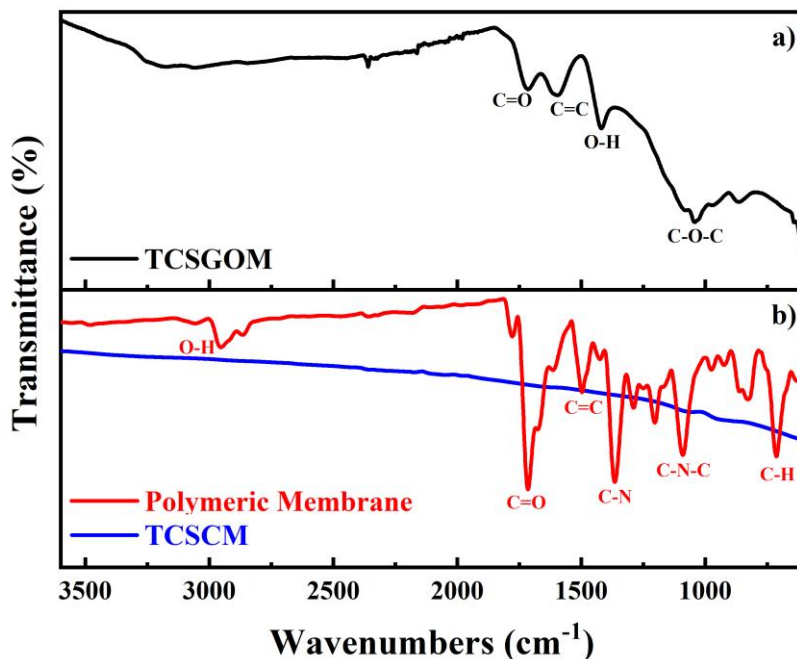


**Figure 2.** FTIR analysis of the a) TCSGOM and b) polymeric precursor membrane and TCSCM (TCSCM: 10% wt. Matrimid and TCSGOM: 1  $\text{mg}\cdot\text{L}^{-1}$  GO solution).

Figure 3 (a-d) shows the microstructural analysis of the two carbon-based membranes, taken in the top surface and the cross-section. Based on Figure 3(a-b), the surface of both the TCSCM and TCSGOM appears to be defect-free and smooth but looks differently in pore size. The average pore size of TCSCM was estimated to be 25 nm, while it was 12 nm for TCSGOM. Consistent with previous research, the current results indicate that the pore size of a flat ceramic-supported graphene-oxide membrane is smaller than that of a flat carbon membrane. On the other hand, opposite results were found for the carbon layer thickness, which was deposited on the top of the ceramic support. The thickness was measured as 1.10 and 2.11  $\mu\text{m}$ , respectively, for TCSCM and TCSGOM. The carbonization of TCSCM at a high temperature resulted in forming a thinner carbon layer than that of

TCSGOM [25]. However, the layer was asymmetric, tightly packed, and strongly attached to the tubular support in both cases.

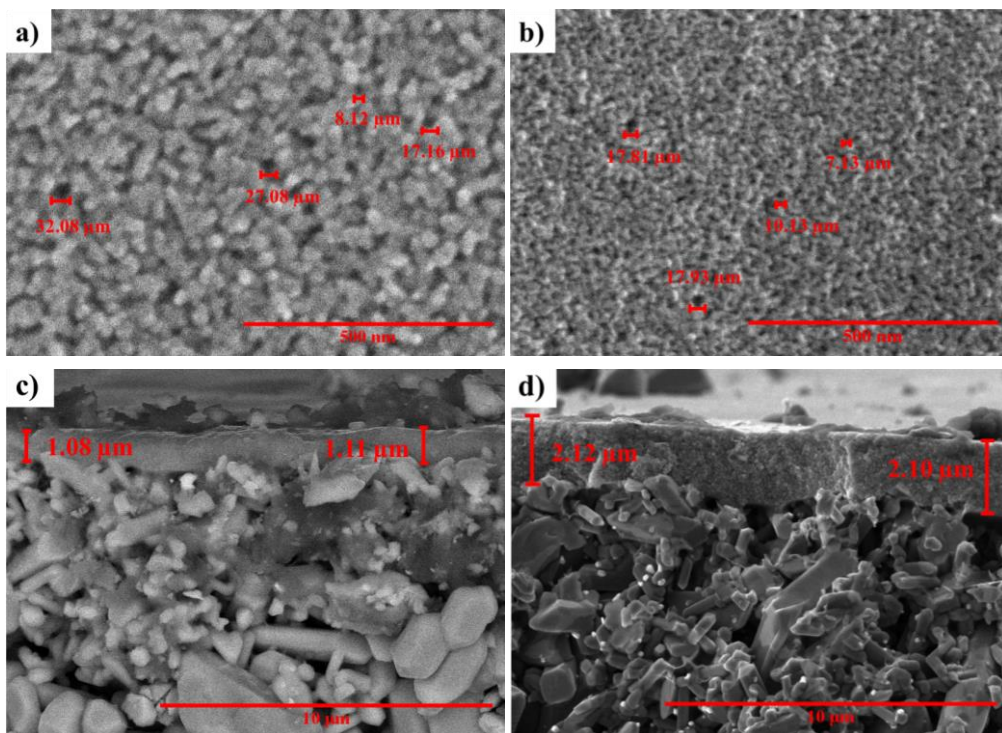


**Figure 3.** FESEM microscopy images a-b) the surface of TCSCM and TCSGOM, and c-d) the cross section of TCSCM and TCSGOM (TCSCM: 10% wt. Matrimid and TCSGOM: 1 mg·L<sup>-1</sup> GO solution).

### 3.2 Permeate Flux and Hydraulic Resistance of the Tubular Carbon-based Membranes

To evaluate the effect of the various carbon layers deposited over the tubular ceramic supports, the TCSCM and TCSGOM membrane flux, i.e., pure water permeance (PWP), and hydraulic resistance ( $H_R$ ) was evaluated using Milli-Q water. Three filtration tests over either tubular ultrafiltration membrane (tubular ceramic support, TCS), TCSCM, and TCSGOM were conducted within a range of transmembrane pressures (TMP). As shown in



Figure 4, the TCS, because of the absence of any additional carbonaceous layer, exhibited the highest permeate flux ( $197.4 \text{ L}\cdot\text{m}^{-2}\cdot\text{h}^{-1}$ ) as well as water permeance ( $247.3 \text{ L}\cdot\text{m}^{-2}\cdot\text{h}^{-1}\cdot\text{bar}^{-1}$ ) at the TMP of 0.80 bar. With respect the other two, the TCSGOM owed the lowest permeate flux,  $18.2 \text{ L}\cdot\text{m}^{-2}\cdot\text{h}^{-1}$ , and PWP,  $22.8 \text{ L}\cdot\text{m}^{-2}\cdot\text{h}^{-1}\cdot\text{bar}^{-1}$ , which is 90% and 60%, respectively, lower than the TCS and TCSCM (Flux:  $45.6 \text{ L}\cdot\text{m}^{-2}\cdot\text{h}^{-1}$  and PWP:  $56.9 \text{ L}\cdot\text{m}^{-2}\cdot\text{h}^{-1}\cdot\text{bar}^{-1}$ ). The variation of the hydraulic resistance was depicted in Figure 4, too, as a bar chart. Following the permeances, the TCSGOM displayed the highest hydraulic resistance ( $1.78 \pm 0.01 \times 10^{13} \text{ m}^{-1}$ ), while TCS had the lowest ( $1.62 \pm 0.01 \times 10^{12} \text{ m}^{-1}$ ).

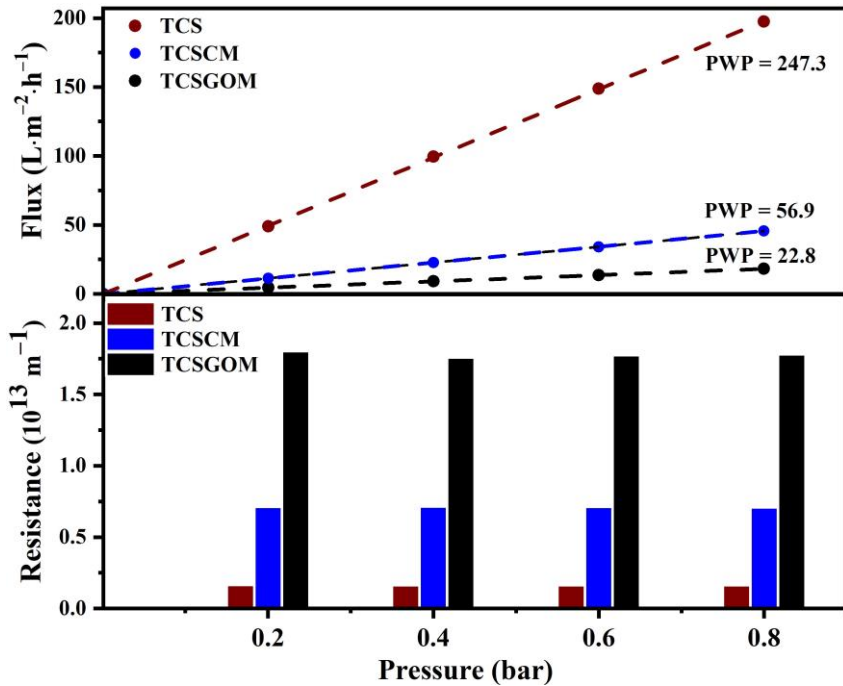


**Figure 4.** Variation of membrane flux, water permeance, and hydraulic resistance as a function of TMP for TCS, TCSCM and TCSGOM.

Compared to TCS, the decrease in membrane flux of TCSCM and TCSGOM is predominantly due to the deposition of an additional carbon layer on the ceramic support inner surface. Again, the distinction of flux between these two carbon-based membranes depends on the thickness and pore size of the carbon layers that cover the membrane surface. As shown in the FESEM images (Figure 3 a-d), the carbon layer thickness of TCSCM was lower than that of TCSGOM. This occurred due to the highly viscous Matrimid solution, which makes evaporation to be slow during the carbonization at a high temperature causing the membrane pores to be larger in size but thinner the carbon layer [26]. On the other hand, the exfoliated GO solution partially penetrated the ceramic support (GO-TiO<sub>2</sub> region) and mostly blocked the support pores. Then, it continues growing to form single or several graphene oxide layers over the tubular support. Amin et al. [15, 16] also observed a similar trend, over flat CSCM that exhibited higher filtration flux and permeance than flat CSGOM. Owing to the little porous and thick graphene oxide layer, TCSGOM demonstrated higher hydraulic resistance than the others.

### 3.3 Role of the Membrane Type on Anaerobic Decolorization of Dyes

Carbon-based membranes (both TCSCM and TCSGOM) and ceramic support (TCS) were examined to assess the color removal from the model azo dye solution. The feed solution contained 50 mg·L<sup>-1</sup> of Acid Orange 7 (AO7), and the anaerobic biodegradation was carried out under dead-end filtration mode at constant permeate flux (0.10 L·m<sup>-2</sup>·h<sup>-1</sup>). The three bioreactors operated with TCS, TCSCM, and TCSGOM are henceforth referred to as B-TCS, B-TCSCM, and B-TCSGOM, respectively. As illustrated in Figure 5, AO7 biodecolorization is drastically dependent on the presence of the carbon layer and microorganisms. Compared to B-TCS, both compact carbon-based

membrane bioreactors (B-TCSCM and B-TCSGOM) demonstrated stable color removal over ten-day periods, in which B-TCSGOM was able to decolorize 95% of AO7 monoazo dye at the highest.

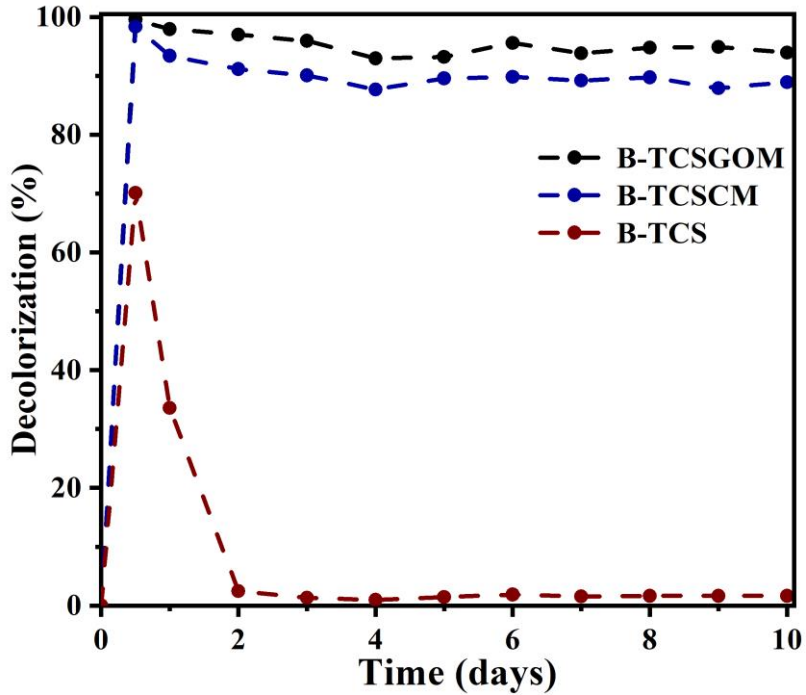


**Figure 5.** Anaerobic decolorization of AO7 in TCS, TCSCM and TCSGOM bioreactors. Flux =  $0.10 \text{ L}\cdot\text{m}^{-2}\cdot\text{h}^{-1}$ ,  $[\text{AO7}]_0 = 50 \text{ mg}\cdot\text{L}^{-1}$  and  $T = 37 \text{ }^\circ\text{C}$ .

Just at starting, all the reactors showed a good dye removal efficiency but, after 12 h of operation, the decolorization of the TCS suddenly dropped from 75% to 33%, and finally, after two days, the bioreactor became unable to remove any color. This suggests that the ultrafiltration ceramic support was neither able to form the needed biofilm to degrade the dye nor to reject, due to its too large pores, the dye molecules from the feed solution. In turn, after three days of operation, the decolorization in the carbon-based membrane bioreactors remained highly stable throughout the experiments. B-TCSGOM demonstrated the most effective decolorization (95%), and the B-TCSCM

showed the least 88% color removal. It appears that the nanoporous carbon layer of both carbon-based membranes was well suited for the anaerobic decolorization process under these conditions. As elsewhere stated [27, 28], these membranes served a triple role: they support microorganisms to grow a biofilm, immobilize the pollutants, and enhance electron transfer between bacteria and dye molecules under anaerobic conditions. Contrarily to findings in some previous research [29, 30], graphene oxide has no detrimental effect on bacteria, allowing biofilm growth and attachment over the membrane surface. However, the graphene layers are more conductive than the carbonized Matrimid layer, resulting in a faster electron shuttle mediator effect [31]. Thus, the enhanced microbial metabolism in TCSGOM provides a higher anaerobic decolorization than the others [32].

After each biodecolorization experiment, the membranes were simply cleaned by water backflushing, which apparently was able to remove any dye molecule, adsorbed on either the carbonaceous layer or the ceramic support, as well as to wash out the biofilm from the membrane surface. This is evidenced by the fact that the initial flux was recovered without compromising the membrane properties, allowing it to be reused in subsequent decolorization tests giving comparable performance.

### **3.4 TCSCM and TCSGOM Performance for Decolorization of Azo Dyes**

The effect of feed concentration of three structurally different azo dyes (monoazo AO7, diazo RB5, triazo DB71) on the biodecolorization performance was investigated for both B-TCSCM and B-TCSGOM. Three different feed solution concentrations were explored in the experiments: 50, 75, and 100 mg·L<sup>-1</sup>. In all cases, the bioreactors were operated under a constant permeate flux of 0.10 L·m<sup>-2</sup>·h<sup>-1</sup>, which was controlled by adjusting regularly the TMP.

Figure 6 (a-i) illustrates the extent of the color removal for the three dye solutions. It can be seen that the decolorization depends on the feed concentration, the number of azo bonds, and, probably, the other functional groups present in the dye molecules. The decolorization performance was also significantly influenced by the type of carbonaceous layer. As expected, irrespective of the feed concentration, the monoazo AO7 gave the highest color removal, 92-97% in TCSGOM and 75-88% in TCSCM. Table 1 collects the dye removal and decolorization rate for the B-TCSCM and B-TCSGOM processes using the different feed concentrations and dyes. Notably, as feed concentration increases, decolorization decreases but the hourly normalized amount of decolorized dye increases. Regardless of the membrane bioreactor, the maximum amount of dye removal ( $9.2 \text{ mg}\cdot\text{m}^{-2}\cdot\text{h}^{-1}$  for B-TCSGOM and  $7.5 \text{ mg}\cdot\text{m}^{-2}\cdot\text{h}^{-1}$  for B-TCSCM) was obtained for  $100 \text{ mg}\cdot\text{L}^{-1}$  of AO7 while DB71 at the same feed concentration gave the lowest  $6.2$  and  $7.8 \text{ mg}\cdot\text{m}^{-2}\cdot\text{h}^{-1}$  for B-TCSCM and B-TCSGOM, respectively.

Overall, color removal was significantly higher and stable in all experiments in the bioreactors operated with the tubular graphene oxide membrane. Under the same operating condition and feed solution, the reason for the superior performance of TCSGOM than the carbonized tubular Matrimid membrane may be attributed to its conductive surface, which enhances the role as a redox mediator due to its better electron transfer capacity during biodegradation. This way, it boosts the quick electron transfer from the bacteria to the azo bonds, followed by breaking the azo bonds of dye molecules to give a colorless product [33]. Accordingly, for any azo dye and concentration applied, TCSGOM removed color significantly better than TCSCM does.

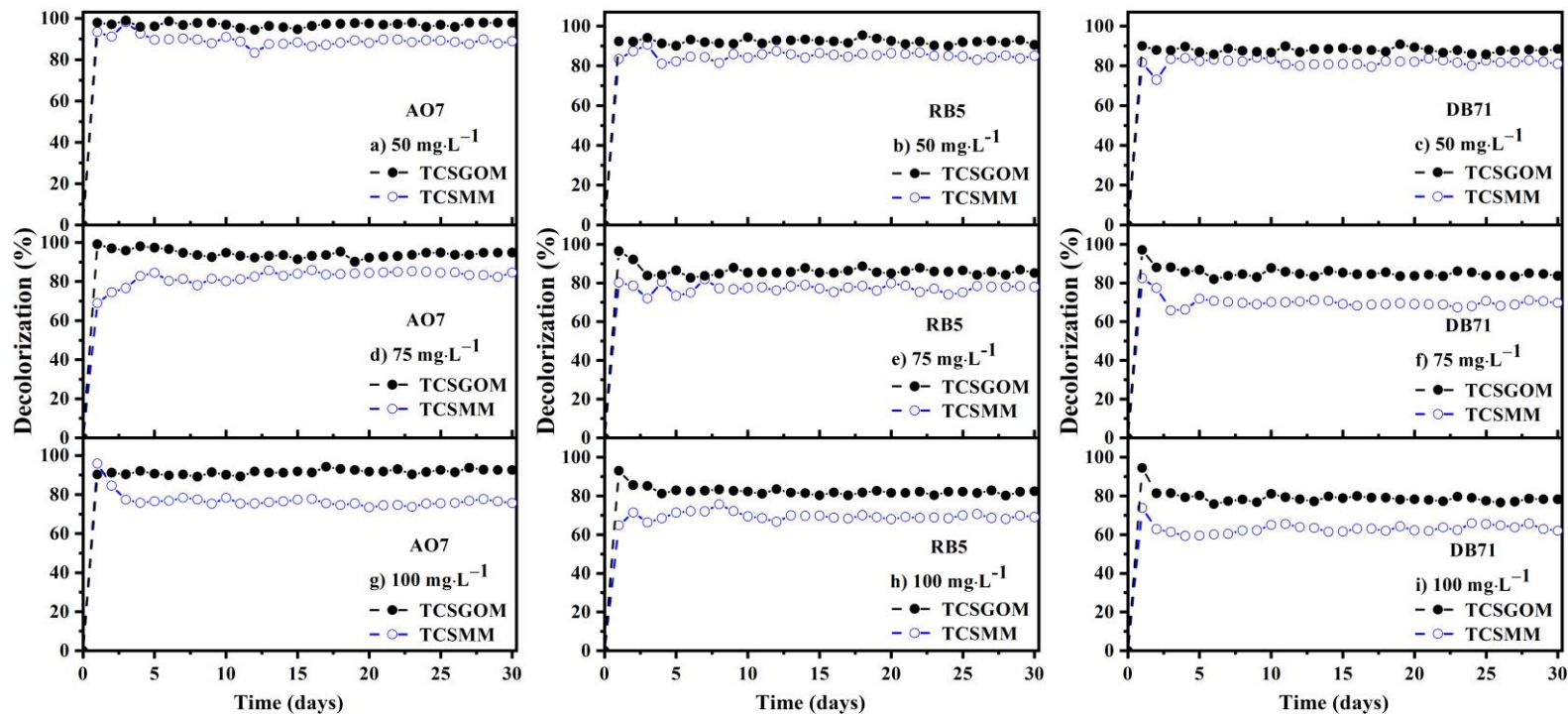


**Figure 6.** Anaerobic decolorization of Acid Orange 7, Reactive Black 5, and Direct Blue 71 at 37 °C for various feed dye concentrations; a-c) 50 mg·L<sup>-1</sup>, d-f) 75 mg·L<sup>-1</sup> and g-i) 100 mg·L<sup>-1</sup>. TCSM: 10% wt. of Matrimid and TCSGOM: 1 mg·mL<sup>-1</sup> of GO.

**Table 1.** Summary of the decolorization and removal of azo dyes

Dye	Concentration (mg·L <sup>-1</sup> )	B-TCSCM		B-TCSGOM	
		Decolorization (%)	Dye Removal Rate (mg·m <sup>-2</sup> ·h <sup>-1</sup> )	Decolorization (%)	Dye Removal Rate (mg·m <sup>-2</sup> ·h <sup>-1</sup> )
AO7	50	90	4.5	97	4.9
	75	84	6.3	94	7.1
	100	75	7.5	92	9.2
RB7	50	84	4.2	90	4.5
	75	77	5.8	85	6.4
	100	69	6.9	82	8.2
DB71	50	80	4.0	88	4.4
	75	69	5.2	84	6.3
	100	62	6.2	78	7.8

There is evidence that decolorization of azo dyes generally depends on the existence of one or more azo bonds connected to sulphonates, -OH and NH<sub>2</sub> groups, and the molecular weight of the dye molecules [34, 35]. The triazo DB71 contains three azo bonds as well as more chromophores and auxochromes groups than AO7 and RB5. Increased presence of such reactive groups in the dye readily reduced microbial growth [36]. Additionally, compared to monoazo dye, the greater toxicity in diazo and triazo molecules resulted in a decline of the decolorization effectiveness by ruining the biofilm or active sites of the microorganisms. This was also found in the present research work. Thus, Figure (a-i) shows that the decolorization rate decreases (90-80% for B-TCSCM and 97-88% for B-TCSGOM) when the feed solution contains more azo, aromatic, and functional groups. This means that, for both bioreactors, the steady color removal followed the order: AO7 > RB5 > DB71. Franciscon et al. [37] and Amin et al. [15, 16] previously observed that the monoazo dye removal was faster and more efficient than diazo and triazo using bacterial bioreduction processes, while a similar trend was also obtained by Garcia et al. [38] using the electro-Fenton method. Once again, it was evident that the faster electron transport is crucial for the anaerobic decolorization of azo dye solutions.

As expected, the dye removal was better in the bioreactors operated at a low feed concentration. For instance, the adverse effect of a growing feed concentration on the dye removal of B-TCSGOM was followed (as shown in Figure 6) by increasing the feed concentration first from 50 to 75 mg·L<sup>-1</sup> and later up to 100 mg·L<sup>-1</sup>. Accordingly, the decolorization for the AO7, the RB5, and the DB71 solutions were declined from 97 to 92%, 90 to 82%, and 88 to 78%, respectively. A similar trend was obtained for B-TCSCM, where the reductions were as follows: 90 to 75% for AO7, 84 to 69% for RB5, and 80 to 62% for DB71. It is well-known that a low feed concentration in the reactor system allows the dye molecules to interact suitably with bacteria to reach significant biodegradation [39]. Under these circumstances, the biomass present was adequate to support almost complete bioreduction. On the other hand, increasing feed concentration in the bioreactors introduces higher dye load with additional chromophores and auxochromes content in the anaerobic biodegradation pathways. Therefore, excess amounts of these functional groups (-SO<sub>3</sub>H, -R, -NH<sub>2</sub>, -SO<sub>2</sub>NH<sub>2</sub>, etc.) severely reduce microbial growth in the reactors, consequently, lessen the decolorization performance [40-42]. In addition, the toxic substances limit the biomass content and microorganism tolerance, which lowers the decolorization rate, too.

This trend was already observed in our previous research, where the anaerobic decolorization of azo dyes was performed using flat ceramic-supported carbonized Matrimid and graphene oxide membrane bioreactors [15, 16]. Using CSCM, the biodecolorization achieved in those experiments was 36-57%, 30-42%, and 26-34% for AO7, RB5, and DB71, respectively. In comparison to the flat membrane bioreactor [15], TCSCM demonstrated about 33, 50, and 66% greater dye removal rates for AO7, RB5, and DB7, respectively. The tubular bioreactor provides better coverage and roughness,



where the surface area of the biofilm and the amount of biomass are increased; this contributed to improve the decolorization rate. However, comparing B-TCSGOM to B-CSGOM, i.e., tubular versus flat, except for the high permit outflow, the percentage of color removal was almost identical [16]. On the other hand, the degree of decolorization declines as the feed concentration increases. The amount of dye removed increases steadily, and the highest dye removal was obtained with  $100 \text{ mg}\cdot\text{L}^{-1}$  of each azo dye solution (Table 1).

## 4. Conclusions

To summarize, two tubular carbon-based membranes to be used as bioreactors were successfully prepared using a carbonized polymer precursor (TCSCM) or graphene oxide (TCSGOM) over a ceramic filtration element as support. To the best of our knowledge, this is the first-time that tubular ceramic-supported carbon-based membranes (TCSCM and TCSGOM) have been integrated with an anaerobic biodegradation process for azo dye decolorization. The TCSGOM had a water permeance of  $22.8 \text{ L}\cdot\text{m}^{-2}\cdot\text{h}^{-1}\cdot\text{bar}^{-1}$ , showing that the GO membrane nanoporous surface was responsible for its lower permeance than the tubular support and TCSCM.

The overall performance of TCSCM and TCSGOM were evaluated with different types of azo dyes (mono-, di- and tri-azo dyes) and several feed concentrations. In all experiments, regardless of the type of azo dye and operating conditions, the TCSGOM bioreactor gave better color removal than the TCSCM. The highest biodecolorization using B-TCSGOM was 97% for AO7, 94% for RB5, and 92% for DB71 at the lowest feed concentration; in turn, for B-TCSCM, it was 90%, 85%, and 80%, respectively.

As a result, the newly developed compact tubular carbon-based membrane may pave the way for novel methods to treat raw textile wastewater using integrated methods in single compact units. This intensified bioreactor should also be easily scaled-up to confirm its applicability in industrial wastewater treatment.

### References:

1. Ismail, G. A. and Sakai, H., Review on effect of different type of dyes on advanced oxidation processes (AOPs) for textile color removal. *Chemosphere*, 2022. 291, 132906.
2. Chung, K.-T., Azo dyes and human health: A review. *Journal of Environmental Science and Health, Part C*, 2016. 34(4), 233-261.
3. Senthil Rathi, B. and Senthil Kumar, P., Sustainable approach on the biodegradation of azo dyes: A short review. *Current Opinion in Green and Sustainable Chemistry*, 2022. 33, 100578.
4. Solís, M., Solís, A., Pérez, H. I., Manjarrez, N., and Flores, M., Microbial decolouration of azo dyes: A review. *Process Biochemistry*, 2012. 47(12), 1723-1748.
5. Teh, C. Y., Budiman, P. M., Shak, K. P. Y., and Wu, T. Y., Recent Advancement of Coagulation–Flocculation and Its Application in Wastewater Treatment. *Industrial & Engineering Chemistry Research*, 2016. 55(16), 4363-4389.
6. McYotto, F., Wei, Q., Macharia, D. K., Huang, M., Shen, C., and Chow, C. W. K., Effect of dye structure on color removal efficiency by coagulation. *Chemical Engineering Journal*, 2021. 405, 126674.

7. Andreozzi, R., Caprio, V., Insola, A., and Marotta, R., Advanced oxidation processes (AOP) for water purification and recovery. *Catalysis Today*, 1999. 53(1), 51-59.
8. Hansson, H., Kaczala, F., Marques, M., and Hogland, W., Photo-Fenton and Fenton Oxidation of Recalcitrant Industrial Wastewater Using Nanoscale Zero-Valent Iron. *International Journal of Photoenergy*, 2012. 2012, 11.
9. Koyuncu, İ. and Afşar, H., Decomposition of dyes in the textile wastewater with ozone. *Journal of Environmental Science and Health. Part A: Environmental Science and Engineering and Toxicology*, 1996. 31(5), 1035-1041.
10. Uddin, M. J., Islam, M. A., Haque, S. A., Hasan, S., Amin, M. S. A., and Rahman, M. M., Preparation of nanostructured TiO<sub>2</sub>-based photocatalyst by controlling the calcining temperature and pH. *International Nano Letters*, 2012. 2(1), 1-10.
11. Moreno-Benito, M., Yamal-Turbay, E., Espuña, A., Pérez-Moya, M., and Graells, M., *Optimal recipe design for Paracetamol degradation by advanced oxidation processes (AOPs) in a pilot plant*, in *Computer Aided Chemical Engineering*, A. Kraslawski and I. Turunen, Editors. 2013, Elsevier. p. 943-948.
12. Kumar, V. and Shah, M. P., *1 - Advanced oxidation processes for complex wastewater treatment*, in *Advanced Oxidation Processes for Effluent Treatment Plants*, M.P. Shah, Editor. 2021, Elsevier. p. 1-31.
13. Islam, M., Amin, M., and Hoinkis, J., Optimal design of an activated sludge plant: theoretical analysis. *Applied Water Science*, 2013. 3(2), 375-386.

14. Obotey Ezugbe, E. and Rathilal, S., Membrane Technologies in Wastewater Treatment: A Review. *Membranes*, 2020. 10(5), 89.
15. Amin, M. S. A., Stüber, F., Giralt, J., Fortuny, A., Fabregat, A., and Font, J., Comparative Anaerobic Decolorization of Azo Dyes by Carbon-based Membrane Bioreactor. *Water*, 2021. 13(8), 1060.
16. Amin, M. S. A., Stüber, F., Giralt, J., Fortuny, A., Fabregat, A., and Font, J., Ceramic-supported graphene oxide membrane bioreactor for the anaerobic decolorization of azo dyes. *Journal of Water Process Engineering*, 2022. 45, 102499.
17. Giménez-Pérez, A., Bikkarolla, S. K., Benson, J., Bengoa, C., Stüber, F., Fortuny, A., Fabregat, A., Font, J., and Papakonstantinou, P., Synthesis of N-doped and non-doped partially oxidised graphene membranes supported over ceramic materials. *Journal of Materials Science*, 2016. 51(18), 8346-8360.
18. Lourenço, N. D., Novais, J. M., and Pinheiro, H. M., Effect of some operational parameters on textile dye biodegradation in a sequential batch reactor. *Journal of Biotechnology*, 2001. 89(2), 163-174.
19. Khehra, M. S., Saini, H. S., Sharma, D. K., Chadha, B. S., and Chimni, S. S., Decolorization of various azo dyes by bacterial consortium. *Dyes and Pigments*, 2005. 67(1), 55-61.
20. El Bouraie, M. and El Din, W. S., Biodegradation of Reactive Black 5 by *Aeromonas hydrophila* strain isolated from dye-contaminated textile wastewater. *Sustainable Environment Research*, 2016. 26(5), 209-216.
21. Elshahawy, M. F., Mahmoud, G. A., Raafat, A. I., Ali, A. E.-H., and Soliman, E. s. A., Fabrication of TiO<sub>2</sub> Reduced Graphene Oxide Based Nanocomposites for Effective of Photocatalytic Decolorization of Dye

- Effluent. *Journal of Inorganic and Organometallic Polymers and Materials*, 2020. 30(7), 2720-2735.
22. Sazali, N., Salleh, W. N. W., Md Nordin, N. A. H., Harun, Z., and Ismail, A. F., Matrimid-based carbon tubular membranes: The effect of the polymer composition. *Journal of Applied Polymer Science*, 2015. 132(33), 1-12.
  23. Barsema, J. N., Klijnstra, S. D., Balster, J. H., van der Vegt, N. F. A., Koops, G. H., and Wessling, M., Intermediate polymer to carbon gas separation membranes based on Matrimid PI. *Journal of Membrane Science*, 2004. 238(1), 93-102.
  24. Ismail, N. H., Salleh, W. N. W., Sazali, N., Ismail, A. F., Yusof, N., and Aziz, F., Disk supported carbon membrane via spray coating method: Effect of carbonization temperature and atmosphere. *Separation and Purification Technology*, 2018. 195, 295-304.
  25. Sazali, N., Salleh, W. N. W., Nordin, N. A. H. M., and Ismail, A. F., Matrimid-based carbon tubular membrane: Effect of carbonization environment. *Journal of Industrial and Engineering Chemistry*, 2015. 32, 167-171.
  26. Ismail, N. H., Salleh, W. N. W., Sazali, N., and Ismail, A. F., Effect of intermediate layer on gas separation performance of disk supported carbon membrane. *Separation Science and Technology*, 2017. 52(13), 2137-2149.
  27. Ming, J., Sun, D., Wei, J., Chen, X., and Zheng, N., Adhesion of Bacteria to a Graphene Oxide Film. *ACS Applied Bio Materials*, 2020. 3(1), 704-712.

28. Mezohegyi, G., Bengoa, C., Stuber, F., Font, J., Fabregat, A., and Fortuny, A., Novel bioreactor design for decolourisation of azo dye effluents. *Chemical Engineering Journal*, 2008. 143(1), 293-298.
29. Wu, P.-C., Chen, H.-H., Chen, S.-Y., Wang, W.-L., Yang, K.-L., Huang, C.-H., Kao, H.-F., Chang, J.-C., Hsu, C.-L. L., Wang, J.-Y., Chou, T.-M., and Kuo, W.-S., Graphene oxide conjugated with polymers: a study of culture condition to determine whether a bacterial growth stimulant or an antimicrobial agent? *Journal of Nanobiotechnology*, 2018. 16(1), 1.
30. Mokkalapati, V. R. S. S., Pandit, S., Kim, J., Martensson, A., Lovmar, M., Westerlund, F., and Mijakovic, I., Bacterial response to graphene oxide and reduced graphene oxide integrated in agar plates. *Royal Society Open Science*. 5(11), 181083.
31. Ma, J., Ping, D., and Dong, X., Recent Developments of Graphene Oxide-Based Membranes: A Review. *Membranes*, 2017. 7(3), 52.
32. García-Martínez, Y., Bengoa, C., Stüber, F., Fortuny, A., Font, J., and Fabregat, A., Biodegradation of acid orange 7 in an anaerobic–aerobic sequential treatment system. *Chemical Engineering and Processing - Process Intensification*, 2015. 94, 99-104.
33. Xiao, X., Li, T.-T., Lu, X.-R., Feng, X.-L., Han, X., Li, W.-W., Li, Q., Yu, H.-Q., A simple method for assaying anaerobic biodegradation of dyes. *Bioresource technology*. 2018. 251, 204-9.
34. Berradi, M., Hsissou, R., Khudhair, M., Assouag, M., Cherkaoui, O., El Bachiri, A., and El Harfi, A., Textile finishing dyes and their impact on aquatic environs. *Heliyon*, 2019. 5(11), e02711.

35. Khan, R., Bhawana, P., and Fulekar, M. H., Microbial decolorization and degradation of synthetic dyes: a review. *Reviews in Environmental Science and Bio/Technology*, 2013. 12(1), 75-97.
36. Shi, Y., Yang, Z., Xing, L., Zhang, X., Li, X., and Zhang, D., Recent advances in the biodegradation of azo dyes. *World Journal of Microbiology and Biotechnology*, 2021. 37(8), 137.
37. Franciscon, E., Zille, A., Fantinatti-Garboggini, F., Silva, I. S., Cavaco-Paulo, A., and Durrant, L. R., Microaerophilic–aerobic sequential decolourization/biodegradation of textile azo dyes by a facultative *Klebsiella* sp. strain VN-31. *Process Biochemistry*, 2009. 44(4), 446-452.
38. Garcia-Segura, S., Centellas, F., Arias, C., Garrido, J. A., Rodríguez, R. M., Cabot, P. L., and Brillas, E., Comparative decolorization of monoazo, diazo and triazo dyes by electro-Fenton process. *Electrochimica Acta*, 2011. 58, 303-311.
39. Rahimi, M., Aghel, B., Sadeghi, M., and Ahmadi, M., Using Y-shaped microreactor for continuous decolorization of an Azo dye. *Desalination and Water Treatment*, 2014. 52(28-30), 5513-5519.
40. Chen, B.-Y., Understanding decolorization characteristics of reactive azo dyes by *Pseudomonas luteola*: toxicity and kinetics. *Process Biochemistry*, 2002. 38(3), 437-446.
41. Popli, S. and Patel, U. D., Destruction of azo dyes by anaerobic–aerobic sequential biological treatment: a review. *International Journal of Environmental Science and Technology*, 2015. 12(1), 405-420.
42. Chen, B.-Y., Chen, S.-Y., and Chang, J.-S., Immobilized cell fixed-bed bioreactor for wastewater decolorization. *Process Biochemistry*, 2005. 40(11), 3434-3440.

## **Chapter 6. Biofilm Model Development and Process Analysis of Anaerobic Bio-digestion of Azo Dyes**

### **Abstract:**

Ceramic-supported graphene oxide membrane bioreactors have already shown their potential for the anaerobic decolorization of wastewater containing azo dyes. The primary goal of this investigation was to develop a mathematical model that would be able to describe the steady-state behavior of this biodegradation process. The developed model was calibrated and validated using independent experimental data sets with various dye structure, feed concentration, hydraulic retention time (HRT) and support materials on which the biofilm was grown. The main aim was to analyze the intrinsic mechanism of the process, which was found to be the hydrolysis that was the rate limiting step of the process. Hydrolysis rate constant were dependent on dye structure and support material. It was decreased when increasing the complexity of the dye structure and also with decreasing the electron carrying capacity of support material. Dye molecules with a higher molecular weight or a more complicated structure had a lower hydrolysis rate. Support materials with high electron transfer capacity increased the biofilm activity, therefore, the hydrolysis rate constant. Increase of the acetate concentration, used as external carbon source, improved the dye removal efficiency, too. However, acetate to dye ratio did not have direct relation to dye removal efficiency. As expected, higher hydraulic retention time (HRT) increased the contact time between dye molecules and biofilm, which enhanced the process efficiency. However, it is essential to impose the right balance between HRT and external carbon sources to make the process feasible.

---





## 1. Introduction

The textile and garment sector still plays a significant role in the growth of the global economy. In the rapid expansion of these industries, several issues have arisen related to huge water pollution. The main cause of this pollution is the extensive use and discharge of dyestuff, especially azo dyes, which represent 70% of the organic colorant chemicals [1]. Industrially, over 100000 types of dyes and pigments are being used, with an annual production volume of 700000 tons [2]. A recent research found that about 744 tons of wastewater are generated while manufacturing one ton of dye [3]. Another statistics reported that nearly 200000 tons of dyes per annum are lost in the effluent streams during the dyeing and printing process, which are discharged into the aquatic system [4]. This enormous amount of dye-containing waste released into the environment consistently pollutes the lakes, rivers, and other water reservoirs [5]. Therefore, it is essential to treat these textile effluents before discharging in order to save and maintain healthy aquatic life.

Numerous approaches, including physical, chemical, physicochemical, and biological processes, were examined independently or combined to treat the dye-containing wastewater. Considering the efficiency, generation of secondary sludge and toxic byproduct, installation, and operating cost, the integration of membrane filtration and anaerobic biodegradation of textile dyes has proven to be very attractive [6-8]. Membranes made of carbonaceous materials with a conductive top layer are often suitable for such treatment method. A recent study demonstrated that the Ceramic-supported Carbon Membrane (CSCM) had the ability to complete decolorization of azo dyes [6]. During the anaerobic biodegradation of azo dye, the nanosized CSCM helps to generate an active biofilm by retaining the microorganism on its

surface. In addition, this layer enhanced the electron shuttle mechanism between the azo bond and microorganisms to increase the biodegradation rate [9]. Aside from that, this membrane improves the treatment performance through the retention of the dye molecules and biodegradable products. Amin et al. [7] also investigated the influence of the conductive Ceramic-supported Graphene Oxide Membrane (CSGOM) derived from the exfoliated graphene oxide (GO) on biodecolorization performance, and the results showed that the CSGOM is more efficient for color removal than the membranes consisting of carbonized Matrimid 5218.

The mechanism of the anaerobic biodecolorization in a compact bioreactor appeared to be initiated through the biosorption of dye molecules on microorganisms and later completed by biodegradation of dyes within microbial cells [10]. During the biosorption, the dye entraps on the surface. However, the biodegradation occurred when the azo bonds of the dye molecules started to cleavage to form aromatic amines with the functional groups of  $-SO_3$ ,  $-OH$ ,  $-COOH$ ,  $-N$ , etc. [11]. Subsequently, under aerobic conditions, those biodegradable aromatic products underwent extensive mineralization resulting highly decolorized treated water [12]. Various researches experiments have been conducted to enhance the performance of anaerobic dye decolorization by biodegradation [13-15]. These studies concluded that the dye reduction process was directly influenced by several factors such as bioavailability, adaptability and selective activity of microbial entities in the aqueous medium, supplementary carbon sources, dye structure and concentration, and retention time.

It has been demonstrated that mixed bacterial cultures outperform single pure cultures in several biological dye-containing wastewater treatment

systems [10, 12]. The mixed bacterial cultures produce a better level of azo dye decolorization than the pure strains due to complementary catabolic pathways within the microbial community and the vulnerability to contamination [16-18]. Moreover, the mixed microbial consortia involved in anaerobic decolorization of dye molecules convert the soluble substrate into volatile acids or alcohols that serve as a competitive substrate for methanogenic, sulfate-reducing, and acetogenic bacteria [19,20]. Additionally, mixed culture is beneficial due to high microbial diversity, which helps to reduce toxicity and improves process stability by resisting variations in quality and amount of wastewater [21]. These anaerobic biodegradation processes are enhanced by the presence of organic carbon or energy sources that act as electron-donors. In such cases, several primary electron source substances such as acetate, glucose, starch and ethanol have been used for bacterial growth to enhance the biodecolorization rate [22].

According to literature, dye structure and concentration in the feed streams significantly affect the anaerobic decolorization kinetics. The dyestuff with simple structure and low molecular weight showed higher biodegradation rate compared to complex and high molecular weight dyes [23, 24]. A recent study [6] on anaerobic decolorization of monoazo Acid Orange 7 (AO7), diazo Reactive Black 5 (RB5), and triazo Direct Blue 71 (DB71) showed that the color removal was 98%, 80%, and 69%, respectively, for AO7, RB5, and DB71. This result indicated that the decolorization rate decreased progressively with increasing molecular weight and substitution -SO<sub>3</sub>H and -N=N- groups. The biodegradation of textile dyes also reduced progressively with increasing initial dye concentration, which was consistent with previous findings. Various dye concentrations were examined and most effective for decolorization were found for lower concentrations [10, 25].

High dye concentrations may inhibit microbial growth therefore reducing microbial dye removal efficiency. The most likely explanation is that presence of more reactive groups of the dye molecules in the anaerobic bioreactor impeded microbial development due to a lack of sufficient biomass concentration in the culture, blockage of active sites of azoreductase, and aromatic metabolites products [26, 27]. It was also found that, after rise of initial dye concentration from 50 to 100 mg·L<sup>-1</sup>, the integrated anaerobic membrane bioreactor fed with different solutions of AO7, RB5, and DB71 exhibited a similar decreasing trend. Besides initial dye concentration, hydraulic retention time (HRT), which must be understood as contact time, has a critical relation with color removal rate; decolorization of dye molecules improved with increasing HRT [24, 28]. Due to the extended HRT, the system may efficiently treat dye-containing wastewater, even at a higher initial feed concentration.

The anaerobic biodegradation of dyes molecules comprises a number of complex process steps including microbial growth, hydrolysis of complex dye molecules, anaerobic degradation of hydrolyzed products, biomass decay, maintenance etc. These steps involve a number of process operation variables. Mathematical models were used to determine the kinetics and process parameters of microbial growth and biodegradation of dyes, as well as to develop adequate process strategies aiming to maximize dye removal. Very few mathematical models have been constructed to analyze the biodegradation of dyes and they are mainly focused on optimization of process variables using response surface methodology [29]. However, to the best of our knowledge, no model is available to analyze the underlying mechanisms for biodegradation of dyes.

With the aforesaid limitations in dyes biodegradation research, this work attempts to understand the mechanism of biodecolorization of azo dye under an integrated anaerobic membrane bioreactor. To analyze the mechanism, a kinetic model was developed based on operation conditions tested for maximum dyes removal. The model was built from a simple set of reaction kinetics and an empirical relation for the hydrolysis rate equation. In more detail, the model was utilized to investigate the influence of the essential operating parameters, for example, dye structures, initial dye concentration, and permeate flux on the dye removal. Therefore, the interaction among the HRT, external carbon source and dye concentration in a biofilm reactor for dye removal has been assessed for the first time. Hydrolysis behavior of complex dye molecules and effect of support materials for biofilm were also assessed. The steady-state model behavior was considered in all cases to evaluate the overall process responses.

## **2. Materials and Methods**

### **2.1 Preparation of Bioreactors**

The biofilm in a single bed bioreactor with ceramic-supported carbon membrane (CSCM) and ceramic-supported graphene oxide membrane (CSGOM) support materials were developed for the bio-digestion of dyes. In order to build the CSCM, a membrane precursor containing 10% wt. Matrimid solution was carbonized over the ceramic support. CSGOM, on the other hand, was created using a standard technique outlined by Gimenez-Perez et al. (2016) [30]. In this case, 1 mg/mL graphene oxide solution was used to make the CSGOM support material. The biofilm was produced seeding secondary anaerobic sludge collected from a municipal WWTP

(Reus, Spain), which was placed over the CSCM and CSGOM support materials.

## 2.2 Process Configuration

A controllable vacuum filtration unit in which CSCM and CSGOM were used as filters and support for biofilm growth was applied. Three different types of dyes, monoazo AO7 (ACROS Organics, ref. 416561000), diazo RB5 (Sigma Aldrich, ref. 306452), and triazo DB71 (Sigma Aldrich, ref. 212407), were selected to generate the artificial wastewater that was mixed with sodium acetate (Sigma Aldrich, ref. 110191) maintaining the absolute concentration (in mg/mL) ratio 1:3. The dye and sodium acetate mixture was then mixed with 1 mL of each basal medium (BM) to make the feed solution. There were six basal mixtures; the elements contained, and composition are listed in Table 1.

**Table 1.** Composition and concentration of the different basal media.

Basal medium (BM)	Minerals	Concentration (mg/L)
<b>BM 1</b>	MnSO <sub>4</sub> ·H <sub>2</sub> O	0.15
	CuSO <sub>4</sub> ·5H <sub>2</sub> O	0.28
	ZnSO <sub>4</sub> ·7 H <sub>2</sub> O,	0.46
	CoCl <sub>2</sub> ·6H <sub>2</sub> O	0.26
	(NH <sub>4</sub> ) <sub>6</sub> Mo <sub>7</sub> O <sub>24</sub> ;	0.28
<b>BM 2</b>	K <sub>2</sub> HPO <sub>4</sub>	21.75
	Na <sub>2</sub> HPO <sub>4</sub> ·2H <sub>2</sub> O	33.40
	KH <sub>2</sub> PO <sub>4</sub>	8.50
<b>BM 3</b>	FeCl <sub>3</sub> ·6H <sub>2</sub> O	29.06
<b>BM 4</b>	CaCl <sub>2</sub>	13.48
<b>BM 5</b>	MgSO <sub>4</sub> ·7H <sub>2</sub> O	15.20
<b>BM 6</b>	NH <sub>4</sub> Cl	190.90

All the chemicals (Sigma Aldrich, Spain) used in this study were analytical grade and the solutions were made with Milli-Q water (Millipore Milli-Q system, Molsheim, France). The feed solution was kept at 1°C to prevent microbial growth in feed solution tank. Nitrogen gas (>99.99 %, Linde) was sparged through the feed tank to maintain it under anaerobic conditions (negative redox potential) and, also, for controlling the permeate flux by setting the needed pressure. The compact bioreactor was run under dead-end filtration mode at a temperature of  $37 \pm 1$  °C. Samples were collected every regular interval and then, the dye concentration, acetate concentration, ammonium concentration and COD immediately analyzed.

### 2.3 Analytical Procedure

The decolorization rate was measured in a visible/UV spectrophotometer (DINKO Instruments, Barcelona, Spain), whereas the maximum absorption wavelength was set at 484 nm for AO7, 597 nm for RB5, and 585 nm for DB71. Acetate concentration in both feed and permeate solution was determined by high-performance liquid chromatography (HPLC) on a C18 Hypersil ODS column applying a gradient of methanol-water mobile phase with a flow rate of 1 mL/min [31]. Portable chemical oxygen demand (COD) test kit (Vario 2420721 and 2420722) was used to measure the wastewater COD. The ammonium-N was determined by the salicylate method (Lovibond method 66) using the Lovibond testing kit (Vario 535650).

### 2.4 Model Development

The anaerobic digestion model was developed based on Activated Sludge Model-2 (ASM2) to examine the anaerobic bio-digestion of dye using a single bed biofilm reactor. An empirical hydrolysis rate equation was developed from the experimental datasets.



The model for anaerobic dye decomposition takes into account four main processes: (1) anaerobic hydrolysis of dye ( $S_S$ ); (2) fermentation of fermentable materials ( $S_F$ ); (3) anaerobic digestion of fermented product ( $S_A$ ) and (4) biomass decay. The model stoichiometry and kinetics are listed in Tables 2 and 3, respectively. The stoichiometric and kinetic parameter values are listed in Table 4.

**Table 2.** Stoichiometric matrix  $A_{ij}$ .

$A_{ij}$	<b>i</b>	$S_S$	$S_F$	$S_A$	$S_H$	$S_{NH}$	$S_{SO2}$	$X_H$	$X_I$
	<b>component</b> →	[mgCOD/ mL]	[mgCOD/ mL]	[mgCOD/ mL]	[mgCOD/ mL]	[mgN/ mL]	[mgS/ mL]	[mgCOD/ mL]	[mgCOD/ mL]
	<b>j process</b> ↓								
1.	Anaerobic hydrolysis	-1	$1 - (V_{NH} + V_S)$			$V_{NH}$	$V_S$		
2.	Fermentation		-1	1					
3.	Anaerobic digestion			$-1/Y_H$	$(1 - Y_H)/Y_H$	$-i_{NXB}$		1	
4.	Decay		$1 - f_I$			$i_{NXB} - f_I i_{NXI}$		-1	$f_I$

**Table 3.** Kinetic rate expressions.

<b>j process</b>	<b>Kinetic rate</b>	<b>Equation</b>
1. Anaerobic hydrolysis	$\rho_H = k_h \cdot S_{S(in)}^{-n} S_S \cdot X_H$	(1)
2. Anaerobic fermentation	$\rho_F = q_{fa} \cdot \frac{S_F}{K_{fe} + S_F} \cdot X_H$	(2)
3. Anaerobic digestion	$\rho_{AD} = \mu_{max}^{AD} \cdot \frac{S_A}{K_A^H + S_A} \cdot \frac{S_{NH}}{K_{NH}^H + S_{NH}} \cdot X_H$	(3)
4. Decay of $X_H$	$\rho_D = b_H \cdot X_H$	(4)

**Table 4.** Stoichiometric and kinetics parameters.

Parameter	Value	Units	Reference
$Y_H$	0.06	mgCOD/mgCOD	[32]
$\mu_{\max}^{AD}$	2.0325	$\text{h}^{-1}$	Estimated
$k_h$	<b>Biofilm on CSGOM support:</b> AO7: $1.3141 \pm 0.061$ RB5: $0.2873 \pm 0.011$ DB71: $0.2621 \pm 0.017$ <b>Biofilm on CSCM support materials:</b> DB71: $0.0410 \pm 0.0040$	$(\text{mgCOD})^{n-1}/(\text{L}^{n-1} \cdot \text{h})$	Estimated
$n$	$1.6852 \pm 0.018$		Estimated
$K_A^H$	0.0760	mgCOD/mL	[32]
$K_{NH}^H$	0.0300	mgN/mL	[32]
$b_H$	0.00083	$\text{h}^{-1}$	[32]
$q_{fe}$	2.0325	$\text{h}^{-1}$	Assumed same as $\mu_{\max}^{AD}$
$K_{fe}$	0.0040	mgCOD/mL	[33]
$i_{NXB}$	0.0700	mgN/mgCOD	[33]
$i_{NXI}$	0.0700	mgN/mgCOD	Assumed same as $i_{NXB}$
$f_I$	0.0800	mgCOD/mgCOD	[33]
$V_{NH}$	<b>Fraction of nitrogen in dye:</b> Acid Orange 7: 0.0422 Reactive Black 5: 0.062 Direct Blue 71: 0.0570	mgN/mgCOD	From stoichiometric calculation
$V_S$	<b>Fraction of sulphur in dye:</b> Acid Orange 7: 0.0481 Reactive Black 5: 0.1700 Direct Blue 71: 0.0740	mgS/mgCOD	From stoichiometric calculation
$D_{NH}$	0.0625	$\text{cm}^2 \cdot \text{h}^{-1}$	[34]
$D_{O_2}$	0.0917	$\text{cm}^2 \cdot \text{h}^{-1}$	[35]
$D_S$	0.0417	$\text{cm}^2 \cdot \text{h}^{-1}$	[36]
$D_H$	0.0538	$\text{cm}^2 \cdot \text{h}^{-1}$	[37]
$D_{SO_2}$	0.0917	$\text{cm}^2 \cdot \text{h}^{-1}$	Assumed same as $D_{O_2}$

- (1) After unit conversion, using a typical biomass composition of  $\text{CH}_{1.8}\text{O}_{0.5}\text{N}_{0.2}$ , corresponding with 1.3659 mgCOD/mg [38]
- (2) 1 mg Sodium acetate = 0.78 mgCOD, 1 mg Acid Orange 7 = 1.987 mgCOD, 1 mg Reactive Black 5 = 1.331 mgCOD, 1 mg Direct Blue 71 = 1.790 mgCOD (theoretically calculated)
- (3) Conversion of ASM2 and ASM2d-values given by Henze et al. (2000) [33] at 10°C and 20°C to 37°C using temperature relationship proposed by these authors (in ASM3):

$$k(T) = k(20\text{ }^\circ\text{C}) \cdot \exp(\theta_T \cdot (T - 20\text{ }^\circ\text{C}))$$

$$\theta_T = \frac{\ln(k(T_1) / k(T_2))}{T_1 - T_2}$$

It is assumed that all dyes undergo hydrolysis first and then anaerobic fermentation and subsequent digestion. The first process, hydrolysis of dye ( $S_S$ ), followed simple reaction kinetics, proportional to dye concentration and presence of microorganisms. As a result, the fermentable materials ( $S_F$ ) were produced through hydrolysis of complex dye molecules. Fermentable materials then are converted to fermented products ( $S_A$ ) by following anaerobic fermentation (second process) that followed Monod kinetics as described in ASM2 [33]. It must be noted that, in this study, acetate was considered as the fermented product ( $S_A$ ). The  $S_A$  was then transformed through anaerobic digestion (third process) and converted to carbon dioxide and methane ( $S_H$ ). Anaerobic digestion depends on the  $S_A$  and ammonium concentration. The growth of microorganisms resulted from the anaerobic digestion, where ammonium nitrogen played a significant role. According to ASM2, it was also considered that hydrolysis and fermentation did not take part in microbial growth. The microorganisms ( $X_H$ ) produced by digestion process took part in all biological activities. The amine group and sulphur

present in dye molecules were converted to the ammonium and hydrogen sulphite through anaerobic hydrolysis.

Therefore, the process was stated as completely anaerobic, so oxygen was not considered as an operating variable in this study. Carbon dioxide and methane produced during digestion did not affect the process and hence was not accounted in the global kinetics.

The biomass decay followed the death-regeneration concept in which the living cells were directly converted to soluble organic substrate and a fraction of inert materials [39]. Decay was first order kinetics and its rate limited steps over the hydrolysis of decay product. Therefore, hydrolysis merged with the decay and fermentable materials were directly produced from the decay of biomass [40].

## **2.5 Reactor Configuration, Simulation Parameters and Initial Conditions**

A one-dimensional biofilm model, only considering gradients through biofilm depth was set up to describe the process. The model was implemented in the Aquasim software [41]. The reactor had a fixed volume of 5 mL; same as that experimentally used. A layer of biomass was assumed to grow on the support materials (CSCM or CSGOM) with a surface area of 13.1 cm<sup>2</sup> for a predefined biofilm thickness of 2 μm. The biofilm was generally dense and rigid and biofilm porosity was assumed to be constant (25%). The density of the biomass and inert materials were considered as 60 mg VSS/mL [42] and, according to Henze et al., (2000), it corresponds to 80 mg COD/mL [33].

The process was evaluated in both experimental and model simulation for an influent containing dye and acetate maintaining the concentration ratio 1:3, even when dye flow rate varied from 0.0655 to 0.131 mL/h. The dye

concentration ranged from 0.05 mg/mL to 0.10 mg/mL. It was assumed that there was initially no other fermentable organic matter ( $S_F$ ) in the inflow. The initial concentrations of dye and substrate in the bulk liquid was assumed equal to influent concentrations. The processes were operated at 37°C. Steady-state simulations were performed to evaluate the process. The interactive effect of dye concentration, HRT, and influent fermented product ( $S_A$ ) were investigated by performing steady-state calculations for different combinations of their concentrations and variation of feed flow rate.

## 2.6 Model Calibration and Validation

The model calibration was performed to determine model parameters represented by constant variables from available data. The parameters were estimated by AQUASIM by minimizing the sum of the squares of the weighted deviations between measurements and simulation outcomes as per Eq. 5.

$$\chi^2(P) = \sum_{i=1}^m \left( \frac{y_{\text{exp},i} - y_{i(P)}}{\sigma_{\text{exp},i}} \times 100 \right)^2 \quad (5)$$

Here,  $y_{\text{exp},i}$  is the experimental value,  $\sigma_{\text{exp},i}$  is its standard deviation,  $y_{i(P)}$  is the simulated value of the corresponding model parameter  $P$ , and  $m$  is the number of data points.

The model validation was conducted through the visual comparison of experimental values and steady-state simulation outcomes. Moreover, the validation was confirmed by calculation of percentage deviation (%) defined by Eq. 6. Less than 9% deviations were considered as acceptable value in this study.

$$\% \text{ deviation} = \left( \frac{y_{\text{exp}, i} - y_{i(P)}}{y_{\text{exp}, i}} \times 100 \right) \quad (6)$$

### 3. Results and Discussions

#### 3.1 Model Calibration

To describe the anaerobic biodegradation of dye, the developed model was calibrated on independent experimental datasets. For the model calibration, continuous mode biodegradation was selected using monoazo AO7 dye with different feed concentrations and flow rates. In this case, the biofilm was developed on ceramic-supported graphene oxide membrane (CSGOM). In all the cases, acetate was set three times higher than dye concentration (in mg/mL), although it was fully consumed through the biodegradation process. The results showed that steady state AO7 concentration in permeate was increased with increasing feed concentration and decreasing HRT. Maintaining 76.3 h of HRT, the permeate AO7 concentration was increased from  $0.00166 \pm 0.00052$  mgCOD/mL to  $0.00520 \pm 0.00096$  mgCOD/mL with increasing feed concentration from 0.099 mgCOD/mL (0.05 mg/mL) to 0.190 mgCOD/mL (0.10 mg/mL).

Accordingly, the removal was decreased from 98.3% to 97.4% (Table 5). Decreasing HRT increased the permeate concentration so lowered the efficiency of the biodegradation because higher feed flow rate reduces the HRT that adversely affects the dye removal efficiency. Thus, the HRT decrease from 76.3 h to 38.2 h, dropped the dye removal efficiency from 97.38% to 94.82% (Table 5).

**Table 5.** Experimental removal of AO7 by CSGOM-biofilm reactor at various hydraulic retention times and dye feed concentration.

HRT (h)	AO7 concentration in feed ( $S_{S(in)}$ ) (mgCOD/mL)	% Dye removal
<b>76.3</b>	0.099	98.3
	0.149	97.8
	0.198	97.4
<b>50.9</b>	0.099	97.5
	0.149	96.8
	0.198	95.9
<b>38.2</b>	0.099	96.8
	0.149	95.9
	0.198	94.8

The hydrolysis rate constant ( $k_h$ ) for AO7 biodegradation, the power index of inflow dye concentration in feeding solution ( $n$ ) and maximum specific growth rate of anaerobic organism ( $\mu_{\max}^{AD}$ ) were determined from the model calibration. The experimental datasets with fixed HRT, 76.3 h, at various inflow dye concentrations, from 0.099 mgCOD/mL to 0.199 mgCOD/mL, were used for the calibration. The estimated value of hydrolysis constant,  $k_h$ , was found to be  $1.314 \pm 0.061$  (mgCOD) $^{n-1}/$  (L $^{n-1}$ ·h), while  $n$  was  $1.685 \pm 0.018$ , and  $\mu_{\max}^{AD}$  was  $2.032$  h $^{-1}$  for all the feed concentrations.

### 3.2 Model Validation

The calibrated model was validated for several HRT in the CSGOM-biofilm reactor, and the different AO7 dye feed concentration. Using the estimated hydrolysis rate constant, the power index ( $n$ ) and maximum specific growth rate of anaerobic organism ( $\mu_{\max}^{AD}$ ), the model could describe the steady state behavior of the biodegradation of AO7 very well with deviations below 8% (Figure 1).

The calculated hydrolysis rate constant was very high compared to literature since, according to ASM2d model, it is  $0.25 \text{ h}^{-1}$  [33]. This hydrolysis constant was even higher than the acidic hydrolysis constant of glucose [43]. The high hydrolysis constant in this study was due to the reduced detachment of biofilm with the support material GO and high electron transfer rate [7] that improve the microbial activities [31] as well as ensure biodegradation of dye with a high efficiency.

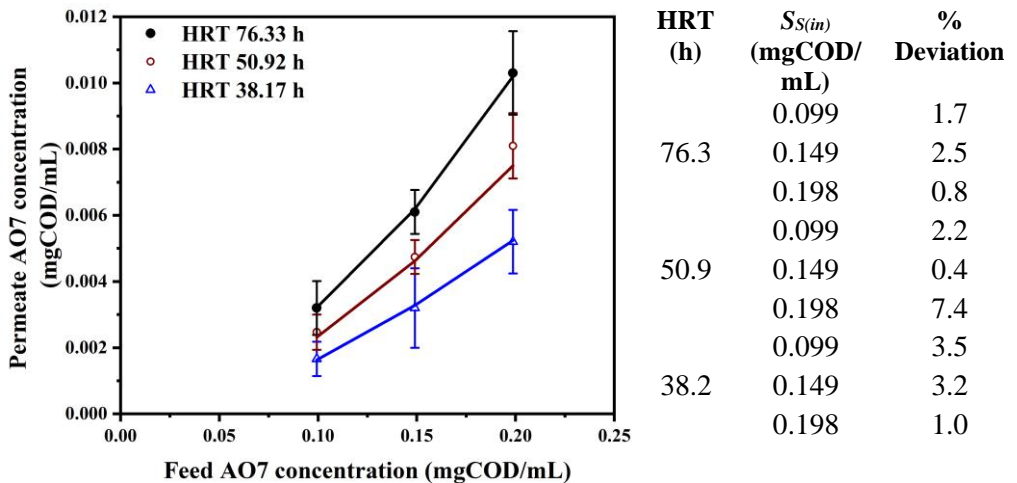


**Figure 1.** Comparison between experimental and predicted outcomes of AO7 removal at steady-state using a CSGOM-biofilm reactor (points are the experimental values and lines are predictions from the model).



### 3.3 Model Evaluation with Various Types of Dye

Anaerobic biodegradation in a CSGOM-biofilm reactor was also evaluated for three different types of dye; in addition to AO7, diazo RB5 and triazo DB71. In both cases, the dye concentration was changed from 0.05 mg/mL ( $\approx$  0.066 mgCOD/mL RB5 and 0.089 mgCOD/mL DB71) to 0.10 mg/mL ( $\approx$  0.133 mgCOD/mL RB5 and 0.179 mgCOD/mL DB71) whilst feed flow rate was varied from 0.065 mL/h to 0.131 mL/h to set the hydraulic retention time from 76.3 h to 38.2 h.

Increasing hydraulic retention time improved the dye removal efficiency and, consequently, decreased the dye concentration in permeate (Table 6). As usual, any increase of the flow rate decreases the HRT that adversely affects the dye removal efficiency. Higher feed concentration also has adverse effect on removal of the dyes. Comparing the three types of dyes; AO7 shown better removal efficiency and DB71 showed the lowest (Table 5 and 6), following the number of azo bonds in the respective molecule.

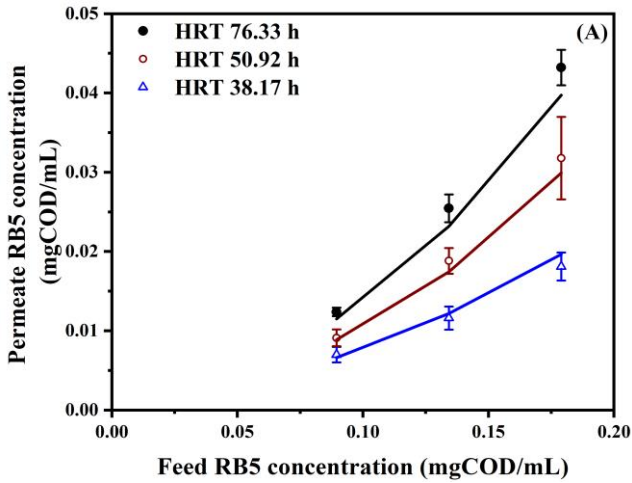
**Table 6.** RB5 and DB71 removal in a CSGOM-biofilm reactor for several hydraulic retention times and dye concentrations.

HRT (h)	Reactive Black 5		Direct Blue 71	
	Feed concentration ( $S_{S(in)}$ ) (mgCOD/mL)	% Dye removal	Feed concentration ( $S_{S(in)}$ ) (mgCOD/mL)	% Dye removal
76.3	0.066	95.9	0.089	92.2
	0.099	94.5	0.134	91.4
	0.133	93.0	0.179	89.9
50.9	0.066	93.4	0.089	89.8
	0.099	90.6	0.134	86.0
	0.133	88.6	0.179	82.2
38.2	0.066	90.6	0.089	86.7
	0.099	88.1	0.134	81.5
	0.133	86.3	0.179	76.0

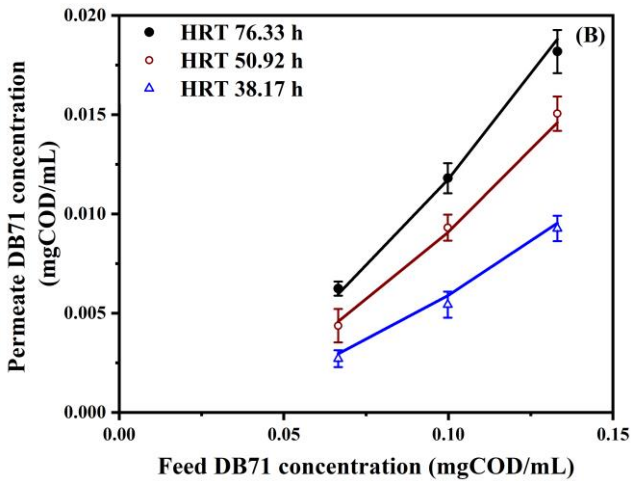
If they are applied the estimated hydrolysis constant ( $k_h$ ), power index of inflow feed concentration ( $n$ ) and maximum specific growth rate of anaerobic organism ( $\mu_{\max}^{AD}$ ) from the biodegradation of AO7, it is not able to describe the steady state behavior of RB5 and DB71 (data was not shown). As the dye structures and functionality were not similar to each other; the hydrolysis rate constant is not the same and needs to be re-estimate for these dyes. The estimated hydrolysis constants ( $k_h$ ) were  $0.287 \pm 0.011$  (mgCOD)<sup>n-1</sup>/ (L<sup>n-1</sup>.h) ( $\chi^2 = 0.00009$ ) for RB5 and  $0.262 \pm 0.017$  (mgCOD)<sup>n-1</sup>/ (L<sup>n-1</sup>.h) ( $\chi^2 = 0.00007$ ) for DB71. Using these re-estimated  $k_h$ , the model predictions agreed well with the experimental values of dye concentration in permeate at steady-state (Figure 2). The percentage deviation associated with HRT, dye feed concentration and dye types were below 9%, which demonstrates the goodness of the model fit.

Hydrolysis rate constant was indeed quite different for each type of dye. Increasing molecular weight as well as complexity of dye structure lowers the hydrolysis capacity of the microorganisms, which becomes in lower hydrolysis constant (Table 7). Tombari et al. (2007) [44] found that the change of configurational and vibrational partition functions has a significant effect on hydrolysis. Kura (1987) [45] analyzed the hydrolysis for different membered inorganic cyclophosphates and found that the lowest membered cyclotriphosphate showed the most rapid hydrolysis,. In addition, there were a wide variation of hydrolysis due to structural variation [46]. Similarly, in this study, it has been found that the hydrolysis rate constant decreased with increasing molecular weight that also correlates here with higher number of azo bonds in the dye molecules (Table 7).

6. Biofilm Model Development and Process Analysis of Anaerobic Bio-digestion of Azo Dyes



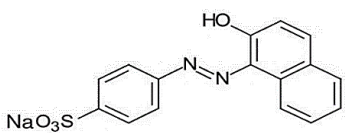
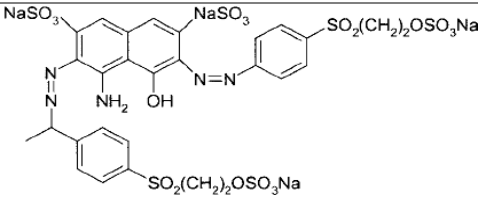
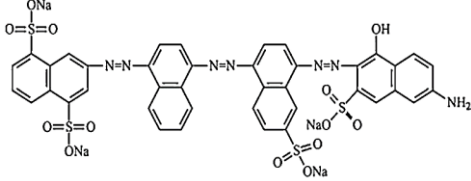
HRT (h)	$S_{S(in)}$ (mgCOD/mL)	% Deviation
76.3	0.066	8.9
	0.099	8.3
	0.133	2.8
50.9	0.066	4.8
	0.099	2.7
	0.133	3.0
38.2	0.066	4.4
	0.099	0.7
	0.133	3.4



HRT (h)	$S_{S(in)}$ (mgCOD/mL)	% Deviation
76.3	0.089	5.3
	0.134	5.0
	0.179	8.5
50.9	0.089	4.7
	0.134	0.9
	0.179	5.9
38.2	0.089	3.1
	0.134	6.7
	0.179	8.1

**Figure 2.** Model validation for (A) RB5 and (B) DB71 removal in a CSGOM-biofilm reactor (points are the experimental values and lines are simulation outcome).

**Table 7.** Relation between the dye properties and hydrolysis constant for CSGOM-biofilm

Dye information	Dye structure	Hydrolysis constant, $k_h$ (mgCOD) <sup>n-1</sup> / (L <sup>n-1</sup> ·h)
Acid Orange 7 C <sub>16</sub> H <sub>11</sub> N <sub>2</sub> NaO <sub>4</sub> S MW = 350.32 g/mol		1.431 ± 0.061
Reactive Black 5 C <sub>26</sub> H <sub>21</sub> N <sub>5</sub> Na <sub>4</sub> O <sub>19</sub> S <sub>6</sub> MW = 991.8 g/mol		0.287 ± 0.011
Direct Blue 71 C <sub>40</sub> H <sub>23</sub> N <sub>7</sub> Na <sub>4</sub> O <sub>13</sub> S <sub>4</sub> MW = 1029.9 g/mol		0.262 ± 0.017

Klaus Hunger; Peter Mischke; Wolfgang Rieper; Roderich Rau; Klaus Kunde; Aloys Engel (2005). "Azo Dyes". Ullmann's Encyclopedia of Industrial Chemistry. Weinheim: Wiley-VCH.

National Center for Biotechnology Information (2021a). PubChem Compound Summary for CID 135442967, Reactive Black 5. Retrieved January 31, 2022, from <https://pubchem.ncbi.nlm.nih.gov/compound/Reactive-Black-5>.

National Center for Biotechnology Information (2021b). PubChem Compound Summary for CID 20427, Direct Blue 71. Retrieved January 31, 2022, from <https://pubchem.ncbi.nlm.nih.gov/compound/Direct-Blue-71>.

### 3.4 Model Evaluation with Differing Supporting Materials

DB71 removal data were employed to find out the effect of support material for the biofilm formation, i.e., CSCM and CSGOM. The removal efficiency was quite higher for the biofilm growing on CSGOM compared to CSCM (Figure 3). Biofilm over CSGOM gives, at steady-state, a dye removal of 92.2 % for 0.089 mgCOD/mL DB71 feed concentration and 76.3 h of HRT, but 22 % less removal was shown for CSCM support. The removal efficiency was also lowered as dye concentration increases and HRT

decreases. For 38.2 h HRT, 50% less removal was encountered for CSCM-biofilm compared to CSGOM-biofilm.

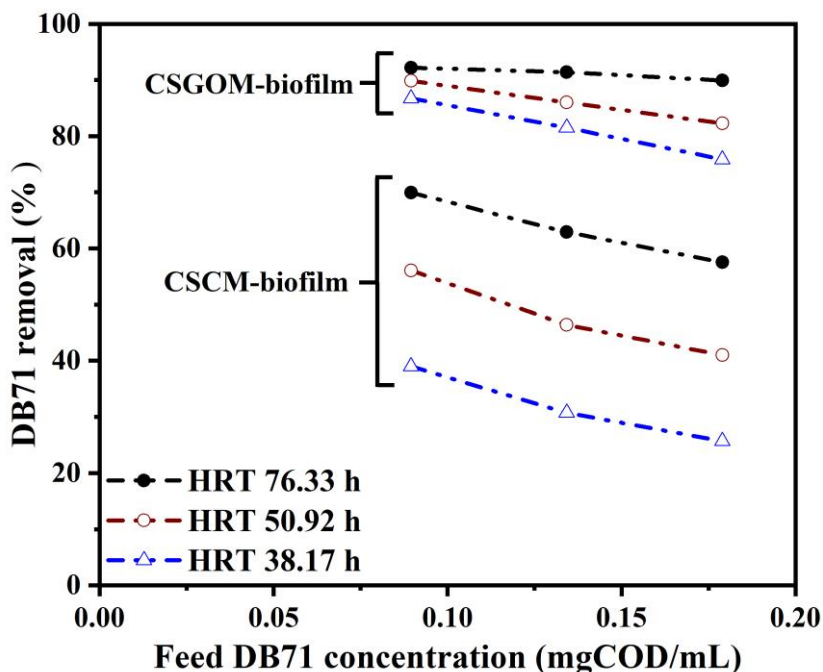


**Figure 3.** Comparison of DB71 removal efficiency of CSGOM-biofilm and CSCM-biofilm.

The developed model was calibrated against data shown in Figure 3 and the estimated hydrolysis constant ( $k_h$ ) for CSCM was calculated to be  $0.041 \pm 0.004$  (mgCOD) $^{n-1}/$  (L $^{n-1}$ ·h) ( $\chi^2 = 0.000098$ ), while it was much higher for CSGOM ( $k_h = 0.262 \pm 0.017$  (mgCOD) $^{n-1}/$  (L $^{n-1}$ ·h)). The low hydrolysis constant for CSCM supporting biofilm is attributed to the lower electron transfer capacity compared to CSGOM. It indicated that the support material with high electron transfer capacity enhances the hydrolysis, which eventually increases the dye removal efficiency. Anyway, the calibrated model was able to reproduce very well the DB71 removal using CSCM based biofilm reactor with deviation below 9% (Figure 4).

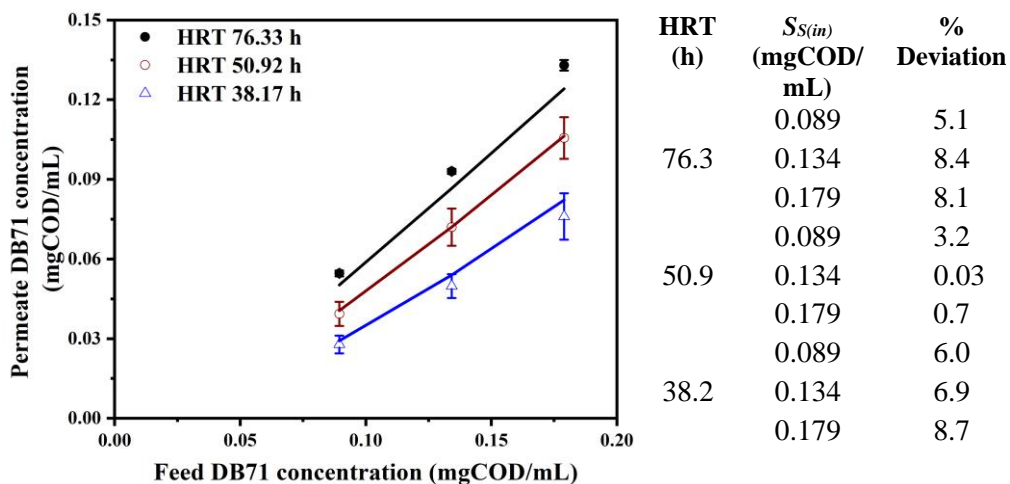


**Figure 4.** Comparison between experimental and predicted behavior at steady-state for DB71 removal using biofilm on CSCM (points are the experimental values and lines are simulation outcome).

### 3.5 Effect of External Carbon Source on Anaerobic Bio-digestion of Dyes

Simulation was conducted with various acetate to dye ratios by changing their concentrations in feed solution. The flow rate as well as HRT was kept constant at 50.9 h. The effect of acetate concentration on dye removal was evaluated based on steady state dye concentration in permeate that was translated as percentage removal as a function of acetate to dye ratio and shown in Figure 5. Results showed that the dye removal efficiency was increased as acetate concentration increases in line with findings from other studies [47, 48]. At the same acetate to dye ratio the removal efficiency was higher for low dye concentration. The dye removal efficiency was also decreased with increasing molecular weight and complexity of dye. In absence of any external organic substrate (acetate), more than 85% AO7 removal was still observed for 0.40 mgCOD/mL dye concentration (Figure 5(A)) but for RB5 it was just 24% (Figure 5(B)) while for DB71 it was 26% (Figure 5(C)). More than 90% dye removal was found for both RB5 and

DB71 by applying an acetate to dye ratio of 5. Easily fermentable organic materials like acetate give advantages to the microorganisms to grow and stimulate the hydrolysis process, thus the removal efficiency. Presence of acetate facilitated the easy transferability of electrons that promoted a faster degradation of azo dye, which suggests that a denser current of electrons helps the reductive break of the azo bond [49]. The increase of external carbon source also promotes an easier development of biofilm and biomass formation and allows reaching higher dye removal rate.

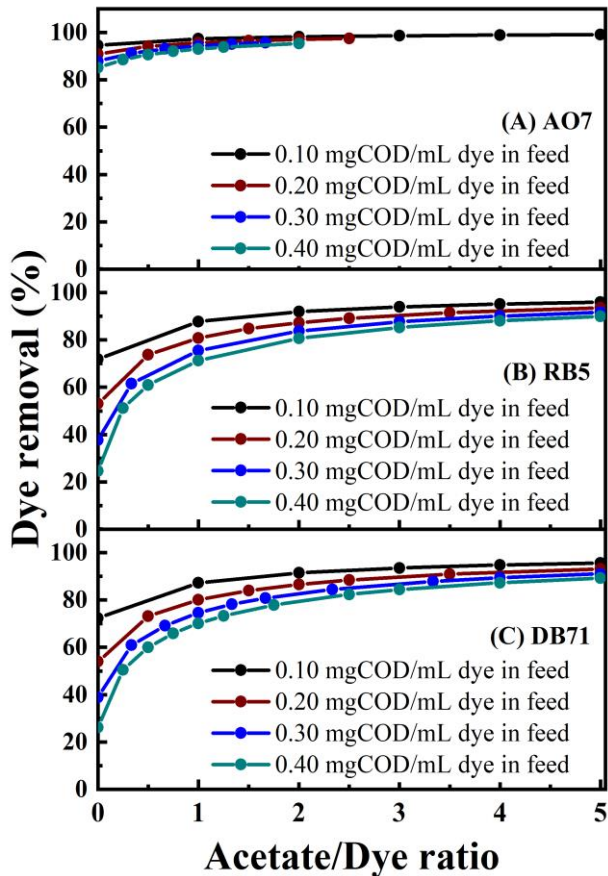


**Figure 5.** Effect of acetate to dye ratio on (A) AO7, (B) RB5 and (C) DB71 removal.

The optimal doses of acetate (external carbon source) for maximum dye removal are not the unique variable that needs to be controlled for efficient process. Another strategy called ratio control: keeping the carbon: dye (Acetate/dye) ratio at a certain level by dosing external carbon for the efficient removal of pollutants. From Figure 5, it was found that ratio alone did not have a straightforward relation to removal achieved, i.e., same ratio did not show same dye removal efficiency. Dye concentration in feed solution also have a significant role. However, this study only was focused to determine the setpoint for minimum external carbon source to meet the effluent standard.

### **3.6 Interaction Between HRT and Acetate to Dye Ratio on Anaerobic Bio-digestion of Dyes**

To evaluate the HRT impact on anaerobic bio-digestion of dyes and find out the interaction between the HRT and acetate to dye ratio on the dye removal process, simulations were conducted at various acetate to dye ratio and HRT. The variation of acetate to dye ratio was done by changing acetate concentration 0-1.2 mgCOD/mL over a fixed 0.40 mgCOD/mL DB71 solution. The HRT was set by changing the feed flow rate from 0.03 mL/h to 1.5 mL/h in the 5 mL bioreactor. The steady state removals reached for each combination are depicted in Figure 6. As expected, HRT enhanced the DB71 removal efficiency. Without adding any acetate in the feed solution (acetate to BD71 ratio 0) the DB71 removal was increased from 6.8% to 74.3% as HRT increases from 33.3 h to 166.7 h. Increasing HRT provides more time to the microorganisms to digest dye and other intermediate products, thus enhancing the dye removal.



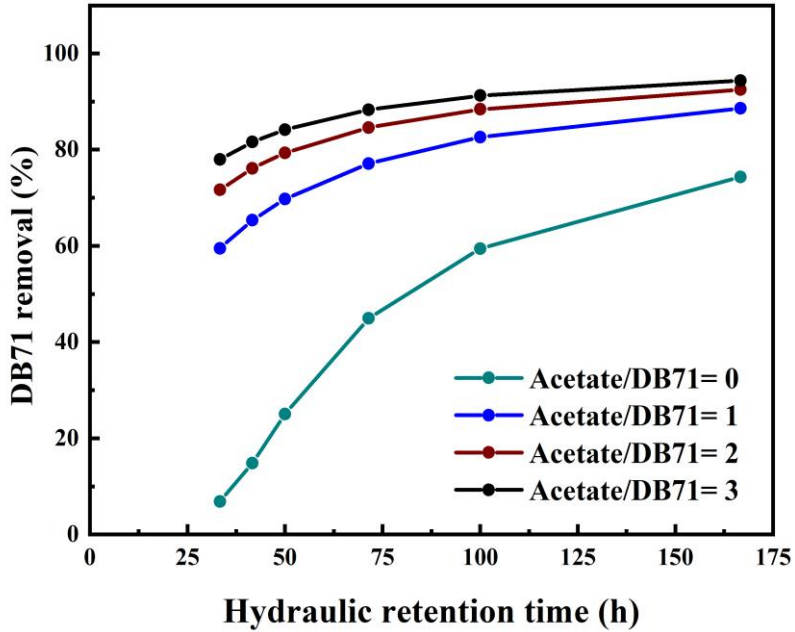


**Figure 6.** Effect of HRT and acetate to DB71 ratio on DB71 removal.

As suspected, both HRT and acetate to dye ratio altered the dye removal efficiency. However, small amount of external carbon source (acetate) is desired since it makes the process more economic, also in terms of lower sludge production. The optimization addressed here is to interactive performance between HRT and external carbon source to dye ratio. The study enables the reduction of use external carbon source by increasing HRT without hampering the effluent water quality, however it should be well balanced with HRT to reduce the investment cost.

## 4. Conclusions

A mathematical model for anaerobic biodegradation of dyes using biofilm reactors coupled with membrane filtration was developed, calibrated and validated with different types of dye, various feed concentrations and several hydraulic retention times.

Hydrolysis played the major role on anaerobic biodegradation of dyes. Hydrolysis rate constant was dependent on dye molecule structure and biofilm support materials. Increasing molecular weight as well as the complexity of dye structure decreased the hydrolysis capacity of dye. Simple dye possesses higher hydrolysis constant compared to more complex (higher molecular weight) dyes.

The support materials, on which the biofilm was formed, has a significant effect on dye removal efficiency. Materials with high electron transfer capacity increases the biofilm activities and hydrolysis as well as enhances the removal efficiency.

External carbon source is also important for the efficient dye removal through anaerobic digestion. Increase of the carbon source dose enhances the dye removal efficiency. The required external carbon source for efficient dye removal also depends on type of dyes; simple dye needs low external carbon dose compared to more complex dyes. Acetate to dye ratio did not have a straightforward relation to dye removal efficiency since dye feed concentration also needs to be taken into account.

Hydraulic retention time (HRT) enhances the dye removal efficiency. It is possible to compensate lower external carbon source doses with higher HRT to achieve a given level of dye removal.

**References:**

1. Berradi, M., Hsissou, R., Khudhair, M., Assouag, M., Cherkaoui, O., El Bachiri, A., and El Harfi, A., Textile finishing dyes and their impact on aquatic enviroins. *Heliyon*, 2019. 5(11), e02711.
2. Rajamohan, N. and Rajasimman, M., Kinetic Modeling of Dye Effluent Biodegradation by *Pseudomonas Stutzeri*. *Engineering, Technology & Applied Science Research*, 2013. 3(2), 387-390.
3. Li, Q., Tang, X., Sun, Y., Wang, Y., Long, Y., Jiang, J., and Xu, H., Removal of Rhodamine B from wastewater by modified *Volvariella volvacea*: batch and column study. *RSC Advances*, 2015. 5(32), 25337-25347.
4. Yilmaz Ozmen, E., Erdemir, S., Yilmaz, M., and Bahadir, M., Removal of Carcinogenic Direct Azo Dyes from Aqueous Solutions Using Calix[n]arene Derivatives. *CLEAN – Soil, Air, Water*, 2007. 35(6), 612-616.
5. Benkhaya, S., M'Rabet, S., and El Harfi, A., Classifications, properties, recent synthesis and applications of azo dyes. *Heliyon*, 2020. 6(1), e03271.
6. Amin, M. S. A., Stüber, F., Giralt, J., Fortuny, A., Fabregat, A., and Font, J., Comparative Anaerobic Decolorization of Azo Dyes by Carbon-based Membrane Bioreactor. *Water*, 2021. 13(8), 1060.
7. Amin, M. S. A., Stüber, F., Giralt, J., Fortuny, A., Fabregat, A., Font, J., Ceramic-supported graphene oxide membrane bioreactor for the anaerobic decolorization of azo dyes. *Journal of Water Process Engineering*. 2022. 45, 102499.

8. Amin, M. S. A., Stüber, F., Giralt, J., Fortuny, A., Fabregat, A., Font, J., Compact Carbon-Based Membrane Reactors for the Intensified Anaerobic Decolorization of Dye Effluents. *Membranes*. 2022. 12(2), 174.
9. Mezohegyi, G., Kolodkin, A., Castro, U. I., Bengoa, C., Stuber, F., Font, J., Fabregat, A., and Fortuny, A., Effective Anaerobic Decolorization of Azo Dye Acid Orange 7 in Continuous Upflow Packed-Bed Reactor Using Biological Activated Carbon System. *Industrial & Engineering Chemistry Research*, 2007. 46(21), 6788-6792.
10. Popli, S. and Patel, U. D., Destruction of azo dyes by anaerobic-aerobic sequential biological treatment: a review. *International Journal of Environmental Science and Technology*, 2015. 12(1), 405-420.
11. Işık, M. and Sponza, D. T., Decolorization of Azo Dyes Under Batch Anaerobic and Sequential Anaerobic/Aerobic Conditions. *Journal of Environmental Science and Health, Part A*, 2004. 39(4), 1107-1127.
12. Saratale, R. G., Saratale, G. D., Chang, J. S., and Govindwar, S. P., Bacterial decolorization and degradation of azo dyes: A review. *Journal of the Taiwan Institute of Chemical Engineers*, 2011. 42(1), 138-157.
13. Yoo, E., Libra, J., and Adrian, L., Mechanism of Dye Reduction of Azo Dyes in Anaerobic Mixed Culture. *Journal of Environmental Engineering- ASCE*, 2001. 127(9), 844-849.
14. van der Zee, F. P. and Villaverde, S., Combined anaerobic-aerobic treatment of azo dyes-A short review of bioreactor studies. *Water Research*, 2005. 39(8), 1425-1440.

15. Pavithra, K. G., P, S. K., V, J., and P, S. R., Removal of colorants from wastewater: A review on sources and treatment strategies. *Journal of Industrial and Engineering Chemistry*, 2019. 75, 1-19.
16. Khehra, M. S., Saini, H. S., Sharma, D. K., Chadha, B. S., and Chimni, S. S., Decolorization of various azo dyes by bacterial consortium. *Dyes and Pigments*, 2005. 67(1), 55-61.
17. Moosvi, S., Kher, X., and Madamwar, D., Isolation, characterization and decolorization of textile dyes by a mixed bacterial consortium JW-2. *Dyes and Pigments*, 2007. 74(3), 723-729.
18. Nigam, P., Banat, I. M., Singh, D., and Marchant, R., Microbial process for the decolorization of textile effluent containing azo, diazo and reactive dyes. *Process Biochemistry*, 1996. 31(5), 435-442.
19. Yoo, E. S., Libra, J., and Adrian, L., Mechanism of Decolorization of Azo Dyes in Anaerobic Mixed Culture. *Journal of Environmental Engineering*, 2001. 127(9), 844-849.
20. Georgiou, D., Metallinou, C., Aivasidis, A., Voudrias, E., and Gimouhopoulos, K., Decolorization of azo-reactive dyes and cotton-textile wastewater using anaerobic digestion and acetate-consuming bacteria. *Biochemical Engineering Journal*, 2004. 19(1), 75-79.
21. Yu, L., Zhang, X.-Y., Wang, S., Tang, Q.-W., Xie, T., Lei, N.-Y., Chen, Y.-L., Qiao, W.-C., Li, W.-W., and Lam, M. H.-W., Microbial community structure associated with treatment of azo dye in a start-up anaerobic sequenced batch reactor. *Journal of the Taiwan Institute of Chemical Engineers*, 2015. 54, 118-124.
22. Pandey, A., Singh, P., and Iyengar, L., Bacterial decolorization and degradation of azo dyes. *International Biodeterioration & Biodegradation*, 2007. 59(2), 73-84.

23. Solís, M., Solís, A., Pérez, H. I., Manjarrez, N., and Flores, M., Microbial decolouration of azo dyes: A review. *Process Biochemistry*, 2012. 47(12), 1723-1748.
24. da Silva, M. E. R., Firmino, P. I. M., de Sousa, M. R., and dos Santos, A. B., Sequential Anaerobic/Aerobic Treatment of Dye-Containing Wastewaters: Colour and COD Removals, and Ecotoxicity Tests. *Applied Biochemistry and Biotechnology*, 2012. 166(4), 1057-1069.
25. Saratale, R., Saratale, G., Kalyani, D., Chang, J.-S., and Govindwar, S., Enhanced decolorization and biodegradation of textile azo dye Scarlet R by using developed microbial consortium-GR. *Bioresource technology*, 2009. 100, 2493-500.
26. Hosseini Koupaie, E., Alavi Moghaddam, M. R., and Hashemi, S. H., Investigation of decolorization kinetics and biodegradation of azo dye Acid Red 18 using sequential process of anaerobic sequencing batch reactor/moving bed sequencing batch biofilm reactor. *International Biodeterioration & Biodegradation*, 2012. 71, 43-49.
27. Jonstrup, M., Kumar, N., Murto, M., and Mattiasson, B., Sequential anaerobic–aerobic treatment of azo dyes: Decolourisation and amine degradability. *Desalination*, 2011. 280(1), 339-346.
28. Oh, Y.-K., Kim, Y.-J., Ahn, Y., Song, S.-K., and Park, S., Color removal of real textile wastewater by sequential anaerobic and aerobic reactors. *Biotechnology and Bioprocess Engineering*, 2004. 9(5), 419.
29. Sonwani, R. K., Swain, G., Giri, B. S., Singh, R. S., and Rai, B. N., Biodegradation of Congo red dye in a moving bed biofilm reactor: Performance evaluation and kinetic modeling. *Bioresource Technology*, 2020. 302, 122811.

30. Giménez-Pérez, A., Bikkarolla, S. K., Benson, J., Bengoa, C., Stüber, F., Fortuny, A., Fabregat, A., Font, J., and Papakonstantinou, P., Synthesis of N-doped and non-doped partially oxidised graphene membranes supported over ceramic materials. *Journal of Materials Science*, 2016. 51(18), 8346-8360.
31. García-Martínez, Y., Bengoa, C., Stüber, F., Fortuny, A., Font, J., Fabregat, A., Biodegradation of acid orange 7 in an anaerobic–aerobic sequential treatment system. *Chemical Engineering and Processing - Process Intensification*. 2015. 94, 99-104.
32. Sun, J., Dai, X., Wang, Q., Pan, Y., Ni, B.-J., Modelling Methane Production and Sulfate Reduction in Anaerobic Granular Sludge Reactor with Ethanol as Electron Donor. *Scientific Reports*. 2016. 6(1), 35312.
33. Henze, M., Gujer, W., Mino, T., and van Loosdrecht, M. C. M., *Activated sludge models ASM1, ASM2, ASM2d and ASM3*. 2000, London: IWA Publishing. 121.
34. Williamson, K. and McCarty, P. L., A model of substrate utilization by bacterial films. *J Water Pollut Control Fed*, 1976. 48(1), 9-24.
35. Picioreanu, C., van Loosdrecht, M. C. M., and Heijnen, J. J., Modelling the effect of oxygen concentration on nitrite accumulation in a biofilm airlift suspension reactor. *Water Science and Technology*, 1997. 36(1), 147-156.
36. Hao, X. D. and van Loosdrecht, M. C. M., Model-based evaluation of COD influence on a partial nitrification-Anammox biofilm (CANON) process. *Water Science and Technology*, 2004. 49(11-12), 83-90.
37. Stewart Philip, S., Diffusion in Biofilms. *Journal of Bacteriology*, 2003. 185(5), 1485-1491.

38. Volcke, E. I., Picioreanu, C., De Baets, B., and van Loosdrecht, M. C., Effect of granule size on autotrophic nitrogen removal in a granular sludge reactor. *Environ Technol*, 2010. 31(11), 1271-80.
39. Van Loosdrecht, M. C. M. and Henze, M., Maintenance, endogenous respiration, lysis, decay and predation. *Water Science and Technology*, 1999. 39(1), 107-117.
40. Mozumder, M. S. I., Picioreanu, C., van Loosdrecht, M. C. M., and Volcke, E. I. P., Effect of heterotrophic growth on autotrophic nitrogen removal in a granular sludge reactor. *Environmental Technology*, 2014. 35(8), 1027-1037.
41. Reichert, P., Aquasim – A Tool for Simulation and Data Analysis of Aquatic Systems. *Water Science and Technology*, 1994. 30(2), 21-30.
42. van Benthum, W. A. J., van Loosdrecht, M. C. M., Tjihuis, L., and Heijnen, J. J., Solids retention time in heterotrophic and nitrifying biofilms in a biofilm airlift suspension reactor. *Water Science and Technology*, 1995. 32(8), 53-60.
43. Zajšek, K. and Goršek, A., A kinetic study of sucrose hydrolysis over Amberlite IR-120 as a heterogeneous catalyst using in situ FTIR spectroscopy. *Reaction Kinetics, Mechanisms and Catalysis*, 2010. 100(2), 265-276.
44. Tombari, E., Salvetti, G., Ferrari, C., and Johari, G. P., Kinetics and Thermodynamics of Sucrose Hydrolysis from Real-Time Enthalpy and Heat Capacity Measurements. *The Journal of Physical Chemistry B*, 2007. 111(3), 496-501.
45. Kura, G., Hydrolysis reaction of inorganic cyclophosphates at various acid strengths. *Polyhedron*, 1987. 6(3), 531-533.



46. Culbertson, J. B., Factors Affecting the Rate of Hydrolysis of Ketimines. *Journal of the American Chemical Society*, 1951. 73(10), 4818-4823.
47. Cui, M. H., Cui, D., Gao, L., Cheng, H. Y., and Wang, A. J., Efficient azo dye decolorization in a continuous stirred tank reactor (CSTR) with built-in bioelectrochemical system. *Bioresour Technol*, 2016. 218, 1307-11.
48. Thung, W.-E., Ong, S.-A., Ho, L.-N., Wong, Y., Ridwan, F., Lehl, H., Oon, Y.-L., and Oon, Y.-S., Biodegradation of Acid Orange 7 in a combined anaerobic-aerobic up-flow membrane-less microbial fuel cell: Mechanism of biodegradation and electron transfer. *Chemical Engineering Journal*, 2017. 336, 397-405.
49. Cui, M.-H., Cui, D., Gao, L., Wang, A.-J., and Cheng, H.-Y., Azo dye decolorization in an up-flow bioelectrochemical reactor with domestic wastewater as a cost-effective yet highly efficient electron donor source. *Water Research*, 2016. 105, 520-526.

## Appendix:

### List of symbols

$b_h$	: Decay rate constant of anaerobic bacteria, $h^{-1}$
$D_{NH}$	: Ammonium diffusion coefficient in water, $cm^2.h^{-1}$
$D_{O_2}$	: Oxygen diffusion coefficient in water, $cm^2.h^{-1}$
$D_S$	: COD diffusion coefficient in water, $cm^2.h^{-1}$
$D_H$	: $S_H$ diffusion coefficient in water, $cm^2.h^{-1}$
$D_{SO_2}$	: $SO_2$ Ammonium diffusion coefficient in water, $cm^2.h^{-1}$
$f_I$	: Fraction of inert COD generated by biomass lysis
$i_{NXB}$	: Nitrogen content in bacteria, mgN/mgCOD
$i_{NXI}$	: Nitrogen content in inert particulate, mgN/mgCOD
$k_h$	: Hydrolysis rate constant, $h^{-1}$
$K_{fe}$	: Saturation coefficient for fermentation of $S_F$ , mgCOD/mL
$K_A^H$	: Saturation coefficient for anaerobic digestion of $S_A$ , mgCOD/mL
$K_{NH}^H$	: Inhibition coefficient for ammonium-nitrogen on anaerobic digestion, $mgO_2/mL$
$n$	: Power index for hydrolysis
$q_{fe}$	: Maximum rate for fermentation, $h^{-1}$

$S_A$  : Fermented product concentration, mgCOD/mL

$S_F$  : Hydrolyzed organic substrate concentration,  
mgCOD/mL

$S_H$  : Digested product concentration, mgCOD/mL

$S_S$  : Dye concentration, mgCOD/mL

$S_{NH}$  : Ammonium concentration, mgCOD/mL

$S_{SO2}$  : Sulphur concentration, mgCOD/mL

$V_{NH}$  : Fraction of nitrogen in dye

$V_S$  : Fraction of sulphur in dye

$X_I$  : Inert particulate concentration, mgCOD/mL

$X_H$  : Anaerobic bacteria concentration, mgCOD/mL

$Y_H$  : Anaerobic Yield coefficient

$\mu_{\max}^{\text{AD}}$  : Maximum specific growth rate of anaerobic bacteria,  $\text{h}^{-1}$

\* in: inflow, \*\* ini: initial

## **Chapter 7. Conclusions and Future Work**

The final chapter of this thesis summarizes the significant findings and provides the most pertinent conclusions. Lastly, several recommendations for further work are made.

---



## 1. General Conclusions

The following are the key conclusions that were achieved from the research findings arising from this thesis:

- The anaerobic biodegradation of azo dye was investigated using ceramic-supported carbon-based membrane bioreactors, where membranes were synthesized from Matrimid 5218 (CSCM) and exfoliated graphene oxide solution (CSGOM) using flat ceramic filtration elements as support. The most significant consideration during the membrane synthesis is the selection of precursor concentration, and it was found that 10% wt. Matrimid solution and 1 mg·mL<sup>-1</sup> of GO solution was the best composition for CSCM and CSGOM, respectively.
- In each reactor, the maximum decolorization of the dye solutions was observed (> 95%) at lower feed concentration (50 mg·L<sup>-1</sup>) and permeate flux (0.05 L·m<sup>-2</sup>·h<sup>-1</sup>). The color removal rate decreased with increasing feed concentration and permeate flux regardless of the structurally different dyestuff molecules tested. Compared to the CSCM bioreactor (B-CSCM), the CSGOM bioreactor (B-CSGOM) showed better biodecolorization due to the better conductive surface and enhanced electron shuttle mechanism of graphene oxide.
- Further studies were focused on microbial identification and growth during the decolorization of azo dyes in B-CSGOM. The results obtained from the electron microscopic images demonstrated that the micro-sized (1.53 μm) biofilm was formed over the CSGOM. Using the DNA Illumina sequencing of the biofilm, it is found that the

anaerobic *Geobacter* and *Pseudomonas Guangdongensis* are the prevalent bacteria for dye decolorization.

- Both the B-CSCM and B-CSGOM were successfully implemented for the removal of multi-azo dyes, azo dye mixtures (ADM), phenothiazine Methylene Blue (MB), and sticky fluorescence Rhodamine B (RhB) dye solutions. In all cases, B-CSGOM performed better than B-CSCM in terms of color removal.
- Tubular ceramic-supported carbon-based membranes (TCSCM and TCSGOM) were synthesized and successfully implemented for anaerobic decolorization of azo dyes for first time to the best of our knowledge. Compared to the flat membrane bioreactor, it was found that the tubular membranes were capable of removing the color from model azo dye solutions with enhanced permeate flow. Not surprisingly, the tubular graphene oxide membrane displayed a higher decolorization rate than the carbonized Matrimid membrane.
- A mathematical model for bioreduction of anaerobic azo dyes in the biofilm of CSGOM reactor was developed, calibrated, and validated using a variety of dye types in a wide range of feed concentration and hydraulic retention time. In this model, hydrolysis was critical in the anaerobic biodegradation of dyes. The rate constant for hydrolysis was dependent on the structure of the dye molecule as well as the hydraulic retention time and biofilm support material.

## 2. Future Work

As a guide for future research, considering the main findings and conclusions obtained from this research work, some proposals are given below for possible future development of this topic.

- Further investigation of membrane precursors (such as carbon nanotubes or fibers, polyaniline, polydopamine, polyacetylene, etc.) is required in order to enhance the electron shuttle mechanism during the biodecolorization of dye solution.
- The doping of selected functional groups (nitrate, phenyl, hydroxyl, methyl, etc.) to the graphene oxide membrane can be studied to increase its porosity, chemical, and thermal stability.
- It would be of interest the design and operation of CSCM and CSGOM in a microbial fuel cell for the simultaneous power generation during wastewater treatment.
- Instead of azo dyes, the T-CSCM and TCSGOM bioreactors can be used to decolorize a variety of other dye solutions and even other compounds likely to be degraded by reductive pathways.
- Another recommendation for color removal of dye molecules would be the integration of the tubular ceramic-supported carbon membrane bioreactor filled with biological activated carbon.
- A topic worthy of development in the future is determining the bioreactor real-time COD, redox potential, and microbial growth to enhance the decolorization rate.



UNIVERSITAT ROVIRA I VIRGILI

CARBON-BASED MEMBRANE BIOREACTORS FOR THE ANAEROBIC DECOLORIZATION OF DYES

Mohammad Shaiful Alam Amin

UNIVERSITAT ROVIRA I VIRGILI

CARBON-BASED MEMBRANE BIOREACTORS FOR THE ANAEROBIC DECOLORIZATION OF DYES

Mohammad Shaiful Alam Amin



**UNIVERSITAT  
ROVIRA i VIRGILI**